NOVEL SiH_2X_2 DERIVATIVES

by

DAVID G. ANDERSON

Doctor of Philosophy

University of Edinburgh

1987

EDINBURGEN. EX BIBL. UNIV.

"NOVEL SiH_2X_2 DERIVATIVES"

CONTENTS

DECLARATION

I hereby declare that the work involved in the compilation of this thesis was carried out solely by myself unless otherwise stated and that the only work previously published is that contained in Appendix III.

ACKNOWLEDGEMENT

Principally, I would like to thank my supervisor Dr. Stephen Cradock for all his encouragement and assistance throughout the duration of this work. I am also indebted to Professor E.A.V. Ebsworth, and particularly Dr. D.W.H. Rankin for his advice on electron diffraction.

My thanks also go to Dr. A.J. Blake for undertaking the x-ray crystal structure determinations, Mr. J. Millar and Mr. L. Bell for running my n.m.r. samples and Dr. S.D. Henderson for his wit and wisdom.

Finally, I would like to thank Dorothy Pilling for typing this thesis and the Department of Chemistry for providing me with a Demonstratorship.

DEDICATION

In memory of the good times.

CHAPTER 1

STRUCTURE DETERMINATION BY ELECTRON DIFFRACTION

1.1 HISTORICAL BASIS

The basis for modern gas-phase electron diffraction derives from the initial scattering experiments of Rutherford,[1] Davisson and Germer,[2] Debye[3,4] and Thomson,[5,6] which illustrated the particle and wave like duality of the electron predicted by de Broglie.[7] Subsequently, Mark and Weirl[8] carried out the first gas-phase electron diffraction experiments on a variety of simple di- and tri-atomic compounds using equipment which, in principle, is essentially the same as that used today, although various significant improvements have now been incorporated. Most notable amongst these, was the introduction of a heart shaped metal sector which compensates for the fall off of scattering intensity with angle, by attenuating the electrons scattered at narrow angles. This, in conjunction with high vacuum techniques, accurate microdensitometry and modern computing methods has meant that gas-phase electron diffraction has become a widely used and relatively routine structural technique.

1.2 THEORY

In an analogous manner to Young's double Slit experiment, scattering of electrons by a molecule will yield a pattern with alternate regions of constructive and destructive interference. In an electron diffraction experiment, these are observed as a series of concentric rings on a photographic plate and here too, if the wavelength of the radiation and the scattering angle are known, then the interatomic distances (cf. the slit separation) can be calculated. The total scattering intensity (I) is given by the expression:

$$I\ (\text{total}) = I(\text{extraneous}) + I(\text{inelastic}) + I(\text{atomic}) + I(\text{molecular})$$

The inelastic scattering arises when an electron electronically excites an atom, thus changing its momentum. At the accelerating potentials used in an electron diffraction experiment, however, this effect is almost negligible. This, together with the extraneous scattering due to multiple collisions or reflections from the chamber walls, can be subtracted from the total scattering intensity, as a background, after subtraction of the atomic scattering. The atomic scattering which is dependent upon the scattering factors[9] of the atoms, gives a rapidly declining function which can be calculated and hence deducted from I(total). This then leaves the molecular scattering intensity, which contains the structural information in the form of interatomic distances.

The molecular scattering intensity is a function of the parameter, S:

$$S = \frac{4\pi\ \mathrm{Sin}\ (\theta/2)}{\lambda} \qquad (1)$$

where θ = the scattering angle and λ = wavelength of the electron beam. S generally has the units nm^{-1} and is useful for comparing scattering data from different sources, since it is independent of the dimensions of the experiment.

For a rigid molecule, the molecular scattering intensity[10] is given by:

$$Im(S) = \frac{2R^2}{S^4} \sum_{ij} \underbrace{(Z_i - F_i(S))(Z_j - F_j(S)).\mathrm{Cos}\ (n_i - n_j)}_{=A_{ij}(S)} \frac{\mathrm{Sin}(Sr_{ij})}{Sr_{ij}} \qquad (2)$$

where $R = \frac{8\pi me^2}{h^2}$

and m and e are the mass and charge of the electron, h is Planck's constant, Zi and Fi(S) are the atomic number and scattering factor[9] of element i at point S and $n_i - n_j$ is the phase shift on scattering from the atom pair i and j at point S. This function is found to be inadequate, however, since on Fourier transformation of this molecular intensity expression, a series of single lines representing the inter-nuclear distances r_{ij} is obtained in the radial distribution curve. In practice, the radial distribution curve does not contain single lines, but peaks, since the interaction time of the electron with the molecule is several orders of magnitude smaller than period of a molecular vibration. It is therefore necessary to include a probability function, $P_{ij}(r)$, which allows for the range of different values around r_{ij} associated with a molecular vibration:

$$Im(S) = \frac{2R^2}{S^4} \sum_{ij} n_{ij} A_{ij}(S) . \int P_{ij}(r) \quad \frac{Sin(Sr)dr}{Sr} \qquad (3)$$

where n_{ij} = number of symmetrically equivalent atom pairs of a specific type.

$$P_{ij}(r) = (\pi U^2_{ij})^{-1/2} \quad exp. \ (-\Delta r \ /2U^2_{ij}) \qquad (4)$$

Where U_{ij} = root mean square amplitude of vibration

and $\Delta r_{ij} = r - r_{ij}^e$ and r_{ij}^e = equilibrium value of the inter-nuclear distance.

Expansion of the integral then yields (5).

$$Im(S) = \frac{2R^2}{S^4} \sum_{ij} n_{ij} A_{ij}(S) . exp \ (-u^2_{ij} S^2/2) . \frac{Sin \ (Sr_{ij}^*)}{Sr_{ij}^*} \qquad (5)$$

Where $r_{ij}^* = r_{ij}^e - u^2_{ij} \ / r_{ij}^e$

Finally, the anharmonic nature of a vibration,[11,12] a_{ij}, must be considered and this is related to the Morse anharmonicity, a, where $a_{ij} = au^4/6$, yielding (6).

$$Im(S) = \frac{2R^2}{S^4} \sum_{ij} n_{ij} A_{ij}(S) . \exp(-U_{ij}^2 S^2/2) \frac{Sin(Sr_{ij}^* - a_{ij}S^3)}{S . r_{ij}^*} \quad (6)$$

a_{ij} is set equal to $200pm^{-1}$ for bonded atoms and this accounts for the asymmetric, non Gaussian, appearance of the peaks observed in the radial distribution curve.

1.3 ELECTRON DIFFRACTION APPARATUS

This Section discusses and deals with the apparatus required for electron diffraction experiments. Discussion is centred around the equipment used in Edinburgh, although the devices and components of any electron diffraction apparatus are essentially very similar.

The fundamental requirement for any experiment of this type is a stable monochromatic electron beam. This is provided by passing a sufficiently large current through a tungsten filament to emit electrons. The electrons are then accelerated through an anode containing a hole using a voltage of approximately 45kV. Since

$$\lambda = \frac{h}{p} \quad (7)$$

$$\text{and } Ve = P^2/2m \quad (8)$$

$$\text{then } \lambda = \frac{h}{(2meV)^{1/2}} \quad (9)$$

Where V = accelerating potential and λ = wavelength of the electron. This equation for the electron wavelength however ignores the relativistic effects which have to be considered for electrons with a velocity close to the speed of light and it can be shown that the

realistic wavelength[13,14] is given by:

$$\lambda = \frac{h}{M_0 C\left[\left(1+\frac{eV}{M_0C^2}\right)^2-1\right]^{1/2}} \qquad (10)$$

Accelerating voltages of the magnitude mentioned above will produce an electron beam with a wavelength of ≃5-6pm which is ideal for structure determination, since molecular bonds lengths generally vary between 100-250pm.

The electron beam is then focussed using magnetic lenses and this can be checked by monitoring the spot produced on a fluorescent screen behind the photographic plates.

The sample is introduced into the apparatus via a narrow nozzle, perpendicular to the electron beam, which can be rotated to give two different nozzle to plate distances giving both narrow and wide angle scattering. In each case, the sample is removed from the diffraction apparatus via a cryogenic pump directly opposite the nozzle inlet.

The scattered electrons are detected using photographic plates stored in the camera unit of the apparatus and a heart-shaped sector device, located between the nozzle and camera, ensures that the detected scattering intensity is in a dynamic range which can be resolved by the photographic emulsion on the plates. Since scattering intensity $\propto S^{-4}$, the sector is shaped such that at small angles (θ) the beam is strongly attentuated and as θ increases, so the attentuation decreases in a known manner.

The whole assembly is encased in a non-magnetic stainless steel, aluminium and brass chamber with lead-glass viewing windows. In order to minimise multiple-scattering, the chamber pressure is held below 10^{-6} torr by a series of oil diffusion and rotary pumps.

1.4 EXPERIMENTAL DETAILS

A pure sample of the compound under investigation is introduced into the apparatus via a ground glass joint attached to the nozzle. With the electron beam focussed and aligned, and the sector rotating, the plate is exposed for a length of time which is dependent upon the scattering power of the sample and the pressure increase in the chamber. Generally three plates were recorded at each of the two camera distances for the sample, along with two benzene plates at each distance. The benzene plates[15] were used to accurately determine the camera distance and electron wavelength used in the subsequent calculations on the sample compound. The samples examined in this work were all run at room temperature, although the facility to vary the nozzle temperature now exists.

The exposed plates are then removed from the camera, and developed and washed, before being sent to be traced by the microdensitometer service at Daresbury.

1.5 TRACING PROCESS AND WAVELENGTH CALCULATION

The electron diffraction plates for benzene and the sample compound are traced on the Joyce-Loebl Microdensitometer 6[16] located at Daresbury. This process firstly involves tracing the benzene plates using initially assumed values for the electron wavelength and the short (S) and long (L) camera distances. This results in the production of incorrect parameters for benzene, but these can be used in conjunction with the accurately known values,[15] to scale the wavelength and camera distances to yield the actual values for the benzene plates. (See below).

$$\lambda = \frac{\lambda_{in.} 139.70}{r(C\text{-}C)} \qquad (11)$$

$$S = \frac{Sin.r(C-C)}{r(C-C)s} \qquad (12)$$

$$L = \frac{Lin.r(C-C)}{r(C-C)_L} \qquad (13)$$

(Where 139.70pm is the literature C-C distance in benzene).

The corrected camera distances and wavelength are then used in conjunction with coordinates of the centre of the sample plates by the microdensitomer, to determine the optical density of the plates. This is carried out by automatic scanning of one thousand points equally spaced around a ring of constant S value for each plate. This process is repeated five times before moving, by an increment ΔS, to the next S value where the whole procedure is again repeated. In this way, the whole plate is scanned, before finally subtracting a background value (which has been determined from an unexposed region of the plate) from all readings.

This yields a list of optical densities for each plate which have an accuracy of $\pm$0.0001D.

This method of tracing has the added advantage that flaws or imperfections in plates can be excluded from tracing by specifying the unwanted sector or region, and also of reducing correlation between adjacent points, since interpolation between S values is no longer necessary.

1.6 DATA REDUCTION AND REFINEMENT

The data reduction and subsequent refinement of structures was carried out using the Edinburgh Regional Computing Centre ICL 2976 mainframe computer. Data reduction involved the use of a modified version of an existing program[17] which used the optical densities direct from Daresbury.

Initially, corrections for the flatness of the plates and saturation of the photographic emulsion are applied to the data, along with the sector equation. This then yields the uphill curve which contains all the various scattering intensities (Itotal). The program then requires a list of all the atom types in the sample and their multiplicities which then enable the atomic scattering to be deducted using the appropriate atomic scattering factors.[9] This leaves the molecular and extraneous scattering intensities, and at this point a molecular model, which generates the atomic coordinates, together with a list of the estimated molecular parameters, amplitudes of vibration and anharmonicities is inserted into the system. This then allows calculation of the theoretical molecular intensity curve. The structure can then be refined using an updated version of an existing least squares refinement program[18] which seeks to find the best fit of the experimental intensity curve with the theoretical one. The difference between these should be attributable to the extraneous scattering and this can be subtracted from the experimental data by either drawing a smooth curve through the difference intensity curve, or automatically by the use of spline functions.

The closeness of the fit between the experimental and theoretical intensity curves is given by the R gen factor, which is related to the R diag factor shown below:

$$R\ diag = \frac{\sum(Iexpt - Itheory)^2}{\sum Iexpt^2} = \frac{\sum D^2}{\sum I^2} \qquad (14)$$

This can be expressed in matrix form as:

$$R\ diag = \frac{D'WD}{I'WI} \qquad (15)$$

Where W is a weight matrix containing only diagonal elements.

This treatment, however, does not consider the correlation between adjacent data points. The standard deviation obtained using a weighting matrix containing only diagonal elements is proportional to $n^{-1}/2$, where n is the number of observations or data points. This is incorrect, however, since it implies that the standard deviation can be reduced by increasing n. As the number of data points (n) increases, so the distance between them decreases and the correlation increases. This is significant in data obtained in an electron diffraction experiment and therefore a weight matrix containing off diagonals to compensate for this must be considered.[19] The elements of this matrix, W, are as follows:

<u>diagonal</u>: $W_{ii} = (S_i - Smin)/(S_1 - Smin)$ where $Smin < S_i < S_1$

$W_{ii} = 1$ where $S_1 < S_i < S_2$

$W_{ii} = (Smax - S_i)/(Smax - S_2)$ where $S_2 < S_i < Smax$

<u>off diagonal</u>: $W_{ij} = 0$ Where $i \neq j \mp 1$

$W_{ij} = 0.5\ (W_{ii} + W_{jj})/(p/h)_R$ where $i = j \mp 1$

Where S_1 and S_2 are weighting points chosen between Smin and Smax for a distance R and $(p/h)_R$ is the correlation parameter at that distance. The correlation parameter is found to equal to negative the off diagonal terms of the weighting matrix if the diagonal terms are equal to unity and its magnitude is always less than 0.5.

The R gen factor can thus be written:

$$R\ gen = \left[\frac{D'WD}{I'WI}\right]^{1/2} \qquad (16)$$

Where W is a weighting matrix containing off diagonal terms and I is the vector of the intensities, with D the difference vector. R gen is, therefore, a better estimate of the standard deviation, although R diag is also quoted in the refinements mentioned in subsequent chapters.

In principle the refinement program allows refinement of all parameters and amplitudes, but in practice some of these remain fixed and amplitudes are sometimes refined as a group with fixed relative ratios.

The program also allowed the observed and difference intensity and radial distribution curves to be plotted out, and those obtained in the final refinement cycle for a given sample, are illustrated in the appropriate chapters.

1.7 LIMITATIONS

In principle, any compound with a vapour pressure greater than 2mm of Hg can be studied by electron diffraction. The number of compounds in this category has increased with the advent of high temperature nozzles, although the thermal stability of the sample is still a limiting factor.

Problems which arise from the atomic arrangement in a molecule are shrinkage effects, overlap of peaks in the radial distribution curve and the presence of light atoms. Shrinkage effects[21] arise from the deformational modes of groups in a molecule, which occur on a longer timescale than the interaction of an electron with a molecule. Thus, 'floppy' groups (i.e. groups which undergo large amplitude, low frequency bending modes) which are actually linear or planar, will appear bent or non-planar, since on average, they will be bent or non-planar most of the time.

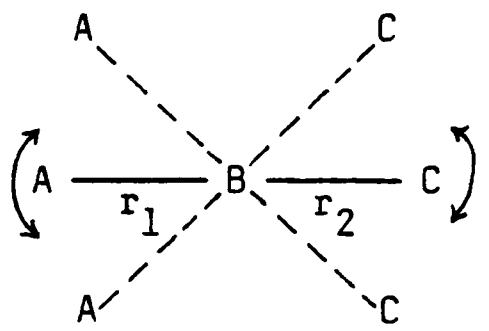

i.e. $AC < r_1 + r_2$

This effect makes structures determined by electron diffraction, strictly incompatible with those determined by microwave Spectroscopy,[22] although a correction can be applied to yield, r_∞:

$$r_\infty = r_a + \frac{U^2}{r_e} - K \qquad (17)$$

Where r_a is the interatomic distance obtained by e.d.; r_∞ is the interatomic distance obtained by microwave and U is the amplitude of vibration. Since $^{u^2}/r_e$ is small, r_e can be substituted with r_a and K, which is a perpendicular amplitude correction for harmonic atomic displacements orthogonal to the vector $\underline{r}$, must be obtained from a normal coordinate analysis of the molecule involved. For simple molecules, data from the two sources generally show good agreement after corrections have been applied.[23]

Problems associated with the radial distribution curve are those of overlapping peaks and light atoms. Where two or more peaks are only 5-10pm apart, generally one or more of the parameters or amplitudes involved has to be fixed, leading to undetermined structures, since independent refinement yields badly determined parameters which are highly correlated.

The area of peaks in the radial distribution curve is proportional to the multiplicity of the distance involved and the atomic numbers of the atoms, and inversely proportional to the distance between them. Generally, therefore, distances involving

hydrogen atoms give rise to only very small peaks and this usually requires fixing the parameters or amplitudes involved to values obtained from spectroscopy or from structure determinations of similar compounds.

The structures discussed in the following chapters are all r_a structures and normal coordinate analyses were not carried out for any of the molecules.

CHAPTER 2

EXPERIMENTAL TECHNIQUES

2.1 INTRODUCTION

In this chapter, details of the experimental techniques involved in the handling of volatile samples, and of the various techniques and instruments used in obtaining Infra-red, Raman and Nuclear Magnetic Resonance spectra are given. The last section concerns the preparation and purification of the samples.

2.2 VACUUM TECHNIQUES

All of the compounds under investigation were either gases or volatile liquids at room temperature, and most were both air and moisture sensitive. This therefore required that all samples were handled using a standard vacuum line.

The vacuum line facilitated easy handling of any compound with a vapour pressure >2mm at room temperature, but with essentially no vapour pressure at 77K (liquid nitrogen temperature).

The vacuum line consisted of two trap sections for the storage and trap-to-trap distillation of samples, and various 'take-off' points which allowed the introduction to, or removal of samples from, the line. The taps in the line were sealed using Apiezon 'N' grease and the joints were sealed with Apiezon 'L'. The vacuum in the line was achieved with a mercury diffusion pump and rotary oil pump. This enabled a line pressure of $\simeq 10^{-5}$mmHg to be reached. The pressure due to samples in the line was monitored or measured by a spiral deflection gauge in conjunction with a manometer in the 'back section' of the line. The spot from the spiral deflection gauge/lamp gave zero deflection when the pressures in the line and back section were equal. Knowing the volume of the line and the 'spiral

sensitivity', allowed specific quantities of samples to be measured out.

All of the samples used in this work were stored in traps surrounded by Dewar flasks containing liquid nitrogen. Purification of the samples was achieved by trap-to-trap fractional distillation through baths containing an organic solvent and either liquid nitrogen or solid carbon dioxide. These 'slush baths' allowed a range of fractionation temperatures to be achieved.

Gas phase Infra-red spectra were recorded by attaching a 10cm cell fitted with either KBr or CsI plates to the line and vapour pressure measurements were made by allowing a sample to volatilise into the spiral section from the 'cold finger' at a specific temperature (usually 273K). Molecular weight determinations were made by allowing a known pressure and weight of gas into a molecular weight bulb of known volume.

Gas—phase Infra-red spectra were recorded using a Perkin Elmer 598 spectrophotometer ($4{,}000 \longrightarrow 200cm^{-1}$). Solid phase and matrix isolated spectra were recorded by spraying samples directly onto a CsI window fitted to Perkin Elmer 225 spectrometer connected directly to a vacuum line ($4{,}000 \longrightarrow 200cm^{-1}$). The window of this spectrometer was held at a controlled temperature down to 10K by an Air Products DE-202 helium microrefrigerator, and a vacuum, generally below 10^{-6}mmHg, was obtained with a metal vacuum line connected to a mercury diffusion pump and a rotary pump.

Preparation of matrix isolated samples involved mixing the sample gas with nitrogen, the inert matrix gas, in a ratio between 1:400 and 1:1,000, parts sample to parts nitrogen respectively. Samples of this mixture were then pulsed onto the spectrometer window at 10K. For both solid and matrix isolated spectra, the final

recorded spectra were run after no further changes in band position and intensity were noted after annealing of the samples.

Both liquid and solid Raman spectra were recorded using either a Cary 83 or a Spex Ramalab Raman Spectrometer between 4,000 → 100cm^{-1}, both with an argon-ion laser with a 488nm source. Samples were sealed in glass tubes approximately 5cm long and with an internal diameter of roughly 2-3mm. These were then placed in the beam and manipulated until an optimum signal was obtained. Solid phase spectra were obtained by streaming cold nitrogen gas over the sample with the temperature being monitored by a thermocouple. The solid phase spectra were again of the annealed sample.

Nuclear Magnetic Resonance spectra were run on a Bruker WP80 (^{1}H and ^{19}F, operating at 80.13 and 75.39 MHz respectively), a Bruker WH200 (^{29}Si and ^{13}C, operating at 39.76 and 50.32MHz respectively) and a Bruker WH360 (^{15}N operating at 36.50 MHz). Generally between 0.2 and 0.3 mmol of sample was used, and in each case the NMR Solvent used was d^{8}-toluene.

Only one mass spectrum was recorded, and this was obtained using an AEI MS902 spectrometer, using 70eV electron energy.

2.3 PREPARATION OF SAMPLES

In this section, details of the reactions carried out in the course of this work are given. The first part lists the preparation of all starting materials, with references to the original work where appropriate. The second Section deals with any new compounds which were prepared, and gives details of fractionation temperatures, and physical properties such as melting point and vapour pressure where appropriate. Finally, a brief description of other reactions which were attempted, but which were unsuccessful is given.

2.3.1 Germane

Germane was prepared by dropping a basic solution of germanium dioxide and KBH_4 into acetic acid.[24]

$$GeO_2 + KOH + KBH_4 \rightarrow GeH_4 + \text{etc.}$$

2.3.2 Germyl chloride

Germyl chloride was prepared by chlorination of germane with stannic chloride.[25]

$$GeH_4 + SnCl_4 \rightarrow GeH_3Cl + HCl + SnCl_2$$

2.3.3 Germyl bromide

Germyl bromide was synthesised by halide exchange of germyl chloride with HBr.[26]

$$GeH_3Cl + HBr \longrightarrow GeH_3Br + HCl$$

2.3.4 Germyl Fluoride

Germyl fluoride was prepared by passing germyl bromide through a column of freshly prepared PbF_2

$$2GeH_3Br + PbF_2 \rightarrow 2GeH_3F + PbBr_2$$

2.3.5 Germyl formate

Germyl formate was prepared by the exchange reaction of germyl bromide with tributyl tin formate. This reaction is analogous to method used to prepare silyl formate.[27]

$$GeH_3Br + Sn(But)_3\ OCOH \rightarrow GeH_3\ OCOH + Sn(But)_3Br$$

2.3.6 Hydrogen bromide

Hydrogen bromide was prepared by bromination of tetrahydronaphthalene with bromine.[28]

$$4Br_2 + C_{10}H_{12} \longrightarrow 4HBr + C_{10}H_8Br_4$$

2.3.7 Boron Trifluoride

Boron trifluoride was prepared by the reaction of ammonium fluoroborate and boric oxide in concentrated sulphuric acid.[29]

$$6NH_4BF_4 + B_2O_3 + 6H_2SO_4 \longrightarrow 8BF_3 + 6NH_4\ HSO_4 + 3H_2O$$

2.3.8 Isocyanic Acid

Isocyanic acid was prepared by subliming $(HNCO)_3$ in a nitrogen atmosphere at reduced pressure.[30]

$$(HNCO)_3 \longrightarrow 3\ HNCO$$

2.3.9 Hydrogen thiocyanate

Hydrogen thiocyanate was prepared by the reaction of potassium thiocyanate and potassium hydrogen sulphate.[31]

$$KNCS + KHSO_4 \longrightarrow K_2SO_4 + HNCS$$

2.3.10 Silver cyanate

Silver isocyanate was prepared by mixing solutions of silver nitrate and potassium cyanate and filtering off the product. This was then successively washed with water, ethanol and ether and finally dried on a vacuum line. The sample was kept in the dark to reduce decomposition.

$$AgNO_3 + KNCO \longrightarrow AgNCO + KNO_3$$

2.3.11 Silver thiocyanate

Silver isothiocyanate was prepared in the same manner as silver isocyanate, but starting with potassium thiocyanate.

2.3.12 Lead fluoride

Lead fluoride was prepared by mixing solutions of sodium fluoride and lead nitrate and filtering off the product. This was then successively washed with water and acetone and finally dried on a vacuum line.

$$Pb(NO_3)_2 + 2NaF \longrightarrow PbF_2 + 2NaNO_3$$

2.3.13 ^{15}N Labelled Dimethylamine

^{15}N labelled dimethylamine was prepared by heating ^{15}N labelled dimethylammonium chloride with calcium oxide under vacuum.

2.3.8 Isocyanic Acid

Isocyanic acid was prepared by subliming $(HNCO)_3$ in a nitrogen atmosphere at reduced pressure.[30]

$$(HNCO)_3 \longrightarrow 3\ HNCO$$

2.3.9 Hydrogen thiocyanate

Hydrogen thiocyanate was prepared by the reaction of potassium thiocyanate and potassium hydrogen sulphate.[31]

$$KNCS + KHSO_4 \longrightarrow K_2SO_4 + HNCS$$

2.3.10 Silver cyanate

Silver isocyanate was prepared by mixing solutions of silver nitrate and potassium cyanate and filtering off the product. This was then successively washed with water, ethanol and ether and finally dried on a vacuum line. The sample was kept in the dark to reduce decomposition.

$$AgNO_3 + KNCO \longrightarrow AgNCO + KNO_3$$

2.3.11 Silver thiocyanate

Silver isothiocyanate was prepared in the same manner as silver isocyanate, but starting with potassium thiocyanate.

2.3.12 Lead fluoride

Lead fluoride was prepared by mixing solutions of sodium fluoride and lead nitrate and filtering off the product. This was then successively washed with water and acetone and finally dried on a vacuum line.

$$Pb(NO_3)_2 + 2NaF \longrightarrow PbF_2 + 2NaNO_3$$

2.3.13 ^{15}N Labelled Dimethylamine

^{15}N labelled dimethylamine was prepared by heating ^{15}N labelled dimethylammonium chloride with calcium oxide under vacuum.

2.3.14 Tributyl tin formate

Tributyl tin formate was prepared by refluxing bis(tributyl tin) oxide and formic acid in toluene for approximately an hour. The water formed was azeotroped out of the solution, and then the toluene was removed by heating the solution in a water bath on a rotary evaporator. The product was finally dried by overnight pumping on a vacuum line.[32]

$$(But_3\ Sn)_2O + 2HOCOH \longrightarrow But_3SnOCOH + H_2O$$

2.3.15 Bis(N,N-dimethylamino) silane

This compound was first prepared by Aylett and Peterson[33] from SiH_2I_2 and $NHMe_2$. It has been prepared here by an analogous method using SiH_2Cl_2 as the starting material. Dimethylamine (4 fold excess) was streamed into dichlorosilane via a double-bulb apparatus at room temperature. This gave the desired product and any excess amine. Fractionation at 227K stops $SiH_2(NMe_2)_2$ and passes $NHMe_2$. The final yield was 85%.

$$SiH_2Cl_2 + 4NHMe_2 \longrightarrow SiH_2(NMe_2)_2 + 2NH_2Me_2Cl$$

2.3.16 Dibromosilane

Acid cleavage of Si-N bonds is well known and this type of reaction can be used to prepare dihalo-silanes. A four-fold excess of HBr was streamed into bis(N,N-dimethylamine)silane via a double-bulb system at room temperature. This gave SiH_2Br_2 and trace of $SiHBr_3$. Fractionation at 209K stops any $SiHBr_3$ and allows the product to pass. The yield was 70%.

$$SiH_2(NMe_2)_2 + 4HBr \longrightarrow SiH_2Br_2 + 2NH_2Me_2Br$$

2.3.17 Diiodosilane

Diiodosilane was prepared in the same manner as dibromosilane. The product was found to stop on fractionation at 227K.

$$SiH_2(NMe_2)_2 + 4HI \longrightarrow SiH_2I_2 + 2NH_2Me_2I$$

These reactions are the reverse of the synthetic routes to the formation of $SiH_2(NMe_2)_2$

2.3.18 Dichlorosilyl-N,N-dimethylamine

Dichlorosilyl-N,N-dimethylamine was prepared by spraying dimethylamine in a two-fold excess into trichlorosilane, at room temperature, via a double-bulb apparatus. Fractionation of the volatile products at 209K stopped $SiHCl_2(NMe_2)$ and passed either of the starting materials. The final yield was 95%. The product was a colourless liquid with a vapour pressure of 13mm at 271K. The melting point of dichlorosilyl-N,N-dimethylamine was found to be 165K.

$$SiHCl_3 + 2NHMe_2 \longrightarrow SiHCl_2(NMe_2) + NH_2Me_2Cl$$

2.3.19 Chlorosilyl-N,N-dimethylamine

This compound was first isolated by Emsley,[34] but the synthetic route gave a lowish yield and a mixture of other products. This work has yielded a better route to this interesting compound. The compound was prepared by mixing a 2-fold excess of dimethylamine with dichlorosilane at room temperature in a double-bulb apparatus. Subsequent fractionation of the volatile products at 227K stopped any $SiH_2(NMe_2)_2$ formed and passed the product. The yield obtained was 92%. $SiH_2Cl(NMe_2)$ is a colourless liquid with a vapour pressure of 46mm Hg at 273K. On cooling, crystallisation tends to occur and the compound was found to have the anomalously high melting point of 193 ± 1K. This suggested that intermolecular association was occurring in the solid and this was subsequently proven by X-ray crystallography.

$$SiH_2Cl_2 + 2NHMe_2 \longrightarrow SiH_2Cl(NMe_2) + NH_2Me_2Cl$$

2.3.20 ^{15}N Labelled Chlorosilyl-N,N-dimethylamine

$$SiH_2Cl_2 + 2^{15}NHMe_2 \longrightarrow SiH_2Cl(^{15}NMe_2) + {}^{15}NH_2Me_2Cl$$

2.3.21 Bromosilyl-N,N-dimethylamine

Bromosilyl-N,N-dimethylamine was prepared by cleaving $SiH_2(NMe_2)_2$ with a two-fold excess of hydrogen bromide at room temperature in a double-bulb apparatus. Fractionation of the volatile products at 209K stops $SiH_2Br(NMe_2)$ and passes any unwanted dibromosilane. The final yield obtained was 89%.$SiH_2Br(NMe_2)$ has a vapour pressure of 16mmHg a 273K and under normal conditions it is found to sublime rather than melt. Like SiH_2ClNMe_2, SiH_2BrNMe_2 tends to crystallise easily.

$$SiH_2(NMe_2)_2 + 2HBr \longrightarrow SiH_2Br(NMe_2) + NH_2Me_2Br$$

2.3.22 Iodosilyl-N,N-dimethylamine

Iodosilyl-N,N-dimethylamine, like SiH_2ClNMe_2 is briefly mentioned by Emsley,[34] but as with the chloro compound the synthetic route is poor and no information is given about the compound. SiH_2INMe_2 was prepared here in an analogous manner to SiH_2BrNMe_2 but using HI instead of HBr. Fractionation of the volatile products proved difficult since both SiH_2INMe_2 and $SiH_2(NMe_2)_2$ stopped at 240K. The % yield for the reaction was not determined, because of the very low volatility of the compound (2mm at 289K). SiH_2INMe_2 like SiH_2BrNMe_2 tends to crystallise easily and it too sublimes under vacuum.

$$SiH_2(NMe_2)_2 + 2HI \longrightarrow SiH_2INMe_2 + NH_2Me_2I$$

2.3.23 Fluorosilyl-N,N-dimethylamine

Attempts were made to prepare, fluorosilyl-N,N-dimethylamine by three different reactions which are listed below. In each case yields were low and the compound was found to be thermally unstable, disproportionating to give SiH_2F_2, $SiHF_2(NMe_2)$ and other related compounds.

Reaction of SiH_2BrNMe_2 and SbF_3

SiH_2BrNMe_2 was passed through a thoroughly dried column of alternate bands of antimony trifluoride/sand mixture (1:1) and glass wool. The volatile products were fractionated at 153K and yielded $\simeq$ 20% SiH_2FNMe_2 (stopped) and $\simeq$ 30% SiH_2F_2 (passed). A trace amount of SiF_4 was also detected. The product mixture suggests that as well as exchange of -Br for - F, acidic attack by SbF_3 on the amine group was also occurring along with some disproportionation.

Reaction of SiH_2ClNMe_2 and GeH_3F

A 1:1 mixture of GeH_3F and SiH_2ClNMe_2 were co-condensed in a tap ampoule and allowed to warm to room temperature. White 'smoke' was given off, presumably by formation of an ammonium salt. The volatile products yielded a complex mixture; a trace of SiH_2FNMe_2, SiH_2F_2, SiF_4, GeH_3Cl, GeH_4 and some unreacted SiH_2ClNMe_2. Again disproportionation was obviously occurring and the reaction was abandoned.

Reaction of $SiH_2(NMe_2)_2$ and BF_3

Sujishi and Witz[35] and Ebsworth and Emeleus[36] reported that BF_3 forms 1:1 donor-adducts with a variety of silylamines at low temperature. These were found to disproportionate at higher temperatures cleaving the Si-N bond and forming a new Si-F bond. It was hoped, therefore, that an analogous reaction could be used to prepare $SiH_2F(NMe_2)$ by specifically cleaving one Si-N bond in $SiH_2(NMe_2)_2$. BF_3 and $SiH_2(NMe_2)$ were co-condensed in a 1:1 ratio in the tap ampoule and the mixture was left to stand at 195K for 45 minutes. The mixture was then warmed to room temperature and subsequently fractionated. SiH_2FNMe_2 ($\simeq$20%) was found to stop at 153K with SiH_2F_2 ($\simeq$30%) passing at this temperature. The other product of the reaction, BF_2NMe_2, was found to stop at 195K. It

It appears then, that this reaction is of limited value with some disproportionation again occurring.

2.3.24 Diformatosilane

Diformatosilane was prepared by condensing either dibromosilane or dichlorosilane into a tap ampoule containing excess tributyl tin formate at 77K. The mixture was warmed to room temperature with vigorous shaking, whereupon a significant decrease in the viscosity of the tin compound was observed. The volatile products were then fractionated at 227K where $SiH_2(OCHO)_2$ stopped and any SiH_3OCHO or SiH_4 passed, and at 250K where $SiH_2(OCHO)_2$ passed. The yields obtained were 72% using SiH_2Br_2 and 61% using SiH_2Cl_2. Diformat osilane is a colourless liquid, with a vapour pressure of 1.4mm Hg at 271.7K. On cooling it tends to form a glassy solid.

$$SiH_2X_2 + 2Sn\ But_3OCHO \longrightarrow SiH_2(OCHO)_2 + 2Sn\ But_3X$$

Where X = Cl or Br.

2.3.25 Dipseudohalosilanes

$$SiH_2X_2 + 2AgY \longrightarrow \text{Products where } X = Br \text{ or } Cl$$

$$Y = -NCO \text{ or } -NCS$$

Reactions of the type shown above were carried out in an attempt to prepare dipseudohalosilanes. Reactions of this type generally using SiH_3Br, rather than SiH_3I, and the appropriate silver pseudohalide[37,38] give the desired silyl pseudohalide compound. It was found, however, that this type of reaction was unsuccessful for preparing bis-substituted compounds with disproportionation reaction being favoured. SiH_2Br_2 and AgNCS tended to react to give SiH_3NCS, and SiH_2Br_2 and AgNCO gave $SiH(NCO)_3$ and a trace amount of $SiH_2(NCO)_2$.

2.3.26 Reactions of Bis-N,N-dimethylamine silane with Acids, HX

(Where X = -CN, -NCO, -NCS and $-O_2CCF_3$)

Reactions between $SiH_2(NMe_2)_2$ and HCN, HNCO and HNCS of the general type:

$$SiH_2(NMe_2)_2 + 4\ HX \longrightarrow$$

were carried out in an attempt to cleave both Si-N bonds in the starting material and to form the appropriate dipseudohalosilane. In all cases some white ammonium salt was formed. In the case of HNCS, SiH_4 and SiH_3NCS were the only volatile silicon containing species formed, but some $NHMe_2$ was also produced. HNCO, however, gave mostly SiH_4, SiH_3NCO, $NHMe_2$ and HNCO, along with traces of $SiH_2(NCO)_2$ and $SiH(NCO)_3$. These reactions indicate that disproportionation has occurred in both cases and that $SiH_2(NCO)_2$ must be more stable than "$SiH_2(NCS)_2$" since it has not been detected. The formation of $NHMe_2$, suggests that HNCO and HNCS are not strong enough acids to form the stable ammonium salts which are the thermodynamic driving force behind acid cleavage reactions of this type.

Reaction of $SiH_2(NMe_2)_2$ with HCN gave only starting materials, although some white salt was initially formed, but this appeared to diminish with time. This suggests that after initial ammonium salt formation, the salt decomposed and allowed re-attack on any 'product' by $NHMe_2$ to give the starting material.

Reaction of $SiH_2(NMe_2)_2$ with CF_3CO_2H, in the stoichiometric ratio 1:2 respectively, in an attempt to prepare the 'mixed' compound $SiH_2(NMe_2)(CO_2CF_3)$, failed. The only detectable volatile products were SiH_4, $SiH_3(CO_2CF_3)$ and CF_3CO_2H. Again disproportionation reactions appear to have occurred.

CHAPTER 3

THE GAS PHASE STRUCTURES OF $SiH_2X(NMe_2)$ WHERE X = Cl,Br & I AND $SiHCl_2(NMe_2)$

3.1 INTRODUCTION

The structures of silyl-amines have merited a considerable amount of work and research effort, after it was initially found by Hedberg[39] that $(SiH_3)_3N$ had a planar structure in the gas-phase. This result, together with experimental findings that this amine, and all other silyl-amines, tend to be only weak bases, gave rise to the suggestion that these features were a consequence of (p $\longrightarrow$ d) π back-bonding from the lone-pair of electrons on nitrogen into the appropriate vacant d-orbitals on silicon.

Numerous other structural studies, generally by gas-phase electron diffraction, have subsequently been undertaken, and these have all tended to reinforce the idea of back-bonding from N to Si. These studies have been divided amongst the three most common types of silyl-amines; those containing a central nitrogen atom surrounded by either one, two or three substituents. A lot of work has been carried out on di- and trisilylamines, since both of these groups of compounds are generally found to have planar structures, e.g. $N(SiH_3)_3$[39,40,41] & $N(SiH_2Me)_3$[42] and $NMe(SiH_3)_2$,[43] $NMe(SiH_2Me)_2$[44] & $NMe(SiHMe_2)_2$.[44] An equally large amount of work has also been carried out on mono-substituted silyl-amines, particularly dimethyl silyl-amines, e.g. $NMe_2(SiH_3)$,[45] $NMe_2(SiH_2Me)$,[46] $NMe_2(SiHMe_2)$[46] and $NMe_2(SiMe^3)$.[47] These mono-substituted amines are generally found to have slightly non-planar structures, but these are very different to the strictly pyramidal trialkyl amines.

Most of the attention in these structural investigations is centred on the extent or lack of planarity, as determined by the sum of the angles around nitrogen, and the relatively short Si-N bond length(s). In general, the greater the number of silyl groups around nitrogen, the more planar the structure and the longer the Si-N bond length(s). These observations can be rationalised well by (p $\longrightarrow$ d) π back-bonding considerations, although low frequency, large amplitude out of plane vibrations at nitrogen have to be considered, since an apparently non-planar structure can be explained by these motions in terms of 'shrinkage'. The structure determinations on mono-substituted silyl-amines have all involved silyl groups containing either hydrogen/methyl substituents, or three common halogen atoms, no examples where mixed hydrogen/halide substituents are present, are known. The gas-phase structures of $SiH_2X(NMe_2)$ (where X = Cl,Br & I) are therefore of interest, since the general effects of the halide on the structure can be observed directly, as can any more subtle trends across the series of halides.

3.2 MOLECULAR MODEL FOR $SiH_2X(NMe_2)$ (WHERE X = Cl, Br & I)

The molecular model used in the structure refinements of the three halosilyl-N,N-dimethylamines assumed local C_3v symmetry in the two methyl groups. With this assumption, the molecule could then be described by five bond lengths, six bond angles and two torsion angles. The bond lengths were Si-N, C-N, C-H, Si-X and Si-H; the angles were <CNC, <NCH, <XSiN, <HSiH, SiH_2 tilt and NMe_2 dip; and the two torsion angles were along the Si-N bond and along the two C-N bonds (these were constrained to be equal). The molecule was initially assumed to have C_s symmetry with its plane through the XSiN plane and bisecting the CNC angle, the coordination at nitrogen being planar. The NMe_2 dip was designated positive if the methyl

groups became trans to X with respect to the Si-N bond, and the SiH_2 tilt was considered positive if the two H atoms moved further from X and towards N. The Si-N torsion angle was deemed to be positive if the SiH_2X group rotated in a clockwise direction viewed from Si to N, and the C-N torsion was designated positive if the methyl groups rotated clockwise viewed from C to N. The two SiNC angles were calculated as dependent parameters from the Si-N and C-N distances. An additional parameter, the SiC_2 wag, was introduced into the model for SiH_2INMe_2 which allowed the two SiNC angles to be different, but this parameter was redundant, since it was found that the SiNC angles were equal.

The nozzle to plate distances and operating wavelengths are given in Table 3.1 for the three compounds.

TABLE 3.1

WEIGHTING FUNCTIONS, CORRELATION PARAMETERS AND SCALE FACTORS

Compound	Camera Distance(mm)	ΔS	Smin	S_1	S_2	Smax	P/h	Scale Factor	Wavelength /pm
				nm^{-1}					
SiH_2ClNMe_2	285.4548	2	20	40	120	146	0.2452	0.636(8)	5.708
SiH_2ClNMe_2	128.3699	4	60	80	300	340	-0.1735	0.701(13)	5.709
SiH_2BrNMe_2	285.3000	2	20	40	120	144	0.4703	0.793(10)	5.708
SiH_2BrNMe_2	128.3599	4	60	80	300	344	-0.1487	0.716(26)	5.704
SiH_2INMe_2	285.3201	2	20	40	124	140	0.4005	0.966(19)	5.677
SiH_2INMe_2	286.0100	2	20	40	124	140	0.4485	0.949(21)	5.676
SiH_2INMe_2	128.2599	4	80	100	240	280	-0.3434	1.016(59)	5.677

3.3 REFINEMENT OF THE $SiH_2Cl(NMe_2)$ STRUCTURE

The radial distribution curve for $SiH_2Cl(NMe_2)$ consists principally of peaks at 110pm, 146pm, 169pm and 207pm for the bonded

distances C-H, C-N and Si-H, Si-N and Si-Cl respectively. Of these parameters, all refined well except Si-H which did refine, but with a large esd. This was undoubtedly due to correlation with the C-N distance which was in close proximity.

The other major peaks in the radial distribution curve occurred at 274pm, 314pm and 378/396pm, these were due to the Si···C, N···Cl and the two C···Cl non-bonded distances respectively. The C···C peak appears as a shoulder at 247pm. The C···C distance along with the Si···C distances define the CNC and SiNC angles respectively, and hence the geometry at nitrogen. The CNC angle refined well and the calculated SiNC angles both had small e.s.d's. The NCH and, particularly, the ClSiN angles, also refined well. The dip angle which determines the SiNC angles refined to the value of -17.2°, with a small e.s.d. of 1.1°. The HSiH angle did not refine well and was subsequently fixed at 111°, the SiH_2 tilt was fixed at -5° after investigation by variation of the angle in a series of refinements, -5° giving the minimum R-factor. The Si-N torsion refined to 9.7° but with a large e.s.d. of $\pm$5.1°, this results in the two distinct C Cl peaks. The C-N torsion was fixed at 0°, with the two methyl groups eclipsing each other. Again this was after investigation by an R-factor loop.

The bonded amplitudes of vibration all refined well, although U(C-H) was slightly higher than expected at 8.1pm. Of the non-bonded amplitudes, the Si···C, N···Cl and the two C···Cl amplitudes (constrained to be equal) refined best. The other amplitudes were all either fixed at reasonable values, refined and then fixed, or constrained to refining amplitudes as follows:-

U2 =/

U2 = 0.45 * U4

U6 = 0.43 * U12 U13

U5 = 0.43 * U16

U25 = 1.0 * U26 U27 U28 U29 U30

U10 = 1.0 * U7

in the final refinement. The final molecular parameters are listed in Table 3.2. The least squares correlation matrix is given in Table 3.3. Not surprisingly, this shows strong correlation between the Si-H and C-N distances which are close to each other in the radial distribution curve, and also between the Si-N torsion and the C···Cl amplitudes which are directly related to each other. These phenomena obviously make refinement of the Si-H bond length, and the Si-N torsion angle difficult. The NCH and CNC angles also show some correlation, as do the Si-Cl bond length and NCH angle. The final R-factor was R_G = 0.084 and R_D = 0.081. This indicates a good fit between the theoretical and experimentally determined intensity curves (Figure 3.1). The radial distribution curve is shown in Figure 3.2 and the difference curve indicates that data is well fitted in all regions. Pictures of the molecule are given in Figure 3.3.

3.4 REFINEMENT OF $SiH_2Br(NMe_2)$ STRUCTURE

The radial distribution curve obtained for SiH_2BrNMe_2 is, as would be expected, quite similar to that of SiH_2ClNMe_2 although it involves longer distances because of the presence of the Br atom.

The bonded atoms gave peaks at 115pm, 147pm, 168pm and 225pm for the C-H, C-N and Si-H, Si-N and Si-Br bonds respectively. Although the C-H and Si-N peaks appeared as shoulders on either side of the C-N/Si-H peak, both refined reasonably well. Attempts to refine the Si-H bond length however, proved unsuccessful, and this

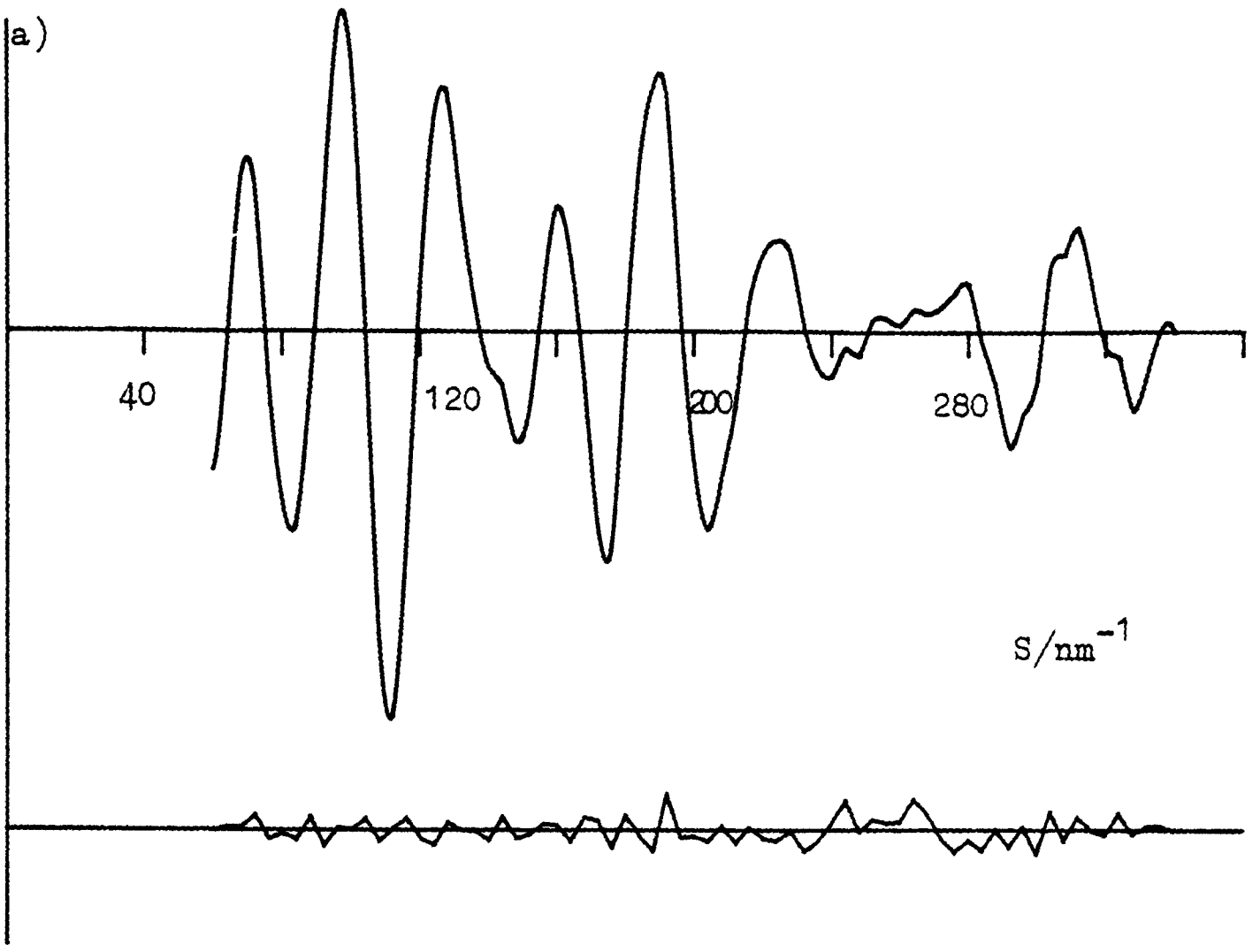

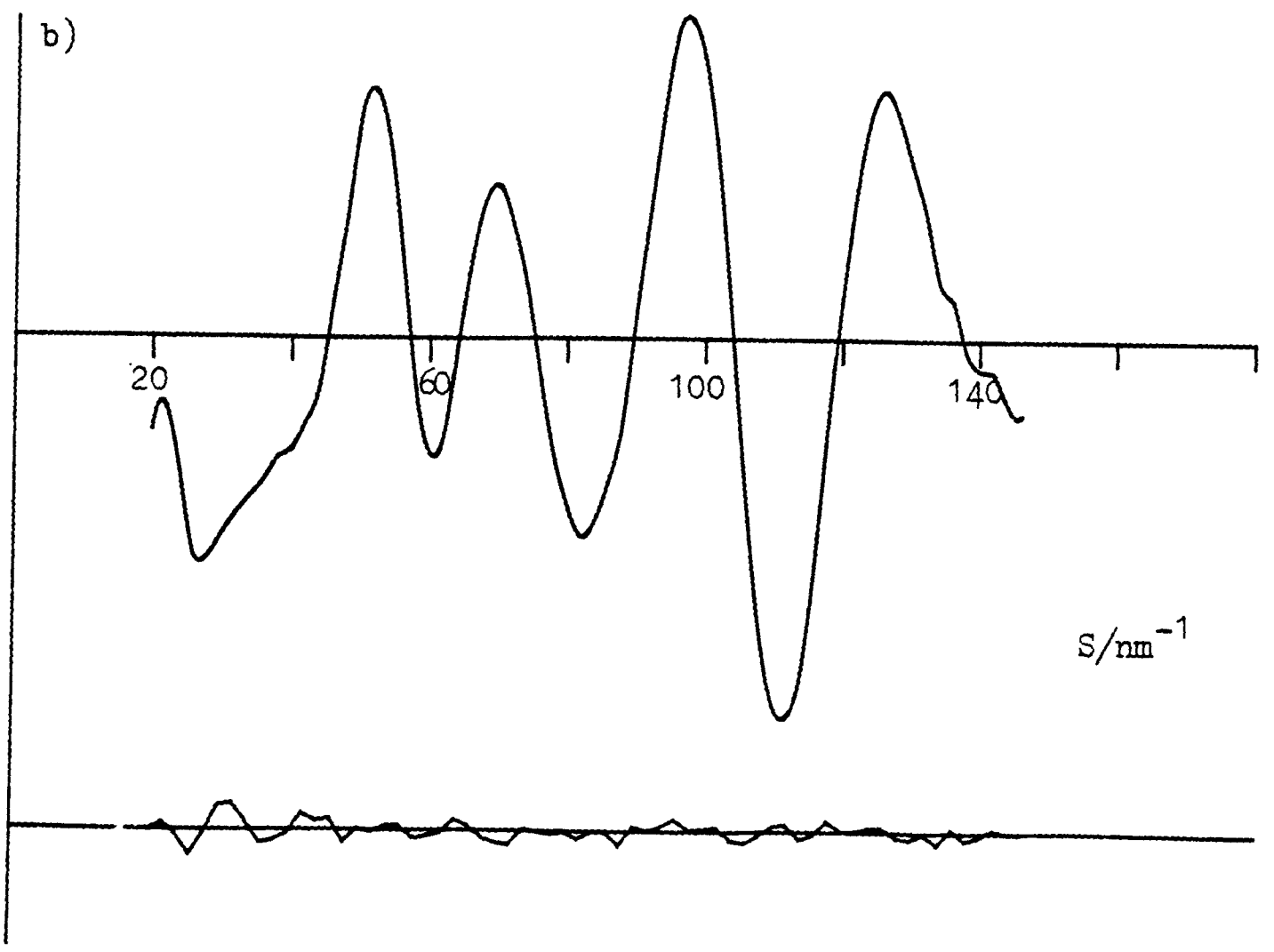

Observed and final weighted difference molecular scattering intensities at camera distances of a) 128mm and b) 285mm.

Figure 3.2 Observed and final difference radial distribution curves for SiH_2ClNMe_2.

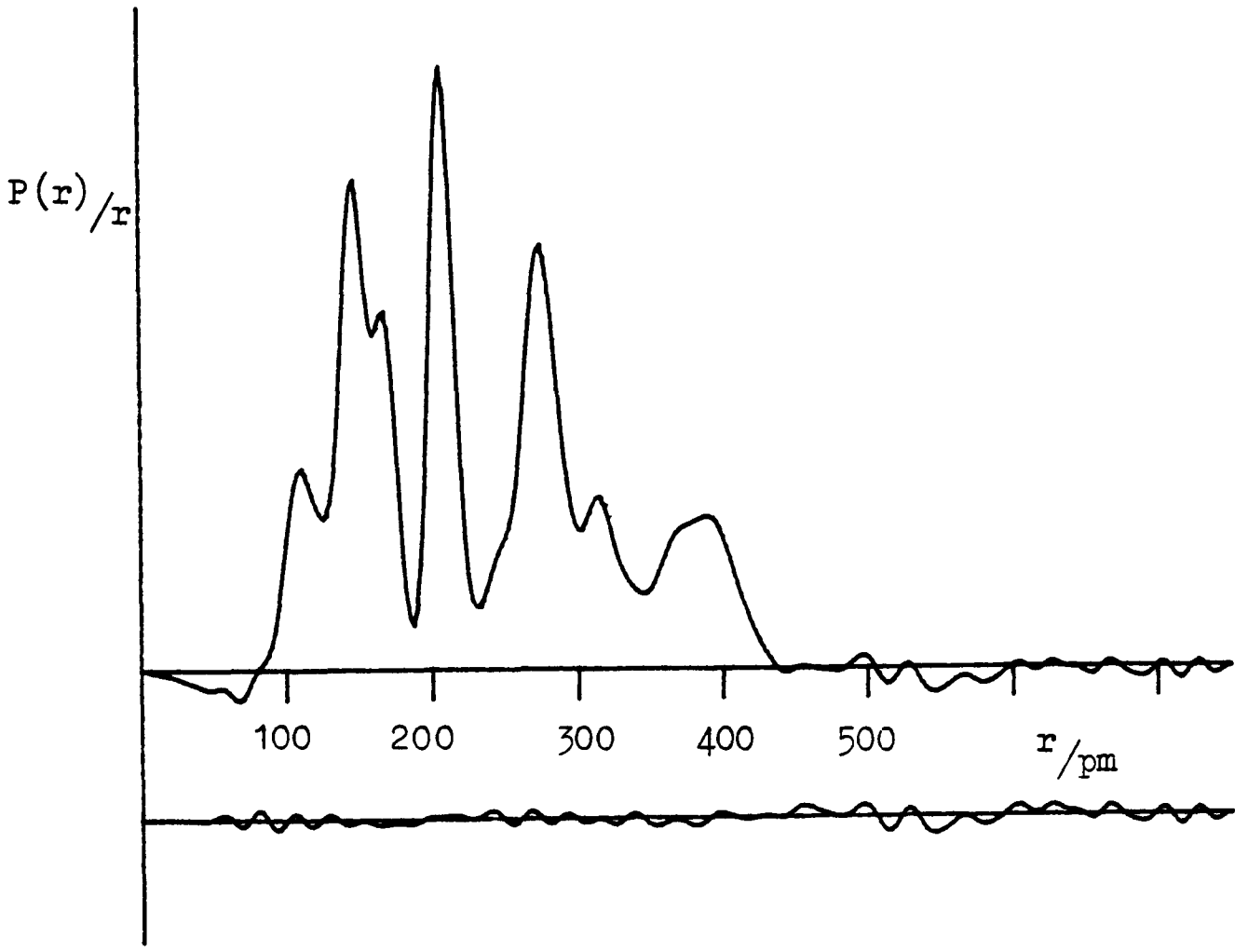

Before Fourier inversion the data were multiplied by $S.\ \exp(-0.00002\ S^2/(Z_{Si}-f_{Si})(Z_{Cl}-f_{Cl}))$.

Figure 3.3 SiH_2ClNMe_2

a)

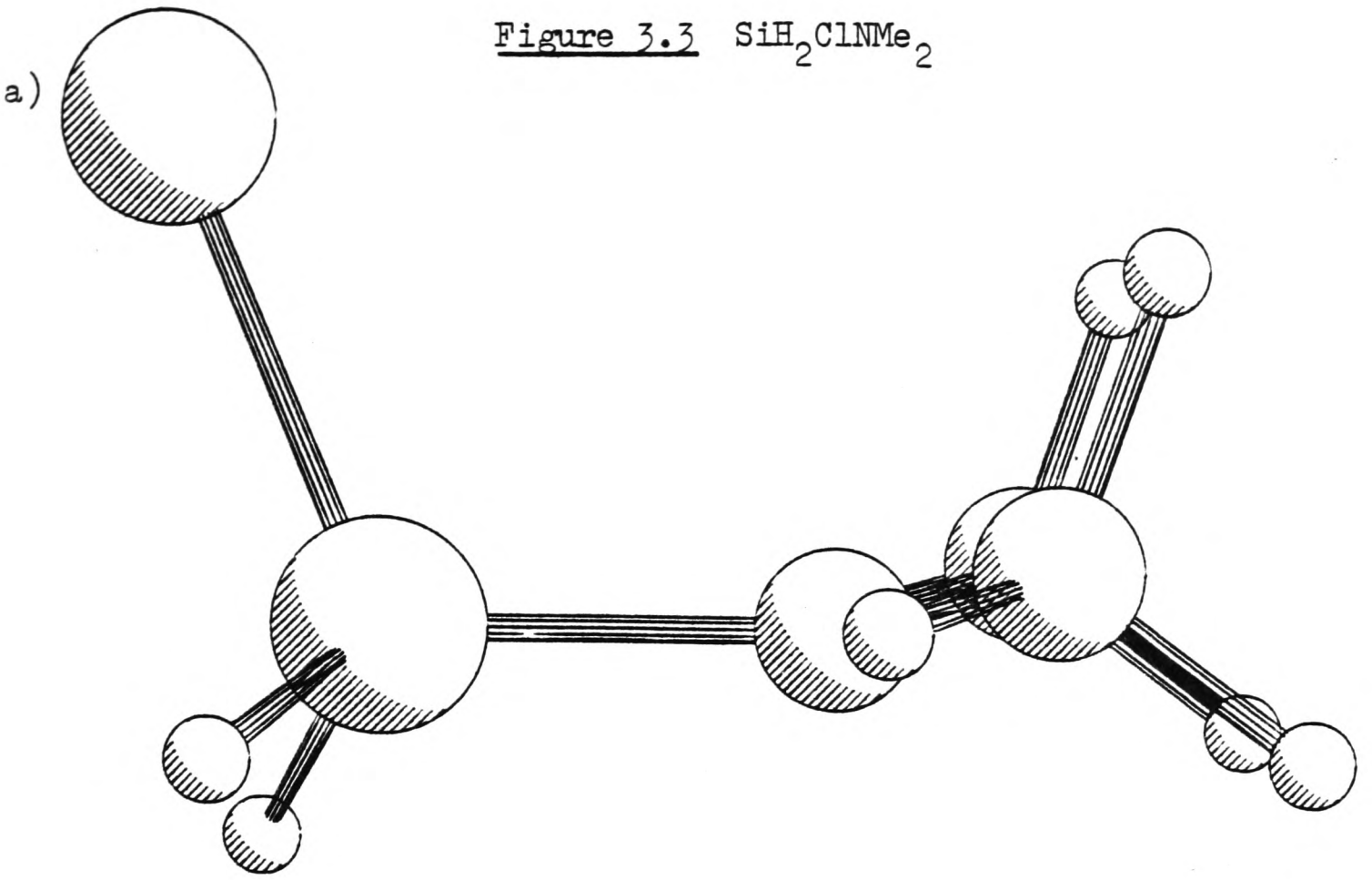

b)

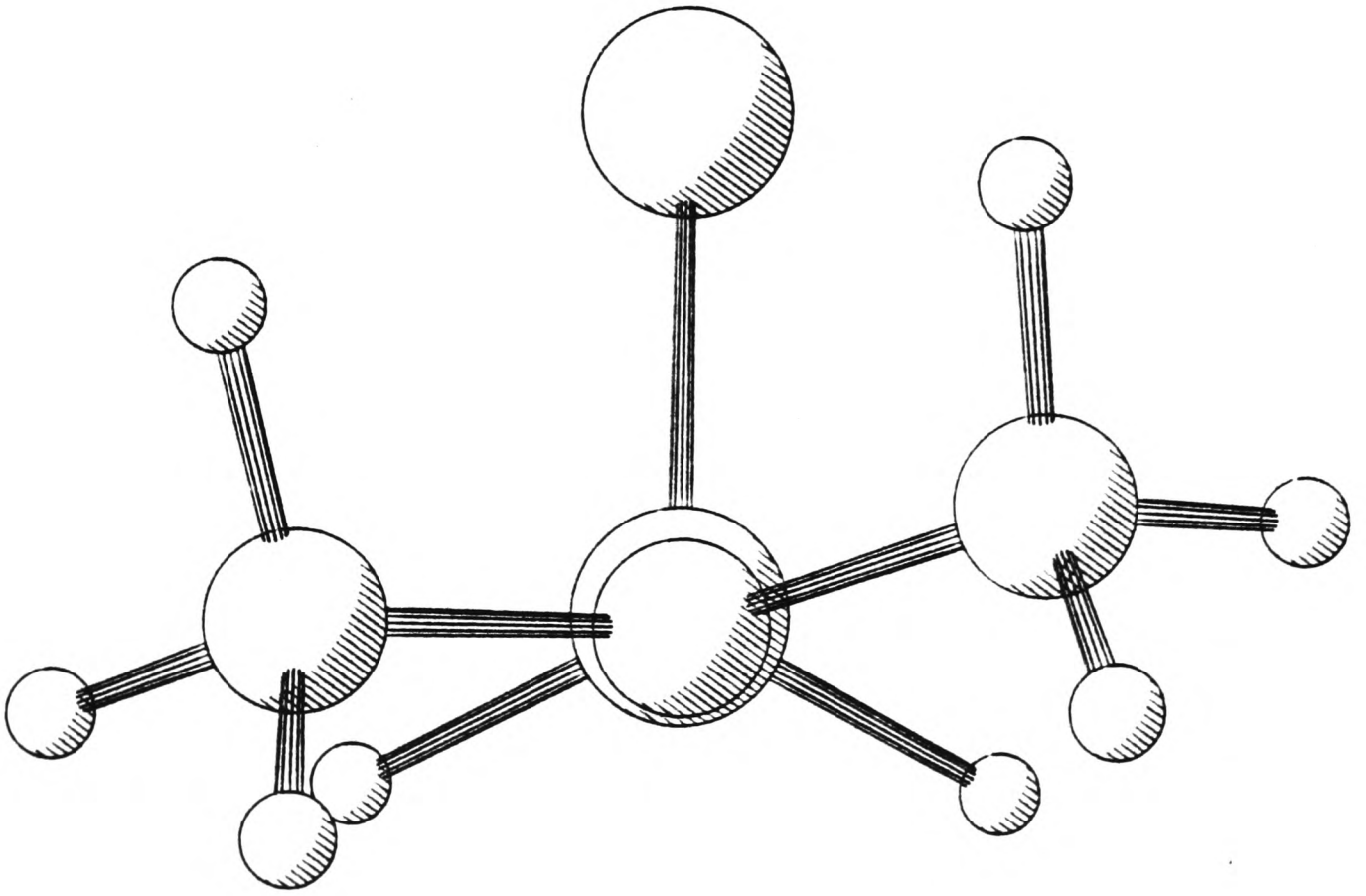

Molecular structure of SiH_2ClNMe_2

a) General view

b) Viewed along the bond from N to Si.

parameter was subsequently fixed at 150pm throughout the refinement. The other major peaks in the radial distribution curve resulted from the Si···C, Br···N and the two Br···C non-bonded distances. The angles which control the geometry around nitrogen are the dip and CNC angles. These were both refined with the CNC angle at 108.6° being close to the value expected for a tetrahedral atom. The other angles refined were the heavy atom BrSiN angle and the NCH angle, although the NCH angle was not particularly well determined with a value of 105.8° ± 2.0. As was the case for SiH_2ClNMe_2, the SiH_2 angle did not refine well and was consequently fixed at 108°, and the SiH_2 tilt angle had to be determined by an R-factor loop. The two remaining torsion angles were both refined; the Si-N torsion being -14.0°(9) and the C-N torsion having a value of 15.3°, but with a large e.s.d. of ±6.2°. This torsion has the two methyl groups in a staggered conformation.

The bonded amplitudes of vibration all refined well, with the exception of Si-H which was fixed at the value of 8.8pm. Of the non-bonded amplitudes, all of those not involving H atoms were refined, except C···C which was fixed at 9.0pm. The two C···Br amplitudes were constrained to be equal. The only amplitude involving a non-bonded H atom to be refined was Br···H (u 18), since this contributed significantly to the total molecular scattering. All other amplitudes of vibration involving H atoms were fixed at reasonable values for a compound of this type. The least-squares correlation matrix is givn in Table 3.4 and shows some correlation the CNC angle and the dip angle, and also the BrSiN angle and dip angle. The parameter list is given in Table 3.5 and the final R-factor was R_G = 0.153 and R_D = 0.13. The molecular intensity curves and the radial distribution curve are given in Figures 3.4 and

Figure 3.4 SiH_2BrNMe_2

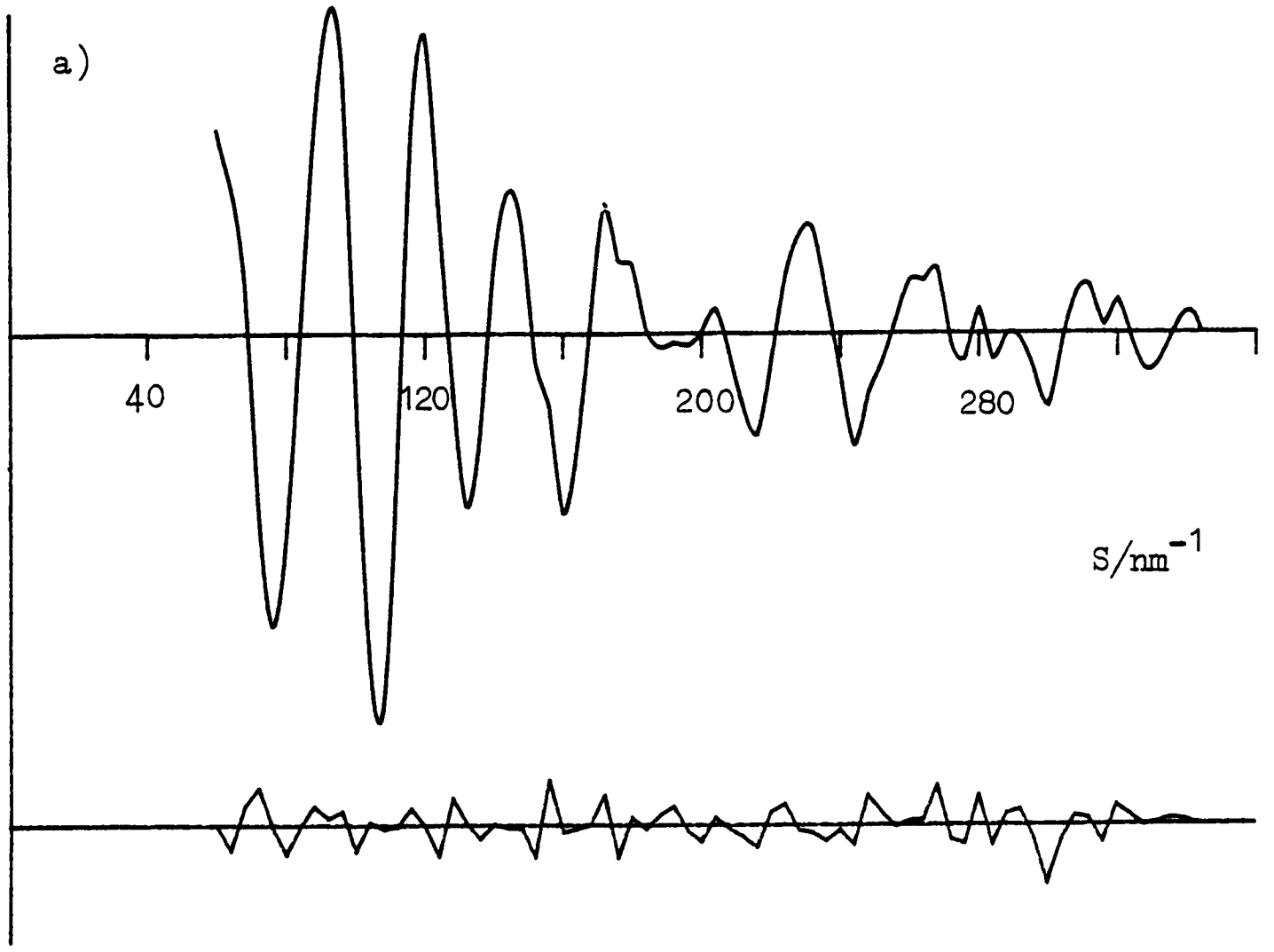

Observed and final weighted difference molecular scattering intensities at camera distances of a) 128mm and b) 285mm.

Figure 3.5 Observed and final difference radial distribution curves for SiH_2BrNMe_2.

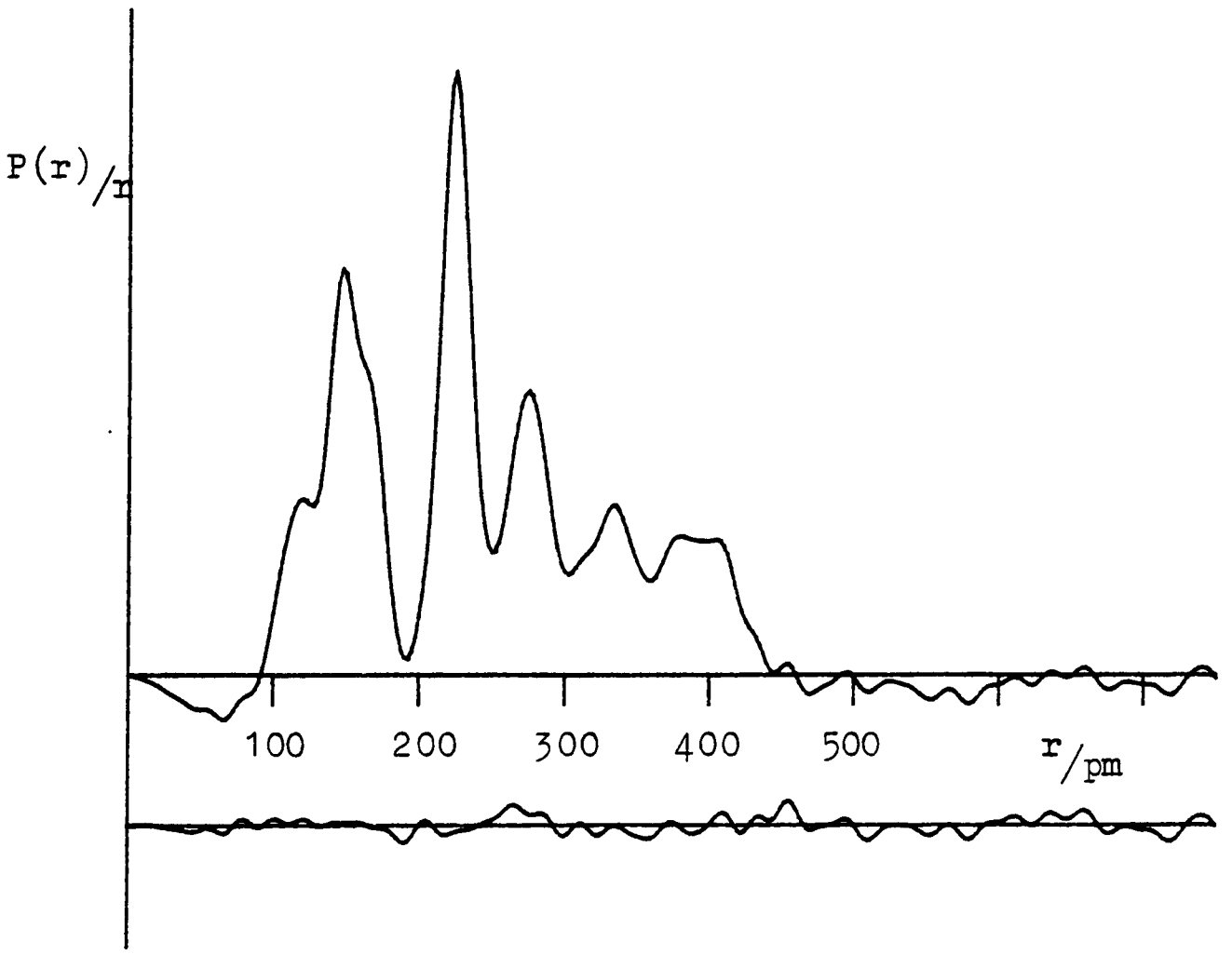

Before Fourier inversion the data were multiplied by $S.\exp(-0.00002\ S^2/(Z_{Si}-f_{Si})(Z_{Br}-f_{Br}))$.

Figure 3.6 SiH_2BrNMe_2

a)

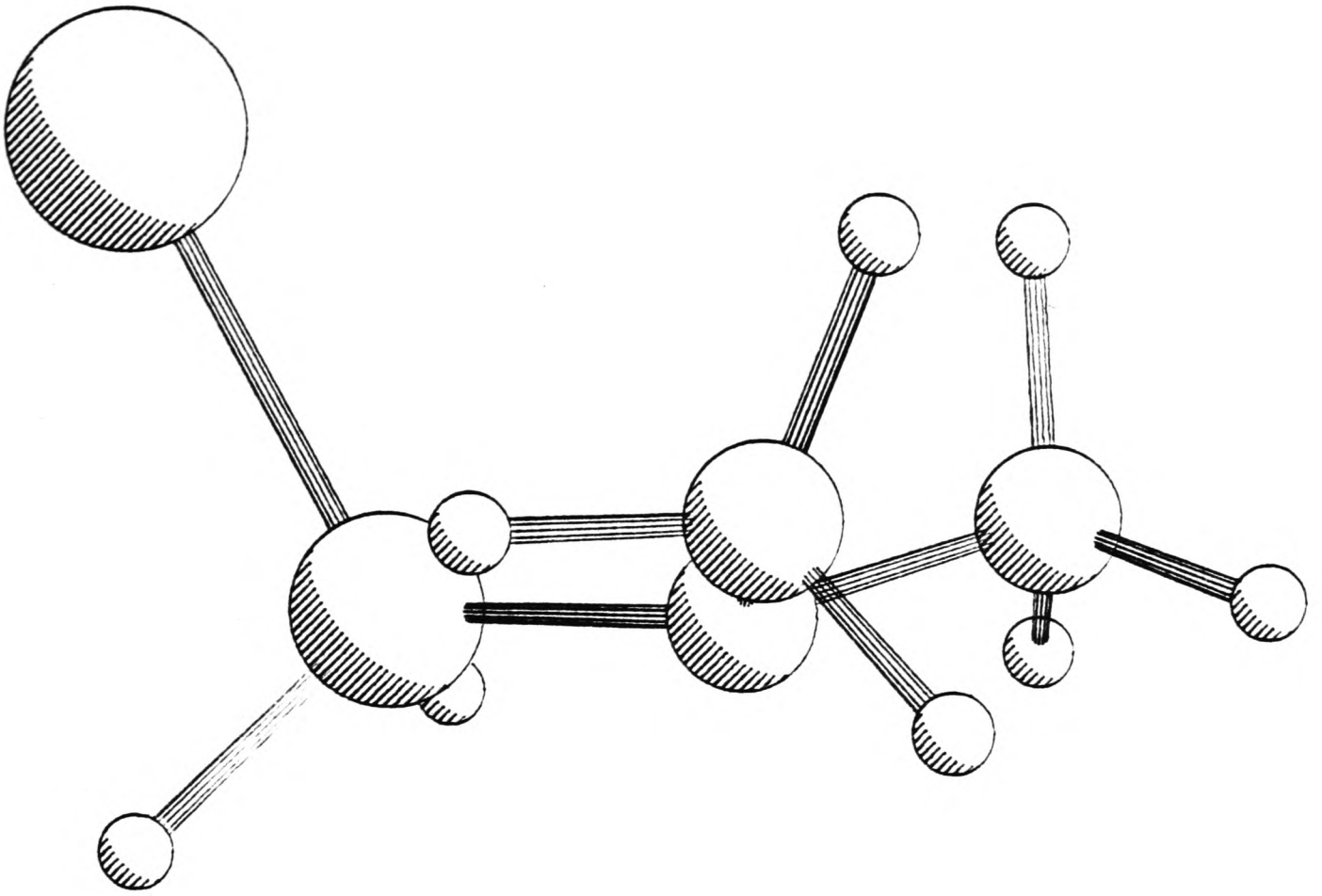

b)

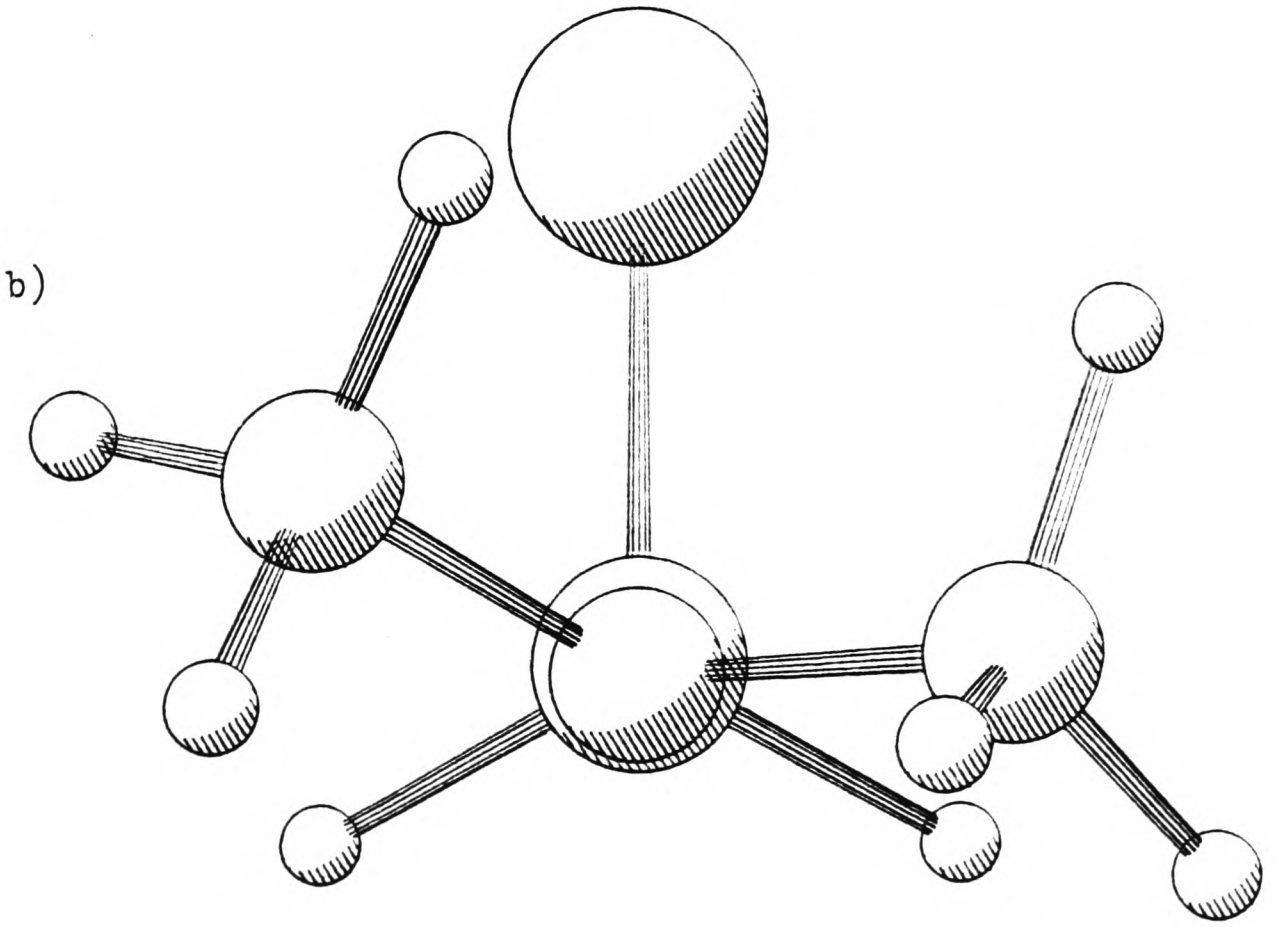

Molecular Structure of SiH_2BrNMe_2

a) General view

b) Viewed along the bond from N to Si.

3.5 respectively. Pictures of the molecule are given in Figure 3.6. From the difference intensity curves it can be seen that the fit between the calculated and experimental curves is not particularly good. The difference radial distribution curve, however, shows no obvious signs of an impurity, so this suggests a problem in the experiment. The plates for this compound were slightly blotchy and this may have been due to reaction between the compound and the photographic emulsion on the plates. This blotchiness will obviously affect the traced optical densities of the plates used in this structure determination.

3.5 REFINEMENT OF THE $SiH_2I(NMe_2)$ STRUCTURE

Recording good quality electron diffraction plates of $SiH_2I(NMe_2)$ proved difficult and, as with $SiH_2Br(NMe_2)$, this seemed to be caused by reaction of the compound with the emulsion on the plates. The short distance plates initially recorded were particularly blotchy and leaving these in the camera overnight on a subsequent run, yielded even poorer quality plates. The plates eventually used in the structure determination contained data from two long and one short distance set of exposures, and it eventually proved necessary to truncate the short distance data set.

The radial distribution curve for $SiH_2I(NMe_2)$ was very similar to that obtained for the chloro and bromosilyl—dimethylamines, although distances involving the halide atom were all longer than the analogous distances in the chloro and bromo compounds. The Si-N, C-N and C-H bond lengths were all refined, with the C-H bond length of 113.1(3)pm being surprisingly well determined and the Si-N bond length appearing quite short at 167.0(2)pm. The Si-I bond length also refined and since this peak overlapped the C···C non bonded distance, the amplitudes were constrained to be equal with the Si-I

amplitude being refined. The other major peaks in the radial distribution curve were all due to non-bonded distances, the largest of which were due to the Si···C, I···C and I···N distances. Unlike the chloro and bromo compounds, the iodide did not yield two distinct X···C peaks (where X = I) peaks hence the Si-N torsion angle was fixed at zero after investigation by a R-factor loop. The Si···C distances showed that like the chloro and bromo compounds, SiH_2INMe_2 was non-planar and these gave a dip angle which refined to the value of -20.8(11)°. The I···N peak determined the ISiN angle and this parameter refined well as did the NCH angle, which gave an N··H non-bonded distance which appeared as a small shoulder on the large Si-I peak. Of the other angles, the methyl torsion (T(CN)) and SiH_2 tilt were both fixed after the parameters had been varied by an R-factor loop, and the HSiH angle was fixed, since it did not refine successfully.

The amplitudes of vibration of the bonded atoms all refined well within the exception u(Si-H), which was fixed at 8.8pm. The non-bonded amplitudes involving heavy atoms were refined, and it proved possible to refine the long distance I··H amplitudes as a group. The following amplitude constraints were applied during refinement:

U5 = 1.00 * U11

U6 = 1.00 * U7

U8 = 1.00 * U9

U22 = 1.00 * U20 21 23 24 25

The least squares correlation matrix is given in Table 3.6 and it shows significant correlation between r(Si-I) and the CNC angle, since the C··C non-bonded distance gives a small peak which overlaps the large Si-I bonded distance peak, and also between the CNC angle

Figure 3.7 SiH_2INMe_2

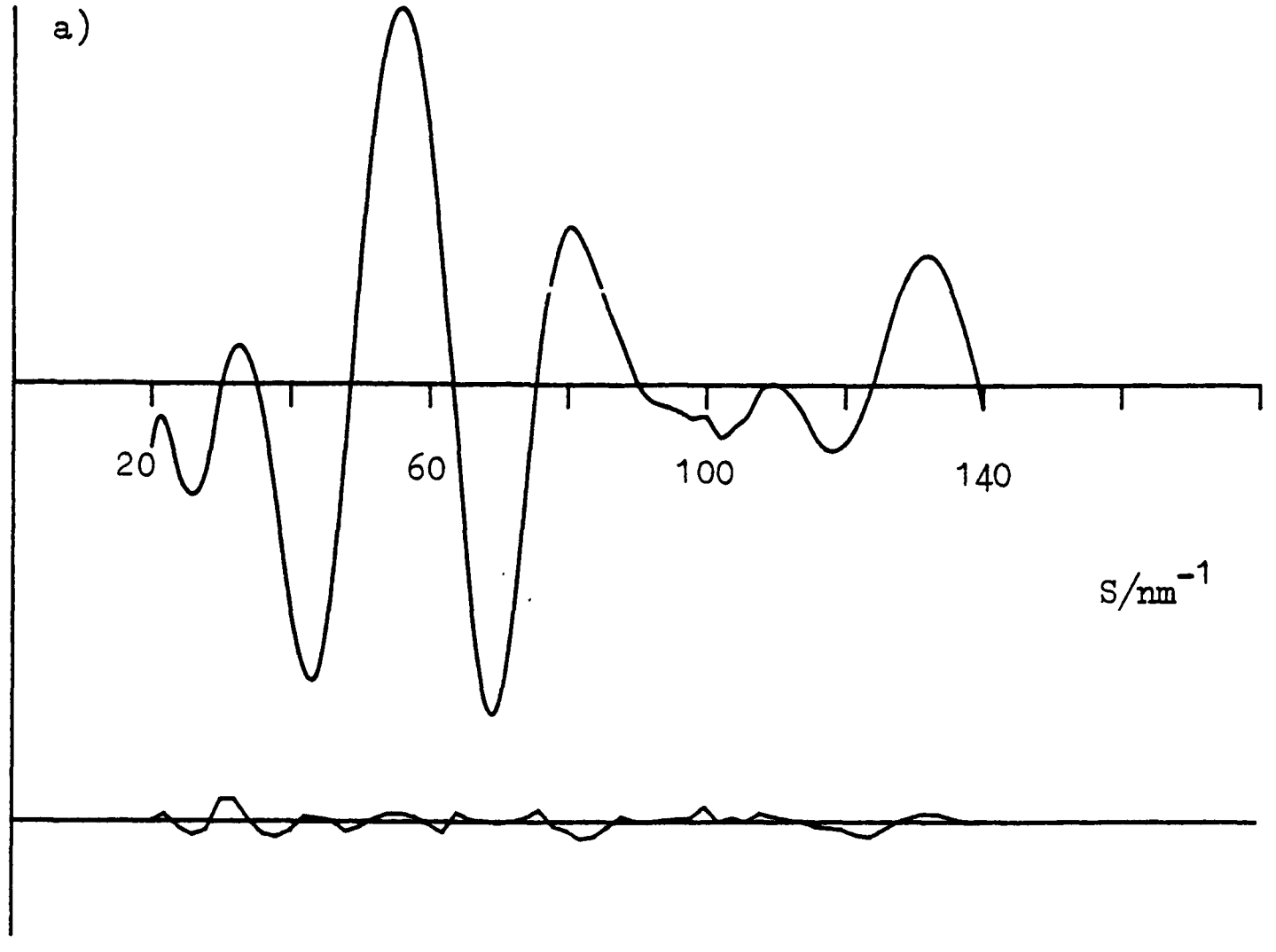

Observed and final weighted difference molecular scattering intensities and camera distances of a) 285mm and b) 286mm.

for SiH_2INMe_2. Before Fourier inversion the data were multiplied by:

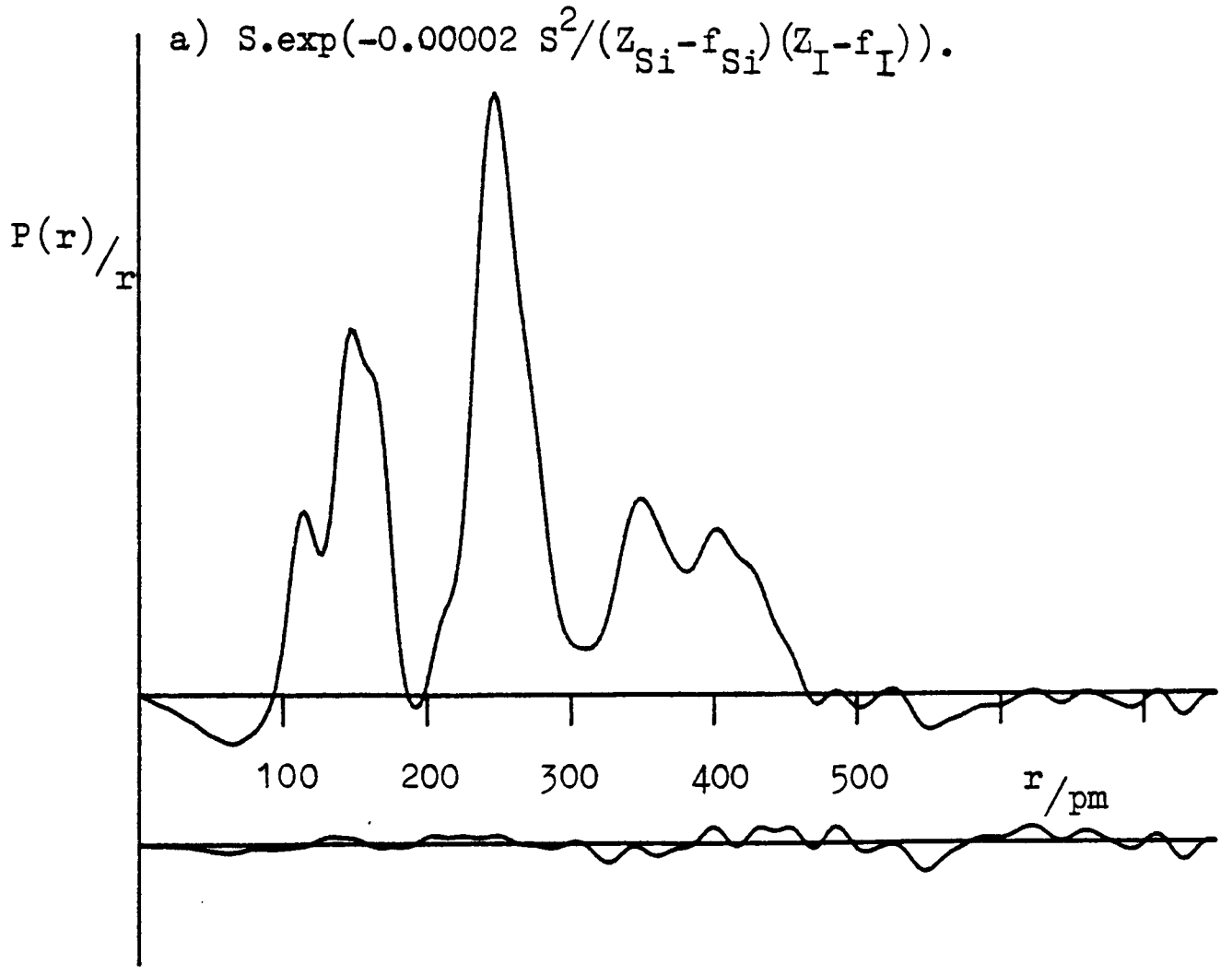

b) Observed and final weighted difference molecular ~~scatter~~ring intensity at a camera distance of 128mm.

Figure 3.9 SiH_2INMe_2

a)

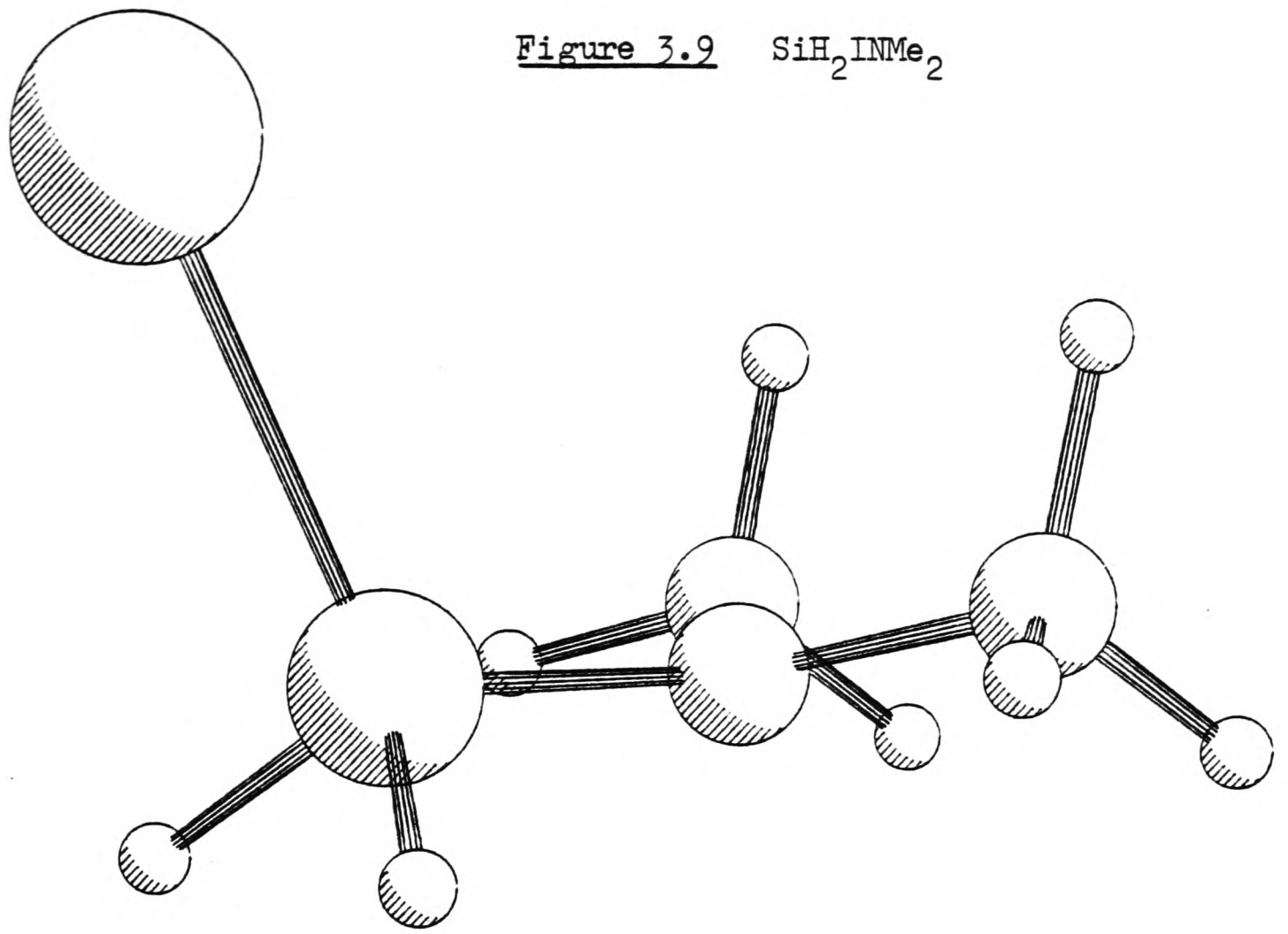

b)

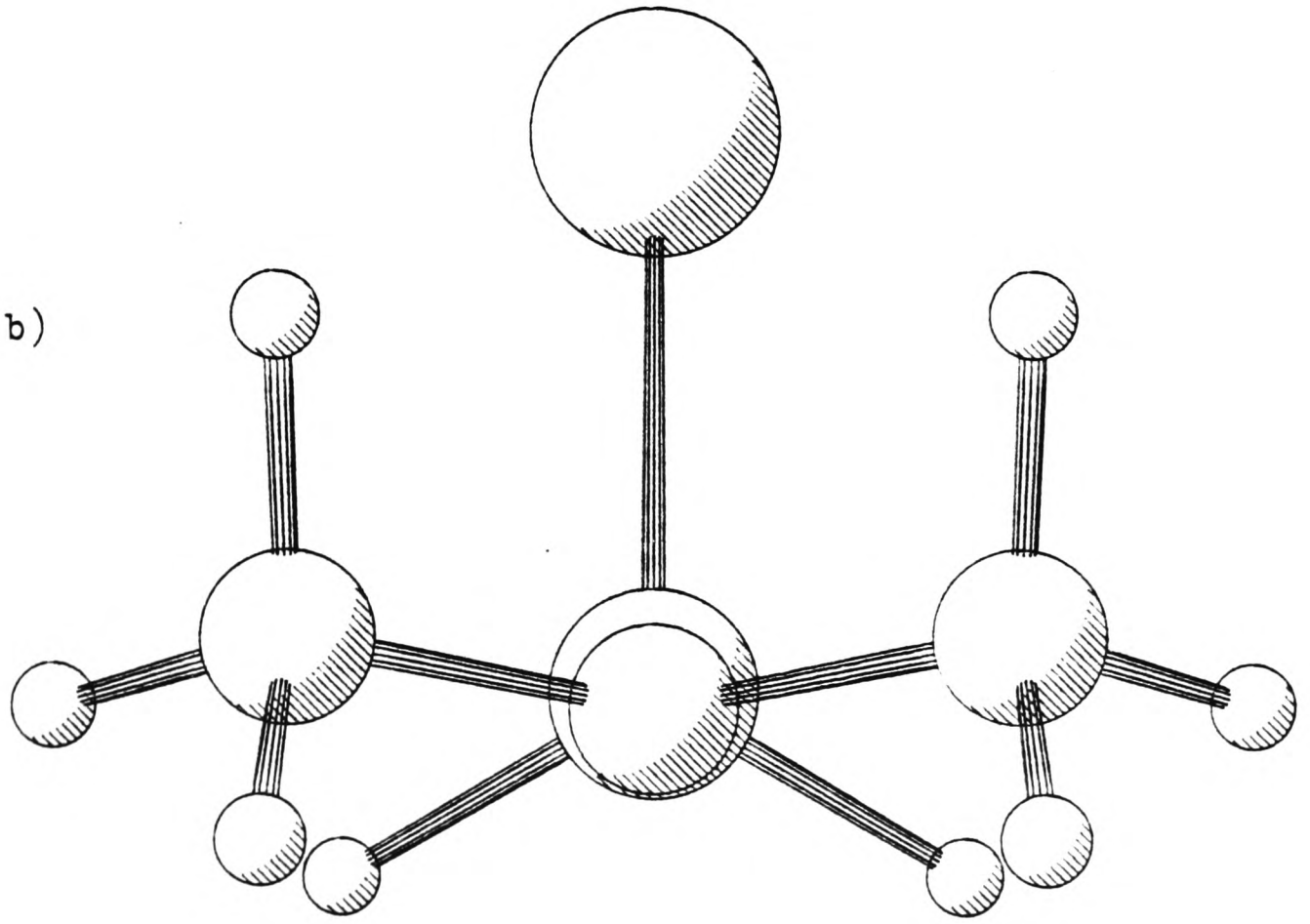

Molecular Structure of SiH_2INMe_2

a) General view.

b) Viewed along the bond from N to Si.

and the dimethyl dip angle. The molecular parameter list is given in Table 3.7 and the final R-factor was R_G = 0.120 and R_D = 0.086. The molecular intensity curves and the radial distribution curve are illustrated in Figures 3.7/8 and 3.8 respectively, and pluto plots of $SiH_2I(NMe_2)$ are given in Figure 3.9.

3.6 RESULTS AND DISCUSSION

The major problem involved in interpreting the determined structures of silyl—amines is whether or not structures which are observed to be slightly non-planar are genuinely so, or whether these observations are simply attributable to shrinkage effects, due to out of plane deformations involving inversion of configuration at nitrogen.

The structures of the three halosilyl-dimethyl amines determined here are remarkably consistent, and all indicate that the geometry at nitrogen is non-planar, although these molecules are distinctly 'flatter' than the pyramidal alkylamines. It would appear, therefore, that mono silyl—amines are genuinely non-planar unlike di and tri silyl-amines, although with increasing substitution of highly electronegative groups or atoms on silicon this 'rule' breaks down. Mono silyl—amines have only one suitable vacant d-orbital on silicon which can become involved in π-bonding to nitrogen, unlike di and trisilyl-amines, hence less of the lone pair electron density on nitrogen is dissipated, although this effect is concentrated and a shorter Si-N bond with more π-character results. (See Table 3.8).

TABLE 3.8

TABLE 3.8

VARIATION OF r(Si-N) WITH THE NUMBER OF SILYL GROUPS BOUND TO NITROGEN

Compound	r(Si-N)/pm	Ref.
$(SiH_3)_3N$	173.5(2)	39
$(SiH_3)_2NMe$	172.6(3)	43
$(SiH_3)NMe_2$	171.5(4)	45
$(SiH_2Cl)NMe_2$	168.7(2)	This work
$(SiH_2Br)NMe_2$	168.3(4)	This work
$(SiH_2I)NMe_2$	167.0(2)	This work

The overall molecular conformation in the three compounds is identical, with a staggered conformation, analogous to that observed for mono halogen substituted ethanes, clearly preferred. The two Si-H bonds and two C-N bonds are thus mutually trans, as are the Si-X bond and the lone electron pair on nitrogen. This would appear to indicate a repulsive interaction between the halogen atom and the lone electron pair on nitrogen. This results in essentially orthogonal XSiN and CNC planes. As the size of the halogen atom is increased, the steric effects become increasingly apparent. The chloro and bromo compounds have Si-N bond torsions of 9.7(51)° and -14.0(9)° respectively, with a resultant small methyl torsion in the bromo compound which moves some of the H atoms closer to the halogen atom and others further away. Finally, in SiH_2INMe_2, the steric effect is particularly marked with t(Si-N) and t(C-N) both zero. This implies that neither methyl group is prepared to move closer to the large iodine atom than the other, hence the iodine atom has essentially 'locked' the conformation into perfect C_s symmetry. It should be noted however, that the Si-N torsions in the chloro and

bromo compounds may be due to a shrinkage effect, although, clearly, this appears to be unimportant for the iodo compound. Further evidence for this hindered rotation about the Si-N bond in $SiH_2I(NMe_2)$ was obtained from the ^{13}C N.M.R. spectrum where the methyl groups were clearly inequivalent at room temperature unlike those of $SiH_2Cl(NMe_2)$ and $SiH_2Br(NMe_2)$. The internal rotational barrier about the Si-N bond in SiH_3NMe_2[48] is calculated as being relatively low at 1.51Kcal/mol. It seems reasonable to predict then, that values for this barrier will become consistently larger as the size of the halogen atom increases for the mono halo silyl compounds, and that this barrier will be particularly high for the iodo compound.

Comparing the Si-N bond lengths of the halo silyl-dimethyl amines with those of $SiH_3(NMe_2)$ and the methyl substituted silyl-dimethyl amines, Table 3.9, it is apparent that the effect of the electronegative halogen atom is to distinctly reduce the Si-N bond length by causing increased π-donation from nitrogen to the more electropositive silicon atom. It is surprising however, that this effect is apparently greatest for the iodo compound. Comparing r(Si-N) for the mono-substituted halo compounds and their tri-halo analogues, as expected, it is observed that the tri-halo compounds contain distinctly shorter Si-N bonds since here silicon will be even more electropositive. It is also noticeable, that the extent of planarity ($\sum$ angles at N) is not always predicted by the Si-N bond length with e.g. r(Si-N) being shorter in $SiH_2I(NMe_2)$ than $SiH_2Cl(NMe_2)$ but $SiH_2Cl(NMe_2)$ being apparently more planar. In general, however, this is a reasonable guide to planarity at nitrogen, since the methyl substituted compounds which have relatively long Si-N bonds are non-planar and the trihalosilyl compounds, which contain some of the shortest known Si-N bonds, are

found to be planar. The SiNC angles for these compounds are consistently wide ($\simeq$120°) as expected due to the stereochemical inactivity of the 'lone pair' on nitrogen caused by π-donation. These angles control the stereochemistry at nitrogen, with angle CNC being more variable. In general angle CNC is, as expected, distinctly wider than the values found for alkyl amines,[49] e.g. 111.8(6)° and 110.6(6)° for $NHMe_2$ and NMe_3 respectively, although it is surprisingly small at 108.6(14)° in $SiH_2Br(NMe_2)$.

It is clear, however, that the observed structures of these mono-halo silyl—amines are non-planar with dip angles of $\simeq$ -20°. These compounds are therefore intermediate between the planar disilylamines or trihalosilylamines and the pyramidal alkylamines, although it must be stressed that the potential energy barrier to inversion at nitrogen will be low and that this can be achieved by a high amplitude out of plane $SiNC_2$ deformation which will give rise to averaged, apparently non-planar structures.

The C-N bond lengths in these compounds ($\simeq$146pm) and in the related methyl substituted compounds are remarkably consistent. This is not unreasonable since π -bonding between carbon and nitrogen is not possible, therefore, varying the substituents on silicon will leave these distances largely unaffected. The C-N bond lengths in the halosilyl—amines however are very slightly longer than those in alkylamines (145.2(6), 145.5(2) and 145.4(2); corrected to 145.9pm in $CH_3\ CH_2\ N(CH_3)_2$ [50] $NH(CH_3)_2$ [49] and $N(CH_3)_3$ [49,51] respectively).

For all three compounds, the angles XSiH (where X = Cl, Br & I) and NSiH were all close to the tetrahedral value as expected, but the angle XSiN was found to be distinctly wider in each case. (113.2(3)°, 115.2(7)° and 115.1(4)° for the chloride, bromide and iodide respectively). With the halide and two methyl groups being mutually

cis with respect to the Si-N bond, this is likely to be due to steric interactions between these groups, particularly for $SiH_2Br(NMe_2)$ and $SiH_2I(NMe_2)$ when the halogen is larger. The geometry around the carbon atoms was as expected, with the refineable NCH and the calculated HCH angles all being close to the tetrahedral value of 109.47°.

A comparison of the silicon-halogen bond lengths in these compounds with those in other halosilanes reveals that they are, predictably, rather long. In general for silyl halides, as the number of halogen atoms around a central silicon atom increases, so the silicon-halogen bond length decreases.[52] This is believed by Pauling,[53] to be caused by ionic and double-bond character of the type shown below.

$$F^- \qquad F - Si = F^+ \qquad F$$

For the fluorosilanes,[52] $(CH_3)_{4-n}SiFn$ (n = 1-3), this is more realistically rationalised by the increasing polar contribution to the Si-F bonds and the contraction of silicons' valence shell.

The Si-Cl bond length of 207.0(1)pm in SiH_2ClNMe_2 is longer than r_o(Si-Cl) = 204.9(3)pm for SiH_3Cl,[54] and also those of $SiHCl_2NMe_2$ and $SiCl_3NMe_2$[55] which are 205.6(1)pm and 202.3(5)pm, respectively. The values obtained for the chlorosilyl-dimethylamines, clearly illustrating the band shortening effect with increasing halogenation.

In SiH_3Br,[54] r_o(Si-Br) is 221.0(3)pm which is shorter than the value of 224.6(2)pm found in SiH_2BrNMe_2. Again, this value is distinctly longer than values of 217.0(1)pm and 217.1(1)pm observed

in $SiHBr_3$[56] and $SiFBr_3$[57] by microwave spectroscopy, where any polar bond character is likely to be more significant.

Finally, the Si-I bond length of 244.6(3)pm in SiH_2INMe_2 is slightly longer than in SiH_3I[54] (243.7(3)pm) and distinctly longer than in SiF_3I,[58] where it is 238.7(20)pm. The slight lengthening of Si-X in the halosilyl—dimethylamines relative to the silylhalides (SiH_3X) is probably attributable to the π-character of the Si-N bonds.

TABLE 3.2

MOLECULAR PARAMETERS FOR $SiH_2Cl(NMe_2)$

a) Independent Parameters

		Distance	Amplitude
r_1	(Si-N)	168.7(2)	4.8(2)
r_2	(C-N)	146.4(2)	4.0(2)
r_3	(C-H)	110.2(4)	8.1(4)
r_4	(Si-H)	147.0(17)	8.8[c]
r_5	(Si-Cl)	207.0(1)	4.7(1)
		Angles	
a_1	<CNC	115.1(6)	
a_2	DIP(CNC)	-17.2(11)	
a_3	<NCH	111.6(8)	
a_4	<ClSiN	113.2(3)	
a_5	<HSiH	111.0(fixed)	
a_6	SiH_2TILT	-5.0(fixed)*	
a_7	T(C-N)	0.0(fixed)*	
a_8	T(Si-N)	9.7(51)	

b) Dependent Parameters

		Angle
a_9	<SiNC(1)	120.8(2)
a_{10}	<SiNC(2)	120.8(2)

All distances and amplitudes of vibration are given in pm and all angles are in degrees. Angles 7 and 8 are torsion angles along the given bond. * = fixed by R-factor plot.

+ = fixed after initially being refined.

TABLE 3.2 (continued)

MOLECULAR PARAMETERS FOR $SiH_2Cl(NMe_2)$

c) Dependent Distances

	Distance	Amplitude
d_2(C-N)	146.4(2)	4.0(2)
d_4(Si-H)	147.0(17)	8.8[c]
d_5(Si-Cl)	207.0(1)	4.7(1)
d_6(Si..C)	274.2(3)	7.1(3)
d_7(Cl..C)	375.8(47)	17.1[c]
d_8(C..C)	247.1(9)	7.4(fixed)[+]
d_9(Cl..N)	314.4(5)	8.5(6)
d_{10}(Cl..)	396.3(60)	17.1(63)
d_{12}(C..Hc')	276.6(20)	16.5[c]
d_{13}(C..Hc')	276.6(20)	16.5[c]
d_{16}(N..Hc)	213.2(10)	10.8[c]
d_{17}(N..HSi)	259.8(14)	11.6[c]
d_{18}(Cl..HSi)	284.3(12)	11.6[c]
d_{19}(Cl..Hc)	368.5(95)	25.5(fixed)[+c]
d_{20}(Cl..Hc)	483.4(43)	25.5(fixed)[+c]
d_{21}(Cl..Hc)	379.2(42)	25.5(fixed)[+c]
d_{22}(Cl..Hc)	403.7(90)	25.5(fixed)[+c]
d_{23}(Cl..Hc)	400.5(79)	25.5(fixed)[+c]
d_{24}(Cl..Hc)	500.3(47)	25.5(fixed)[+c]
d_{25}(Si..Hc)	279.9(12)	9.2(24)[c]
d_{26}(Si..Hc)	359.2(9)	9.2[c]
d_{27}(Si..Hc)	333.7(13)	9.2[c]

TABLE 3.2 (continued)

MOLECULAR PARAMETERS FOR $SiH_2Cl(NMe_2)$

c) Dependent Distances

	Distance	Amplitude
d_{28}(Si..Hc)	279.9(12)	9.2[c]
d_{29}(Si..Hc)	333.7(13)	9.2[c]
d_{30}(Si..Hc)	359.2(9)	9.2[c]

d) Other Amplitudes which were fixed

	Amplitude
(C..Hc')	17.0
(C..Hsi)	20.0
(Hsi..Hsi)	12.0
(Hsi..Hc)	20.0
(Hc..Hc)	11.0
(Hc..Hc')	20.0

TABLE 3.3

LEAST SQUARES CORRELATION MATRIX (X100) FOR $SiH_2Cl(NMe_2)$*

	r5	a2	a3	a8	u3	u10	u25	K1	K2
r2	-83				-40				
r3	45								
r4			-59						
a1		50	60				-43		
a2				40		-47			
a8						-98			
u2									54
u5								41	74
u6							-65		
u9							56		
K1									42

*Only off-diagonal elements with magnitude >40 are shown.

EX BIBL. UNIV. EDINBURGEN.

TABLE 3.4

LEAST SQUARES CORRELATION MATRIX (X100) FOR $SiH_2Br(NMe_2)$*

	a2	a4	u9	u18	K2
r1					43
a1	65	55			
a2		-64			
a3					-51
a7			56	60	
u2					52
u5					54
u6				46	
u9				80	

*Only off-diagonal elements with magnitude >40 are shown.

TABLE 3.5

MOLECULAR PARAMETERS FOR $SiH_2Br(NMe_2)$

a) Independent Parameters

	Distance	Amplitude
r_1(Si-N)	168.3(4)	5.9(4)
r_2(C-N)	147.2(3)	4.6(4)
r_3(C-H)	151.1(8)	8.4(8)
r_4(Si-H)	150.0(fixed)	8.8(fixed)
r_5(Si-Br)	224.6(2)	5.9(2)
	Angles	
a_1 <CNC	108.6(14)	
a_2 DIP(CNC)	-26.8(16)	
a_3 <NCH	105.8(20)	
a_4 <BrSiN	115.3(7)	
a_5 <HSiH	108.0(fixed)	
a_6SiH_2TILT	-6.0(fixed)*	
a_7T(C-N)	15.3(62)	
a_8T(Si-N)	-14.0(9)	

b) Dependent Parameters

	Angle
a_9<SiNC(1)	121.4(5)
a_{10}<SiNC(5)	121.4(5)

All distances and amplitudes of vibration are given in pm and all angles are in degrees. Angles 7 and 8 are torsion angles along the given bond. * = fixed by R-factor plot.

+ = fixed after initially being refined.

TABLE 3.5 (continued)

MOLECULAR PARAMETERS FOR $SiH_2Br(NMe_2)$

c) Dependent Distances

	Distance	Amplitude
d_6(Si..C)	275.3(6)	8.5(7)
d_7(Br..C)	411.9(17)	12.6(20)
d_8(C..C)	239.0(22)	9.0(fixed)
d_9(Br..N)	333.2(12)	11.8(17)
d_{10}(Br..C)	382.3(15)	12.6[c]
d_{18}(Br..HSi)	300.9(4)	11.7(70)

d) Other Amplitudes which were fixed

	Amplitude
(C..Hc')	17.0
(C..Hsi)	20.0
(N..Hc)	11.0
(N..Hsi)	12.0
(Br..Hc)	20.0
(Si..Hc)	11.0
(C..HSi)	20.0
(Hsi..Hsi)	12.0
(Hsi..Hc)	20.0
(Hc..Hc)	11.0
(Hc..Hc')	20.0

TABLE 3.6

LEAST SQUARES CORRELATION MATRIX (X100) FOR $SiH_2I(NMe_2)$*

	a1	a2	u3	u5	u6	u8	u10	u22	K1	K2	K3
r1	44										
r2	46			-53							
r4	-81	-50		46							
a1		69		-55							
a2							40				
a4						48		-58			
u1									68		
u2			76	48					67		
u3				52					70		
u5					74				58	50	44
u6										44	40
u8							54	-74			
u17									42		
K2											44

*Only off-diagonal elements with magnitude ⩾40 are shown.

TABLE 3.7

MOLECULAR PARAMETERS FOR $SiH_2I(NMe_2)$

a) Independent Parameters

	Distance	Amplitude
r_1(Si-N)	167.0(2)	4.8(4)
r_2(C-N)	146.8(3)	6.0(4)
r_3(C-H)	113.1(3)	5.2(5)
r_4(Si-H)	150.0(fixed)	8.8(fixed)
r_5(Si-I)	244.6(3)	7.5(4)
	Angles	
a_1 <CNC	117.3(12)	
a_2 DIP(CNC)	-20.8(11)	
a_3 <NCH	108.6(5)	
a_4 <ISiN	115.1(4)	
a_5 <HSiH	108.0(fixed)	
a_6SiH_2TILT	-2.0(fixed)	
a_7T(C-N)	0.0(fixed)	
a_8T(Si-N)	0.0(fixed)	
a_9WAG(CNC)	0.0(fixed)	

b) Dependent Parameters

	Angles
a_{10}<SiNC(1)	119.1(4)
a_{11}<SiNC(5)	119.1(4)

All distances and amplitudes of vibration are given in pm and all angles are in degrees. Angles 7 and 8 are torsion angles along the given bond. * = fixed by R-factor plot.

+ = fixed after initially being refined.

TABLE 3.7 (continued)

MOLECULAR PARAMETERS FOR $SiH_2I(NMe_2)$

c) Dependent Distances

	Distance	Amplitude
d_6(Si..C)	270.7(5)	8.7(5)
d_7(Si..C)	270.7(5)	8.7[c]
d_8(I..C)	413.0(12)	35.3(23)
d_9(I..C)	413.0(12)	35.3[c]
d_{10}(N..I)	349.8(7)	10.9(8)
d_{11}(C..C)	250.8(18)	7.5[c]
d_{17}(N..H)	211.9(6)	5.1(8)
d_{19}(I..H_{si})	322.7(4)	18.3(fixed)[+]
d_{20}(I..Hc)	410.5(12)	14.7[c]
d_{21}(I..C)	522.2(12)	14.7[c]
d_{22}(I..C)	400.2(27)	14.7(21)
d_{23}(I..C)	410.5(12)	14.7[c]
d_{24}(I..C)	400.2(27)	14.7[c]
d_{25}(I..C)	522.2(12)	14.7[c]

c = amplitude constrained

d) Other Amplitudes which were fixed

	Amplitude
(C..Hc')	17.0
(C..Hsi)	20.0
(N..H)	12.0
(Si..Hc)	18.0
(Hsi..Hsi)	12.0
(Hc..Hc')	20.0
(Hc..Hc)	11.0
(Hsi..Hc)	20.0

TABLE 3.9

GAS-PHASE GEOMETRICAL PARAMETERS FOR SOME MONOSILYL-DIMETHYLAMINES

Compound	Sum of the angles at N	r(Si-N)	r(C-N)	<CNC	<SiNC	Ref.
SiH_3NMe_2	351.1(20)	171.5(4)	146.2(4)	111.1(12)	120.0(4)	45
SiH_2INMe_2	355.5(20)	167.0(2)	146.8(3)	117.3(12)	119.1(4)	This Work
SiH_2BrNMe_2	351.4(23)	168.3(4)	147.2(3)	108.6(14)	121.4(5)	This Work
SiH_2ClNMe_2	356.7(10)	168.7(2)	146.4(2)	115.1(6)	120.8(2)	This Work
$SiHCl_2NMe_2$	359.6(12)	168.1(4)	146.4(3)	115.5(6)	122.1(3)	This Work
$(SiH_2Me)NMe_2$	355.6(15)	171.5(6)	145.5(3)	112.7(8)	121.5(8)	46
$(SiHMe_2)NMe_2$	352.4(18)	171.9(5)	146.0(4)	113.7(15)	119.3(8)	46
$(SiMe_3)NMe_2$	360[f]	171.0(5)	146.2(4)	117.1(10)	121.4(5)	47
SiF_3NMe_2	359.9(62)	165.4(15)	143.3(15)	120.5(30)	119.7(16)	55
$SiCl_3NMe_2$	359.3(34)	165.7(12)	144.6(12)	113.1(18)	123.1(8)	55

f = fixed, all angles are in degrees and all bond lengths are in pm.

3.7 MOLECULAR MODEL FOR $SiHCl_2NMe_2$

The model used to define the atomic coordinates of $SiHCl_2NMe_2$ was essentially the same as that used for the SiH_2XNMe_2 compounds, but with some minor modifications. As before, it was assumed that the two methyl groups possessed local C_{3v} symmetry. The structure was then defined by five bond angles, six bond angles and two torsion angles. These were exactly the same as those for SiH_2XNMe_2, except angle HSiN replaced angle XSiN, angle ClSiCl replaced angle HSiH and the SiH_2 tilt was replaced by the $SiCl_2$ tilt. The additional parameter, the dimethyl wag was introduced allowing the two SiNC angles to be different. This proved to be unnecessary, however, since it was found that the SiNC angles were equal. The dip and the tilt angles were now considered with respect to the H atom on silicon instead of the halide atom, and again the molecule was initially assumed to possess C_s symmetry and to be planar at nitrogen. The SiNC angles were calculated as dependent parameters. The nozzle to plate distances and operating wavelengths are given in Table 3.10.

TABLE 3.10

WEIGHTING FUNCTIONS, CORRELATION PARAMETERS AND SCALE FACTORS

	Distance(mm)	nm^{-1} ΔS	Smin	S_1	S_2	Smax	P/h	Scale Factor	Wavelength pm
$SiHCl_2NMe_2$	128.3999	4	68	80	300	340	0.1078	0.735(17)	5.705
$SiHCl_2NMe_2$	285.1899	2	20	40	120	144	0.4773	0.791(23)	5.705

3.8 REFINEMENT OF THE $SiHCl_2NMe_2$ STRUCTURE

The radial distribution curve for $SiHCl_2NMe_2$ is given in Figure 3.10. Its principal features are essentially the same as

SiH_2ClNMe_2 with the exception of the strong Cl..Cl peak at 326pm and a series of small peaks between 350 and 436pm for the four C..Cl non-bonded distances. The bonded distances all refined well, with the exception of the Si-H distance, which was fixed at 150pm.

The Si-Cl bond length was, unsurprisingly, particularly well defined at 205.6(1)pm. With the clear Si..C peak and the C..C distance appearing as a shoulder in the radial distribution curve, the geometry at the nitrogen atom was well determined. The CNC angle refined to 115.5°(6), and the dependent SiNC angles were both 122.1°(3). Of the angles, the heavy atom ClSiCl angle refined well, but the HSiN angle did not refine satisfactorily and was fixed close to the tetrahedral value at 108°. The NCH angle refined to the high value of 114° and with a large e.s.d.(2°). Attempts to refine the dip angle for the $-NMe_2$ group yielded a small angle with a large e.s.d. which was not particularly satisfactory. It was decided therefore, to find the optimum dip angle by varying the parameter between +10° — -10° in a series of refinements and fixing it at the value which gave the lowest R-factor. The Si-N torsion angle refined satisfactorily to a value of 76.4°(13), which has one methyl group slightly twisted away from eclipsing the Si-H bond. The C-N torsion was fixed at 60° after investigation by an R-factor loop. This conformation has the three pairs of C-H bonds eclipsing one another. The$SiCl_2$ tilt was fixed at 0°, again after an R-factor loop.

The amplitudes of vibration for the Si-N, N-C and Si-Cl bonds all refined well, the C-H amplitude, however, tended to refine to an unrealistically large value and was therefore fixed after initial refinement. The Si-H amplitude was fixed throughout the structure refinement. The heavy atom amplitudes for the non-bonded distances Si..C, Cl..Cl, N..Cl and the four C..Cl distances were all refined

Figure 3.10 Observed and final difference radial distribution curves for $SiHCl_2NMe_2$.

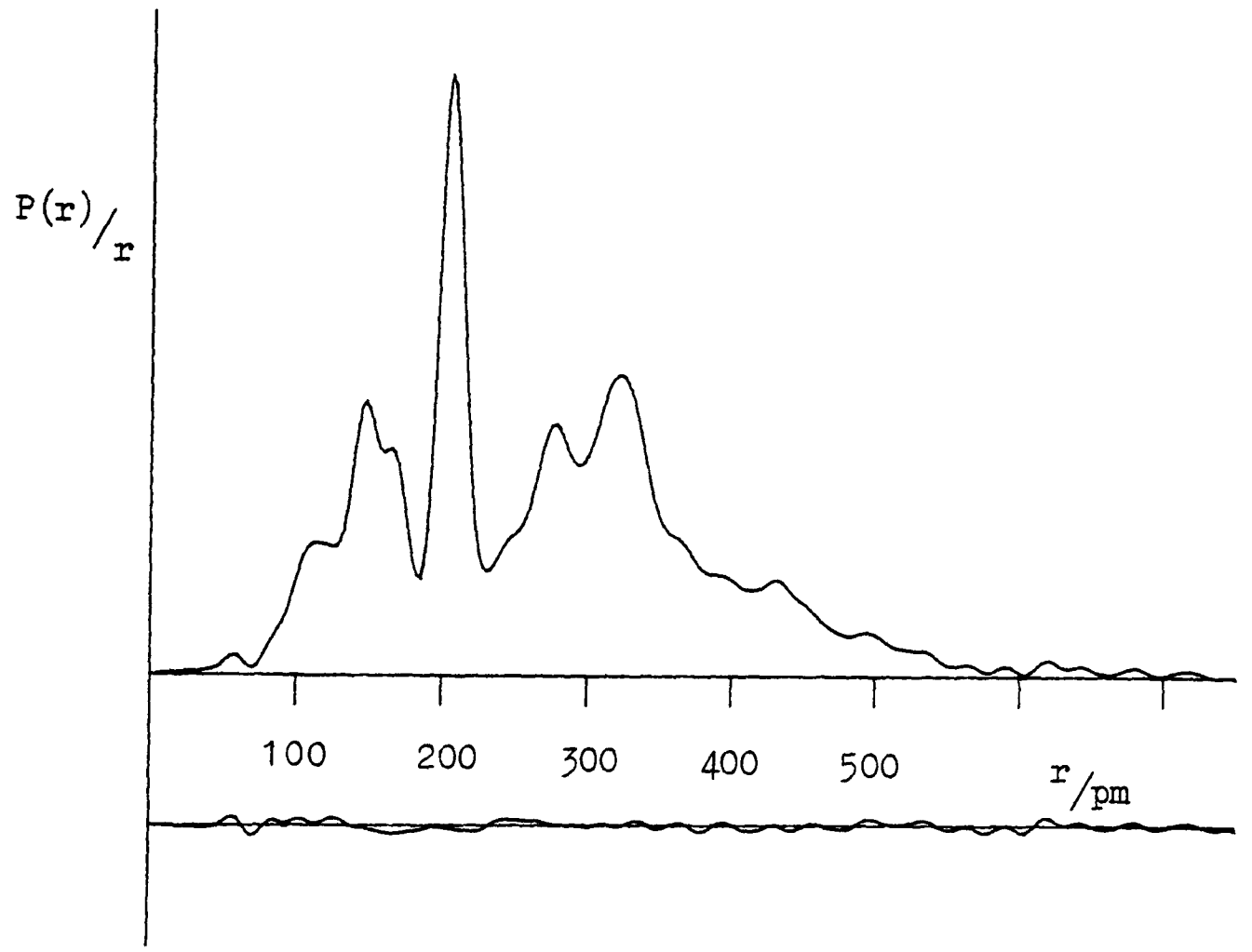

Before Fourier inversion the data were multiplied by $S.\exp(-0.00002\ S^2/(Z_{Si}-f_{Si})(Z_{Cl}-f_{Cl}))$.

Figure 3.11 $SiHCl_2NMe_2$

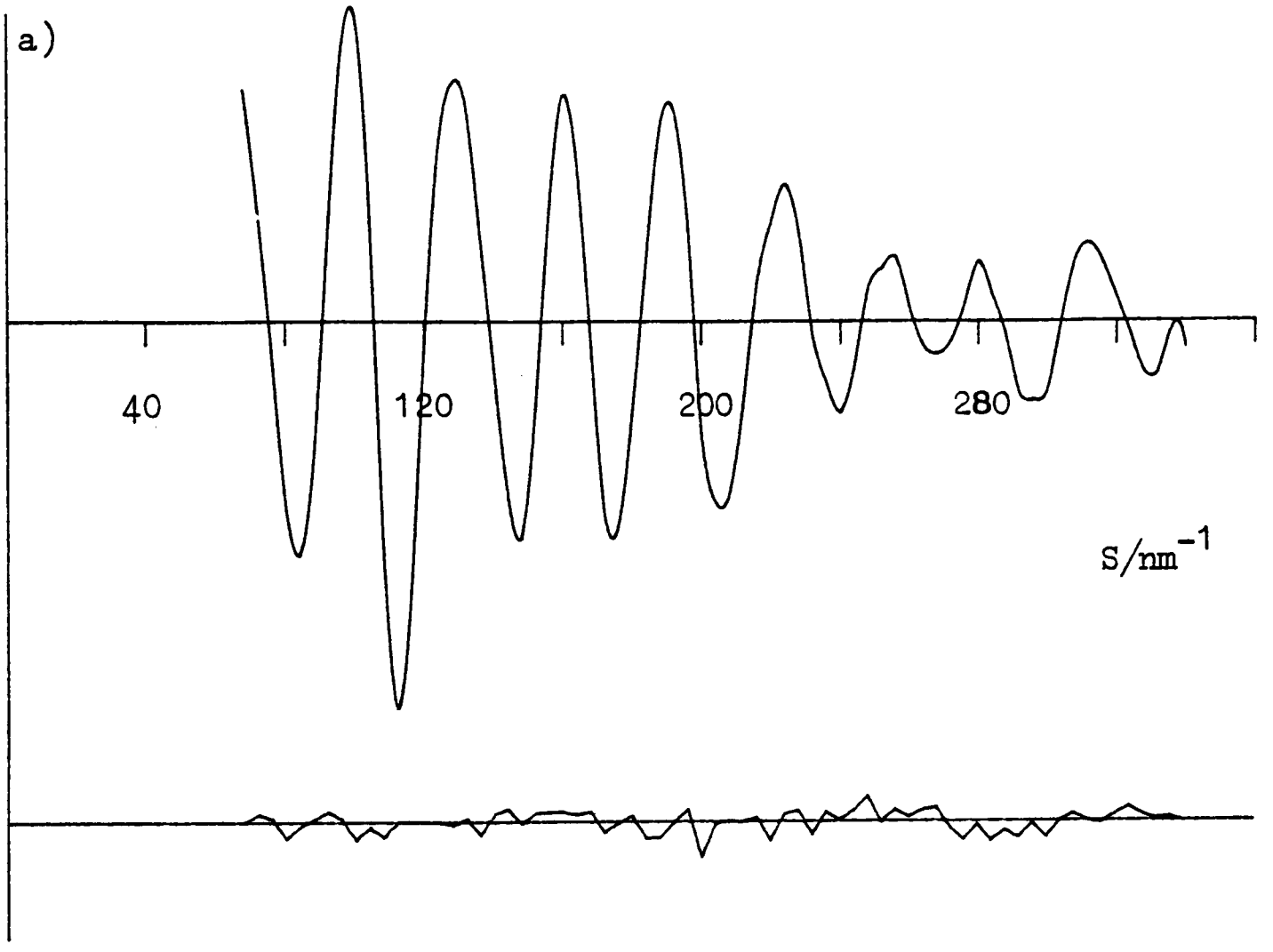

Observed and final weighted difference molecular scattering intensities at camera distances of a)128 mm and b) 285 mm.

Figure 3.12 $SiHCl_2NMe_2$

a)

b)

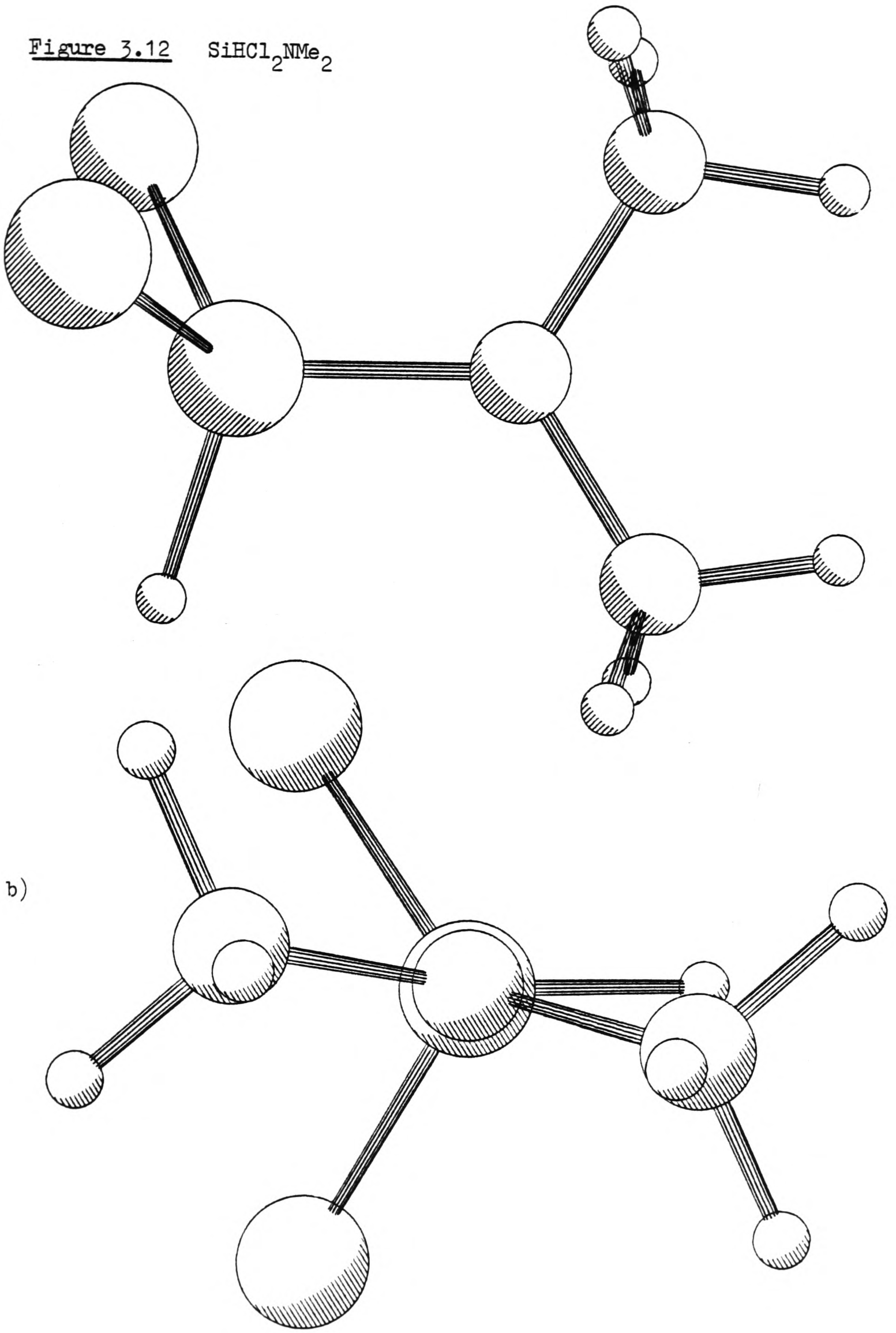

Molecular Structure of $SiHCl_2NMe_2$

a) General View

b) Viewed along the bond from N to Si.

independently. The amplitudes due to the less significant C..C, N..H(U14) and Cl..H(U15) distances were all refined and then fixed at these values. All other inter-atomic distances involved either one or two hydrogen atoms, and these were consequently fixed at reasonable values.

The final list of parameters is given in Table 3.11 and this gave the minimum R-factors (R_G = 0.098 and R_D = 0.084). The least squares correlation matrix (See Table 3.12) reveals a strong correlation between the ClSiCl angle and the N..Cl amplitude and also significant correlation between the C..Cl amplitudes. The intensity curves are given in Figure 3.11 and views of $SiHCl_2NMe_2$ are shown in Figure 3.12.

3.9 RESULTS AND DISCUSSION (INCLUDING THE X-RAY CRYSTAL STRUCTURE OF $SiHCl_2NMe_2$)

The X-ray crystal structure of $SiHCl_2NMe_2$ at 116K was determined by Dr. A.J. Blake. The space group and unit cell parameters were as follows: Space group = P_{2_1}/n, a = 631.29(10), b = 1107.7(7), c = 984.5(3)pm, $\alpha = \gamma = 90^\circ$, $\beta = 104.360(22)^\circ$, Z = 4, D = 1.434gcm^{-3} and R = 0.0453. Some of the molecular parameters obtained are given in Table 3.13 and a view of the molecule is shown in Figure 3.13.

TABLE 3.11

MOLECULAR PARAMETERS FOR $SiHCl_2(NMe_2)$

a) Independent Parameters		
	Distance	Amplitude
r_1(Si-N)	168.1(4)	5.5(4)
r_2(C-N)	146.4(3)	4.4(3)
r_3(C-H)	112.1(8)	9.8(fixed)+
r_4(Si-H)	150.0(fixed)	8.8(fixed)
r_5(Si-Cl)	205.6(1)	5.1(1)
	Angles	
a_1 <CNC	115.5(6)	
a_2 DIP(CNC)	6.0(fixed)*	
a_3 <NCH	114.1(21)	
a_4 <HSiN	108.0(fixed)	
a_5 <ClSiCl	104.8(7)	
a_6SiCl_2TILT	0.0(fixed)*	
a_7T(C-N)	60.0(fixed)*	
a_8T(Si-N)	76.4(13)	
a_9WAG(CNC)	0.0(fixed)*	
b) Dependent Parameters		
	Angles	
a_{10}<SiNC(1)	122.1(3)	
a_{11}<SiNC(2)	122.1(3)	

All distances and amplitudes of vibration are given in pm and all angles are in degrees. Angles 7 and 8 are torsion angles along the given bond. * = fixed by R-factor plot.

+ = fixed after initially being refined.

TABLE 3.11 (continued)

MOLECULAR PARAMETERS FOR $SiHCl_2(NMe_2)$

c) Dependent Distances

	Distance	Amplitude
d_6(Si..C)	275.3(4)	7.8(5)
d_7(Cl..Cl)	325.7(16)	12.1(8)
d_8(C..C)	247.6(10)	7.7(fixed)+
d_9(N..Cl)	308.7(4)	18.5(27)
d_{10}(C..Cl)	436.4(10)	11.2(19)
d_{11}(C..Cl)	407.8(16)	15.1(32)
d_{12}(C..Cl)	350.2(14)	17.3(39)
d_{13}(C..Cl)	369.4(13)	15.2(27)
d_{14}(N..H)	217.8(26)	15.3(fixed)+
d_{15}(Cl..H)	294.8(3)	18.4(fixed)+

d) Other Amplitudes which were fixed

	Amplitude
(Hsi..N)	12.0
(C..Hsi)	20.0
(Cl..Hc)	20.0
(C..Hc)	17.0
(Si..Hc)	18.0
(Hc..Hc)	11.0
(Hc..Hc')	20.0
(Hsi..Hc)	20.0

TABLE 3.12

LEAST SQUARES CORRELATION MATRIX (X100) FOR $SiHCl_2(NMe_2)$*

	a1	a2	u6	u7	u9	u10	u11	u12	u13	K1	K2
r1	45	41								44	
a3				63						52	62
a5			-47		-86				-42		
a8						53	58	46	48		
u2										43	
u5										81	41
u6					59						
u7					47			72		44	59
u9								43			41
u10							76		45		
u11									68		
K1											47

*Only off-diagonal elements with magnitude ⩾40 are shown.

TABLE 3.13

MOLECULAR PARAMETERS FOR CRYSTALLINE $SiHCl_2(NMe_2)$

Bond Lengths(pm)

Cl(1) - Si(1) = 205.48(8)	C(1) - H(11) = 97(3)
Cl(2) - Si(1) = 205.46(8)	C(1) - H(12) = 110(4)
Si(1) - H(1) = 137(3)	C(1) - H(13) = 96(4)
Si(1) - N(1) = 166.41(19)	C(2) - H(21) = 97(3)
N(1) - C(1) = 145.7(3)	C(2) - H(22) = 104(3)
N(1) - C(2) = 145.7(3)	C(2) - H(23) = 104(3)

Angles (°)	Variation of Angles
Cl(1)-Si(1)-Cl(2) = 103.22(3)	N-C-H = 109.7(17) - 114.5(22)
Cl(1)-Si(1)-H(1) = 109.4(13)	H-C-H = 102.3(29) - 111.0(24)
Cl(1)-Si(1)-N(1) = 111.99(7)	
Cl(2)-Si(1)-H(1) = 110.7(13)	
Cl(2)-Si(1)-N(1) = 112.41(7)	
H(1)-Si(1)-N(1) = 109.1(13)	
Si(1)-N(1)-C(1) = 123.87(15)	
Si(1)-N(1)-C(2) = 122.58(15)	
C(1)-N(1)-C(2) = 113.55(18)	

Torsion Angles (°)

H(1)-Si(1)-N(1)-C(1) = -3.3(14)

H(1)-Si(1)-N(1)-C(2) = 177.4(14)

Figure 3.13 The molecular structure of $SiHCl_2NMe_2$ at 116K.

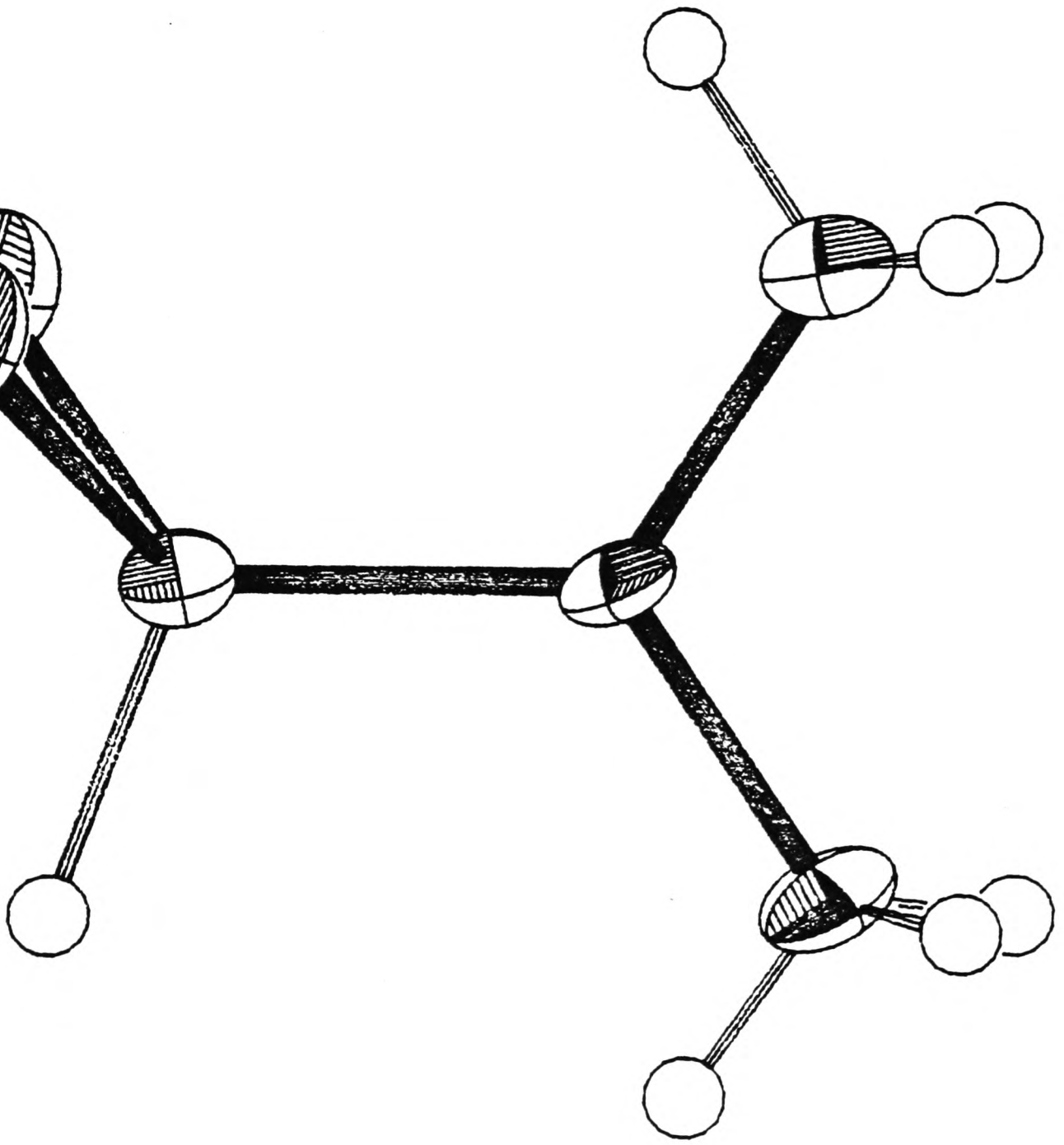

A comparison of the structures of $SiHCl_2NMe_2$ in the gas and solid phases reveals a very close similarity, which contrasts with SiH_2ClNMe_2 where the compound was monomeric in the gas-phase and dimeric as a crystalline solid. The monomeric nature of crystalline $SiHCl_2NMe_2$ is expected for two reasons, firstly because of the high apicophilicity of Cl relative to $-NMe_2$ and particularly H, and secondly for steric reasons. Cavell[59] predicts that highly electronegative substituents will preferentially be axially coordinated rather than equatorially in 5-coordinate phosphorus compounds probably, because of greater ionic character in the bonding in the axial direction. Corriu[60,61] has shown that in contrast to pentacoordinate phosphorus compounds, the apicophilicity of groups (x) attached to pentacoordinate silicon is dependent upon the ease of stretching or polarisability of the Si-X bond and not directly to the electronegativity of X. On this basis, it is therefore predicted that Cl will be axial, H will be equatorial and that $-NMe_2$ may be either axial or equatorial. For dimerisation or pentamerisation[62,63] (cf.SiH_3NMe_2) of $SiHCl_2NMe_2$ either one or both of the Cl atoms would have to be equatorially coordinated which is obviously very unfavourable. Sterically, dimerisation of $SiHCl_2NMe_2$ would also involve essentially eclipsing interactions between the equatorial Si-Cl bond and one of the C-N bonds on both of the amine/"ammonium" groups, and hence this arrangement would be unlikely. Formation of a pentamer would be impossible, since sterically there is insufficient room to accommodate a minimum of five Cl atoms 'inside' the ring structure. It is therefore not unexpected that $SiHCl_2NMe_2$ is monomeric in the solid phase.

Considering the molecular parameters for the gaseous and solid phase structures of $SiHCl_2NMe_2$ it is apparent that these are fairly

similar, although some subtle differences exist. The sum of the angles around nitrogen are 360.0 $\pm$0.5° and 359.6 $\pm$1.2° for $SiHCl_2NMe_2$ in the solid and gaseous phases respectively, and so it is apparent that in the solid phase the compound is perfectly planar at nitrogen, whilst it is very slightly non-planar in the gas-phase (DIP angle = 6°). Strictly speaking, $SiHCl_2NMe_2$ could be said to be planar in gas-phase, within experimental error, and this apparent inconsistency is consistent with the idea that the apparent non-planarity is simply attributable to a shrinkage effect. The planarity of $SiHCl_2NMe_2$ compared to the non-planar SiH_3NMe_2 [45] and SiH_2XNMe_2 (X = Cl, Br & I), is expected from a consideration of the substituted effects. As the number of electron withdrawing halide substituents on silicon is increased, so increased (p-d)π donation occurs from N into the increasingly electropositive Si atom (see Table 3.9).

This results in a more planar nitrogen atom and a slight shortening of the Si-N bond. The Si-N bond length in the gas-phase (168.1pm) is significantly shorter than 180pm predicted by Schomaker and Stevenson[64] and as would also be expected, it is shorter than the values determined for di and trisilyl-amines (173-175pm),[42,43,44] since π-back donation from the central N atom is not dissipated through either two or three silyl groups. This bond length, however, is distinctly longer than the value observed in the solid phase, where r(Si-N) is 166.4pm.

The gas-phase Si-N bond length, in $SiHCl_2NMe_2$, is distinctly shorter than r(Si-N) in any of the methyl-substituted silyl dimethylamines[46] (See Table 3.9) or most of the silyl and methyl silyl pseudohalides,[65] which vary between 170-178pm. This is as expected, since the inductive effect of methyl groups tends to decrease the

ability of the d-orbitals on silicon to accept lone pair electron density from nitrogen and hence a longer Si-N bond is produced. Only compounds which are well substituted with electronegative groups or atoms such as Cl_3SiNCO,[66] (r(Si-N) = 162.6pm), F_3SiNCO[67] (r(Si-N) = 164.8pm) or the trihalosilyl-dimethyl amines[55] tend to give shorter bonds. The Si-N bond, although distinctly shortened, is still much longer than the Si=N bond in $Bu^{\pm}_2Si=N-SiBu^{\pm}_3$[68] (156.8pm), which is likely to have a bond order between 2 and 3.

Comparing the SiNC and CNC angles for $SiHCl_2NMe_2$ in the gas and solid phases, it is apparent that a slight widening of SiNC angle coupled with a distinct narrowing of angle CNC occurs in the solid phase and this is probably due to packing constraints in the crystal. These parameters however, are not signficantly different from those in other monosilyl—dimethylamines (Table 3.9), although the CNC angles for $SiHCl_2NMe_2$ in the gas and solid phase are wider than those observed for alkylamines, e.g. $NHMe_2$[49] (<CNC = 111.8(6)°) and NMe_3[49] (<CNC = 110.6(6)°), where no lone pair delocalisation is possible. Similarly, the C-N bond lengths in $SiHCl_2NMe_2$ in both phases, are fairly consistent with those observed in related compounds. The Si-Cl bond lengths in the gas—phase (205.6(1)pm) and the solid phase (205.48(8) and 205.46(8)pm) are very similar, and these compare with 205pm for SiH_3Cl[69] and 207.0(1)pm for SiH_2ClNMe_2 (see before). The angles around silicon (ClSiN and ClSiH) are both close to the tetrahedral value and do not merit further discussion. The ClSiCl angle of 104.8(7)° and 103.22(3)° in the gas and solid phases respectively, is significant, however. This heavy atom angle which might be expected to be slightly greater than the tetrahedral value is also distinctly narrower than expected in Me_2SiCl_2 [70] (107.5(2)°), in the silacyclopentene,[71] $Cl_2\overline{SiCH_2CHCHCH_2}$ (103.9(5)°) and in other

compounds containing the $\geq SiCl_2$ group. This narrowing is clearly due to the silicon centre, since this effect is not observed in the analogous carbon compounds.

The molecular parameters involving the methyl groups are, unsurprisingly, not particularly well defined in either structure, but the average C-H bond length in the gas phase (112.1(8)pm) is longer than any of the C-H bond lengths in the crystal. This may, however, be a consequence of the X-ray experiment, since the scattering of X-rays is from the centre of electron density and this is shifted away from the H atom in any bond to hydrogen, resulting in a shorter than predicted bond length. The NCH angles in the crystal are mostly greater than 109° and the average NCH angle in the gas phase (114(2)°) is also greater than the tetrahedral value, although this parameter is subject to a large error.

The overall molecular conformation in the gas and solid phases is very similar, with the plane containing the CNC atoms approximately bisecting the ClSiCl angle. This conformation results in one of the C-N bonds essentially eclipsing the Si-H bond, although torsions along the Si-N bond of $\simeq$ 3° and 14° in the solid and gas-phases respectively reduce this interaction. In the gas-phase, however, the larger angle is possibly due to shrinkage associated with the low frequency torsional motion around the Si-N bond. It is apparent however, that the Si-Cl/C-N eclipsing interactions are dominant over the Si-H/C-N interaction in determining the structure and thus a syn conformation occurs, with the Si-H bond and one of the C-N bonds almost eclipsing. The small Si-N torsion in the gas-phase will serve to simultaneously reduce this effect and also reduce the, close to, eclipsing interaction between the lone pair of electrons on nitrogen and one of the Si-Cl bonds. This is consistent with the conformation observed

for $(SiHMe_2)NMe_2$[46] where the CNC plane essentially bisects the CSiC plane, and here too a small Si-N torsion relieves the perfect eclipsing of the Si-H and one of the C-N bonds.

Finally the methyl torsions (rotation about the C-N bonds), which were tied together in the gas-phase, result in an eclipsed conformation between all the C-H bonds, although all the C-H and Si-N interactions are staggered as expected. In the solid phase, again all the C-H bonds are eclipsed, but here two of the C-H bonds are eclipsing the Si-N bond, and this like the narrower CNC angle in the solid is probably due to steric constraints in the molecular packing in the crystal.

It can be seen then, that $SiHCl_2NMe_2$ fits logically between the non-planar monohalosilyl-dimethylamines and the planar disilyl-amines although definitive infra-red information on the Si-N torsion and particularly the $SiCN_2$ in plane deformation (A') would be useful in ascertaining whether there is a genuine hump in the potential energy function for bending at the planar configuration or whether the molecule is genuinely slightly non-planar in the gas-phase.

CHAPTER 4

THE VIBRATIONAL AND MULTINUCLEAR NMR SPECTRA OF $SiH_2X(NMe_2)$ WHERE X = F, Cl, Br & I AND $SiHCl_2(NMe_2)$

4.1 INTRODUCTION

After initially preparing new compounds, it is obviously essential that they are subsequently characterised as fully as possible. The halosilyl-amines which were prepared in the course of this work were all volatile and hence easily studied by gas-phase infra-red spectroscopy. Infra-red and Raman spectra of the compounds in the solid and liquid phases were also recorded, since shifts in absorption frequency and changes in peak intensities are often observed in the condensed phases. It was particularly important to record solid phase spectra for these compounds, since large shifts, particularly for ν Si-N, were sometimes observed which were indicative of intermolecular interactions. If single crystals suitable for X-ray studies were not obtained, then the solid phase spectra provided the only evidence for intermolecular interactions on condensation. These spectra are discussed in detail in Chapter 5. Matrix isolated spectra were also recorded in some cases, since intermolecular interactions are generally removed in an inert matrix and band widths are considerably reduced due to the removal of any rotational structure. As a consequence of this, two absorptions which are overlapping in the gas-phase are sometimes seen as two distinct peaks in the matrix isolated spectrum.

In the gas-phase, band shapes can often give useful information in the assignment of bands. An asymmetric top with three distinct moments of inertia will give rise to three different band shapes for vibrations which involve dipole changes parallel to each of the three axes.

A vibration with a dipole change parallel to the axis with the largest moment of inertia gives a C-type band (prominent Q branch), a vibration parallel to the axis of intermediate moment of inertia gives a B-type band (PR branches), and a vibration parallel to the axis with the lowest moment of inertia will give an A-type band (PQR branches).

The molecules under investigation here, however, all have C_s symmetry and so dipole changes for vibrations are either parallel or perpendicular to the plane of symmetry. This results in either A-C type hybrid bands for vibrations which have A' symmetry, or B-type bands for modes which have A" symmetry.

The Raman spectra tend to be useful in conjunction with the infra-red spectra in assigning bands, since in many cases absorptions which are strong in the infra-red spectrum are only weakly active in the Raman spectrum and vice-versa. For molecules with an inversion centre, the extreme case of mutual exclusion exists, with vibrations which are infra-red active being Raman inactive (since there is no change in polarisability) and vice-versa.

In the liquid Raman spectrum it is also possible to determine which vibrations are fully symmetric with the use of a polarising filter. By placing a polarising filter in the scattered Raman beam with its polarising axis parallel and then perpendicular to the beam, it is found that the signal intensity of a fully symmetric vibration will diminish, whilst the intensities of any asymmetric vibrations remain constant. In general, however, Raman polarisation data was not recorded in this work.

Assignment of the observed bands was generally accomplished by comparison of the experimental data with suitable literature information for related compounds. For the halosilyl-amines reported

here these compounds were dimethylamine,[72,73] dimethylsilylamine[48,74,75] (SiH_3NMe_2), various methylsilylhalides[76] ($MeSiH_2X$) and dihalosilanes[77] (SiH_2X_2). In general, the characteristic absorption frequencies above 1,000cm^{-1} are 3,000cm^{-1} - 2,800cm^{-1} for C-H stretches, ≃2,200cm^{-1} for Si-H stretches, 1,500-1,450cm^{-1} for C-H deformations and 1,310-1,000cm^{-1} for methyl rocking deformations and C-N stretches. Below 1,000cm^{-1}, the Si-H deformations, the Si-N stretch and the Si-X stretch all occur. For compounds containing the $-SiH_2$ group the bending and wagging deformations tend to have a characteristic pattern (the wag always being more intense) in the gas phase IR spectrum and these are found between 1,000 - 800cm^{-1}. The Si-N stretch occurs between 700 and 650cm^{-1}. The region below 400cm^{-1} contains the skeletal bending deformations and the two methyl torsions. Absorption bands in this region tend to be weak and assignment of bands in this region is difficult.

The use of nuclear magnetic resonance spectroscopy allows immediate determination of the purity of the sample and gives conformation of the number and types of atoms or groups present in the molecule. It obviously also gives information on which atoms are bonded, particularly the Si-H and C-H bonds.

4.2 VIBRATIONAL SPECTRA OF $SiH_2Cl^{14}NMe_2$ and $SiH_2Cl^{15}NMe_2$ (EXCLUDING SOLID PHASE SPECTRA)

The infra-red and Raman spectra of $SiH_2Cl^{14}NMe_2$ were recorded and the infra-red spectra are illustrated in Figures 4.1 and 4.2. The gas-phase infra-red spectrum of $SiH_2Cl^{15}NMe_2$ is shown in Figure 4.3. A suggested assignment is given in Table 4.1.

The gas-phase infra-red spectrum of $SiH_2Cl^{14}NMe_2$ is briefly mentioned by Emsley, but no proper assignment of the bands was made. The molecule is found by electron diffraction in the gas-phase, to

Figure 4.1 Infra-red spectrum of $SiH_2Cl^{14}NMe_2$ in the gas-phase.

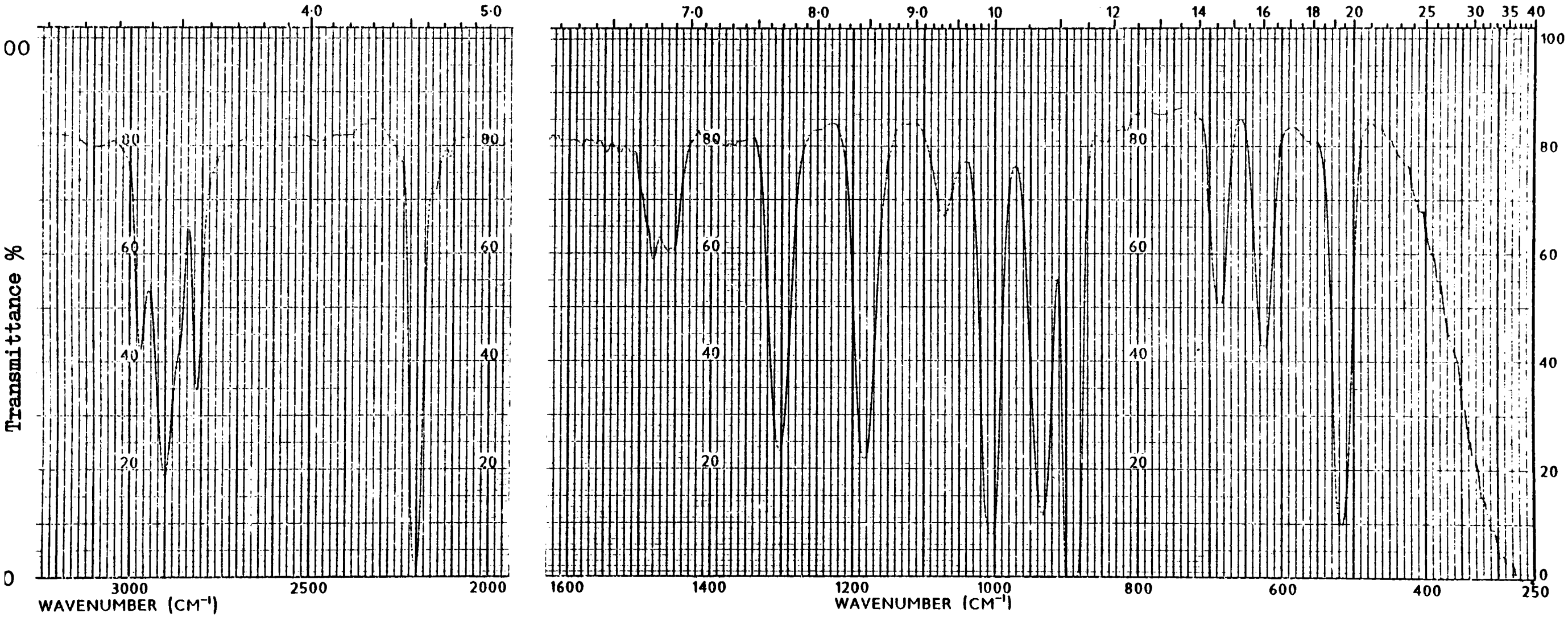

Figure 4.2 Infra-red spectrum of $SiH_2Cl^{14}NMe_2$ in an N_2 matrix (1:580)

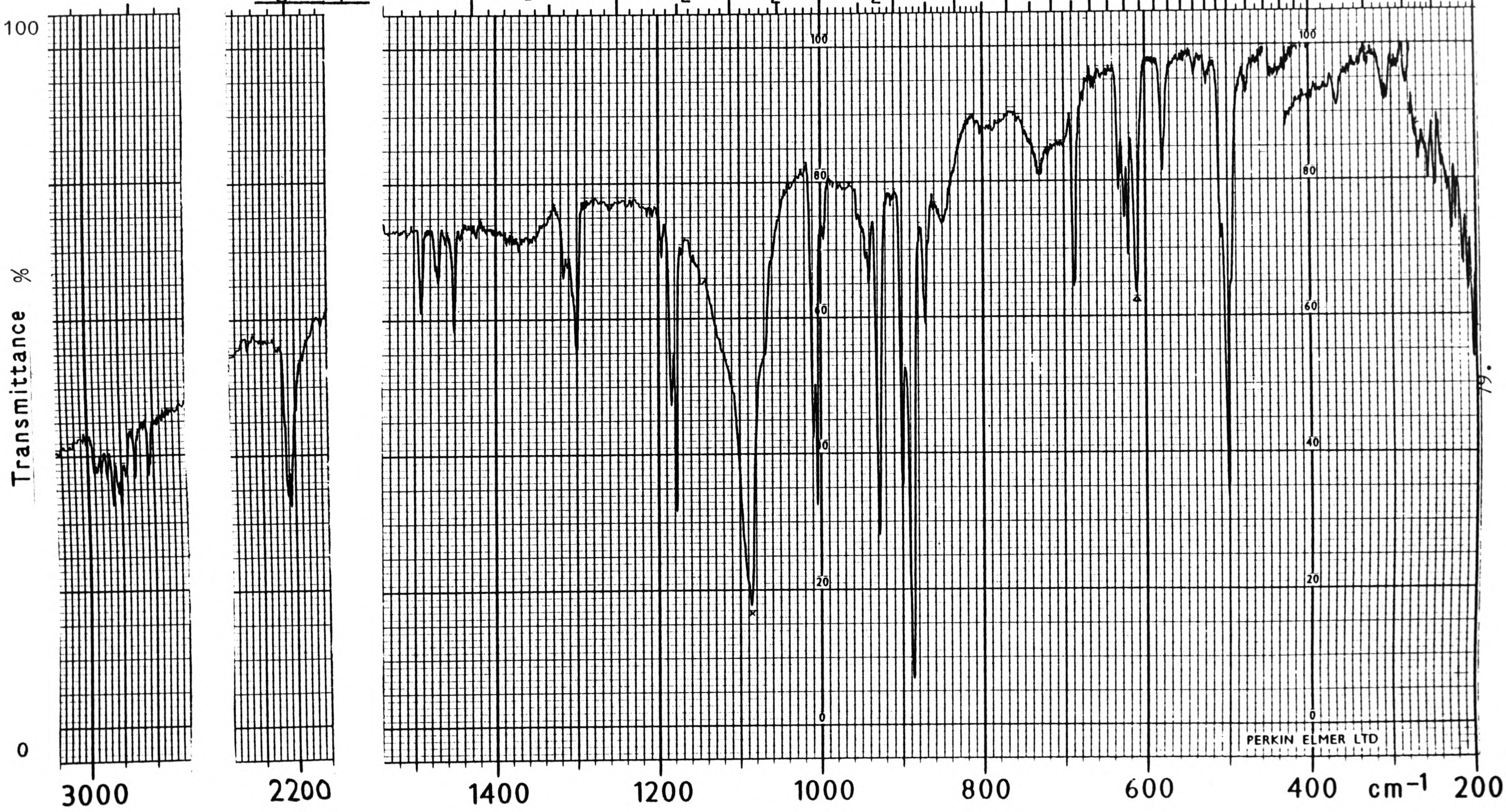

x = Cell blank

△ = Impurity

Figure 4.3 Infra-red spectrum of $SiH_2Cl^{15}NMe_2$ in the gas-phase.

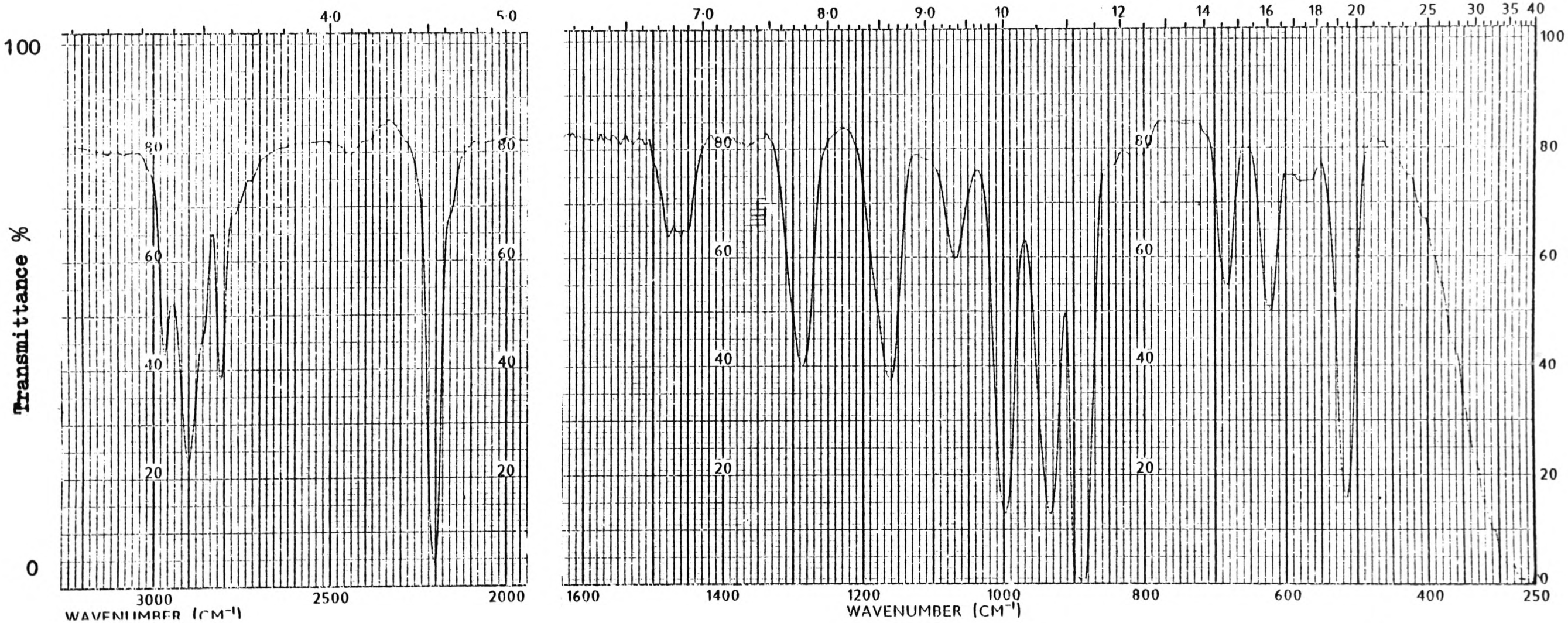

have C_s symmetry and it therefore has 18A' and 15A" modes of vibration, all of which are infra-red and Raman active. The methyl groups will give rise to 6 C-H stretching modes, 6 deformations, 4 rocks and 2 torsional modes about the C-N bonds. The SiH_2 group yields two stretching vibrations (sym/asym) and four deformations. The other stretching modes are for the Si-N, C-N (sym/asym) and Si-Cl vibrations. The remaining modes all involve deformations of the heavy atom $ClSiNC_2$ skeleton, including the Si-N torsional mode.

In the C-H stretching region the gas-phase and the matrix isolated infra-red spectra of $SiH_2Cl^{14}NMe_2$ and the gas-phase IR spectrum of $SiH_2Cl^{15}NMe_2$ are all very similar. Essentially three distinct absorptions occur at $\simeq$2,976cm^{-1}, 2,904cm^{-1} and at 2,816cm^{-1}. The two higher frequency signals are assigned to the asymmetric C-H stretches (2A' + 2A") and the lower frequency absorption to the symmetric stretches (A'+A"). Durig[48] makes more specific assignments for the asymmetric modes, but without any obviously discernable band shapes, this is not really possible here. This region is also complicated by the presence of overtone and combination bands of the methyl deformations. In the liquid Raman spectrum the highest frequency signal is shifted down to 2,965cm^{-1} whilst the other high frequency peak moves up to 2,927cm^{-1}. The absorption assigned to the symmetric stretches is shifted to lower frequency at 2,805cm^{-1}.

The Si-H stretches give rise to strong bands which are found at 2,206cm^{-1} and 2,194cm^{-1} in the gas-phase infra-red and Raman spectra, respectively. In the matrix spectrum however, two peaks are observed at the higher frequencies of 2,224 and 2,215cm^{-1}, and these can be attributed to the asymmetric and symmetric Si-H stretches respectively.

The region between 1,500-1,400cm^{-1} contains the methyl deformations. The infra-red spectra in this region consist of a broad absorption ($\simeq$60cm^{-1} wide) with certain discernable peaks at 1,485cm^{-1}, 1,469cm^{-1}, 1,464cm^{-1} and 1,455cm^{-1} in the gas-phase for $SiH_2Cl^{14}NMe_2$. The spectrum for $SiH_2Cl^{15}NMe_2$ is essentially the same, with the Raman spectrum of $SiH_2Cl^{14}NMe_2$ having bands at 1,485cm^{-1} and 1,442cm^{-1}. By analogy with $NHMe_2$,[72] the bands at 1,455cm^{-1}(IR) and 1,442cm^{-1}(R) are assigned as the symmetric (A'+A") deformations, whilst the remaining high frequency signals are attributed to the asymmetric deformations (2A'+2A"). Again, without accurate polarisation data and gas-phase band shapes, it is unreasonable to make more specific assignments in this region.

Below 1,400cm^{-1}, the four CH_3 rocks and the two C-N stretches occur, but assignments are complicated by the considerable mixing of these modes when the symmetry species are the same.

The band at 1,303cm^{-1} in the gas-phase infra-red and 1,296cm^{-1} in the liquid Raman spectrum is assigned to the CH_3 rock (A') which is coupled to the C-N symmetric stretch. This absorption undergoes an isotopic shift (-12cm^{-1}) on replacement of N^{14} with N^{15}. This band is at considerably higher frequency than the analogous band for $NHMe_2$[72] (1,240cm^{-1}) and it is thought that this is due to additional coupling to the Si-N stretch, also of A' symmetry.[48,74].

The bands at 1,189cm^{-1} in the gas-phase infra-red spectrum of $SiH_2Cl^{14}NMe_2$, have their counterparts in the matrix spectrum at 1,184cm^{-1} and 1,178cm^{-1} (a doublet) and 1,073cm^{-1} respectively. Only one band is observed at 1,074cm^{-1} in the Raman spectrum in this region, although the other signal was probably too weak to detect. These are assigned as the two asymmetric CH_3 rocks(A"), and they will also be coupled, but to the C-N asymmetric stretch(A"). The band at

higher frequency is shifted to lower frequency by 33cm^{-1} on ^{15}N substitution, whilst the other band is essentially unmoved. This effect was also observed for SiH_3NMe_2.[74] The C-N symmetric stretch is assigned as the very strong absorption at 1,009cm^{-1} in the gas-phase infra-red, at 1,008cm^{-1} (weak) in the Raman spectrum and the doublet at 1,010 and 1,005cm^{-1} in the matrix spectrum. This band undergoes a shift to lower frequency of 8cm^{-1} on replacement of ^{14}N with ^{15}N, which is analogous to the shift of 7cm^{-1} observed for SiH_3NMe_2.[74] The fourth CH_3 rock (A') which is assigned to the band at 1,147cm^{-1} [74]/1,149cm^{-1} [48] for SiH_3NMe_2 (in the gas-phase) is not observed in any of the spectra for $SiH_2Cl^{14}NMe_2$ or $SiH_2Cl^{15}NMe_2$. Similarly, the asymmetric C-N stretch, which Durig[48] only observed as a very weak band in the Raman liquid spectrum, is not detected in either the infra-red or Raman of $SiH_2Cl^{14}NMe_2$ or $SiH_2Cl^{15}NMe_2$, presumably due to its weak nature.

The Si-H_2 deformations all occur below 1,000cm^{-1}, with the SiH_2 bend and wag giving rise to a characteristic pattern in the gas-phase infra-red spectrum. These are observed at 936cm^{-1} and 894cm^{-1} respectively for $SiH_2Cl^{14}NMe_2$, and although both bands are very intense, the lower frequency wag is always the stronger. The matrix infra-red spectrum is very similar, although here the wag is seen as a doublet with a splitting of 12cm^{-1}. In the Raman spectrum these modes are observed at 929cm^{-1} and 887cm^{-1}, and here the band is slightly more intense, although both bands are considerably weaker than those observed in the infra-red spectra. These assignments agree well with those of Ebsworth et al[76] for methylsilylhalides. As expected, N^{14}-N^{15} exchange has no effect on the frequencies of these absorptions. The SiH_2 twist is assigned as the very weak band at 769cm^{-1} in the gas-phase infra-red, and at 775cm^{-1} in the Raman

TABLE 4.1

OBSERVED FREQUENCIES (cm^{-1}) AND ASSIGNMENTS FOR CHLOROSILYL-N,N-DIMETHYLAMINE

Infra-Red* Gas	Infra-Red* Matrix(N_2)	Raman* Liquid	Infra-Red+ Gas	Assignment
	2,982w			
2,976m	2,974w	2,965w	2,970m	
	2,962w			
	2,944w			νas (C-H) (2A'+2A") and overtones and combination bands due to $-CH_3$ deformations
	2926w	2,927m		
	2,910w			
2,904s	2,900w	2,897m	2,904s	
2,894m,sh	2,887w		2,888m,sh	
2,867m,sh	2,858w	2,851m	2,868m,sh	
2,816m	2,817w	2,805m	2,812m	
				νs(C-H), (A'+A")
	2,811w			
	2,233m,sh			
	2,227m,sh			
	2,224m			
2,206vs	2,215m	2,194vs(p)	2,203vs	ν (Si-H), (A'+A") s/as
	2,209m,sh			
	2,197m,sh			
1,500w,sh				
1,494w,sh	1,491w			
1,485w		1,485w	1,481w	δ as(C-H), (2A'+2A")
	1,472w,sh			
1,469w	1,470w		1,469w,sh	
1,464			1,463w	

TABLE 4.1 (continued)

OBSERVED FREQUENCIES (cm^{-1}) AND ASSIGNMENTS FOR CHLOROSILYL-N,N-DIMETHYLAMINE

Infra-Red* Gas	Infra-Red* Matrix(N_2)	Raman* Liquid	Infra-Red+ Gas	Assignment
1,455w	1,450	1,442m	1,455w	δs(C-H), (A'+A")
			1,452w,sh	
	1,316w			
	1,311w,sh			ρ(C-H), (A')
	1,304m,sh			
1,303s	1,300m	1,296m	1,291s	
1,189s]	1,184m			
]PR				ρ(C-H), (A")
1,185s]	1,178s		1,166s	
1,079w]	1,073m			
]PR				ρ(C-H), (A")
1,073w]	1,069m	1,074vw	1,072w	
1,015s,sh				
1,009a	1,010s	1,008w	1,001s	νs(C-N), (A')
1,006s,sh	1,005s			
	996w			
941s,sh				δs(Si-H), (A')
936s	929s	929m	937s	
901vs	900s		901vs	
894vs				δw(Si-H), (A')
890vs	888vs	887m	892vs	
833vw	849vw	835vw		
769vw	730vw	775m	n.o.	δt(Si-H), (A")

TABLE 4.1 (continued)

OBSERVED FREQUENCIES (cm^{-1}) AND ASSIGNMENTS FOR CHLOROSILYL-N,N-DIMETHYLAMINE

Infra-Red* Gas	Infra-Red* Matrix(N_2)	Raman* Liquid	Infra-Red+ Gas	Assignment
696m,sh				
689m	688m	695vs	690m	ν(Si-N), (A')
684m,sh	687m			
	632m			
628]	625m	629w	630]	ρ(Si-H),(A")
]PR			]PR	
623]	621m		625]	
523s,sh	508m,sh		523s,sh	
519s	501s	506vs	519s	ν(Si-Cl), (A')
515s,sh	496m,sh		514s,sh	
	476vw			
		378m		δ(CNC), (A')
371vw	367vw	370m		
	309vw,sh			
298vw	305	303		
	283			δ(SiNC), (A")?
		203		
		157		
		111		τ(Si-N), (A")

* $SiH_2Cl(^{14}N\ Me_2)$

+ $SiH_2Cl(^{15}N\ Me_2)$

Abbreviations: w = weak, m = medium, s = strong, v = very, sh = shoulder.

spectrum. This deformation involves only a small dipole change, and is consequently only weakly infra-red active, whilst being significantly stronger in the Raman spectrum. In the matrix infra-red spectrum, this band is shifted down to 730cm^{-1}.

The Si-N stretching vibration (A') is assigned as the strong polarised band at 695cm^{-1} in the Raman spectrum and at 689cm^{-1} in the gas-phase infra-red spectrum. This compares with the values of 670cm^{-1} and 665cm^{-1} for ν(Si-N) in SiH_3NMe_2[48,74] and SiF_3NMe_2[78] respectively, in the gas-phase. It is likely that this band is coupled to the symmetric C-N stretch, and surprisingly this absorption does not shift to lower frequency on isotopic substitution with ^{15}N. The matrix infra-red spectrum has this absorption centred at 688cm^{-1}, which is quite consistent with the other spectra. The final SiH_2 deformation, the rock, occurs at 629cm^{-1} in the Raman liquid spectrum and at 628 and 623cm^{-1} in the gas-phase infra-red spectrum, these clearly being the P and R branches of a B-type band. The matrix infra-red spectrum yields three bands here, centred at 625cm^{-1}.

The Si-Cl stretching vibration (A') is observed as a strong band at 519cm^{-1} in the gas-phase infra-red spectra of both $SiH_2Cl^{14}NMe_2$ and $SiH_2Cl^{15}NMe_2$, this compares with 527cm^{-1} and 551cm^{-1} for CH_3SiH_2Cl[76] and SiH_3Cl[79] respectively, which is not unreasonable on the basis of mass effects. This band is also strong in both the Raman and matrix infra-red spectra, but it is shifted down to 506cm^{-1} and 501cm^{-1} respectively in these spectra. This effect cannot be interpreted as being indicative of any intramolecular association, since no corresponding effect is observed for the Si-N stretch, although it is probably indicative of some bond lengthening.

Below 400cm^{-1}, assignment of the observed bands becomes more

difficult, since far infra-red data was not obtained and the bands expected in this region tend to be weak. For SiH_2ClNMe_2 the bands expected in this region are the two methyl torsions (A'+A"), the ClSiN(A') bend and the CNC and SiNC deformations (2A'+2A") which includes the Si-N torsion. The CNC bend (A') is assigned as the absorption at 384cm^{-1} and 360cm^{-1} in the gas-phase infra-red spectra of $NHMe_2$[72] and SiH_3NMe_2,[48] repectively. $SiH_2Cl^{14}NMe_2$ gives rise to weak bands in the gas phase and matrix infra-red spectra at 371cm^{-1} and 367cm^{-1} respectively. The Raman spectrum in this region contains bands at 378cm^{-1} and 370cm^{-1}, these are therefore assigned as the CNC bend (A').

The remaining two assignments for $SiH_2Cl^{14}NNMe_2$ are for the out of the plane SiNC (A") deformation and the Si-N bond torsion (A") deformation and the Si-N band torsion (A"). These are both tentative and are based upon the observations of Durig et al[48] for SiH_3NMe_2 where they are found at 268cm^{-1} and 115cm^{-1} in the gas-phase infra-red spectrum, respectively. Other bands are observed for $SiH_2Cl^{14}NMe_2$ in this region, but none of these can be firmly assigned to the missing methyl torsions and the in plane SiNC(A') deformation. The Raman spectra of SiH_2ClNMe_2 and SiH_2BrNMe_2 contain similar bands at 157cm^{-1} and 152cm^{-1} respectively, which could be due to δ (SiNC),(A'), but this mode is assigned to a band under one of methyl rocks at $\simeq$234cm^{-1} in SiH_3NMe_2[48]. It is this low frequency, high amplitude deformation involving inversion at nitrogen which is associated with the shrinkage effects which are significant for silylamines with planar or near-planar geometries. Further information in the region below 300cm^{-1} for a series of related compounds with isotopic labelling is required before concrete assignments for this, and the other low frequency modes, can be made.

4.3 VIBRATIONAL SPECTRA OF SiH_2BrNMe_2 (EXCLUDING SOLID PHASE SPECTRA)

The vibrational spectra of SiH_2BrNMe_2 and SiH_2ClNMe_2 are very similar. This is not surprising, since, by a gas-phase electron diffraction study, this molecule is also found to be slightly distorted from C_s symmetry. Assuming this point group then, like SiH_2ClNMe_2 this molecule will have 18A' and 15A" vibrational modes, all of which will be both infra-red and Raman active. The infra-red spectra for SiH_2BrNMe_2 are illustrated in Figures 4.4 and 4.5 and a vibrational assignment is made in Table 4.2, which includes Raman data.

In the C-H stretching region, the gas-phase infra-red spectrum shows three distinct absorptions at 2,974cm^{-1}, 2,907cm^{-1} and 2,815cm^{-1}. These are analogous to those observed for SiH_2ClNMe_2 and similarly the two highest frequency absorptions are assigned to the asymmetric stretches (2A'+2A"), and the remaining band is assigned to the symmetric modes (A'+A"). The matrix isolated spectrum in this region is more complicated, and shows considerable splitting, presumably of the symmetric and asymmetric modes. As with SiH_2ClNMe_2 it is not possible to be more specific about these modes without observing suitable band shapes or having good polarisation data.

The two Si-H stretches appear as a single band in the gas-phase infra-red and Raman (liquid) spectra. In the matrix spectrum, however, a clear doublet splitting of 15cm^{-1} is apparent and this is likely to be due to the symmetric and asymmetric stretches with the asymmetric mode being assigned to the higher frequency absorption.

The methyl group deformations occur below 1,500cm^{-1} and these give rise to broad bands in the gas and liquid phase spectra. The matrix spectrum shows three distinct bands in this region (at $\simeq$1,490,

Figure 4.4 Infra-red spectrum of SiH_2BrNMe_2 in the gas-phase.

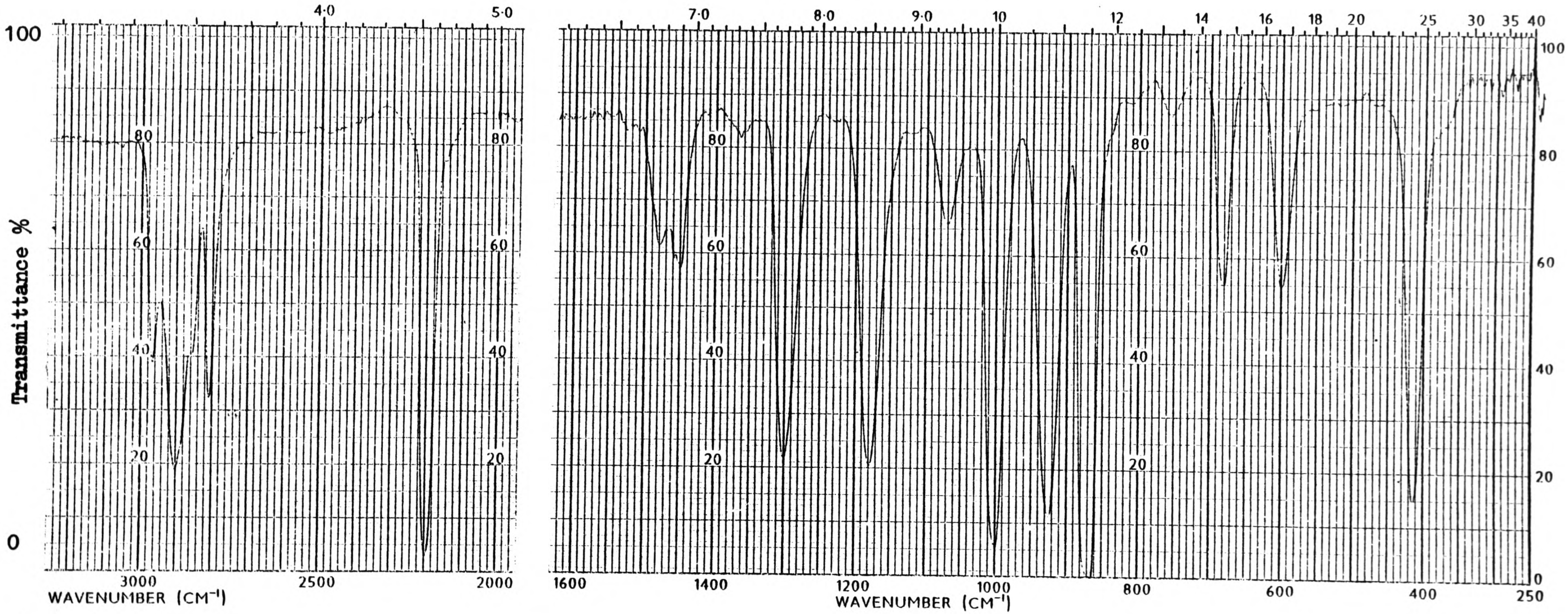

Figure 4.5 Infra-red Spectrum of SiH_2BrNMe_2 in an N_2 matrix (1:578).

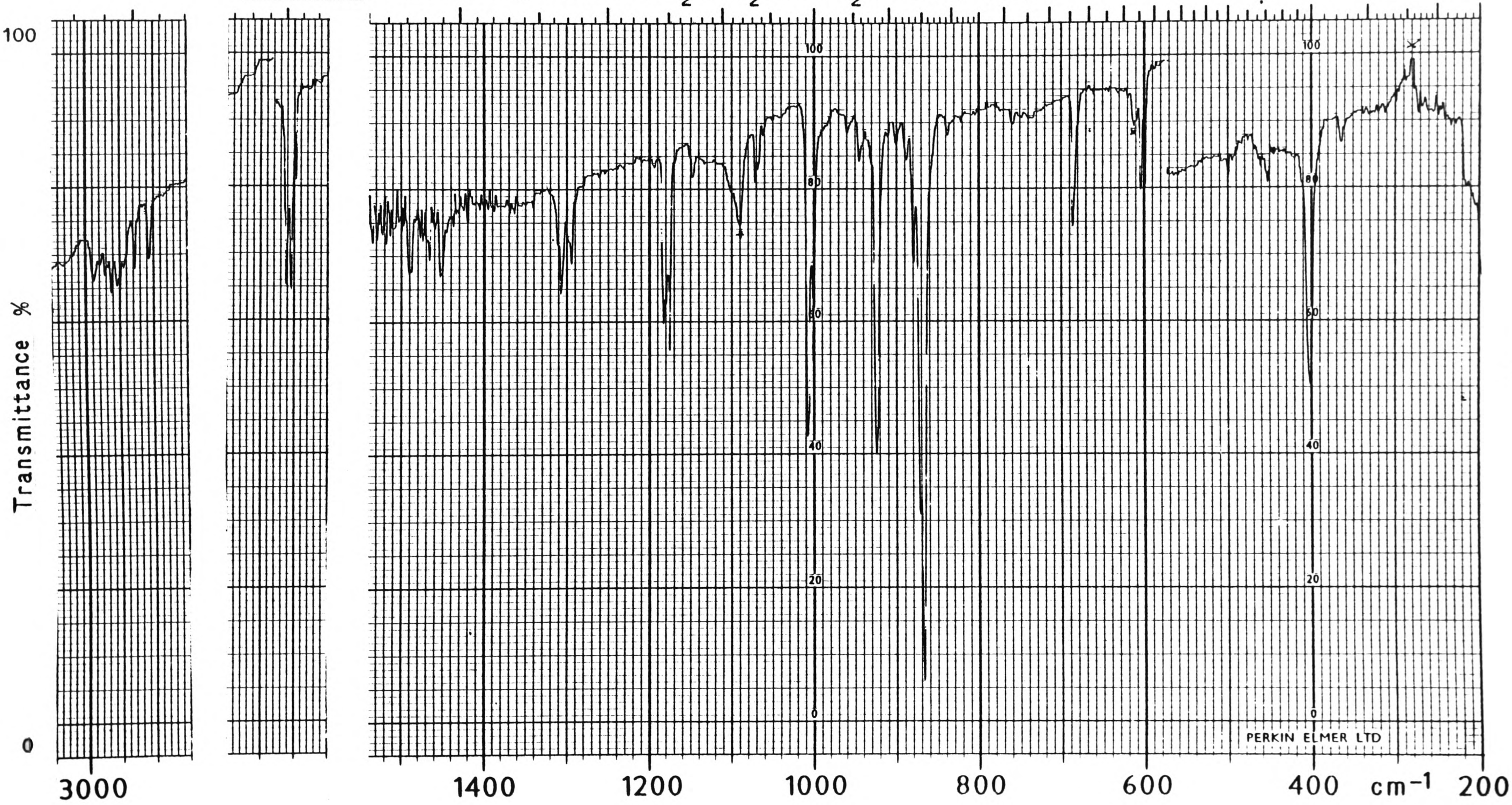

+ = Cell blank

1,468 and 1,450cm^{-1}) and as for $NHMe_2$[72] and SiH_2ClNMe_2 the two highest frequencies absorptions are assigned to the asymmetric modes (2A'+2A") and the remaining band at 1,450cm^{-1} is assigned to the symmetric deformations (A'+A"). As with SiH_2ClNMe_2 good polarisation data in this region would be required to allow individual assignments to be made.

The region between 1,400cm^{-1} and 1,000cm^{-1} contains the absorptions due to the C-N stretches and the methyl group rocks and, in an analogous manner to SiH_3NMe_2[48,74] and SiH_2ClNMe_2 there is considerable mixing of some of these modes. This contrasts with dimethylamine[72] where the two C-N stretches occur at 930cm^{-1}(νs) and 1,022cm^{-1}(νas), and mixing is less significant. The highest frequency band occurs at 1,305cm^{-1} and 1,297cm^{-1} in the gas and liquid phases respectively, and this is attributed to the CH_3 rock (A'), again coupled to the CN symmetric stretch. As with SiH_2ClNMe_2 this band is shifted to higher frequency than the analogous band in $NHMe_2$[72] (1,240cm^{-1}) due to coupling with the Si-N stretch (A').

The band at 1,076cm^{-1} in the gas phase infra-red spectrum has its Raman counterpart at 1,070cm^{-1} and this band, and the strong infra-red bands at $\simeq$1,180cm^{-1} are respectively ascribed to the two CH_3 rocks (A"), both coupled to the asymmetric C-N stretch (A").

Finally, in this region, the symmetric C-N stretch is assigned to the bands at 1,013cm^{-1} and 1,003cm^{-1} in the gas and liquid spectra respectively, by analogy with SiH_3NMe_2.[48,74] The matrix isolated spectrum shows a clear doublet splitting of all of the bands in this region which is similar to that observed for SiH_2ClNMe_2. The asymmetric C-N stretch was not observed in any of the spectra and the remaining methyl rock (A') is only tentatively assigned. This is undoubtedly a consequence of the intrinsically weak nature of these modes.

TABLE 4.2

OBSERVED FREQUENCIES (cm^{-1}) AND ASSIGNMENTS FOR BROMOSILYL-N,N-DIMETHYLAMINE

Infra-Red		Raman	Assignment
Gas	Matrix(N_2)	Liquid	
	2,978m		
2,974m	2,970m		
	2,957m		νas(C-H) (2A'+2A") and overtones and combination bands due to CH_3 deformations
	2,942m		
2,917m	2,924m	Spectrum not obtained in this region	
2,907m	2,908m		
	2,899m		
2,889m	2,888m		
2,862m	2,857m	2,854vw	
2,815m	2,815m	2,800vw	νs(C-H) (A'+A")
2,785m,sh			
	2,229s,sh		
2,206s	2,225,s		νs/as(Si-H), (A'+A")
2,193s	2,210s	2,190s	
	2,205s,sh		
	1,490m		
1,486w/m	1,487m	1,486w	δas(C-H), (2A'+2A")
1,478w/m			
1,470w/m	1,469m		
1,463w/m	1,465m		

TABLE 4.2 (continued)

OBSERVED FREQUENCIES (cm^{-1}) AND ASSIGNMENTS FOR

BROMOSILYL-N,N-DIMETHYLAMINE

Infra-Red		Raman	Assignment
Gas	Matrix(N_2)	Liquid	
1,457w/m	1,452m		δs(C-H) (A'+A")
1,453w/m	1,450m	1,440m	
	1,448m,sh		
	1,311m,sh		
1,305s	1,307m		ρ(C-H), (A')
	1,298m,sh		
	1,294m	1,297m	
1,185s	1,182s		ρ(C-H), (A")
	1,179s,sh		
	1,174s		
		1,143vvw	ρ(C-H), (A')
1,076w	1,070w	1,070vw	
	1,067w		ρ(C-H), (A")
	1,065w,sh		
	1,062w		
1,013s	1,007s	1,003m	
	1,005s,sh		νs(C-N), (A')
1,007s	999s		
930s	923s	917m	δs(Si-H), (A')
881vs	878m		
875vs	870vs		δw(Si-H), (A')
871vs	865vs	859m	
760w	759vw	758m	δt(Si-H), (A")
	737vw		

TABLE 4.2 (continued)

OBSERVED FREQUENCIES (cm^{-1}) AND ASSIGNMENTS FOR BROMOSILYL-N,N-DIMETHYLAMINE

Infra-Red		Raman	Assignment
Gas	Matrix(N_2)	Liquid	
686m	686m	683s	ν(Si-N), (A')
		653	
603m	604m	603w	ρ(Si-H), (A")
	598m	588w	
419s	400s	396vs	ν(Si-Br), (A')
367w	364w	368m	δ(CNC), (A')
		268m	δ(SiNC), (A")
		152m	

Abbreviations: w = weak, m = medium, s = strong, v = very
sh = shoulder

The bending and wagging SiH_2 group deformations give rise to very intense absorptions in the infra-red spectra. These shift from 930cm^{-1} and $\simeq$880cm^{-1} respectively in the gas phase to 923cm^{-1} and $\simeq$874cm^{-1} in the matrix spectrum, and more significantly to 917cm^{-1} and 859cm^{-1} in the Raman spectrum. Shifting of this type, of the $-SiH_2$ deformational modes on condensation is quite common in silyl compounds.[80] Again, a doublet is observed for the 'wag' in the matrix isolated spectrum.

The $-SiH_2$ torsion or twist is assigned to the bonds at 760cm^{-1} and 758cm^{-1} in the gas and liquid phases respectively and predictably this bond is only weakly active in the infra-red spectra.

The Si-N stretch in SiH_2BrNMe_2 is ascribed to the bands at 686cm^{-1} and 683cm^{-1} in the gas and liquid phase spectra respectively, and the absence of any sign of shifting of this mode in the liquid phase suggests that there is no significant intermolecular interaction occurring. As with SiH_2ClNMe_2 this band occurs at relatively low frequency due to coupling with the symmetric C-N stretch, and there is no indication of any splitting of this band in the matrix spectrum.

By analogy with the other monohalosilyl-amines and other $-SiH_2$[76] compounds, the SiH_2 rocking deformation (A") was assigned to the bands at 603cm^{-1} in all three spectra. The gas-phase spectrum gave no indication of a B-type band-shape for this or any other vibrational mode, hence all assignments were made by comparison with other appropriate spectra.

The band due to the silicon-halogen stretching vibration, ν(Si-Br), is observed as an intense band at 419cm^{-1} in the gas-phase infra-red spectrum. This mode occurs at 430cm^{-1} and $\simeq$415cm^{-1} respectively, in the corresponding spectra of SiH_3Br and $MeSiH_2Br$.

This band, like that of ν(Si-Cl) in SiH_2ClNMe_2 shows distinct shifting to lower frequency ($396cm^{-1}$) in the Raman spectrum, and again this is probably due to some bond lengthening in the liquid phase.

Absorptions in the region below $400cm^{-1}$ are again difficult to assign, since the spectra have lower frequency limits of $250cm^{-1}$, $200cm^{-1}$ and $\simeq 100cm^{-1}$ in the gas, matrix and liquid phases respectively. The only band in this region which can be assigned with any certainty is the CNC bend (A') at $367cm^{-1}$ and $368cm^{-1}$ in the gas and liquid phases. The position of this band is quite consistent with that observed in the other halosilyl-amines and in $NHMe_2$[72,73] and SiH_3NMe_2.[48] A medium intensity signal is detected in the Raman spectrum at $268cm^{-1}$ and this is probably due to the out of plane SiNC deformation, since this mode occurs at the same frequency in the gas phase infra-red spectrum of SiH_3NMe_2.[48] The lowest frequency Raman band at $153cm^{-1}$ is analogous to the band at $157cm^{-1}$ for $SiH_2ClN^{14}Me_2$ and is therefore more likely to be due to the in plane SiNC deformation rather than the XSiN bending mode, although its position is inconsistent with the assignment made by Durig.[48] Again, no indication of bands due to the two methyl torsions was observed.

4.4 VIBRATIONAL SPECTRA OF SiH_2INMe_2 (EXCLUDING SOLID PHASE SPECTRA)

In the gas-phase SiH_2INMe_2 is found, by electron diffraction, to have perfect C_s symmetry and it should therefore have analogous vibrational spectra to SiH_2XNMe_2 (X = Cl,Br) with identical numbers of infra-red and Raman active modes. This is certainly the case for the gas-phase infra-red spectrum. The liquid Raman spectrum however, although incomplete, is distinctly different in some regions and this is probably due to presence of extra bands, particularly in the νSi-N

and 1,000-800cm^{-1} regions, caused by decomposition of the sample. This is not unreasonable, since the Raman tube had to be heated to ≃330K to liquify the sample of SiH_2INMe_2 which normally sublimes. The following discussion will therefore exclude any references to the Raman spectrum. The gas-phase infra-red spectrum is shown in Figure 4.6 and a vibrational assignment is given in Table 4.3.

The region between 3,000cm^{-1} and 2,800cm^{-1} contains the C-H stretching modes and again these are very similar to those of SiH_2XNMe_2 (X = Cl & Br) with three principal bands at 2,969cm^{-1}, 2,903cm^{-1} and 2,811cm^{-1}. Comparing the absorption frequencies for the three compounds in the gas-phase, slight shifts to lower frequency are noted as the mass of the halide is increased. Similar shifts of ≃2cm^{-1} are also noted in the positions of the C-H deformations. It is not surprising that these shifts are small since these motions will involve almost only hydrogen atom movements, and hence the halide substituents are unlikely to exert too large an effect on the absorption frequencies.

The two Si-H stretches appear as a single band at 2,198cm^{-1} and are similar to those observed for the other halosilyl-dimethylamines. The SiH bending and wagging deformations are assigned to the strong bands at 925cm^{-1} and 849cm^{-1} respectively, and comparing these with their counterparts in the analogous compounds (Table 4.4) it is apparent that these modes shift to lower frequency as the size of the halogen atom increases. Ebsworth et al[76] observed a similar effect in gas-phase infra-red spectra of methyl silyhalides and it is believed that this is related to the electronegativity rather than the mass of the halogen atom.

It is also apparent that the Si-H torsional and rocking modes are similarly affected by the halogen substituent with the rock being

Figure 4.6 Infra-red Spectrum of SiH_2INMe_2 in the gas-phase.

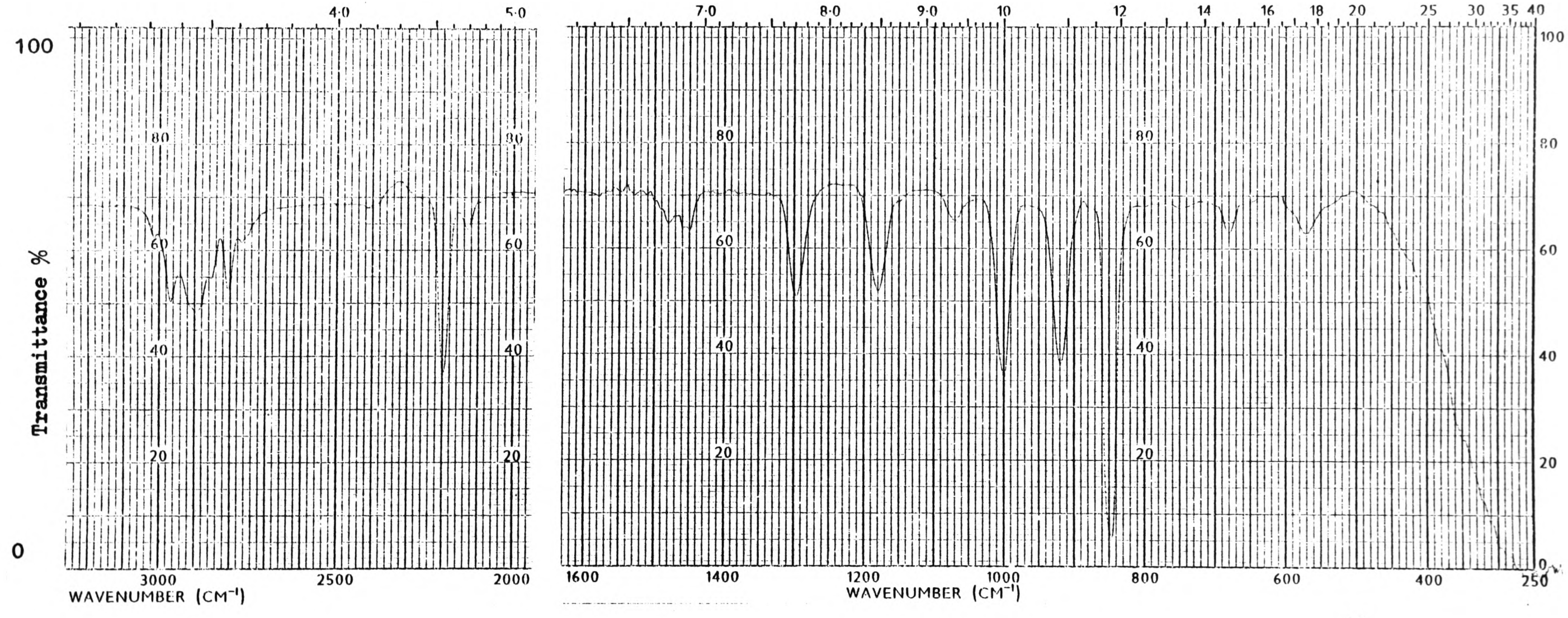

TABLE 4.3

OBSERVED FREQUENCIES (cm^{-1}) AND ASSIGNMENTS FOR IODOSILYL-N,N-DIMETHYLAMINE

Infra-Red Gas	Raman Liquid	Assignment
2,969m		
2,915m,sh	Not recorded	νas (C-H), (2A'+A") and overtones and combination bands due to CH_3 deformations.
2,903m		
2,890m,sh		
2,811m		νs(C-H), (A'+A")
2,198s	2,213s	νs/as (Si-H), (A'+A")
	2,202s	
1,494w/m		
1,483w/m		
1,469w/m	Not recorded	δas (C-H) (2A'+2A")
1,462w/m		
1,452w/m		δs(C-H), (A'+A")
1,301s		ρ(C-H), (A')
1,184s		ρ(C-H), (A")
1,075w	1,098w?	ρ(C-H), (A")
1,009s,sh	991m	νs(C-N), (A')
1,004s	981m	
	952m	
	926s	
	920s	δs(Si-H), (A')
925	914s	
	905w/sh	

TABLE 4.3 (continued)

OBSERVED FREQUENCIES (cm^{-1}) AND ASSIGNMENTS FOR IODOSILYL-N,N-DIMETHYLAMINE

Infra-Red Gas	Raman Liquid	Assignment
855vs,sh	862w	δ_w(Si-H), (A')
849vs		
753w	762w	δ_t(Si-H), (A")
	713m	ν(Si-N), (A')
	706m	
684m	698m	
574w	585w	ρ(Si-H), (A")
383w	Not recorded	δ(CNC), (A')
362m		ν(Si-I), (A')

Abbreviations: w = weak, m = medium, s = strong, v = very, sh = shoulder

TABLE 4.4

SiH_2 DEFORMATION FREQUENCIES FOR
SiH_2XNMe_2 (WHERE X=Cl,Br&I)
IN THE GAS-PHASE (cm^{-1})

Compound	δs(Si-H)	δw(Si-H)	δt(Si-H)	ρ(Si-H)
SiH_2ClNMe_2	936	894	769	625
	-6	-19	-9	-22
SiH_2BrNMe_2	930	875	760	603
	-5	-26	-7	-29
SiH_2INMe_2	925	849	753	574

particularly susceptible to this effect.

The assignments for the methyl rocking modes and the C-N stretches are identical to those of bromo and chloro compounds and the positions of these bands seems to be largely unaffected by the nature of the halogen atom. Again, mixing between some of these vibrations will be significant, and again ν_{as} (C-N) and ρ(C-H), (A') are not observed.

The Si-N stretch occurs at 684^{-1} in the gas-phase infra-red spectrum, so here too shifts of $\simeq -2cm^{-1}$ are detected as Group 7 is descended from Cl. As with the chloro and bromo analogues, there does not seem to any detectable intermolecular association in the liquid phase. It is not possible to correlate the Si-N absorption frequency with bond length, since although ν (Si-N) for SiH_3NMe_2 occurs at $670cm^{-1}$ (i.e. lower frequency than halo-substituted compounds), ν (Si-N) for SiF_3NMe_2 occurs at $665cm^{-1}$ [78] and it contains the shortest Si-N bond.

The other remaining bands above $250cm^{-1}$ are at $383cm^{-1}$ and $362cm^{-1}$. These are assigned as the CNC bend (A') and the Si-I

stretch respectively, on the basis of their intensities and their assignments in related compounds. The Si-I stretching frequencies in SiH_3I[81] and $SiMe_3I$[82] are $\simeq$355cm^{-1} and 331cm^{-1} respectively and these bands will be reasonably strong.

The CNC deformation in $NHMe_2$ however, is relatively weak and occurs at 384cm^{-1}, hence ν(Si-I) is assigned to the lower frequency band. Without further far infra-red or Raman data, no assignments for the $SiNC_2$ group deformations or the methyl torsions can be made.

THE GAS-PHASE INFRA-RED AND MULTINUCLEAR N.M.R. SPECTRA OF SiH_2FNMe_2

4.5 INTRODUCTION

The problems associated with preparing SiH_2FNMe_2 were discussed in chapter 2 and this coupled with its thermal instability (see later) meant that a thorough investigation of its spectroscopic properties was not possible. The presence of the ^{19}F (Spin = $^1/_2$) nuclei, however, allowed a more rigorous characterisation by n.m.r. and this proved invaluable, since the only vibrational information obtained was from a gas-phase infra-red spectrum. This section deals with this spectroscopic data and also details the dissociation products of SiH_2FNMe_2.

4.6 THE VIBRATIONAL SPECTRUM OF SiH_2FNMe_2

The presence of dissociation products, particularly SiH_2F_2 meant that it was difficult to obtain a gas-phase spectrum of a pure sample of SiH_2FNMe_2. A reasonably clean sample was eventually prepared and the spectrum is shown in Figure 4.7. The assignments are listed in Table 4.5, but the frequencies are only approximate, since accurate peak expansions were not recorded. The spectrum merits discussion, however, since it reveals some features which are distinctly different to those of the other monohalosilyl-dimethylamines.

Figure 4.7 Infra-red Spectrum of SiH_2FNMe_2 in the gas-phase.

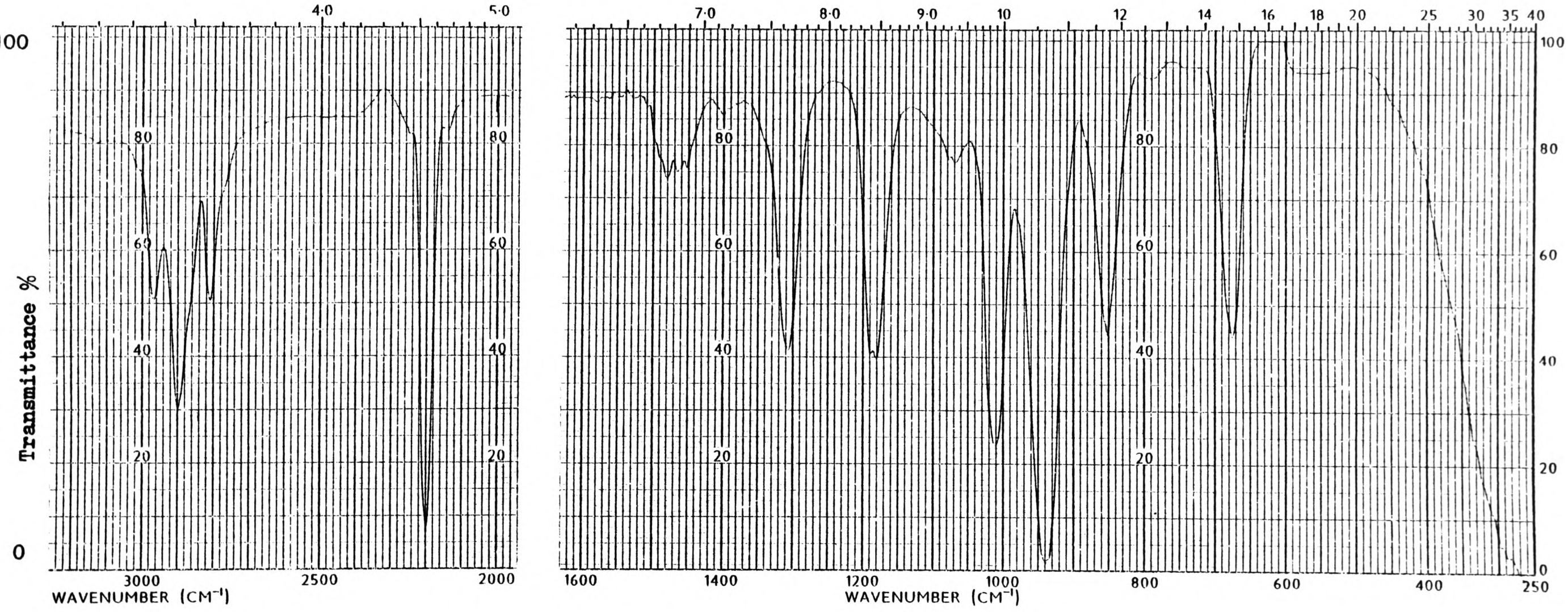

TABLE 4.5

OBSERVED FREQUENCIES (cm^{-1}) AND ASSIGNMENTS FOR FLUOROSILYL-N,N-DIMETHYLAMINE

Infra-Red (gas)	Assignment
2,968m, 2,900s, 2,870m	ν as(C-H), (2A'+2A") and overtones and combination bands due to $-CH_3$ deformations.
2,812m	νs(C-H), (A'+A")
2,200vs	νs/as (Si-H), (A'+A")
1,480m, 1,467m br	δ as(C-H), (2A'+2A")
1,452m	δ s(C-H), (A'+A")
1,308	ρ (C-H), (A')
1,189s, 1,181s PR	ρ(C-H), (A")
1,079w/m, 1,069w/m PR	ρ(C-H), (A")
1,011s	νs(C-N), (A')
940vs,br	δ s(Si-H)+δ w(Si-H)(2A')
852s	ν (Si-F),(A')
790vw	δ t(Si-H),(A")
676s	ν(Si-N)+ρ(Si-H),(A'+A")

N.B. Spectrum was not recorded below $400cm^{-1}$

Abbreviations: w = weak, m = medium, s = strong, v = very, br = broad.

The C-H stretching and bending regions, and the Si-H stretching region are very similar to those of the other SiH_2XNMe_2 compounds and therefore will not be discussed further. The methyl rocking region between 1,350cm^{-1} and 1,000cm^{-1} is however distinctly different. Here, two of the bands, at ≃1,185cm^{-1} and ≃1,075cm^{-1} clearly show B-type band shapes with distinct P&R branches. This feature is only apparent in the expanded spectra of the chloride and is not present in either the bromide or the iodide, due to their greater moments of inertia. This confirms the assignments of Durig[48] for SiH_3NMe_2 that these are the two out-of-plane rocking modes (A"), rather than fully symmetric modes. Once more, the fourth methyl rock is too weak to be observed.

Of the two C-N stretches, again only the symmetric mode is observed and the position of this band is consistent with that of the other halosilyl-dimethylamines. Again, there will be considerable mixing of the modes in this region.

The Si-H deformations between 900cm^{-1} and 1,000cm^{-1} give rise to a distinctly different pattern to those of the other compounds, SiH_2XNMe_2. In SiH_2FNMe_2 the wag is shifted up to higher frequency, resulting in only one broad, very intense bond being observed, with both absorptions being superimposed.

The Si-F stretch occurs at 852cm^{-1} and this is consistent with the values of 872cm^{-1} and ≃858cm^{-1} for SiH_3F[79] and CH_3SiH_2F[76] respectively.

Of the remaining bands, the Si-H torsional mode gives rise to a very weak absorption at 790cm^{-1}, the band at 676cm^{-1}, however, is again more interesting. This is where the Si-N stretch is expected to occur, but as with the Si-H bending mode, the Si-H rocking deformation is shifted to considerably higher frequency, relative to

Figure 4.8 ^{19}F Nmr Spectrum of SiH_2FNMe_2.

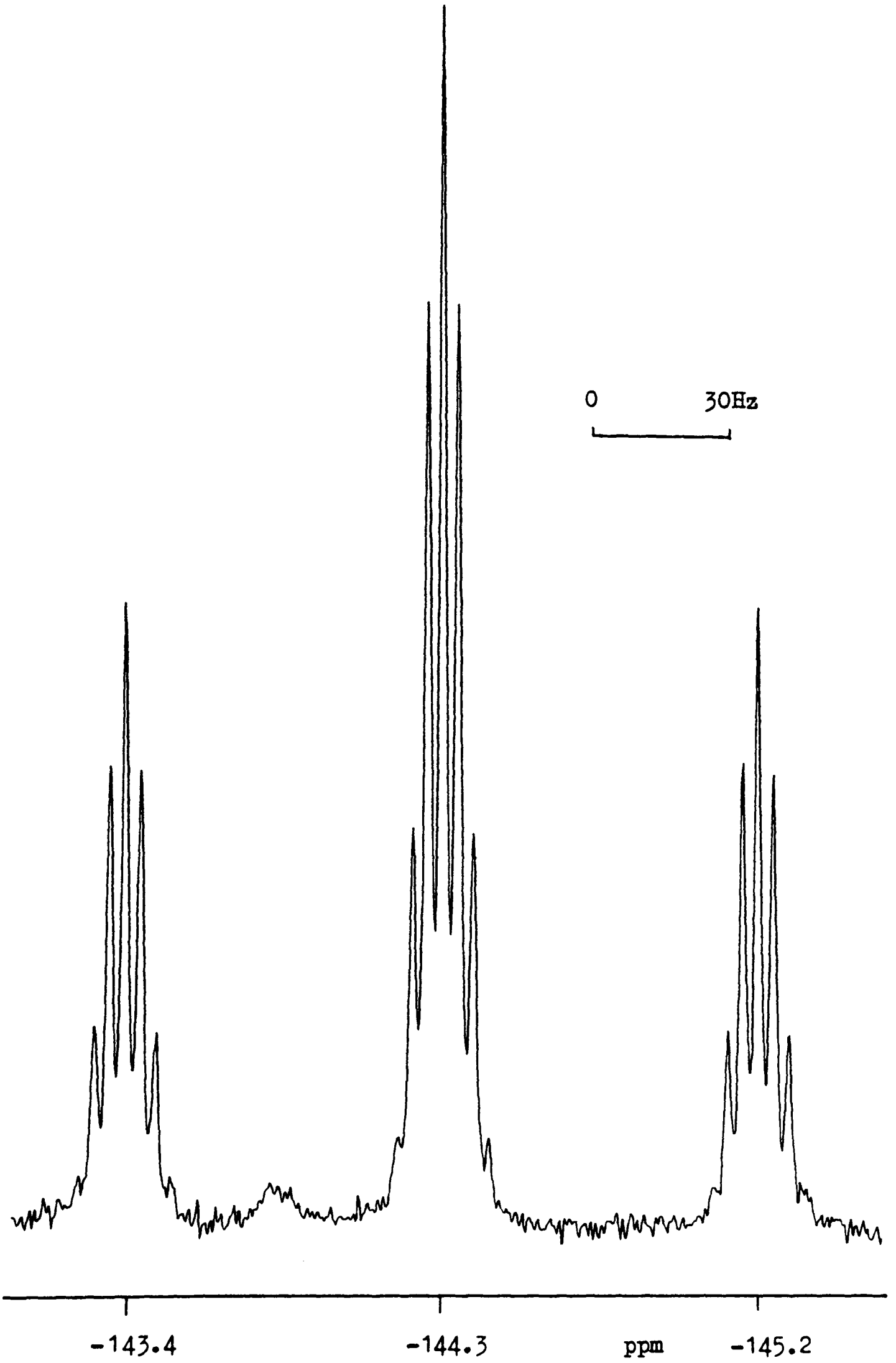

Figure 4.9 ^{19}F Nmr Spectrum of $SiHF_2NMe_2$.

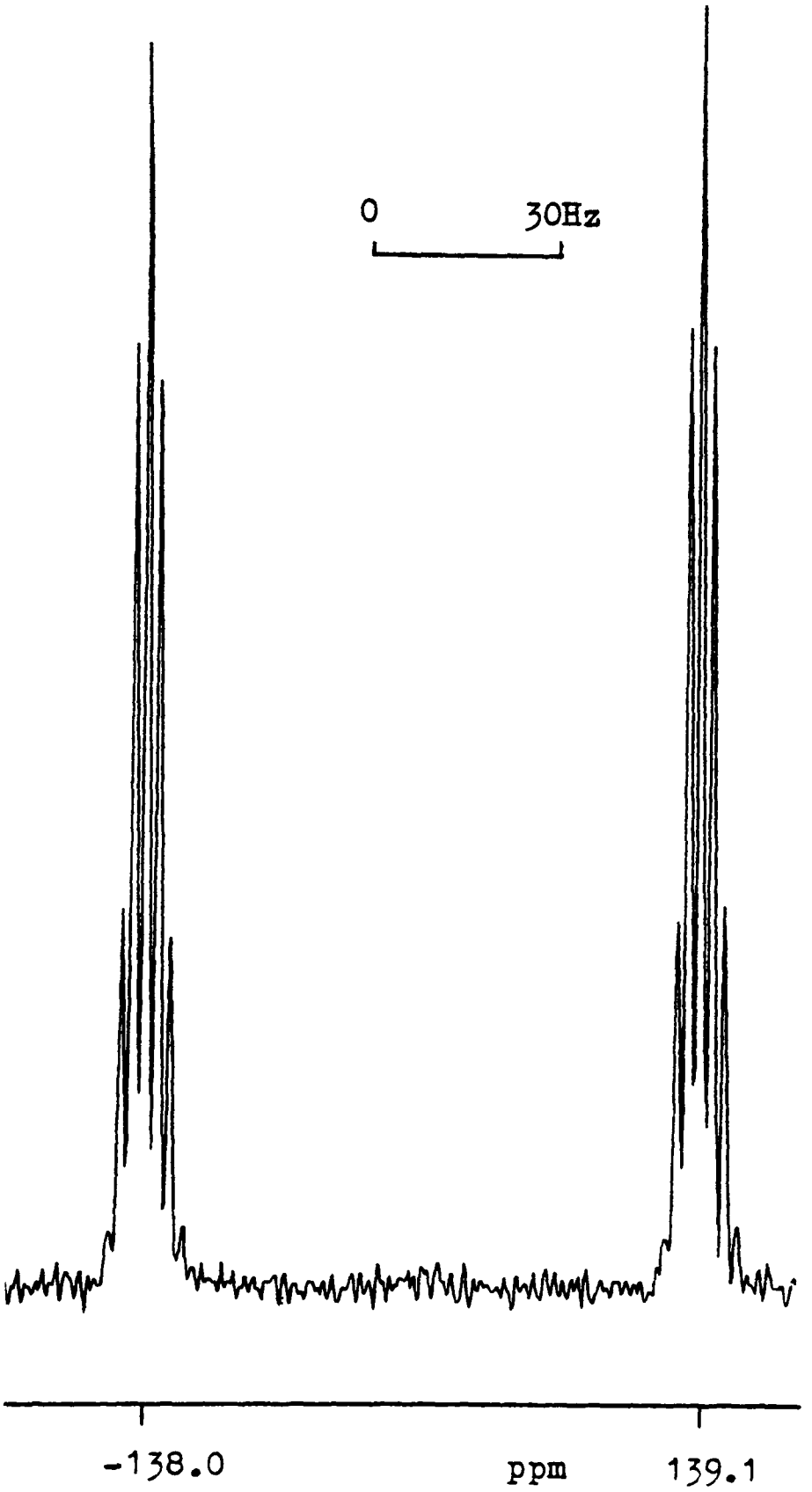

the value of $625cm^{-1}$ for SiH_2ClNMe_2 again resulting in a superimposition of the two bands. This results in a distinctly more intense band than would be predicted for the Si-N stretching vibration alone.

No other bands were observed above $400cm^{-1}$.

4.7 N.M.R. SPECTRA OF SiH_2FNMe_2

Proton, ^{29}Si, ^{19}F and ^{13}C n.m.r. spectra of SiH_2FNMe_2 were recorded and these gave a doublet (with ^{29}Si satellites), a doublet of triplets, a triplet of septets (with ^{29}Si satellites) and a quartet of doublets respectively. The parameters were as follows:

$\delta H_{Si} = 4.39$, $\delta Hc = 2.24$, $\delta^{29}Si = -22.6$, $\delta^{19}F = -144.3$ and $\delta^{13}C = 36.9$

$^2J_{H-F} = 69.5$, $^1J_{Si-H} = 249.9$, $^1J_{H-C} = 133.1$, $^1J_{Si-F} = 307.7$, $^3J_{C-F} = 2.8$ and $^4J_{H-F} = 3.4$

δ's are in p.p.m. and J in Hz.

The ^{19}F spectrum, however, clearly indicated the presence of $SiHF_2NMe_2$ (see Figures 4.8 and 4.9) and on re-running this spectrum overnight at room temperature it was apparent that much of the SiH_2FNMe_2 had disproportionated to yield more $SiHF_2NMe_2$ along with small quantities of SiH_2F_2, $SiHF(NMe_2)_2$ and some other unidentifiable species. The relative broadness of the peaks due to SiH_2FNMe_2 was also noted in the ^{19}F spectrum.

The proton coupled and decoupled ^{29}Si spectra also revealed that a significant amount of $SiH(NMe_2)_3$ was present.

The parameters for $SiHF_2NMe_2$ determined from the ^{19}F spectrum are given below:

$\underline{SiHF_2NMe_2}$: $\delta^{19}F = -138.6$, $^2J_{H-F} = 86.0$, $^1J_{Si-F} = 274$ and $^4J_{H-F} = 1.9$.

$\underline{SiHF(NMe_2)_2}$: $\delta^{19}F = -143.2$, $^2J_{H-F} = 87.7$, $^1J_{Si-F} = N.O.$ and $^4J_{H-F} = 1.8$

N.O. = not observed.

Thus, the thermal instability of SiH_2FNMe_2 at room temperature is clearly illustrated by n.m.r. spectroscopy.

Since the major disproportionation product is $SiHF_2NMe_2$, this may be indicative of the increased thermodynamic stability on formation of a greater number of Si-F bonds.

4.8 VIBRATIONAL SPECTRA OF $SiHCl_2NMe_2$

Infra-red and Raman spectra for $SiHCl_2NMe_2$ have been recorded in various phases, and the infra-red spectra are illustrated in Figures 4.10 and 4.11. A vibrational assignment is given in Table 4.6. The spectra have been interpreted on the basis that the molecule has C_s symmetry, after studies in the gas and solid phases by electron and x-ray diffraction revealed that in both cases the molecule contained a mirror plane. The molecule is therefore expected to have 20A' + 13A" modes of vibration, all of which should be both infra-red and Raman active. The methyl groups give rise to six stretches, six deformations, four rocks and two torsional modes. The Si-H group produces one stretching mode and two deformations.

Finally, the heavy atom $SiCl_2NC_2$ skeleton gives rise to five stretching modes, and seven deformations and bends, including the Si-N bond torsion. The gas-phase infra-red spectrum showed no sign of any distinct band shapes.

In the C-H stretching region the spectra obtained for $SiHCl_2NMe_2$ are essentially the same as those obtained for SiH_2XNMe_2 (where X = Cl,Br,I) and hence the assignment is the same. The distinct band at lowest frequency ($\simeq$2,810cm^{-1}) in all four spectra is assigned to the symmetric C-H stretches (2A'), whilst the remaining bands at higher frequency (2,970-2,850cm^{-1}) are assigned as the asymmetric stretches (2A'+2A"). Again, without the benefit of

Figure 4.10 Infra-red Spectrum of $SiHCl_2NMe_2$ in the gas-phase.

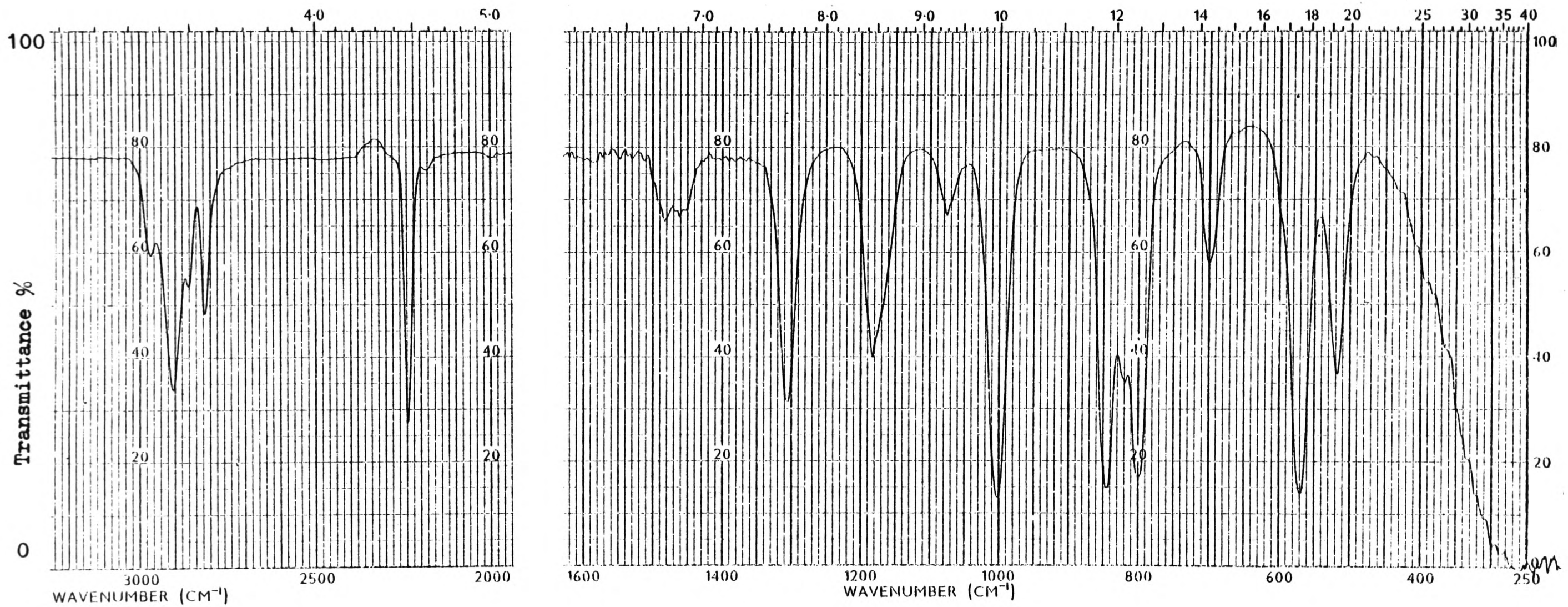

Figure 4.11 Infra-red spectrum of $SiHCl_2NMe_2$ in the solid phase.

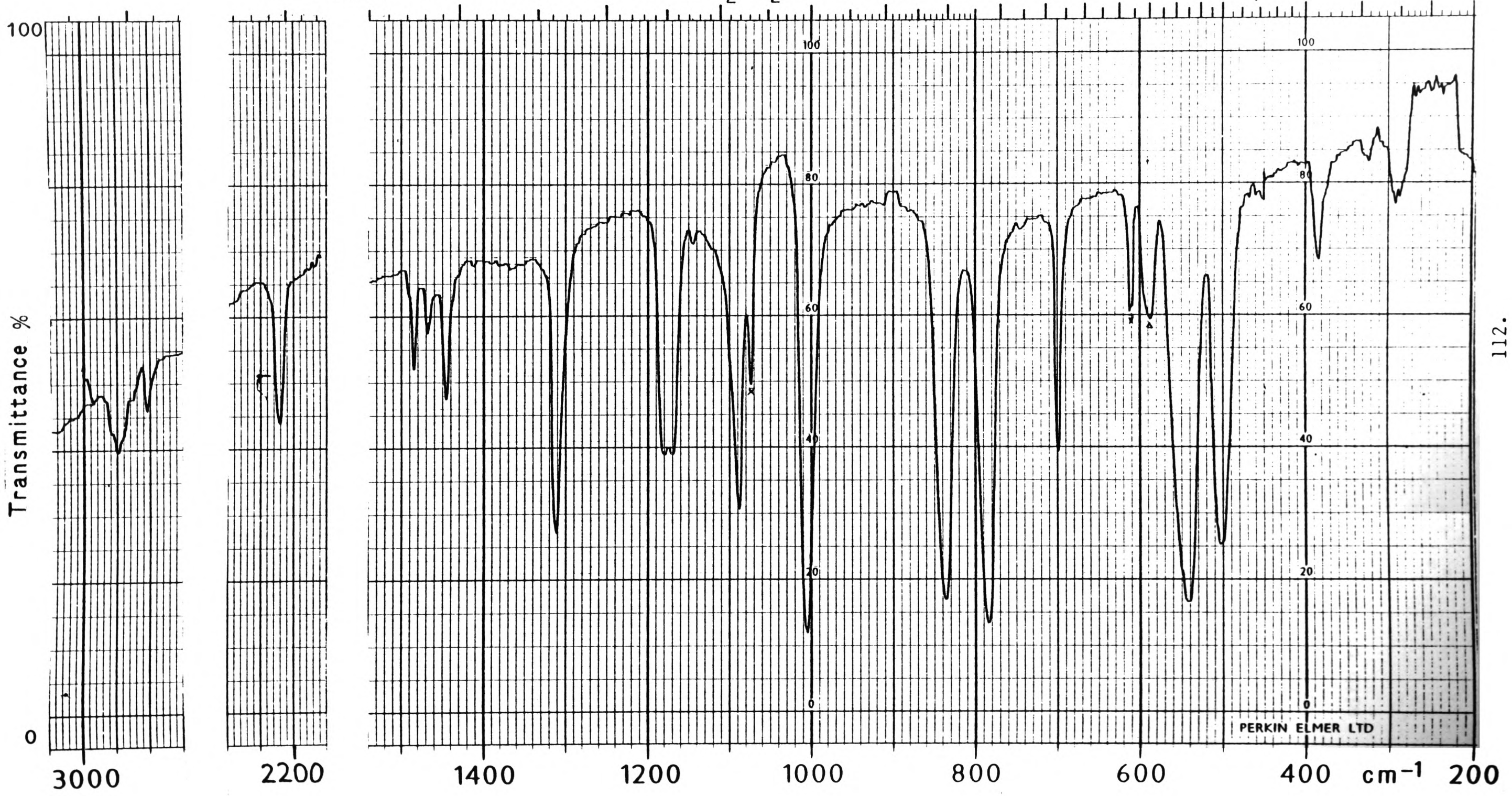

△ = Impurity

distinct band shapes or polarisation data, more specific assignments cannot be made. All of the C-H stretching modes are relatively weak in intensity in the Raman spectra. The Si-H stretch is observed at 2,241cm^{-1} in the gas-phase, and at 2,244cm^{-1} in the solid phase infra-red, and in the solid phase no splitting such as that seen for the symmetric and asymmetric modes in -SiH_2 compounds is observed.

In the region between 1,500 and 1,400cm^{-1}, the C-H deformations appear as a broad band in the gas-phase infra-red spectrum. These absorptions sharpen and split up into five bands in the Raman solid phase spectrum and three bands with shoulders in the solid phase infra-red spectrum. In the Raman spectra, the three principal bands occur at $\simeq$1,488, 1,441 and 1,412cm^{-1} whilst in the infra-red spectra they appear at 1,486, 1,461 and 1,445cm^{-1}, hence a distinct shift of the two lower frequency bands in the Raman spectra is noted. The lowest frequency band in each case is assigned to the symmetric deformations (2A'), whist the remaining bands are assigned as the asymmetric deformations (2A'+2A"). This is analogous to the assignment for SiH_3NMe_2 [48,74] and again good polarisation data would make more specific assignments possible.

The region between 1,400cm^{-1} and 1,000cm^{-1} contains the bands assigned to the 4 methyl rocking modes and the 2 C-N stretches, and again assignments are complicated by mixing of some of the vibrations. This is further complicated in $SiHCl_2NMe_2$ since both the symmetric and asymmetric C-N stretches will have A' symmetry and should also couple unlike the monohalosilyl-dimethylamines. The strong bands in the infra-red and the weak bands at $\simeq$1,310cm^{-1} in the Raman spectra are assigned to the symmetric methyl rock, coupled to both the C-N symmetric and asymmetric stretches; this compares with the value of 1,293cm^{-1} for SiH_3NMe_2.[48] This band is shifted to

slightly higher frequency than the analogous band for the monohalo compounds and this is probably due to the additional coupling to the asymmetric C-N stretch. It should be noted that coupling to the Si-N stretch will also occur. In both the liquid and solid Raman spectra, weak bands are observed at $\simeq$1,147cm^{-1} and 1,102cm^{-1}, which are absent in infra-red spectra, these are assigned to the other symmetric methyl rocking mode and the asymmetric C-N stretch respectively, which were not observed in the spectra of the monohalo-silyl compounds. νas(C-N) is shifted to a distinctly higher frequency for $SiHCl_2NMe_2$ than it is in SiH_3NMe_2[48] (1,030cm^{-1}) and this is probably due to coupling to the symmetric C-N stretch. The remaining two bands in this region are at $\simeq$1,077cm^{-1} (in all four spectra) and at $\simeq$1,185cm^{-1} in the infra-red spectra. These bands are analogous to those observed at 1,189cm^{-1} and 1,075cm^{-1} SiH_3NMe_2[48] in the gas-phase and are therefore assigned as the two asymmetric methyl rocks (A").

Finally, in this region, the very strong infra-red bands at 1,006cm^{-1} and the medium intensity bands at 1,004cm^{-1} and 1,003cm^{-1} in the liquid and solid Raman spectra are assigned to the C-N symmetric stretch. These frequencies are consistent with those observed for SiH_3NMe_2[48,74] and the monohalosilyl-dimethylamines, and are not shifted.

The two Si-H deformations (in plane and out of plane) were assigned to the very strong gas-phase absorptions at 846 and 808cm^{-1}, respectively. These compare with the values of 742-706cm^{-1} and 637-636cm^{-1} for the modes in the series of compounds Me_2SiHX[83,84] where (X = F, Cl,Br,I). It is apparent therefore, that these deformational motions must be distinctly more similar in $SiHCl_2NMe_2$ than in the dimethylsilyl-halides. The lower frequency, out of plane

TABLE 4.6

OBSERVED FREQUENCIES (cm^{-1}) AND ASSIGNMENTS FOR DICHLOROSILYL-N,N-DIMETHYLAMINE

Infra-Red		Raman		Assignment
Gas	Solid	Liquid	Solid	
2,970m	2,972m	2,968w	2,978w	
	2,934m,sh	2,929w	2,931w	
2,911s	2,918s			ν_{as} (C-H) (2A'+2A")
	2,900S		2,903w	and overtones and combination bands
	2,886m,sh			due to CH_3 deformations
2,865m	2,851m	2,856m/w	2,858w	
2,818m	2,809m	2,811m	2,810m	ν_s(C-H), (2A')
2,249sh,s			2,246vs,sh	
2,241s	2,244s	2,236vs	2,243vs	ν(Si-H),(A')
2,233sh,s				
1,494m	1,491m,sh			
1,487m	1,486m	1,487m	1,488m	δ_{as}(C-H), (2A'+2A")
1,469m	1,469m	1,443m/s	1,441m	
1,465m	1,465m,sh		1,433m	
1,456m	1,449m,sh		1,427m,sh	
	1,445m	1,419	1,412	δ_s(C-H), (2A')
	1,437m,sh			
1,309s	1,314vs	1,307m	1,310w/m	ρ(C-H), (A')
		1,146w/m	1,149w/m	ρ(C-H), (A')
1,189sh,s				
1,187s	1,183s			ρ(C-H), (A")
1,179sh,s	1,171s			
		1,103vw	1,101w	ν_{as}(C-N),(A')

TABLE 4.6 (continued)

OBSERVED FREQUENCIES (cm^{-1}) AND ASSIGNMENTS FOR DICHLOROSILYL-N,N-DIMETHYLAMINE

Infra-Red		Raman		Assignment
Gas	Solid	Liquid	Solid	
1,085sh,m				)
				)
1,080m	1,074m	1,075w	1,079w/m	) ρ(C-H), (A")
1,073sh,m				)
				)
			1,008m	)
				) νs(C-N)(A')
1,006vs	1,006vs	1,004m	1,003m	)
849vs			840m/s	)
				) δi(Si-H)(A')
846vs	834vs	842m	835m/s	)
820s				)
				) δo(Si-H)(A")
808vs	782vs	792m	776vs	)
708sh,m				)
				) ν(Si-N)(A')
702m	699s	700s	701m	)
			524sh,w	)
				) νas(Si-Cl)(A")
573vs	537vs	560m	517m	)
527sh,s				)
				) νs(Si-Cl)(A')
520s	502vs	503s	504vs	)
530vw	451vw			
407vw	385sh,m	326vs	330s	)
				) δ(CNC)(A')
397vw	381m			
	329w			
	306w?			
	295sh,m			)
				)
310ww	291m	297sh,m	285m	) δ(SiNC)(A")
				)
300ww	285m		264m	)

TABLE 4.6 (continued)

OBSERVED FREQUENCIES (cm^{-1}) AND ASSIGNMENTS FOR DICHLOROSILYL-N,N-DIMETHYLAMINE

Infra-Red		Raman		Assignment
Gas	Solid	Liquid	Solid	
		188s	196s	)
				)
		175s	177m?	) $\delta(SiCl_2)(A')$
				)
			169m	)
		134m	152s	
		110m?	116m/s	$\tau(Si-N)(A'')$

Abbreviations: w = weak, m = medium, s = strong, v = very,

sh = shoulder

mode, shifts from 808cm^{-1} to 792cm^{-1} in the transition between the gas and liquid phases, and shifts further to 782cm^{-1}(IR) and 776cm^{-1}(R) in the solid phase. This type of behaviour is often observed for deformational modes in silicon hydrides on condensation.

The band at ≃700cm^{-1} in both infra-red and Raman, and in all phases is assigned as the Si-N stretching mode. The position of this band is very consistent with the absorption frequencies noted for the monohalosilyl-dimethylamines, although the appearance of one band at 699cm^{-1}(IR) and 701cm^{-1}(R) in the solid phase for $SiHCl_2NMe_2$ contrasts strongly with the two bands observed for these compounds in each of the solid phase spectra. This is completely consistent with the X-ray diffraction data for $SiHCl_2NMe_2$ which shows that no polymerisation occurs in the crystalline state involving Si-N...Si-N dative interactions, and the physical observation of the relatively low melting point (165K). In this way the Si-N absorption frequency in the solid phase, with respect to the gas-phase value, can be used to predict whether multimers are present in the solid phase, i.e. whether significant intermolecular interactions occur on condensation. The asymmetric and symmetric Si-Cl stretches are assigned to the strong bands at 573cm^{-1} and 520cm^{-1} respectively in the gas—phase infra-red spectrum. The corresponding modes in SiH_2Cl_2[77] are found at 590/587cm^{-1} and 527cm^{-1}. Both of these modes shift to lower frequency in $SiHCl_2NMe_2$ on condensation particularly the asymmetric stretch which moves to 560cm^{-1} in the Raman liquid spectrum, and to 537cm^{-1} and 517cm^{-1} in the solid phase infra red and Raman spectra respectively. This is perhaps surprising, since no intermolecular interactions occur in the solid phase and the Si-Cl bond lengths in the gas and solid phases are remarkably similar.

The remaining unassigned modes are the two methyl torsions, the Si-N torsion and the NSiCl (A'+A"), CNC (A') and SiNC(A'+A") deformations. All of these vibrational modes are expected to absorb energy below 400cm^{-1} and assignments in this region are not definitive. Absorptions at 407/397cm^{-1} and 381cm^{-1} in the gas and solid phase infra-red spectra are assigned to the CNC bend (A') since in SiH_3NMe_2[48] this mode is observed at 360cm^{-1} in the gas-phase. The Raman counterparts of this mode may be the bands observed at 326cm^{-1} and 330cm^{-1} in the liquid and solid phase spectra respectively. The out of plane SiNC (A") deformation occurs at 268cm^{-1} for SiH_3NMe_2[48] in the gas-phase infra-red spectrum, hence the Raman solid bands at 285cm^{-1} and 264cm^{-1} may be tentatively assigned to this mode. The $SiCl_2$ bend is assigned to the bands at 188/175cm^{-1} and 196cm^{-1} in the liquid and solid phase Raman spectra. This assignment is made on the basis that the same mode occurs in SiH_2Cl_2[77] at 188cm^{-1} in the gas-phase. Finally, bands occur at 152cm^{-1} and possibly 110cm^{-1} in the Raman spectra. Similar bands appear in the Raman spectra of SiH_2XNMe_2 (X = Cl&Br) and the higher frequency band is possibly due to the in-plane SiNC (A') bending mode. Again, this assignment is tentative, since it contrasts with that of Durig.[48] The lower frequency absorption however, has its counterpart at 115cm^{-1} for SiH_3NMe_2[48] in the gas-phase infra-red spectrum and is thus assigned as the Si-N bond torsional mode. As with the monohalo silyl-dimethylamines, no evidence for the two methyl torsions (2A") was observed. Again, far infra-red spectra and good quality Raman data for this compound and its isotopic analogues are required before a definitive assignment of the low frequency modes can be made.

4.9 NUCLEAR MAGNETIC RESONANCE STUDIES OF HALOSILYL-DIMETHYLAMINES

INTRODUCTION

The chemical shifts and coupling constants for the halosilyl-dimethylamines have all been determined, with the exception of $SiH_2Cl^{15}NMe_2$, for samples with isotopes in their natural abundance. Signal to noise ratios in ^{13}C and ^{29}Si spectra are therefore relatively poor, since these spin = $^1/_2$ nuclei are present in only 1.1% and 4.7% respectively. Generally, therefore, spectra of these nuclei were obtained by the use of polarisation transfer techniques to enhance sensitivity.

The presence of naturally occurring ^{14}N (Spin = 1) quadrupolar nuclei in these compounds has the effect of broadening the signals in the spectra making small couplings in e.g. the ^{29}Si spectra difficult to detect. This effect can be removed however, by substitution with ^{15}N (Spin I = $^1/_2$) and this also allows extra coupling constants to be determined.

All of the compounds prepared in the course of this work have been studied by ^1H, ^{13}C and ^{29}Si n.m.r. and the solvent, temperature and concentrations have been kept constant in each case. All chemical shifts have been measured with respect to $Si(CH_3)_4$, (TMS).

4.10 RESULTS AND CONCLUSIONS

The n.m.r. spectra of the halosilyl-dimethylamines confirm the molecular structures proposed by vibrational spectroscopy and electron diffraction and also indicate that there is no rapid exchange of atoms or groups in any of the samples. The ^{13}C n.m.r. spectra also indicate that, with the exception of SiH_2INMe_2, the two methyl groups in each compound are equivalent at room temperature. The two distinct ^{13}C resonances and the presence of the $^3J_{C-H_c}$

coupling constant for the iodide indicate that the methyl groups must be inequivalent due to the significantly higher barrier to internal rotation about the Si-N bond, caused by the presence of the large iodine atom. As previously mentioned, this result seems to be confirmed by electron diffraction, where the molecule is found to possess perfect C_s symmetry unlike the chloride or bromide.

A comparison of the parameters obtained from the spectra (see Table 4.7) indicate that as the electronegativity of the halogen atom decreases, δH_{Si} increases whilst δH_C decreases. The ^{13}C and ^{29}Si chemical shifts, however, seem to be fairly insensitive to the halogen substituent, although the value of $\delta^{29}Si$ for SiH_2INMe_2, (-47.2 p.p.m.) presumably indicates the shielding effect of the iodine atom. $^1J_{C-H}$ is also fairly insensitive to the halogen atom, but $^1J_{Si-H}$ appears to increase slightly as the halogen atom becomes less electronegative. As expected, $^1J_{Si-H}$ is significantly larger for $SiHCl_2NMe_2$ than any of the monohalo compounds.

Examples of some of the more interesting spectra are given in Figures 4.12 - 4.14.

In an attempt to detect the change from tetra- to pentacoordinate silicon which accompanies the dimerisation process which these compounds undergo at low temperature, (see Chapter 5) a sample of neat SiH_2ClNMe_2 was prepared and this tube studied at various temperatures down to -78°C. Both ^1H and ^{29}Si spectra were recorded, but the significant shift to higher frequency expected for $\delta^{29}Si$ in a 5-coordinate complex[85,86] was not detected at any stage and thus further attempts to detect dimerisation were abandoned.

Figure 4.12 ^{29}Si Nmr Spectrum of $SiH_2Cl^{14}NMe_2$.

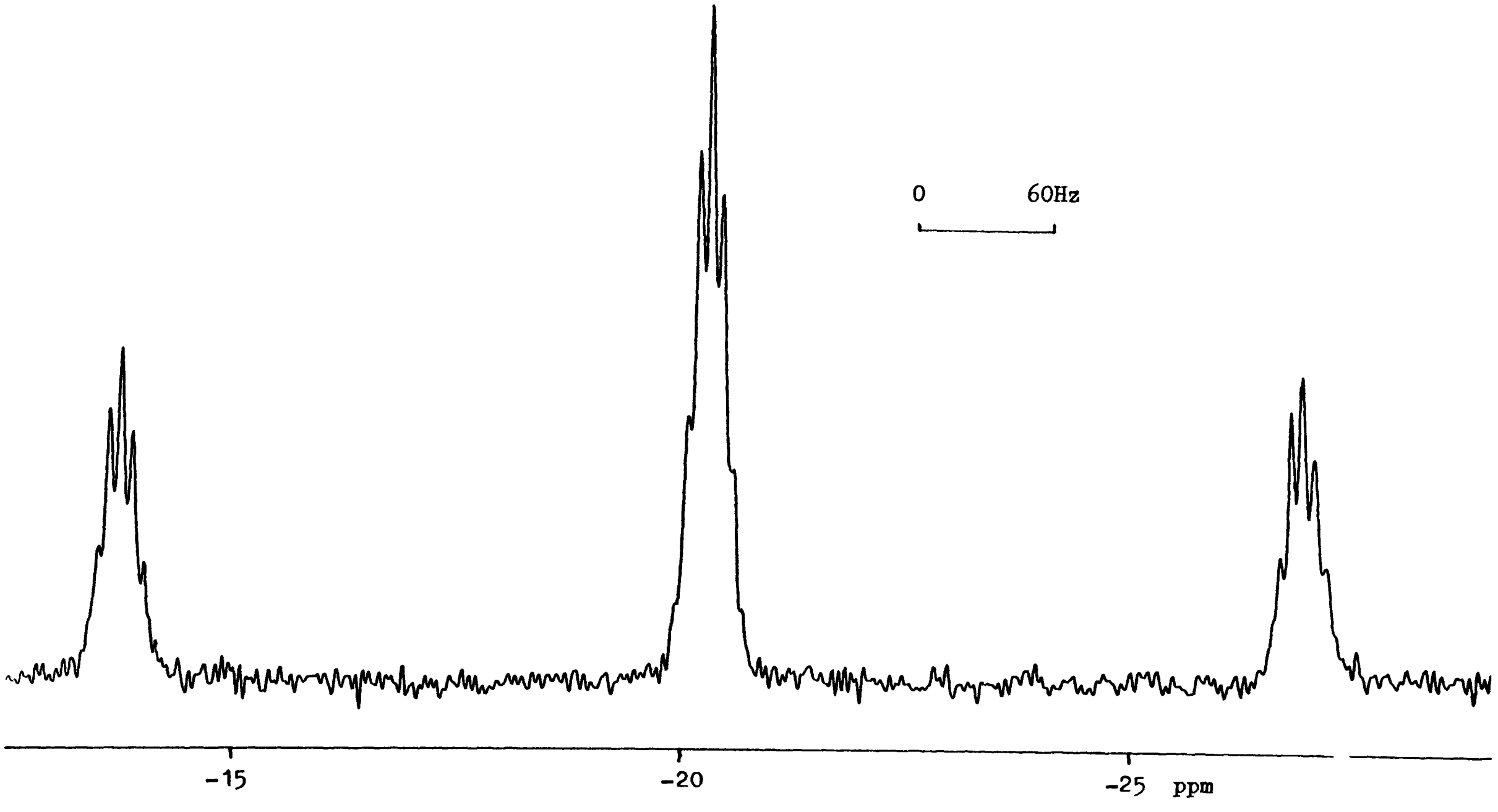

Figure 4.13 ^{15}N Nmr Spectrum of $SiH_2Cl^{15}NMe_2$.

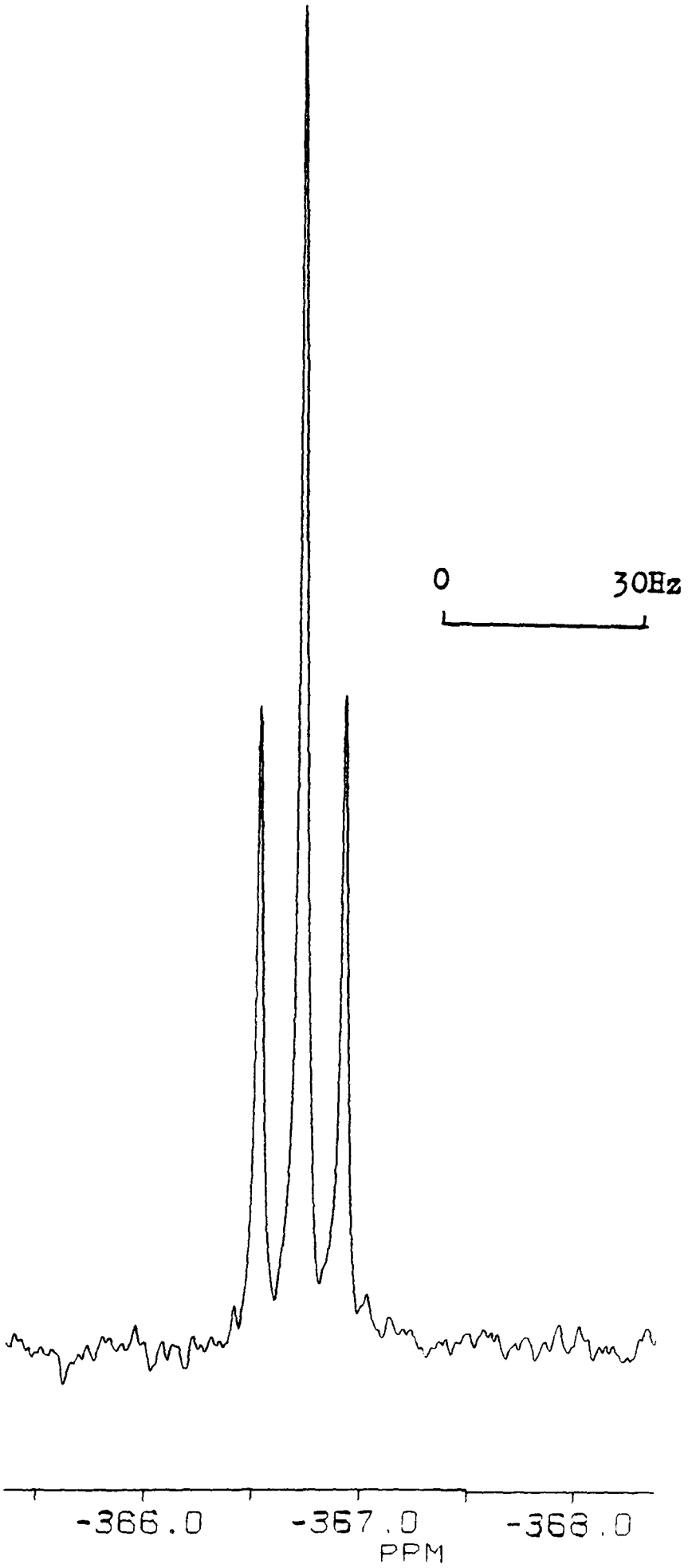

Figure 4.14 ^{13}C Nmr Spectrum of SiH_2INMe_2.

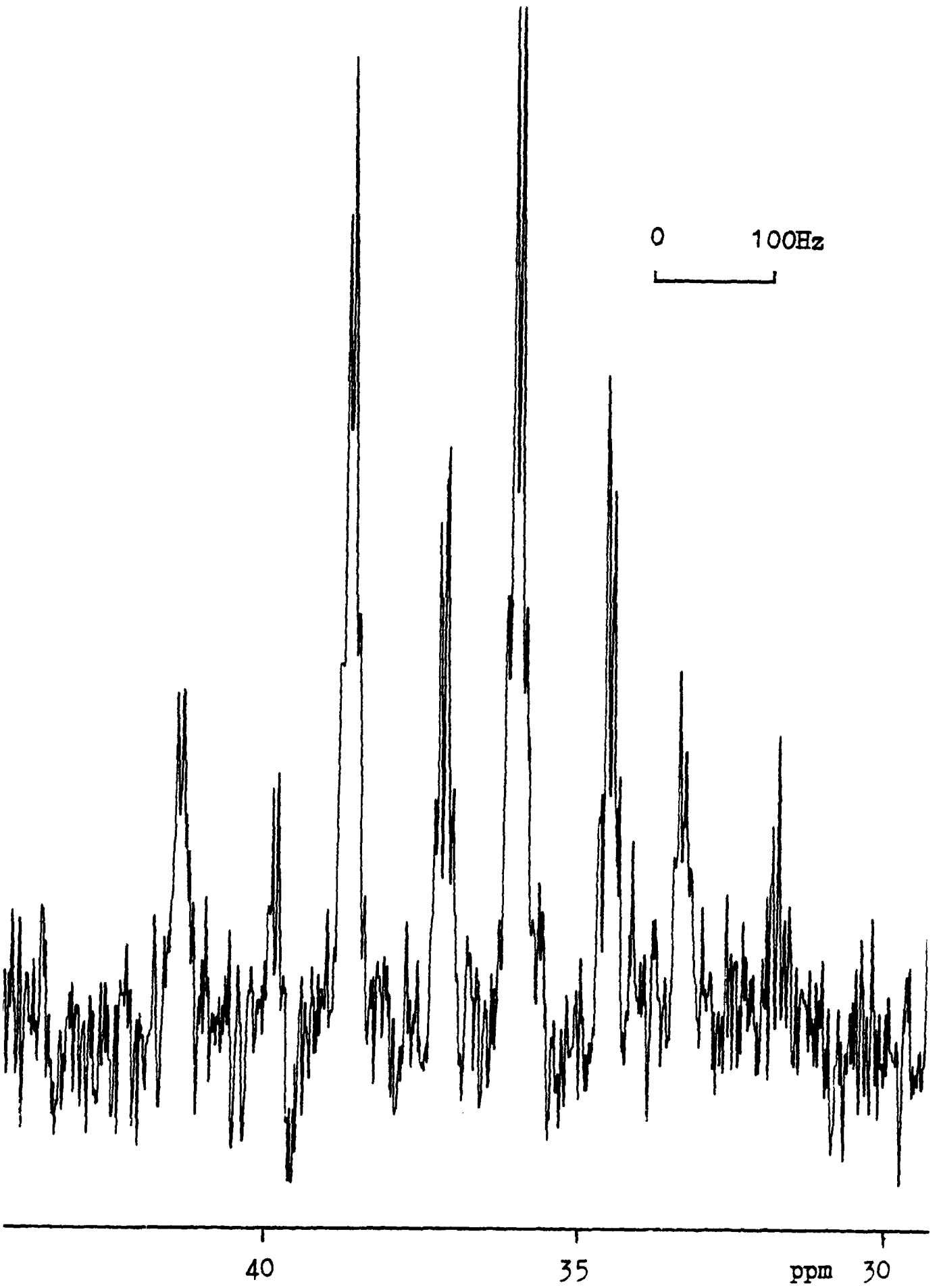

TABLE 4.7

SUMMARY OF THE NMR PARAMETERS OF HALOSILYL-DIMETHYLAMINES

Compound	δH_{Si}	δH_C	$\delta^{13}C$	$\delta^{13}C$	$\delta^{29}Si$	$\delta^{15}N$	$^1J^{13}C\text{-}^1H$	$^1J^{29}Si\text{-}^1H$	$J^{15}N\text{-}^{29}Si$	$^2J^{15}N\text{-}^1H_{Si}$	$^3JC\text{-}H_C$	$^3J^{29}Si\text{-}^1H$
SiH_2FNMe_2	4.39	2.24	36.9	-	-22.6	-	133.1	249.9	-	-	-	N.O.
SiH_2ClNMe_2	4.78	2.17	36.9	-	-21.0	-	134.8	260.2	-	-	-	5.0
$SiH_2Cl^{15}NMe_2$	4.79	2.15	N.R.	-	-20.8	-366.7	≃135.6	259.3	22.5	7.3	-	N.O.
SiH_2BrNMe_2	4.85	2.12	39.1	-	-27.6	-	135.2	263.0	-	-	-	N.O.
SiH_2INMe_2	4.84	2.01	35.9	37.4	-47.2	-	135.1	262.8	-	-	5.0	N.O.
$SiHCl_2NMe_2$	5.27	2.18	34.5	-	-21.8	-	136.0	322.0	-	-	-	N.O.

All δ in p.p.m., all J in Hz.

$^2J_{^1H_C\text{-}^{15}N}$ was not observed and must be < 0.06Hz.

CHAPTER 5

THE VIBRATIONAL SPECTRA OF $SiH_2X(NMe_2)$ WHERE X=Cl,Br&I IN THE SOLID PHASE AND THE X-RAY CRYSTAL STRUCTURE OF $SiH_2Cl(NMe_2)$

5.1 INTRODUCTION

The ability of silicon to form complexes with a coordination number greater than four, i.e. five or six is well known.[87] These compounds fall into three general categories:

i) penta or hexahalo anions which are stabilised by large cations in lattices, e.g. SiF_6^{2-} and SiF_5^-,

ii) complexes stabilised by chelating ligands, e.g. $Si(bipy)_3$ and $SiPh_3bipy^+$, and

iii) adducts of 4-coordinate species with coordinating organic bases, e.g. $SiF_4.(Pyr)_2$ and $SiF_4.(bipy)$.

Examples, where 4-coordinate silicon compounds (in the gas-phase) polymerise to become 5-coordinate (in the solid-phase) are, however, limited and apart from the silyl halides and pseudohalides, SiH_3X (where X = F,[88] I,[89] -CN,[90] -NCO[91]), the only other known example is SiH_3NMe_2.[62,63] Polymerisation generally occurs via a "head to tail" process producing chains, although in SiH_3NMe_2 the ends of the chains are linked, forming discrete cyclic pentamers. The ability of silicon to become pentacoordinate is possibly because of its vacant d-orbitals, which are low enough in energy to accept electron density from suitable neighbouring atoms with lone pairs. This is essentially an S_{N^2} process[92,93,94] and the 'product' formed is a stable trigonal-bipyramidal silicon compound which is analogous to the 5-coordinate transition state which is postulated in S_{N^2} processes in carbon chemistry.

It appears that the potential energy surface for an S_{N^2} process

involving a silicon centre has a clear minimum between the levels for the reactants and products, unlike that of carbon.

The physical manifestation of this polymerisation or pentacoordination is a tendency for silicon compounds which are liquids or gases at room temperature to form distinct crystals, as opposed to glasses, at low temperature. These intermolecular interactions will also produce a clear raising of the melting point of the solid to an unexpectely high value. This is the case in SiH_3NMe_2,[35] where the melting point is found to be an anomalously high, 276.3°K. The three compounds SiH_2XNMe_2 (X=Cl,Br&I) all tend to crystallise at low temperature, but the melting point of SiH_2ClNMe_2 is found to be 193K compared with 151K and 169K for SiH_2Cl_2 and $SiH_2(NMe_2)_2$[33] respectively. It was therefore decided to attempt to obtain crystals of SiH_2ClNMe_2 and SiH_2BrNMe_2 suitable for x-ray crystallography, but although both compounds crystallised easily, only SiH_2ClNMe_2 yielded single crystals.

5.2 X-RAY CRYSTAL STRUCTURE OF SiH_2ClNMe_2

The X-ray crystal structure of SiH_2ClNMe_2 at 116K was determined by A.J. Blake. The space group and unit cell parameters were as follows: a monoclinic crystal, space group $C_{2/m}$, a = 676.59(22), b = 995.0(3), c = 849.40(27)pm, $\alpha=\gamma=90°$, β = 114.70(4)°, Z = 4, D = 1.402gcm^{-3} v = 0.5195nm^3 and R = 0.0970.

The final molecular parameters are given in Table 5.1 and a view of the molecule is given in Figure 5.1.

As with SiH_3NMe_2 the contrast between the gas and solid phase structures of SiH_2ClNMe_2 is marked, but SiH_2ClNMe_2 chooses to dimerise rather than form pentameric rings like SiH_3NMe_2. The dimer with C_{2h} symmetry is more accurately described as two strongly-interacting monomers, since the 4 Si-N bonds are not all equivalent

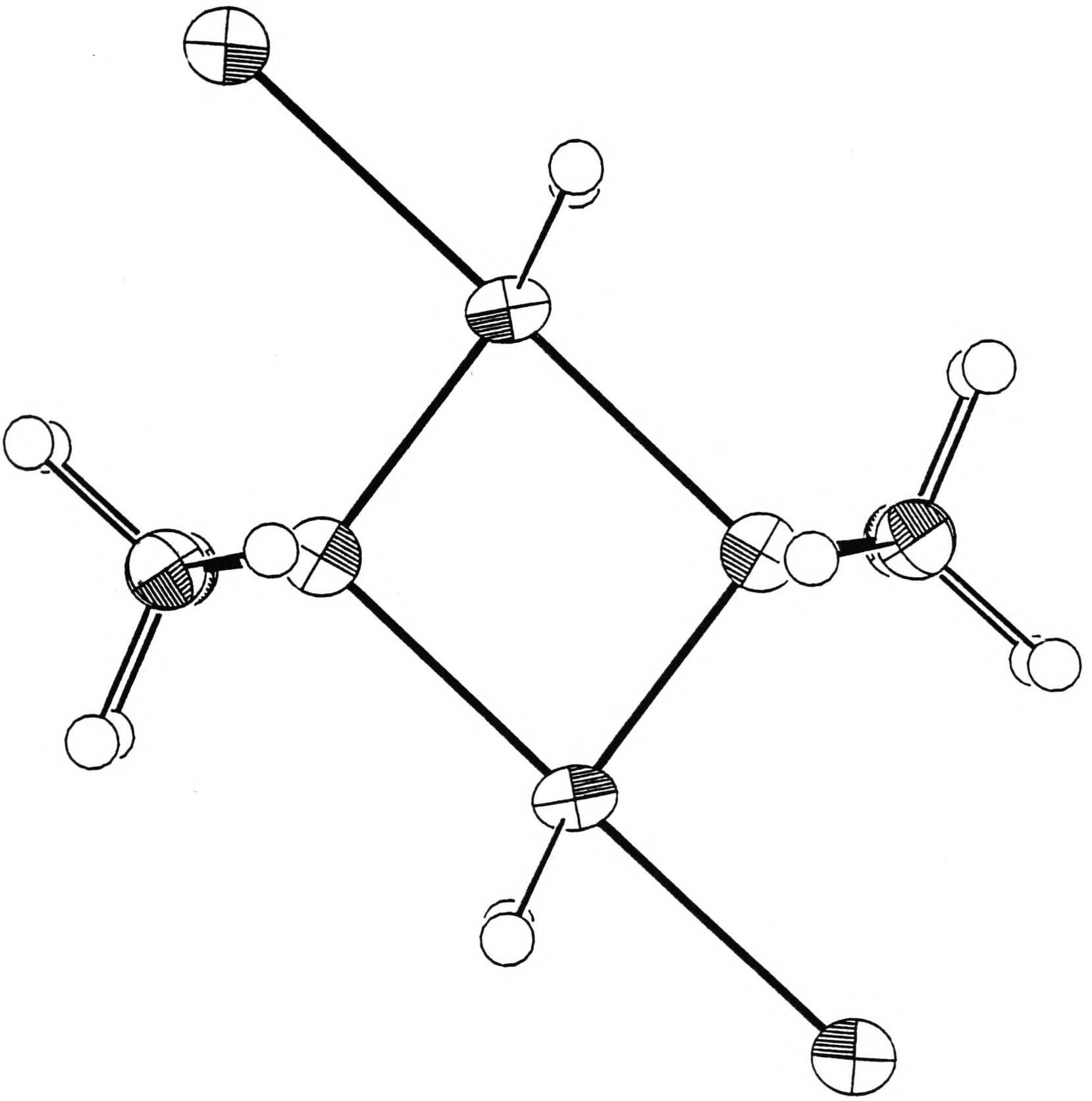

Figure 5.1 The SiH_2ClNMe_2 dimer viewed perpendicular to the $Si_2N_2Cl_2$ plane.

TABLE 5.1

MOLECULAR PARAMETERS FOR CRYSTALLINE SiH_2ClNMe_2

Bond Lengths (pm)

Si-Cl = 223.1(6)	Si-H(4) = 149(11)
Si-N = 181.4(13)	N-C = 149.8(18)
Si-N = 205.4(13)	C-H (2) = 108.0(17)

Interbond Angles (°)

Cl-Si-N = 96.1(5)	C-N-Si' = 112.5(9)
Cl-Si-H(4) = 81(4)	C-N-C = 108.8 (14)
N-Si-H(4) = 126(4)	N-C-H (1) = 105.5 (12)
H(4)-Si - H(4) = 107(8)	N-C-H(2) = 108.4(12)
Cl-Si-N' = 179.0(4)	N-C-H(3) = 114.4(12)
N-Si-N' = 83.0(5)	H(1)-C-H(2) = 109.3(14)
H(4)-Si-N' = 100(4)	H(1)-C-H(3) = 109.6(14)
Sil-N-C = 112.8(9)	H(2)-C-H(3) = 109.5(14)
Si-N-Si' = 97.0(6)	

Torsion Angles (°)

Cl-Si-N-C = 61.9(9)	Cl-Si-N'-C = 0
H(4)-Si-N-C = -21(5)	H(4)-Si-N'-C' = 0
Si-N-C-H(1) = 167(1)	

and the 4-membered ring is not equilateral. Formation of a dimeric species, rather than a cyclic pentameter or a chain arrangement, is not surprising since Corriu et al have shown[61,95,96] that for S_N2 type reactions the nature of nucleophile and the leaving group will control the stereochemistry of the intermediate. Leaving groups like -Cl, which has a high apicophilicity, or easily polarisable Si-Cl bond, always assume an axial position and thus the incoming nucleophile, the nitrogen atom from a neighbouring molecule, will attack at the other axial site. This trigonal-bipyramidal arrangement is also expected, since Corriu has also shown[97] that hydrogen atoms have a high equatorial preference in 5-coordinate silicon complexes. Thus SiH_2ClNMe_2 contrasts with SiH_3NMe_2 where nitrogen atoms occupy the axial positions and a perfect trigonal bipyramidal arrangement occurs with all Si-N bond lengths being equal.

Sterically, formation of a pentameric ring would be very unfavourable unless the equatorial Cl atoms all pointed away from the outside of the ten-membered ring.

The Si-N and SiN' bond lengths of 181.4(3) and 205.4(13)pm respectively can be compared to the 'idealised' Si-N bond lengths of 197.44(18) and 198.04(19)pm in pentameric SiH_3NMe_2 and it is apparent that the short bond is attributable to the 'monomer' unit whilst the longer bond is due to the coordinating $-NMe_2$ group from the neighbouring monomer. This longer bond is, however, considerably shorter than the Si...N bond lengths in compounds 1,[98] 2[61] and 3[61] below:

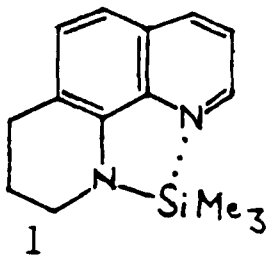

1

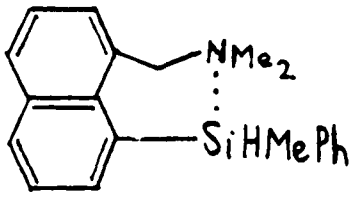

2

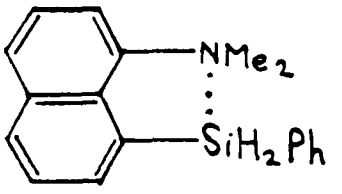

3

r(Si...N):-	268.9(8)pm	266(1)pm	258.4(3)pm

indicating that the coordinating Si...N bond is relatively strong, although not as strong as that found in SiH_3NMe_2. The Si-Cl bond length of 223.1(6)pm is distinctly longer than that observed in the gas-phase, 207.0(1)pm, and this is expected since -Cl is the 'leaving group'. The Si-Cl distance is more realistically compared to those trans to N in the comparable compound 4 below:[99]

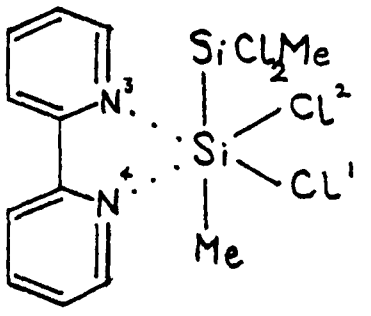

4

$r(Si\text{-}Cl^1)$ = 227.4(8)pm $\quad$ $r(Si\text{-}Cl^2)$ = 239.2(10)pm

$r(Si..N^3)$ = 202.9(12)pm $\quad$ $r(Si...N^4)$ = 200.7(11)pm

The C-N bond lengths show clear lenghthening in the crystal (149.8(18)pm versus 146.4(2)pm) relative to the gas-phase as the two nitrogen atoms become tetrahedrally coordinated. The Si-H bond lengths also appear to increase as silicon becomes pentacoordinate, but since these bond lengths are not particularly well defined in either structure, this difference is probably not significant.

The bond angles in the crystal structure are also distinctly different to those of the gas-phase monomer. The NSiCl and HSiCl angles are drastically reduced from 113.2(3)° and 105.6° respectively in the gas-phase to 96.1(5)° and 81(4)° in the crystal, allowing coordination of the N' atoms, making Si pentacoordiante and forming a planar Si_2N_2 ring. The Si-N...Si' angle of 97.0(6)° can be considered to be a compromise between the tetrahedral value of 109.47° and value of 90° expected if the Si_2N_2 ring was square. This angle induces an N-Si...N' angle of 83.0(5)°, which is distinctly smaller than the value of 90° expected for trigonal-bipyramidal

silicon, indicating the ease with which the geometry of a 5-coordinate silicon centre can be distorted. Further evidence of this is the wide N'...Si-H angle of 100(4)° which can probably be attributed to the eclipsing interactions from the two C-N bonds. This type of arrangement is clearly found to be unfavourable in the gas-phase.

The remaining angles around nitrogen are as expected, close to the tetrahedral value with angle CNC decreasing to 108.8(14)° from the gas-phase value of 115.1(6)° where the geometry at nitrogen is between pyramidal and planar. Similarly, the Si-N-C angle drops from 120.8(2)° in the gas-phase to 112.8(9)°.

With the Cl-Si...N' angle being 179.0(4)°, the axial preference of -Cl and the S_{N^2} nature of the interaction is confirmed, and thus the dimer can be considered to be a 'frozen' intermediate at a stage earlier in the reaction pathway than that of SiH_3NMe_2 in the solid phase.

5.3 VIBRATIONAL SPECTRA OF SiH_2XNMe_2 IN THE SOLID PHASE

INTRODUCTION

In the previous section, the x-ray crystal structure of SiH_2ClNMe_2 has been discussed, and this reveals that the compound exists in the form of discrete dimeric units in the crystalline state. In this section, and also in the subsequent sections for SiH_2BrNMe_2 and SiH_2INMe_2 the vibrational spectra of these compounds will be discussed assuming that in the solid phase, the spectra obtained are of dimeric SiH_2XNMe_2 (where X = Cl,Br,I). This assumption is not unreasonable, since these compounds are naturally crystalline in the solid phase and they all show analogous spectroscopic behaviour. As far as possible, the samples were annealed until no further changes occurred in the spectra.

The tabulated bands are those which are due to dimeric material, any monomer bands visible in the spectra have been excluded, although in some cases where annealing was incomplete, this occasionally proved difficult to establish.

A discrete dimer with crystallographic C_2h symmetry will have 72 modes of vibration: 20Ag + 16Bg + 17Au + 19Bu. Assigning all of these bonds, particularly the modes involving the methyl group motions, will be difficult without Raman polarisation data and hence, with the exception of the methyl group rocks, only the skeletal modes (i.e. those involving the $[SiH_2XNC_2]_2$ unit) will be considered. These will give rise to 11Ag + 7Bg + 8Au + 10Bu vibrations. Since the dimer contains an inversion centre, the rule of mutual exclusion will apply with the Ag and Bg modes being Raman active and the Au and Bu modes being infra-red active. Table 5.2 lists the expected skeletal modes and their activity.

TABLE 5.2

SKELETAL NORMAL MODES OF VIBRATION FOR THE SiH_2XNMe_2 DIMER

Species	Vibration	Activity
Ag	$\nu s(SiX)$, $\nu s(SiH)$, $\nu s(CN)$, $\nu(Si_2N_2)_R$, $\nu(Si_2N_2)_R$, $\beta(SiX)$, $\beta(SiH)_w$, $\beta(SiH)_B$, $\beta(CN)_w$, $\beta(CN)_B$, $\beta(Si_2N_2)_R$.	Raman
Au	$\nu as(SiH)$, $\nu as(CN)$, $\gamma(SiX)$, $\gamma(SiH)$, $\tau(SiH)$, $\gamma(CN)$, $\tau(CN)$, $\gamma(Si_2N_2)_R$.	Infra-red
Bg	$\nu as(SiH)$, $\nu as(CN)$, $\gamma(SiX)$, $\gamma(SiH)$, $\tau(SiH)$, $\gamma(CN)$, $\tau(CN)$.	Raman
Bu	$\nu as(SiX)$, $\nu s(SiH)$, $\nu s(CN)$, $\nu(Si_2N_2)_R$, $\nu(Si_2N_2)_R$, $\beta(SiX)$, $\beta(SiH)_w$, $\beta(SiH)_B$, $\beta(CN)_w$, $\beta(CN)_B$.	Infra-red

Abbreviations: β = in plane deformation, γ = out of plane deformation

τ = torsion, B = Bend, W = wag, R = Ring

5.4 VIBRATIONAL SPECTRA OF $SiH_2Cl^{14}NMe_2$ AND $SiH_2Cl^{15}NMe_2$ IN THE SOLID PHASE

The solid phase infra-red spectra of $SiH_2Cl^{14}NMe_2$ and $SiH_2Cl^{15}NMe_2$ are shown in Figures 5.2 and 5.3 and a list of vibrational assignments is given in Table 5.3.

The assignments for the skeletal, Si-N, stretches and the Si-Cl stretches have been made reasonably confidently, some of the other modes however, e.g. the Si-H deformations and the bands observed around $1,000cm^{-1}$, are assigned only tentatively, since there have been no other studies on similar compounds with which comparisons can be made.

The Si-H bond stretching vibrations should give rise to two active modes in each of the infra-red and Raman spectra. Two bands are observed in the infra-red spectrum of $SiH_2{}^{14}NMe_2$, and these are assigned with the asymmetric mode at higher frequency. Only one band is observed in the Raman spectrum, however. It is noted that the infra-red band at $2,242cm^{-1}$, $\nu_{as}(SiH)$, is shifted to a distinctly higher frequency relative to the gas-phase value of $2,206cm^{-1}$.

The methyl group rocking modes and the C-N stretches are found in the region between $1,300cm^{-1}$ and $950cm^{-1}$ and in general these are shifted to lower frequencies relative to the gas-phase values. Four methyl rocks and two C-N stretches are expected in both the infra-red and Raman spectra with the infra-red active rocks having 2Au + 2Bu symmetry, whilst the Raman active rocks possess 2Ag + 2Bg symmetry. The two active C-N stretches in each of the spectra possess the same symmetry species as the active rocks, thus similar problems, due to the mixing of vibrations, to those which occurred in the spectra of the monomeric material are expected. In the dimer, however, the active Si_2N_2 ring stretching modes also have the same symmetry, and hence these too will mix with the appropriate ν(C-N) mode in each case.

Figure 5.2 Infra-red Spectrum of $SiH_2Cl^{14}NMe_2$ in the solid phase.

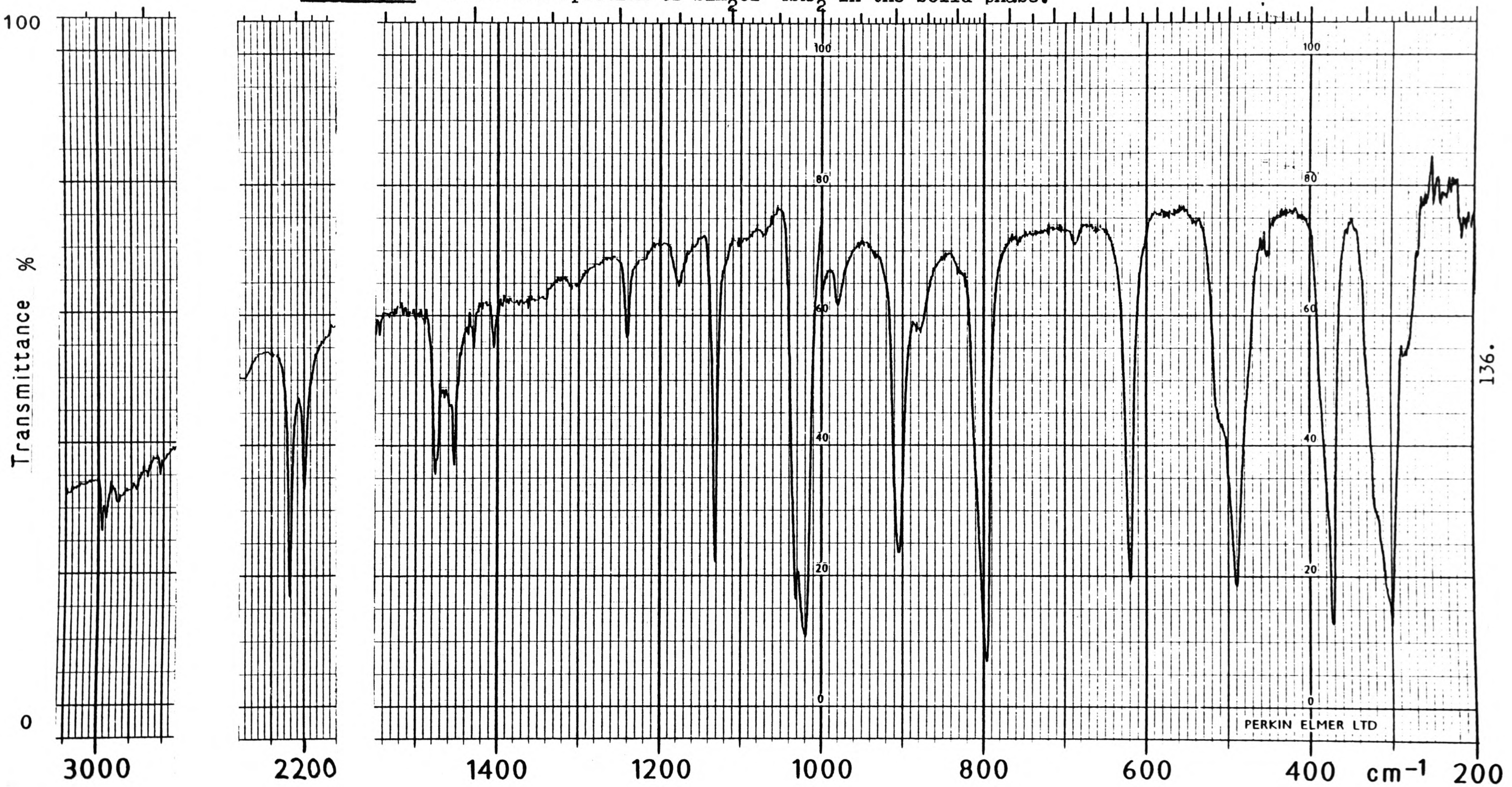

Figure 5.3 Infra-red Spectrum of $SiH_2Cl^{15}NMe_2$ in the solid phase.

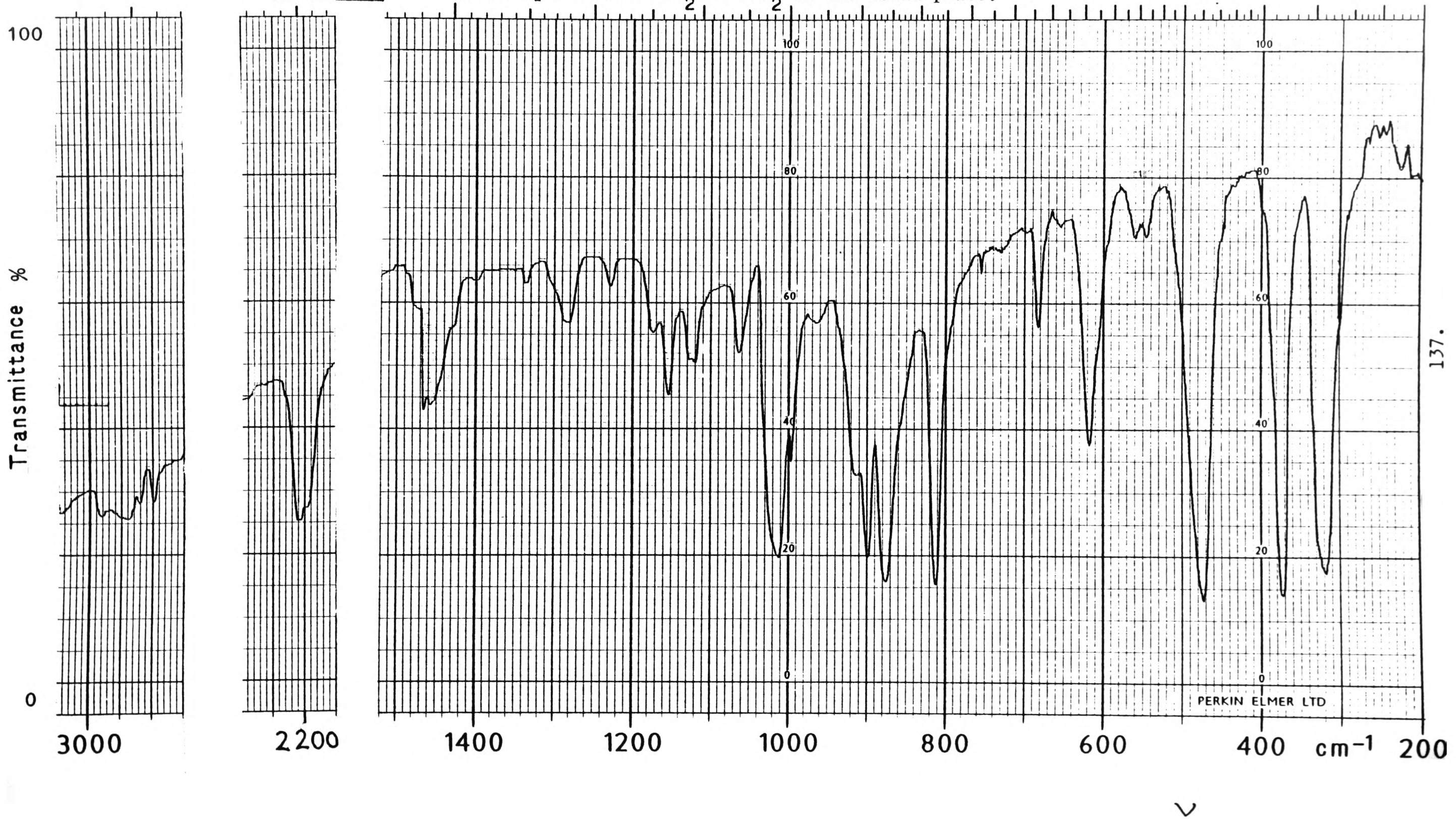

Three of the four active rocks have been assigned in both infra red and Raman spectra and these are all shifted to lower frequency compared to the gas-phase values with clear ^{15}N shifts also apparent. In the case of $SiH_2Cl^{15}NMe_2$ the symmetric C-N stretching mode is assigned at a higher frequency than the lowest frequency rock in the infra-red spectrum, and this attributed to the mixing of this mode with $\nu as(Si-N)$ at $\simeq 800cm^{-1}$. This is also why this mode is shifted to higher frequency, relative to the gas-phase value. The asymmetric C-N stretch which is too weak to be observed in either the infra-red or Raman spectra of the monomer is therefore assigned to the weaker bands at $\simeq 970cm^{-1}$ in both the infra-red and Raman spectra, since these modes, which are again mutually exclusive, will not mix with either of the active ring Si_2N_2 modes in either of the spectra.

The active bending and wagging Si-H deformations are tentatively assigned to the remaining bands between 900-1,000cm^{-1} in the infra-red and Raman spectra on the basis of their position and intensity.

On annealing a sample of either $SiH_2Cl^{14}NMe_2$ or $SiH_2Cl^{15}NMe_2$ after initially depositing it on the cold window inside the infra-red spectrometer, it is clear that the monomeric Si-N stretch at $\simeq 690cm^{-1}$ is replaced by two bands at $\simeq 800cm^{-1}$ and $620cm^{-1}$. These are assigned to the two active Si_2N_2 ring-stretching modes in each of the spectra and this large splitting can again be attributed to mixing between these modes which have Bu symmetry in the infra-red spectrum and Ag symmetry in the Raman spectrum. It is this effect which must cause the band for the ^{15}N labelled sample ($814cm^{-1}$) to befound at a higher frequency than the band of the ^{14}N species ($794cm^{-1}$) in the infra-red spectra.

Between 500-600cm^{-1}, absorptions are assigned to the remaining Si-H deformations; the torsional and rocking modes, but again these

TABLE 5.3

OBSERVED FREQUENCIES (cm^{-1}) AND ASSIGNMENTS FOR THE SiH_2ClNMe_2 DIMER

Infra-Red		Raman	Assignment
$SiH_2Cl^{14}NMe_2$	$SiH_2Cl^{15}NMe_2$	$SiH_2Cl^{14}NMe_2$	
2,990w	Unclear, since annealing was incomplete	Absorptions too weak to be observed	νs/as(C-H),
2,977w			3Au+3Ag+3Bg+3Bu
2,940v			
2,885vw			
2,849vw			
2,810			
2,242s			νas(SiH), Au
2,197m			νs(SiH), Bu
		2,210s	νas(SiH), Bg νs(SiH), Ag
1,475m		1,476s	
1,462?			δ s/as(CH),
1,453m		1,448m	
1,429w		1,436m	3Au+3Ag+3Bg+3Bu
1,405w		1,431?	
		1,256vw	
		1,249vw	ρ(CH), Ag
		1,242vw	

TABLE 5.3

OBSERVED FREQUENCIES (cm^{-1}) AND ASSIGNMENTS FOR THE SiH_2ClNMe_2 DIMER (continued)

Infra-Red		Raman	Assignment
$SiH_2Cl^{14}NMe_2$	$SiH_2Cl^{15}NMe_2$	$SiH_2Cl^{14}NMe_2$	
1,238m	1,233w		ρ(CH), Au
		1,101w	ρ(CH), Bg
1,129vs	1,123		ρ(CH), Bu
		1,024w	ρ(CH), Bg
1,031vs	1,003vs		ρ(CH), Bu
		1,019w	νs(CN), Ag
1,020vs	1,016vs		νs(CN), Bu
		975w	νas(CN), Bg
979w/m	969w/m		νas(CN), Au
		941w	
		926s	β(SiH), Ag(bend)
902vs	900vs		β(SiH), Bu(wag)
		908w	β(SiH), Ag(wag)
794vs	814vs		ν as(SiN), Bu
		794s	νs(SiN), Ag
618vs	620vs		νas(SiN), Bu
		602vs	νs(SiN), Ag
		587w	τ(SiH), Bg
507s,sh			γ(SiH), Au(rock)
		499m	ν s(SiCL), Ag
488vs	476vs		ν as(SiCl), Bu
438vw?		441vw?	

TABLE 5.3

OBSERVED FREQUENCIES (cm^{-1}) AND ASSIGNMENTS FOR THE SiH_2ClNMe_2 DIMER (continued)

Infra-Red		Raman	Assignment
$SiH_2Cl^{14}NMe_2$	$SiH_2Cl^{15}NMe_2$	$SiH_2Cl^{14}NMe_2$	
		380m	β(CNC), Ag(bend)
371vs	376vs		β(CNC), Bu(bend)
		324s	
318vs,sh	325vs		
299vs			
284m,sh			
		268s	
		207s	
192m?	184m		
		177s	
		115s]	
		]	
		109s]	
		76m?	
		58s	

Abbreviations: w = weak, m = medium, s = strong, v = very and sh = shoulder

assignments are only tentative.

The assignments for the Si-Cl stretches can be made fairly confidently, since these clearly shift to lower frequency on annealing and give rise to strong bands. The Raman active band at 499cm^{-1} can be compared with the values of 489cm^{-1} and 424cm^{-1} for ν(Si-Cl) axial in $SiCl_3H.NMe_3$ and $SiCl_3F.NMe_3$ respectively.[100] Shifts of ν(SiX) to lower frequency in the solid phase are well known in the silyl halides, SiH_3X,[80] and since dimeric SiH_2ClNMe_2 contains considerably longer Si-Cl bonds than in the monomer, a shift of this type is not unexpected.

The last two bands which can be assigned confidently, are the in-plane CNC bending modes. These occur at similar frequencies to the symmetric CNC bend in the unassociated monomer, but become much more intense in the solid phase infra-red spectra.

Below 400cm^{-1}, the remaining CNC deformations, the in-plane and out of plane Si-Cl deformations, the Si_2N_2 ring deformations and the methyl torsional modes are all expected, but the spectra in these regions are too complex to attempt to assign.

5.5 VIBRATIONAL SPECTRA OF SiH_2BrNMe_2 IN THE SOLID PHASE

The solid phase infra-red spectrum of SiH_2BrNMe_2 is illustrated in Figure 5.4 and a list of assignments is given in Table 5.4 which includes Raman data. The spectra are essentially analogous to those obtained for SiH_2ClNMe_2 and thus the assignments are also very similar.

In the Si-H stretching region, again two IR active bands are observed and these are assigned to the symmetric and asymmetric stretches. The Raman spectrum contains one band with a shoulder, presumably with both active modes superimposed.

In the methyl rocking region, assignments are again made more

Figure 5.4 Infra-red Spectrum of SiH_2BrNMe_2 in the solid phase.

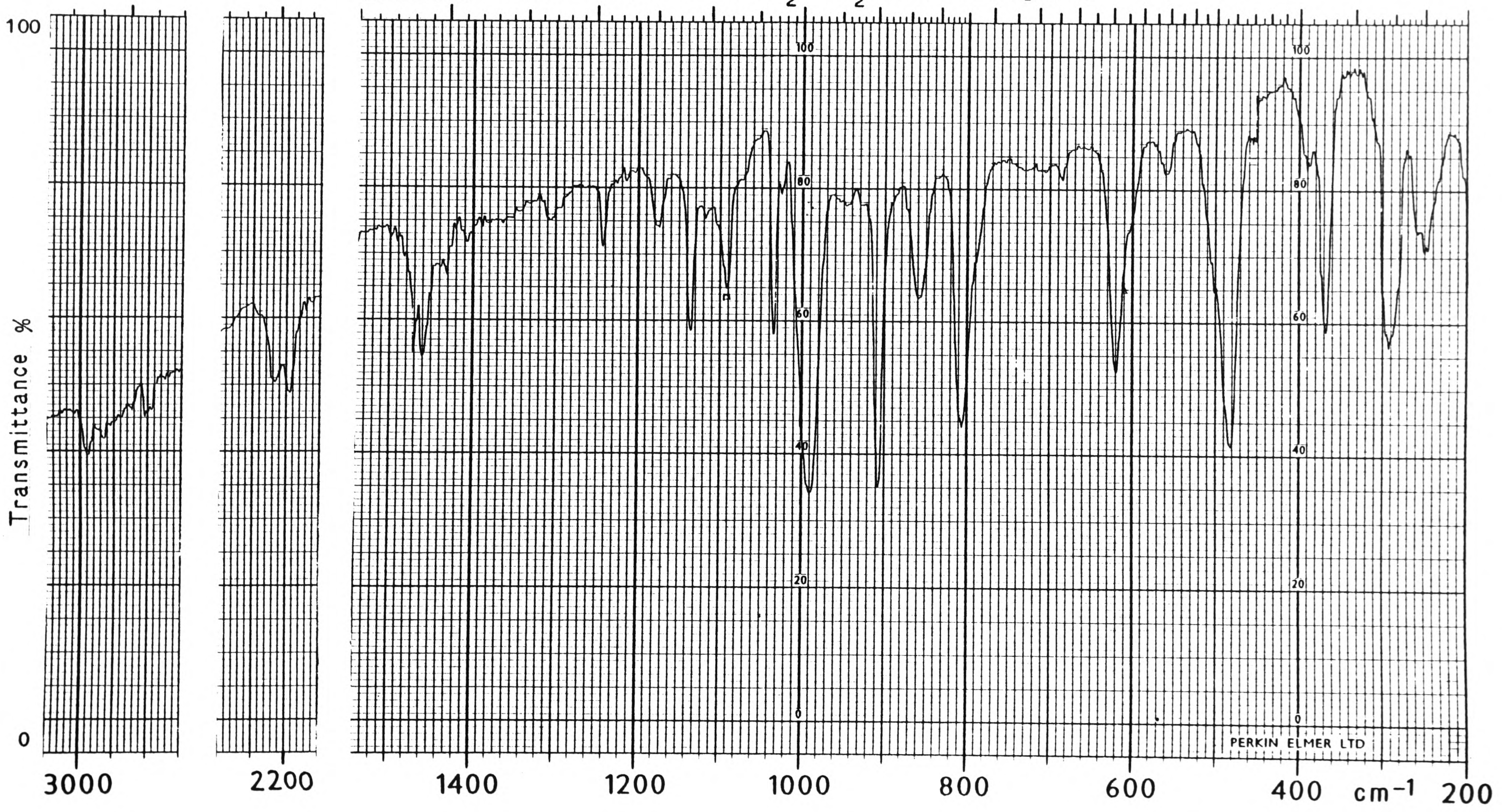

difficult, due to the possibility of mixing with both the C-N stretches and the ring Si_2N_2 modes.

It is apparent, however, that the three highest frequency bands are again due to methyl rocks, shifted to lower frequency and these are assigned as before. The fourth rock, which was not observed in either of the spectra of SiH_2ClNMe_2 is possibly the weak band at $1,001cm^{-1}$ in the Raman spectrum. The infra-red spectrum just below $1,000cm^{-1}$ is identical to that of SiH_2ClNMe_2 and thus the symmetric C-N stretch is attributed to the strong band at $986cm^{-1}$ with the weak band at $944cm^{-1}$ being assigned to the asymmetric mode. Again, the symmetric stretch must be strongly mixed with the two ring Si_2N_2 modes.

Very strong bonds are observed in the Raman spectrum at $918cm^{-1}$ and $904cm^{-1}$ in the infra-red. These absorptions are assigned to the active Si-H bend and wag respectively and are again analogous to those observed for SiH_2ClNMe_2.

In the Si-N stretching region, the monomer band expected at $\simeq 680cm^{-1}$ is once more replaced by two very strong bonds in both the infra-red and Raman spectra at $\simeq 800cm^{-1}$ and $600cm^{-1}$. These are assigned to the two active Si_2N_2 ring stretching vibrations in each case, and again these will be extensively mixed and are thus separated by $\simeq 180cm^{-1}$.

Assignments have been made for the mode for the two rocking and torsional Si-H deformations at $\simeq 490cm^{-1}$ and $556cm^{-1}$ respectively, but these are again only tentative.

Of the remaining bands, only the Si-Br stretching and one of the CNC bending modes can be assigned. With the Si-Br bonds being considerably weakened in the dimer, the bands for the stretching modes will be shifted to lower frequencies and these occur at similar

TABLE 5.4

OBSERVED FREQUENCIES (cm^{-1}) AND ASSIGNMENTS FOR THE SiH_2BrNMe_2 DIMER

Infra-Red(Solid) SiH_2BrNMe_2	Raman(Solid) SiH_2BrNMe_2	Assignment
2,971w	2,988w	νs/as(CH),
2,927w	2,928w	
2,908] broad		3Au+3Ag+3Bg+3Bu
]		
2,876] w		
	2,856w	
2,843w	2,841w	
2,799w	2,787w	
2,231m/s		νas(SiH), Au
	2,205s,sh	νas(SiH), Bg
2,189m/s		νs(SiH), Bu
	2,200s	νs(SiH), Ag
1,470m/s	1,470m	δs/as (CH),
1,458m/s	1,441m	
1,432w	1,426m	3Au+3Ag+3Bg+3Bu
1,405w		
1,241w/m	Region not recorded	ρ(CH), Au
1,135s		ρ(CH), Bu
	1,100w	ρ(CH), Bg
1,032s		ρ(CH), Bu
	1,013m	ρ(CH), Bg

TABLE 5.4

OBSERVED FREQUENCIES (cm^{-1}) AND ASSIGNMENTS FOR THE SiH_2BrNMe_2 DIMER (continued)

Infra-Red(Solid) SiH_2BrNMe_2	Raman(Solid) SiH_2BrNMe_2	Assignment
1,000vs,sh]		ν_s(CN),Bu
]		
986vs]		
	1,001w	ρ(CH), Ag?
	992w]	ν_s(CN), Ag
	]	
	982w]	
944w/m		ν_{as}(CN), Au
	946w	ν_{as}(CN), Bg
	939w	
	918vs	β(SiH), Ag(bend)
904vs		β(SiH), Bu(wag)
	906w]	β(SiH), Ag(wag)
	897w]	
	870w?	
	836w?	
802vs		ν_{as}(SiN), Bu
	783m,sh]	ν_s(SiN), Ag
	]	
	776s]	
618vs		ν_{as}(SiN), Bu
	649s	
	595vs]	ν_s(SiN), Ag
	586vs,sh]	
556w		τ(SiH), Au

TABLE 5.4

OBSERVED FREQUENCIES (cm^{-1}) AND ASSIGNMENTS FOR THE SiH_2BrNMe_2 DIMER (continued)

Infra-Red(Solid) SiH_2BrNMe_2	Raman(Solid) SiH_2BrNMe_2	Assignment
	497s	γ(SiH), Bg
498]vs,sh		γ(SiH), Au
482]vs		
	434vs]	
	423vs,sh]	
386m?		
	377s	ν_s(SiBr), Ag
366vs		ν_{as}(SiBr), Bu
	352m	β(CNC), Ag(bend)
291]vs		
283]vs,sh		
	292vs	
254]m/s		
248]m/s		
	275s	
	263vs	
190?		
	166s	
	155s	
	128vs	
	113w	
	92w	
	79w	

frequencies to the CNC bends making assignments more difficult. It is expected that the silicon-halogen stretches will give rise to strong bands in both the infra-red and Raman spectra, and so these modes are assigned to the bands at 366cm^{-1} and 377cm^{-1} respectively. In $SiCl_3Br.NMe_2$,[100] -Br is axial and ν(Si-Br) occurs at 386cm^{-1} and 384cm^{-1} in the infra-red and Raman spectra respectively, although here this mode is mixed with an Si-Cl stretch at lower frequency. The Raman active CNC bend is assigned to the band at 352cm^{-1}, although the infra-red active mode is either very weak or shifted to lower frequencies.

5.6 VIBRATIONAL SPECTRA OF SiH_2INMe_2 IN THE SOLID PHASE

The vibrational spectra of SiH_2INMe_2 in the solid phase have been recorded and the infra-red spectrum is illustrated in figure 5.5. Vibrational assignments are given in Table 5.5. The spectra obtained are once again consistent with dimer formation.

The Si-H stretching modes which are infra-red active are assigned to the two bands close to 2,200cm^{-1}. These are analogous to those obtained for the chloride and bromide and show a splitting of 31cm^{-1}. This frequency difference clearly decreases as the halogen atom becomes heavier, since values of 41cm^{-1} and 45cm^{-1} were obtained for the bromide and chloride respectively.

The methyl rocking modes occur at very similar frequencies to those of SiH_2BrNMe_2 and thus assignments are identical. Shifting of all these modes to low frequency, relative to the gas-phase positions, is again clearly apparent.

The C-N stretches occur to low frequency of the methyl rocks with two active bands in each spectrum. These occur at $\simeq$990cm^{-1} and 950cm^{-1} with the high frequency band assigned to the symmetric mode, due to mixing with the Si_2N_2 ring modes. The other modes between 900 and 1,000cm^{-1} are assigned to the Si-H bending and wagging

Figure 5.5 Infra-red Spectrum of SiH_2INMe_2 in the solid phase.

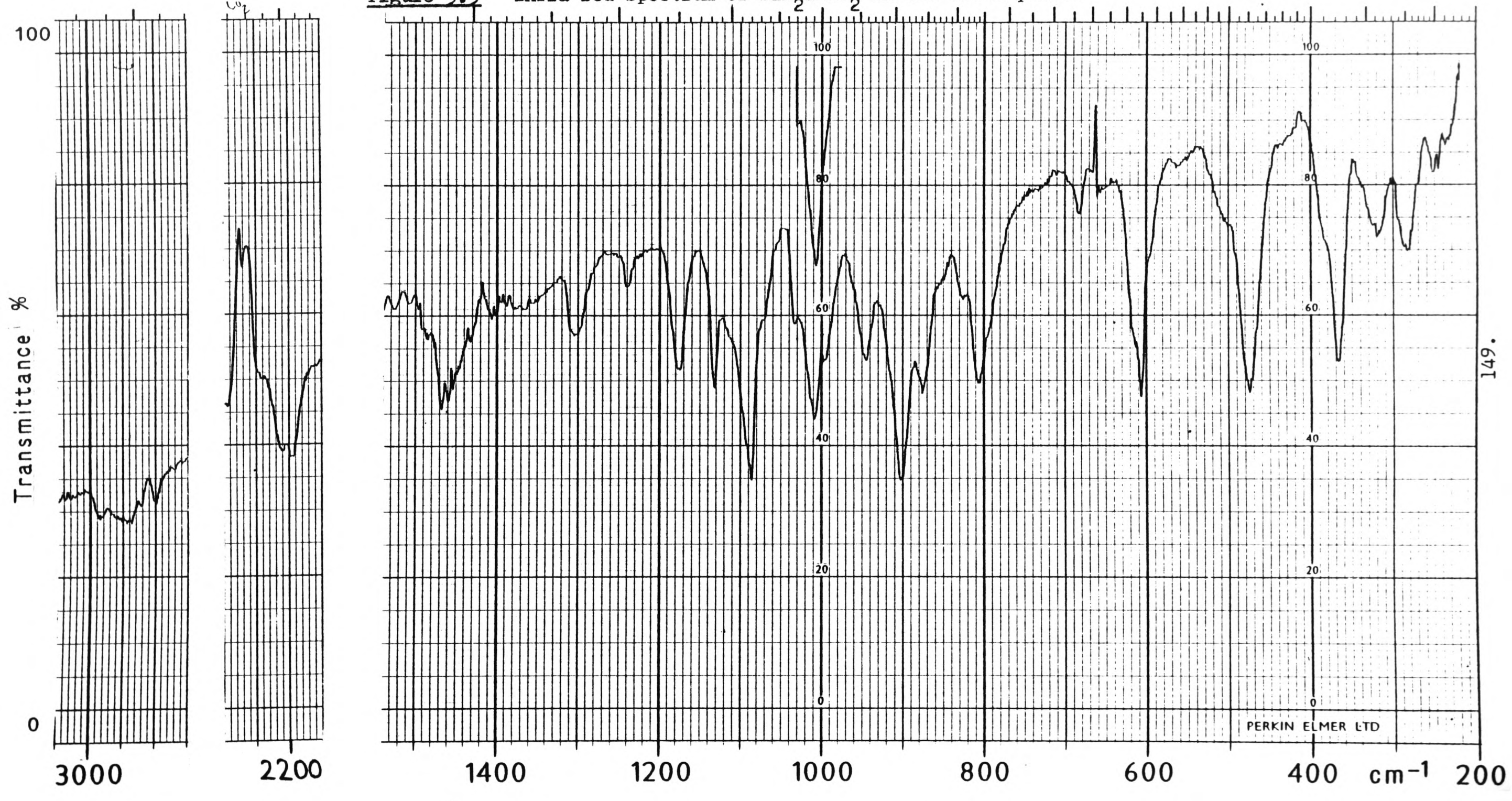

deformations, and these are encouragingly consistent with those observed for the chloride and bromide.

The two characteristic Si_2N_2 ring stretching bands were again evident in both spectra, with a particularly large splitting of $199cm^{-1}$ in the infra-red spectrum. In the Raman spectrum, however, a much smaller separation of $157cm^{-1}$ was noted. Although the Raman spectrum was recorded at 180K, this region of the spectrum was also recorded at room temperature showing clearly that the solid sample was almost completely dimeric even then.

Between $480cm^{-1}$ and $600cm^{-1}$, the active bands are tentatively assigned to the Si-H torsional and rocking modes, and not unexpectedly the infra-red active torsion is too weak to be observed.

Of the remaining bands, the CNC in plane deformations are assigned to the absorptions at around $375cm^{-1}$, in keeping with those observed for SiH_2ClNMe_2. The Si-I stretching modes, however, are more difficult to assign, since these will be shifted down into the region below $350cm^{-1}$. By comparison with the spectra obtained for SiH_2XNMe_2 (X = Cl, Br and I), these are assigned to the absorptions at $324cm^{-1}$ and $314cm^{-1}$ in the infra-red and Raman spectra, respectively. These values compare with $334cm^{-1}$ (infra-red) and $329cm^{-1}$ (Raman) for ν(SiI) in $SiCl_3I.NMe_3$,[100] although here this mode is strongly mixed with ν(SiCl).

Again, these shifts to low frequency (ν(SiI), $362cm^{-1}$ in the gas-phase) are consistent with a much weakened silicon-iodine bond, characteristic of a strong intermolecular interaction.

TABLE 5.5

OBSERVED FREQUENCIES (cm^{-1}) AND ASSIGNMENTS FOR THE $SiH_2I(NMe_2)$ DIMER

Infra-Red(Solid) SiH_2INMe_2		Raman(Solid) SiH_2INMe_2		Assignment
2,970w	)		)	
	)		)	
2,885w,br	) Not		)	ν s/as(CH),
	) well		)	
2,846w	) defined		)	3Au+3Ag+3Bg+3Bu
	)		)	
2,799w	)	NOT	)	
		RECORDED		
2,224m				νas/(SiH), Au
2,193m				νs(SiH), Bu
		1,487w	)	
			)	
1,470m		1,470s	)	
			)	
1,460m		1,454m	)	δs/as(CH),
			)	
		1,444)w	)	
		)	)	3Au+3Ag+3Bg+3Bu
		1,440)m	)	
			)	
1,434w		1,429s	)	
			)	
1,408w		1,411w	)	
			)	
		1,398w	)	
1,240w		NOT		ρ(CH), Au
1,134m		RECORDED		ρ(CH), Bu
		1,096m		ρ(CH), Bg
1,033m				ρ(CH), Bu
		1,015m		ρ(CH), Bg
1,010s	)			νs(CN), Bu
	)			
999m,sh	)			

TABLE 5.5

OBSERVED FREQUENCIES (cm^{-1}) AND ASSIGNMENTS FOR THE $SiH_2I(NMe_2)$ DIMER (continued)

Infra-Red(Solid) SiH_2INMe_2	Raman(Solid) SiH_2INMe_2	Assignment
	991vw)) 980vw)	νs(CN), Ag
949m		νas(CN), Au
	958w)) 946m)	νas(CN), Bg
919m,sh?		β(SiH), Bu(bend)
	924w	β(SiH), Ag(bend)
906s		β(SiH), Bu(wag)
	903m	β(SiH), Ag(wag)
810s))		ν as(SiN), Bu
798m,sh)		
	753m	νs(SiN), Ag
	656w	
618s,sh)) 611s)) 601m,sh)		νas(SiN), Bu
	596vs	νs(SiN), Ag
	585w/m	τ(SiH), Au
500m,sh)) 480s)		γ(SiH), Au(rock)
	488s	γ(SiH), Bg(rock)
371s		β(CNC), Bu

TABLE 5.5

OBSERVED FREQUENCIES (cm^{-1}) AND ASSIGNMENTS FOR THE $SiH_2I(NMe_2)$ DIMER (continued)

Infra-Red(Solid) SiH_2INMe_2	Raman(Solid) SiH_2INMe_2	Assignment
	378m	β(CNC), Ag
324m		ν_{as}(SiI), Bu
	314w	ν_{s}(SiI), Ag
286m		
	293s	
257w))? 250w)		
	273m)) 262m)	
	153)) 147)	
	113	
	87	
	38	

CHAPTER 6

THE GAS-PHASE STRUCTURE OF $SiH_2(NMe_2)_2$

6.1 INTRODUCTION

Bis(dimethylamino) silane was first prepared and characterised by Aylett and Peterson,[33] but unlike most other silyl-amines, no structural data exists for this compound. The molecular structure is of interest, since studies of other silyl-amines with a central silicon atom with more than one amine group are very rare indeed. As with other related compounds, the geometry at nitrogen is the most important feature, although here the possibility of inequivalent $-NMe_2$ groups exists. These have been shown by Ebsworth et al[101] to be equivalent at room temperature by ^1H n.m.r.

6.2 MOLECULAR MODEL FOR $SiH_2(NMe_2)_2$

The molecular model used to define the atomic coordinates of $SiH_2(NMe_2)_2$ was very similar to that used in solving the structures of the compounds SiH_2XNMe_2. A subroutine, assuming local C_{3V} symmetry in the methyl groups, was written using the Si-N, C-N and C-H bond lengths and the CNC, NCH, NMe_2 dip, NMe_2 wag, C-N bond torsion and Si-N bond torsion angles. The dip, wag and torsions angles all being designated positive as before, although the Si-N torsion was now considered positive if the $-NMe_2$ group rotated in a clockwise sense viewed along the Si-N bond from N to Si. This routine was then called again to generate the other $-NMe_2$ group in conjunction with an angle, NSiN, thus allowing the two groups to be inequivalent. At various stages in the refinement the model was altered to fix equivalent parameters in the two groups to have identical values. Again, all of the SiNC angles were calculated as dependent parameters. The nozzle to plate distances and the operating wavelengths are given in Table 6.1.

TABLE 6.1

WEIGHTING FUNCTIONS, CORRELATION PARAMETERS AND SCALE FACTORS

	Distance(mm)	nm^{-1} Δs	Smin	S_1	S_2	Smax	P/h	Scale Factor	Wavelength pm
$SiH_2(NMe_2)_2$	128.3800	4	60	80	300	340	0.2510	0.736(18)	5.699
$SiH_2(NMe_2)_2$	285.3401	2	20	40	124	144	0.2343	0.867(9)	5.699

6.3 REFINEMENT OF THE $SiH_2(NMe_2)_2$ STRUCTURE

The radial distribution curve for $SiH_2(NMe_2)_2$ is illustrated in Figure 6.1 and it shows distinct peaks for the bonded C-H, C-N and Si-N distances and non-bonded Si...C distances (two overlapping peaks). The non-bonded N...H and two C...C distances (short) appear as shoulders of the Si...C peak, at 212pm and ≃240pm respectively, whilst the remaining 4C...N and 4C...C distances (long) give rise to broad overlapping peaks between 340 and 530pm. The bonded distances all refined well except Si-H which was fixed and it proved impossible to distinguish two different Si-N bond lengths, therefore these were constrained to be identical. The angles around nitrogen, CNC, C'N'C', SiNC and SiN'C', were all well defined with angles CNC and C'N'C' refining easily to different values. This inequivalence was also apparent in the two different dip angles, although the e.s.d's. were again large, like those of the monohalosilyl—dimethylamines. Both Si-N torsion angles, defined by the C...N and C...C non-bonded distances, refined acceptably and again the two SiNC angles in each $-NMe_2$ group were found to be equal. Of the remaining angles, both NCH and NSiN were refined, although angle NSiN was poorly defined due to its strong correlation with both dip angles, the N...N and Si...C

distances being very similar. The C-N torsion angles for both $-NMe_2$ groups were investigated by R-factor plots and in both cases, minima were obtained when the angles were zero, hence these angles were constrained to be equal at this value.

Finally, the $-SiH_2$ tilt and HSiN angles were fixed, again after a series of refinements where these parameters had different values.

The amplitudes of vibration of the bonded atom pairs all refined easily, except u(Si-H), which was fixed throughout refinement. Most of the heavy atom non-bonded amplitudes were also refined and the following constraints were applied.

u 9 = 1 x u 10/11/12

u16 = 1 x u 13/14/15

u40 = 1 x u 5/ 7/41

All other amplitudes which were not refined, were fixed at reasonable values.

The correlation matrix (Table 6.2) revealed strong correlation between the inter-related dip(s), CNC(s) and t(Si-N)(s) angles and the Si...C non-bonded amplitudes. The final parameter list is given in Table 6.3 and the corresponding R-factors are R_G = 0.063 R_D = 0.052. The molecular intensity curves and pluto plots of the molecule are illustrated in Figures 6.2 and 6.3 respectively.

Figure 6.1 Observed and final difference radial distribution curves for $SiH_2(NMe_2)_2$.

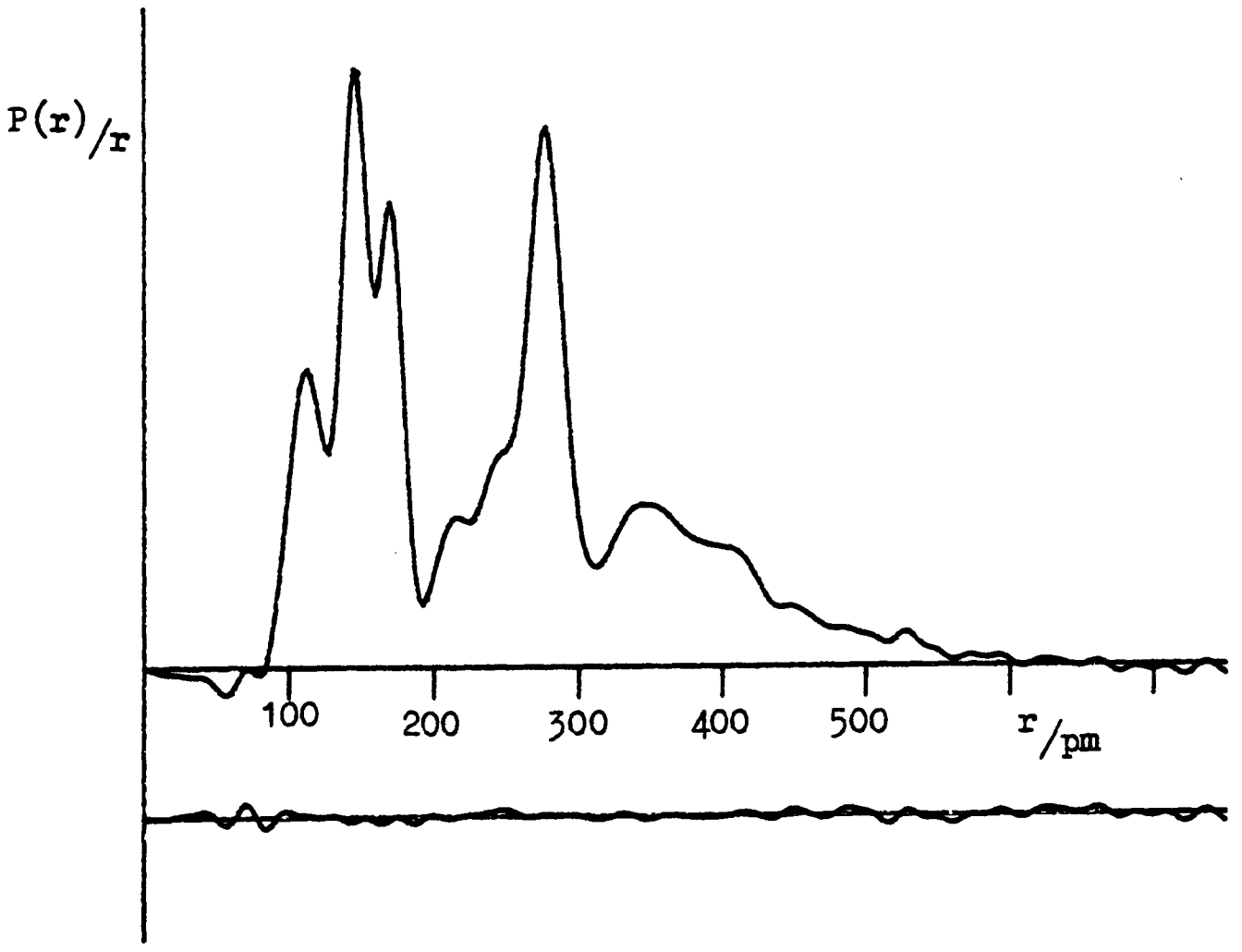

Before Fourier inversion the data were multiplied by $S.\exp(-0.00002\,S^2/(Z_{Si}-f_{Si})(Z_N-f_N))$.

Figure 6.2 $SiH_2(NMe_2)_2$

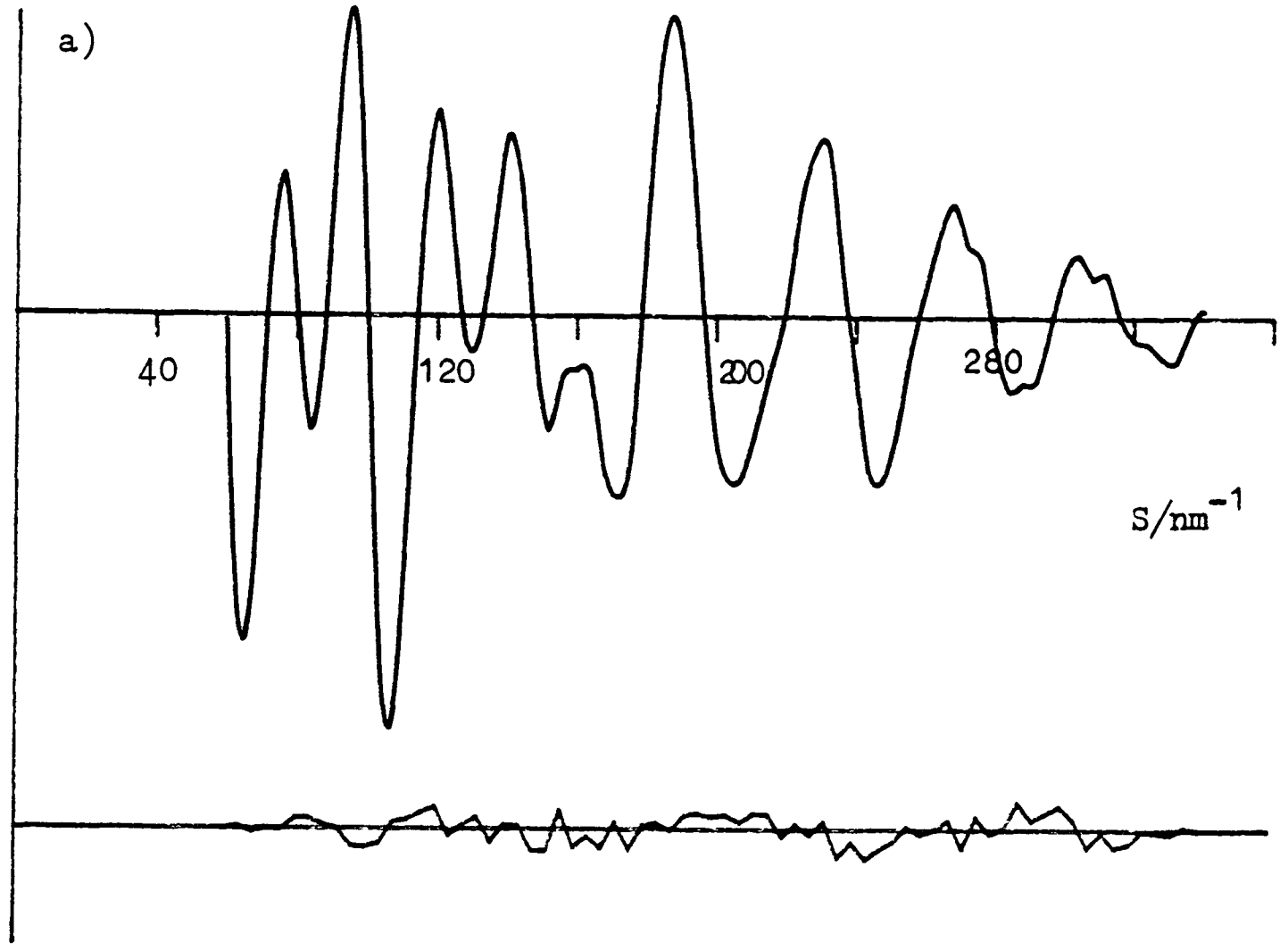

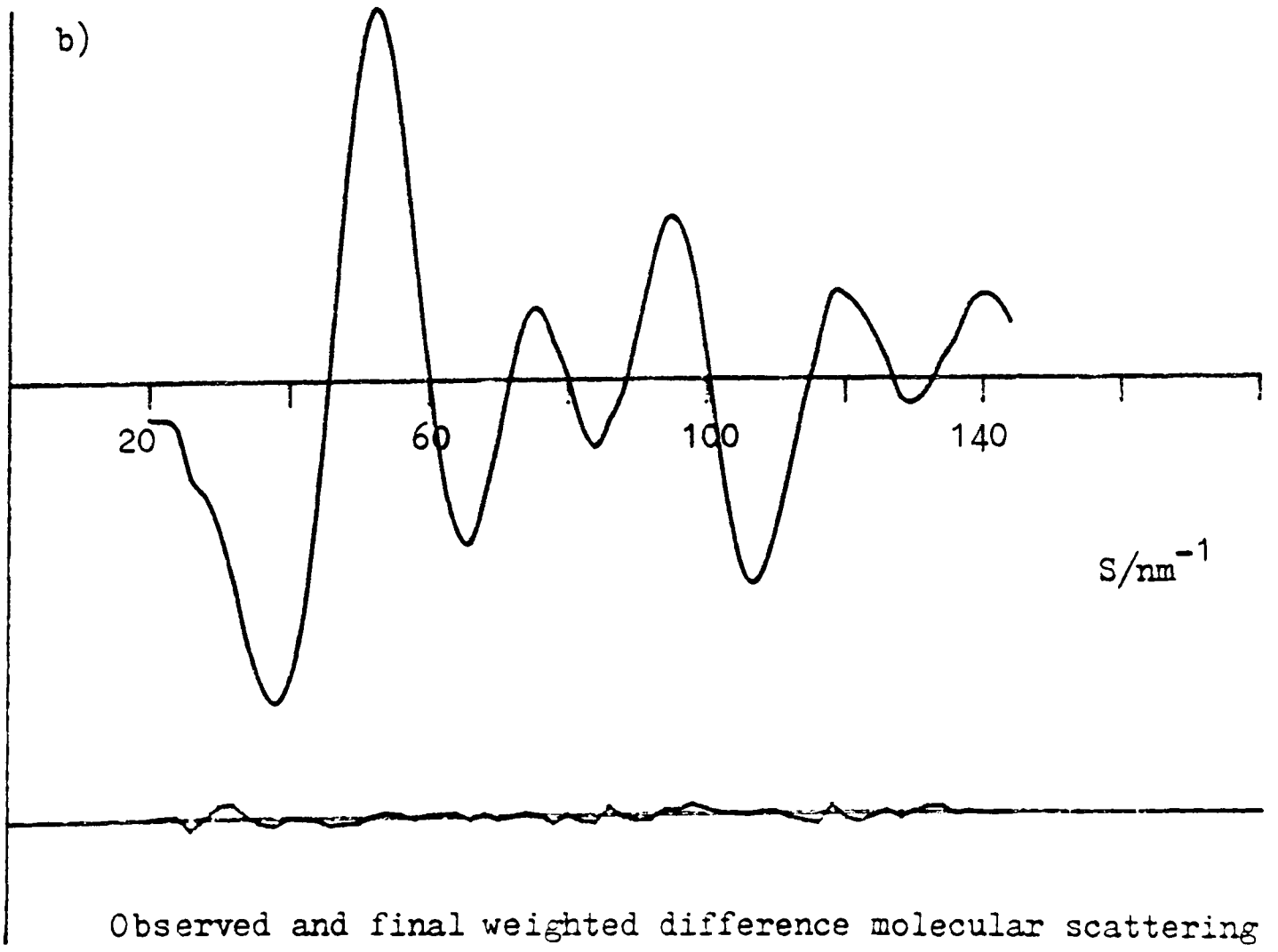

Observed and final weighted difference molecular scattering intensities at camera distances of a) 128mm and b) 285mm.

Figure 6.3 $SiH_2(NMe_2)_2$.

a)

b)

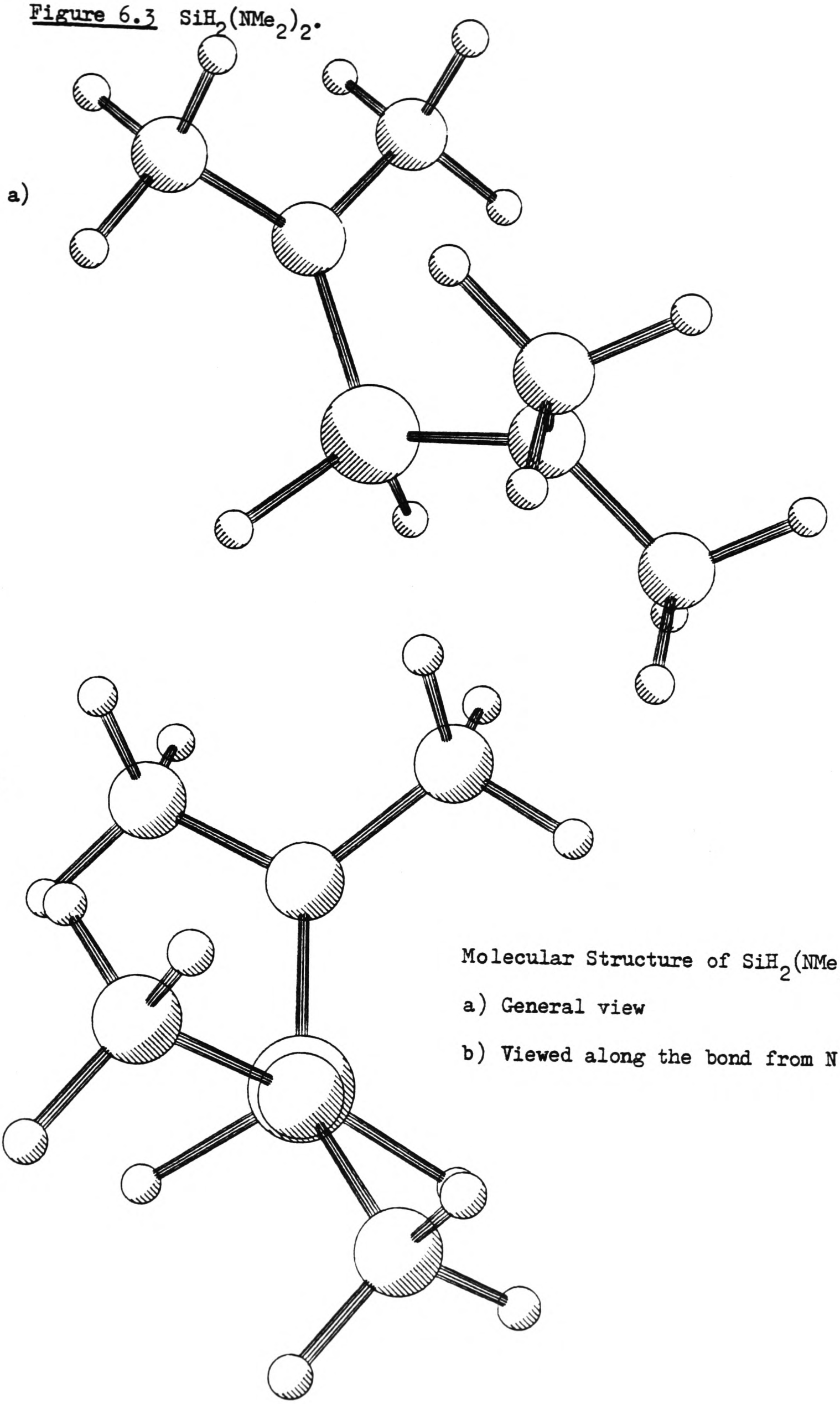

Molecular Structure of $SiH_2(NMe_2)_2$

a) General view

b) Viewed along the bond from N to Si.

TABLE 6.2

LEAST SQUARES CORRELATION MATRIX (X100) FOR $SiH_2(NMe_2)_2$*

	r3	a2	a3	a5	a7	a10	a11	a13	u9	u16	u40	k1	k2
r2	54												
a1		-40	54	40		40	42					-47	
a2				-83	-56	-78	-76	-72			83		
a3												-49	
a5					66	94	88	52			-91		
a7						51	48	56			-62		
a10							92		-43		-85		
a11									-41	45	-79		
a13											-62		
u2													65
u3													40
k1													40

*Only off-diagonal elements with magnitude ≥ 40 are shown.

TABLE 6.3

MOLECULAR PARAMETERS FOR $SiH_2(NMe_2)_2$

a) Independent Parameters

		Distance	Amplitude
r_1	(Si-N)	170.8(1)	5.6(2)
r_2	(C-N)	146.0(1)	5.1(2)
r_3	(C-H)	111.7(2)	8.8(2)
r_4	(Si-H)	148.0(fixed)	8.8(fixed)
		Angles	
a_1	<CNC	108.4(6)	
a_2	DIP(CNC)	22.8(36)	
a_3	<NCH	109.9(5)	
a_4	<HSiH	108.0(fixed)	
a_5	<NSiN	112.1(23)	
a_6	T(C-N)	0.0(fixed)*	
a_7	T(Si-N)	40.9(18)	
a_8	WAG(CNC)	0.0(fixed)*	
a_9	WAG(C'N'C')	0.0(fixed)*	
a_{10}	DIP(C'N'C')	14.4(58)	
a_{11}	T(Si-N')	17.5(20)	
a_{12}	SiH_2 TILT	3.0(fixed)*	
a_{13}	<C'N'C'	115.4(9)	

b) Dependent Parameters

		Angles
a_{14}	<SiNC(1/5)	122.6(9)
a_{15}	<SiN'C'(13/17)	121.2(11)

TABLE 6.3

MOLECULAR PARAMETERS FOR $SiH_2(NMe_2)_2$ (continued)

All distances and amplitudes of vibration are given in pm and all angles are in degrees. Angles 6, 7 and 10 are torsion angles along the given bond. * = fixed by R-factor plot.

+ = fixed after initially being refined.

c) Dependent Distances

	Distance	Amplitude
d^5(Si...C(1))	278.2(11)	8.4[c]
d^6(C(1)...C(5))	236.8(9)	6.0(fixed)
d^7(Si...C'(13))	276.2(16)	8.4[c]
d^8(N...N)	283.3(38)	10.0(fixed)
d^9(N(9)...C(13))	345.7(25)	15.2(13)
d^{10}(N(9)...C(17))	378.1(16)	15.2[c]
d^{11}(N(21)...C(1))	413.6(34)	15.2[c]
d^{12}(N(21)...C(5))	349.3(35)	15.2[c]
d^{13}(C(1)...C(13))	458.4(32)	14.8[c]
d^{14}(C(1)...C(17))	520.2(14)	14.8[c]
d^{15}(C(5)...C(13))	415.9(67)	14.8[c]
d^{16}(C(5)...C(17))	397.3(22)	14.8(16)
d^{17}(C(1)...H(6))	335.0(9)	14.5[+]
d^{18}(C(1)...H(7))	261.8(16)	14.5[+]
d^{19}(C(1)...H(8))	261.8(16)	14.5[+]
d^{21}(N(9)...H(2))	211.9(5)	10.5(4)
d^{40}(Si...C(5))	278.2(11)	8.4(5)
d^{41}(Si...C(17))	276.2(16)	8.4[c]
d^{43}(C(13)...C(17))	246.8(12)	6.0(fixed)

TABLE 6.3

MOLECULAR PARAMETERS FOR $SiH_2(NMe_2)_2$ (continued)

d) Other Amplitudes which were fixed

	Amplitude
C(1)...H(11)	20.0
N(9)...H(12)	15.0
Si...H(2)	18.0
C(13)...H(2)	20.0
C(17)...H(2)	20.0
N(9)...H(14)	20.0
C(1)...H(18)	20.0
H(2)...H(12)	20.0
H(2)...H(3)	11.0
H(2)...H(7)	20.0
H(11)...H(12)	12.0
H(2)...H(14)	25.0

Molecular Numbering

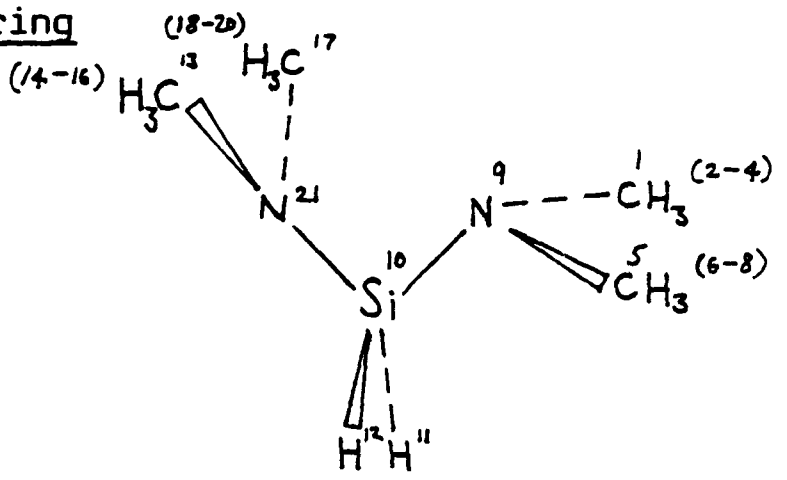

Atoms C^{1} and C^{5} = "C", atoms C^{13} and C^{17} = "C'".

Atom N^{9} = "N", atom N^{21} = "N'".

6.4 RESULTS AND DISCUSSION

The overall molecular conformation of bis(dimethylamino)silane is, like the monohalosilyl—dimethylamines, controlled by the eclipsing interactions of the Si-H and C-N bonds. In the compounds SiH_2XNMe_2 (X=Cl,Br and I) the Si-H and C-N bonds were mutually trans with respect to the Si-N bond and in $SiH_2(NMe_2)_2$ this arrangement might also be expected to be preferred. Here, however, the steric interactions of the four methyl groups must be considered, and this arrangement would result in very short and unfavourable contacts. The resultant structure, with non-planar nitrogen atoms, has one group (C'N'C') mutually trans to the two Si-H bonds and the other (CNC) mutually cis. The CNC group is then twisted about the Si-N bond by 41° to relieve the potentially eclipsing Si-H/C-N interactions, (see Figure 6.3). A torsion of greater magnitude than this, resulting in the Cl-N9 bond being perfectly staggered, would give rise to shorter contacts between three of the methyl groups (C_{13}, C_{17} and C_5) and would result in a smaller $C_5\ N_9\ SiN_{21}$ dihedral angle. This torsion also ensures that the CNC group lone pair is not eclipsing the Si-N' bond. The Si-N' torsion angle of 18° serves to reduce crowding of the three methyl groups by moving C_{17} towards the CNC group, but more significantly C_{13} further away.

The geometry at nitrogen in both $-NMe_2$ groups is non-planar with dip angles of 23° and 14°, and $\sum$[2x(SiNC)+CNC] of 353.6(24)° and 357.7(32)° for the CNC and C'N'C' groups respectively. This is expected, since the monosilyl-amines are generally non-planar and it is therefore unlikely that one silicon centre will be able to 'absorb' a sufficient amount of the lone pair electron density from two $-NMe_2$ groups to confer planarity on either one or both of the nitrogen centres. It is, therefore, surprising to note that the

C'N'C' group is flatter than in any of the monohalosilyl—amines, although the e.s.d. in $\sum$is large.

A gas-phase electron diffraction study[102] of $Si(NMe_2)_3Cl$ has shown that the $-NMe_2$ groups are planar, although this is undoubtedly due to steric rather than electronic factors. Shrinkage effects may also be more important for $SiH_2(NMe_2)_2$, since a planar $-NMe_2$ group would be expected to have a short Si-N bond. In $SiH_2(NMe_2)_2$, both Si-N bond lengths were found to be 170.8(1)pm which is not particularly short and is comparable with r(Si-N) for $Si(H_nMe_{3-n})NMe_2$ [46,47] (where n = 0,1,2 or 3).

The Si-N bond length in $Si(NMe_2)_3Cl$ is 171.5(2)pm, which is also comparable, and so steric effects may also influence the geometry at nitrogen (N') in $SiH_2(NMe_2)_2$.

Further evidence that it is the (wide) SiNC angles rather than angle CNC which determine the geometry at nitrogen, for any given dip angle, is afforded by the presence of SiNC(x2) and SiN'C'(x2) angles of 122.6(9)° and 121.2(11)° respectively. These are consistently wide, as in other silylamines, whilst the CNC and C'N'C' angles have the vastly differing values of 108.4(6)° and 115.4(9)°. The C'N'C' angle being comparable with that found in other silyl—amines (see Table 3.9) whilst angle CNC is very similar to that found in the pyramidal alkylamines $NHMe_2$[49] and NMe_3.[49]. This structure would therefore seem to indicate the ease with which the $-NMe_2$ group can be deformed, and hence the importance of shrinkage effects in considering the observed structures.

Of the remaining bond angles, NCH, and the calculated HCH's were all close to the tetrahedral value. The angle NSiN, although poorly defined at 112.1(23)°, is slightly greater than tetrahedral, and can probably be compared with the widened angles XSiN in the

halosilyl-dimethylamines.

The C-N and C-H bond lengths of 146.0(1)pm and 111.7(2)pm respectively are both very similar to those in other silyl-amines and do not require further comment.

Finally, the hydrogen atoms in both $-NMe_2$ groups were found to be fully eclipsed and the torsion angles were 0^o in each case.

CHAPTER 7

THE GAS-PHASE STRUCTURE OF $SiH_2(OCHO)_2$ BY ELECTRON DIFFRACTION

7.1 INTRODUCTION

Interest in the structural aspects of silyl and germyl esters has recently become quite marked following gas-phase structure determinations of silyl formate[103] and silyl acetate.[104] These molecules have essentially cis conformations with respect to the C-O bond, although small torsions ensure that the Si-O and C=O bonds are not perfectly eclipsed. This conformation gives rise to short intramolecular contacts (≃280pm) between the Si and carbonyl O atoms. This compares with a value of 350pm for the sum of the van der Waals' radii for the two atoms. Intramolecular contacts of this type are also known for the carbon analogues of these esters, where this cis conformation yields a C...O distance of 268pm in the gas-phase for methyl formate[105] and the sum of the van der Waals' radii is 320pm. It is apparent therefore, that this intramolecular interaction is more significant for silicon compounds. Structural investigations of these compounds in the solid phase have also been carried out, since in the crystal additional intermolecular interactions are possible. In crystalline silyl acetate, the Si...O(carbonyl) intermolecular contact (273pm) is even shorter than intramolecular contact (283pm).

Crystal structure determinations of the carbon analogues, e.g. methyl acetate[104] reveal that although the short intramolecular contact is present, no intermolecular interactions exist, in contrast to the silyl esters. The crystal structure of silylmonothio-acetate,[106] also contains a short intramolecular contact between the Si and S atoms (319pm) and an intermolecular contact between Si and S

of 338pm. Here the sum of the van der Waals' radii for Si and S is 390pm. This reflects the poorer electron donor properties of sulphur relative to oxygen. Compounds of this type are obviously also of interest, because of the possibility of isomerism by either O or S binding to silicon. The structure of $SiH_2(OCHO)_2$ in the gas-phase is therefore of interest since it contains two formate groups which can interact with the central silicon atom and obviously here steric constraints may also be influential on the molecular structure.

7.2 MOLECULAR MODEL FOR $SiH_2(OCHO)_2$

The molecular model used to generate the atomic coordinates of deformatosilane assumed that the OCHO groups were planar, and that the bond lengths and bond angles in both formate groups were the same. The molecule was then defined by fourteen parameters: five bond lengths, five bond angles and four torsion angles. The bond lengths were Si-H, Si-O, O-C, C=O and C-H, the angles were HSiH, OSiO, SiOC, OCO and HCO (carbonyl oxygen). The four torsion angles were for the Si-O and C-O torsions in each of the two formate groups. This meant that the torsions in each group were completely independent. The nozzle to plate distances and operating wavelengths used in the $SiH_2(OCHO)_2$ experiment are given in Table 7.1.

TABLE 7.1

WEIGHTING FUNCTIONS, CORRELATION PARAMETERS AND SCALE FACTORS

	Distance(mm)	nm^{-1} ΔS	Smin	S_1	S_2	Smax	P/h	Scale Factor	Wavelength (pm)
$SiH_2(OCHO)_2$	285.4800	2	20	40	124	144	-0.1282	0.639(4)	5.693(6)
$SiH_2(OCHO)_2$	128.3599	4	68	80	300	328	-0.0746	0.771(13)	5.693(6)

7.3 REFINEMENT OF THE $SiH_2(OCHO)_2$ STRUCTURE

The radial distribution curve for $SiH_2(OCHO)_2$ (Figure 7.1) consists of two peaks below 200pm. The first of these at ≃125pm is broad and contains overlapping peaks for the C-H, C=O and C-O distances, the second contains the Si-O and SiH peaks and is centred at 167pm. The C=O and C-O bond lengths both refined well, but attempts to refine the C-H bond length, which was only a smaller contributor to the overall molecular intensity, proved impossible and so this parameter was subsequently fixed. The Si-O and Si-H bond lengths were also both refined, although the Si-H bond had a predictably larger e.s.d. than any of the other bond lengths.

The principal peaks in the radial distribution curve due to the non-bonded distances were at 225pm for the O...O distance within the formate group, 264pm for the two equivalent Si...C distances (with a shoulder at 290pm due to the two Si...O (carbonyl) distances) and at 445pm due to the overlapping C...C and O...O (carbonyl O on one formate group to Si bound O on the other) distances. The Si...C and O...O 225pm distances determine the SiOC and OCO angles respectively, and these distinct peaks gave well determined values for the two angles.

Of the other angles, angle OSiO was refined but it had a significantly larger e.s.d. than either SiOC or OCO, and angles HSiH and HCO were fixed at 110° and 120° respectively. The long distance O...O (carbonyl-carbonyl), C...C and the four C...O peaks will determine the overall molecular conformation and this is controlled by the four torsion angles. Initially R-factor loops were performed on the torsion angles in an attempt to investigate all of the conformations which might possibly fit the data. After this had been completed, and one preferred conformation had been established, all

four torsions were allowed to refine simultaneously.

The amplitudes of vibration for the bonded atoms were all refined except Si-H and C-H, which were fixed at 7.7 and 7.0pm respectively. The non-bonded amplitudes not involving H atoms were all refined at some stage, but in the final refinement only O...O(U_6), Si...C(U_7) and Si...O(U_9) were refining. Problems were encountered when attempts were made to constrain some of the amplitudes, particularly Si...O(U_9) and Si...O(U_{10}). With this constraint applied the fit was considerably worsened, and ultimately when these amplitudes were refined independently, they had considerably different values. It was also found that some of the amplitudes tended to refine to very large values, particularly O...O(U_8), Si...O(U_{10}) and O...C(U_{12}). All of the amplitudes involving one or more H atoms were fixed at reasonable values throughout the refinement. The final list of parameters is given in Table 7.2. The molecular intensity curves are given in Figure 7.2, and the very close agreement between the experimental and calculated intensity distributions is revealed in the difference curve and the final R-factors, of R_G = 0.053 and R_D = 0.059. The least squares correlation matrix (Table 7.3) shows the significant correlation between angle OSiO and one of the SiO torsions, and between some of other torsion angles. This explains why these parameters did not tend to refine well. Pluto plots of $SiH_2(OCHO)_2$ are given in Figure 7.3.

7.4 RESULTS AND DISCUSSIONS

Diformatosilane like SiH_3OCHO,[103] SiH_3OCOCH_3[104] and the carbon analogues of these esters was found to have both formate groups in a cis conformation with respect to the C-O bond, yielding two short intramolecular Si...O contacts. Two O-Si-O-C linkages are also

Figure 7.1 Observed and final difference radial distribution curves for $SiH_2(OCHO)_2$.

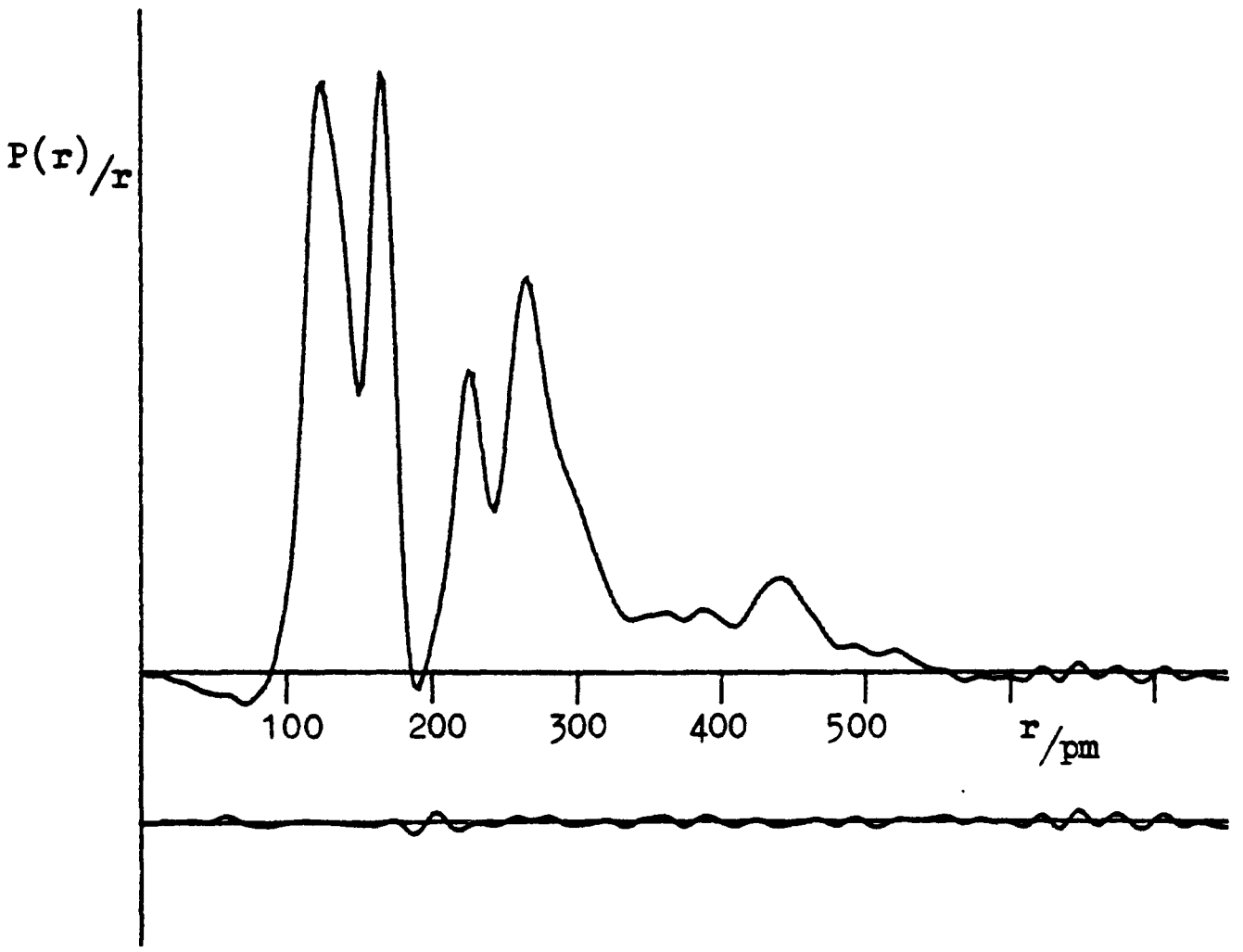

Before Fourier inversion the data were multiplied by $S.exp\ (-0.00002\ S^2/(Z_{Si}-f_{Si})(Z_O-f_O))$.

Figure 7.2 $SiH_2(OCHO)_2$

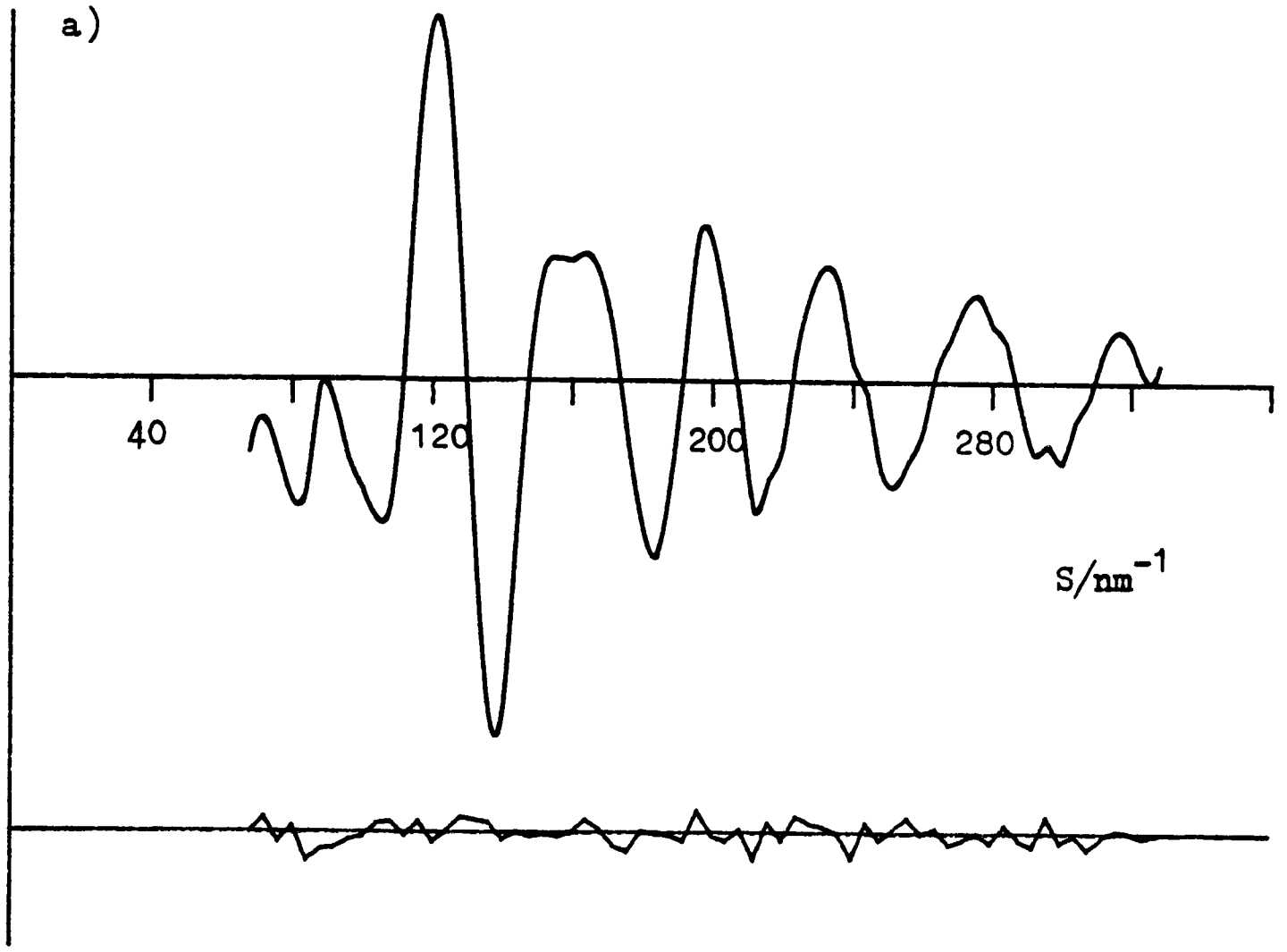

Observed and final weighted difference molecular scattering intensities at camera distances of a) 128mm and b) 285mm.

Figure 7.3 $SiH_2(OCHO)_2$

a)

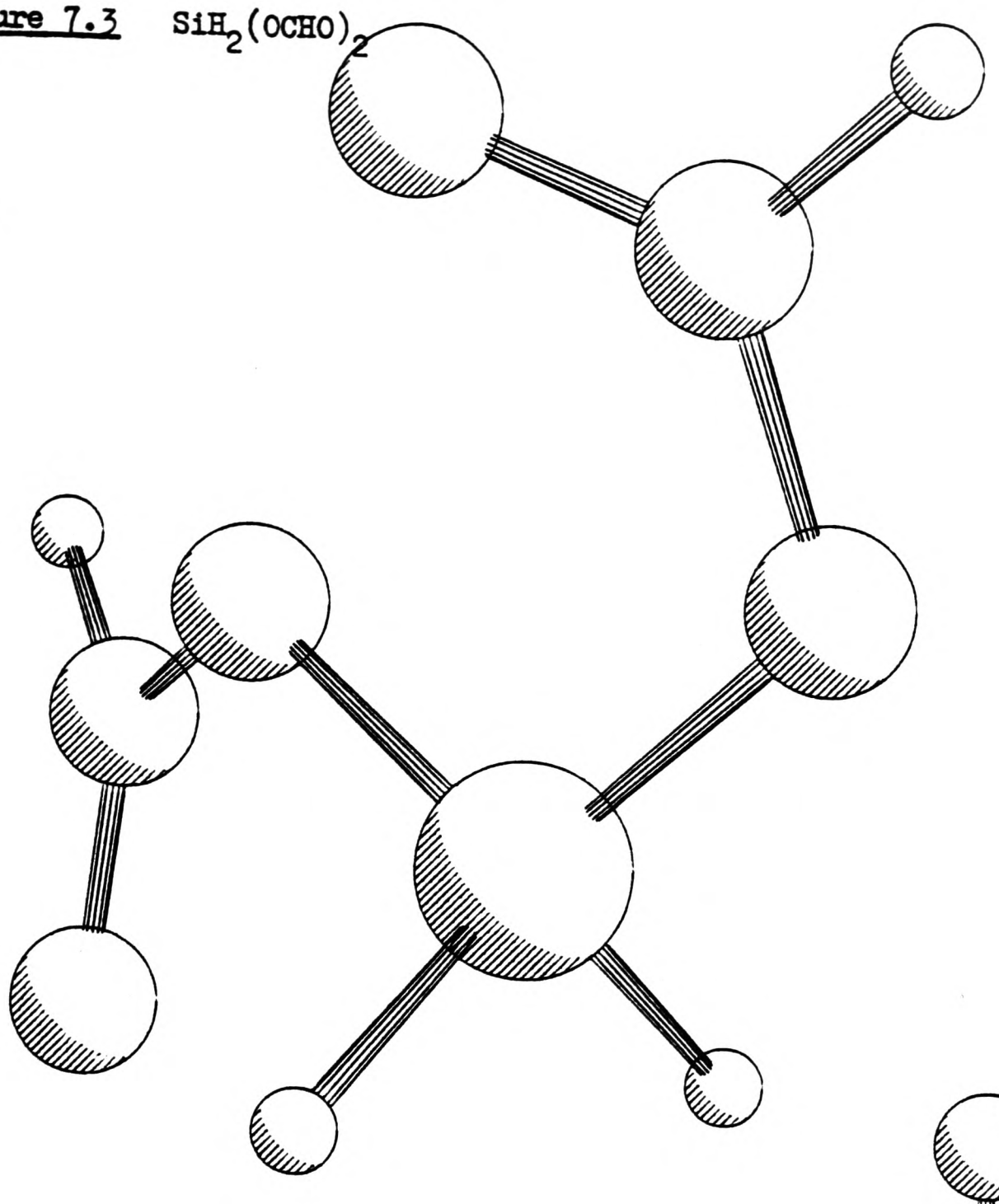

b)

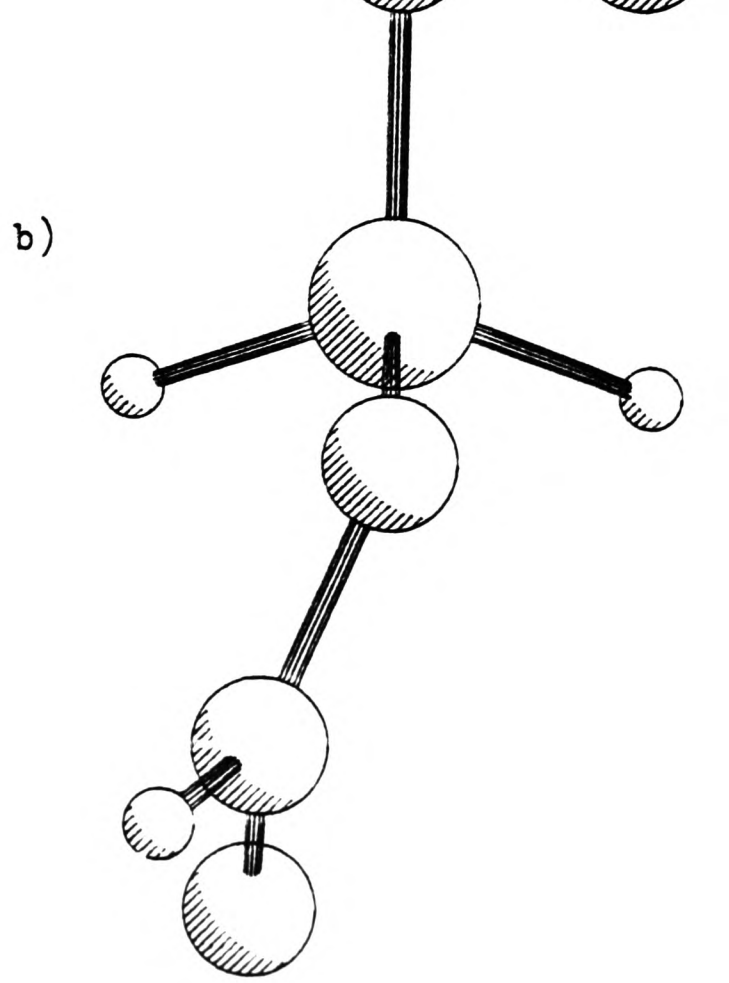

Molecular Structure of $SiH_2(OCHO)_2$

a) General view

b) Viewed through the OSiO plane.

TABLE 7.2

MOLECULAR PARAMETERS FOR $SiH_2(OCOH)_2$

a) Independent Parameters

	Distance	Amplitude
r_1(Si-H)	151.6(9)	7.7(fixed)
r_2(Si-O)	166.7(1)	5.1(1)
r_3(C-O)	136.7(1)	5.4(2)
r_4(C=O)	121.4(1)	4.1(2)
r_5(C-H)	110.6(fixed)*	7.0(fixed)
	Angles	
a_1 <HSiH	110.0(fixed)	
a_2 <OSiO)	109.3(17)	
a_3 <SiOC	120.4(3)	
a_4 <O-C=O	121.3(2)	
a_5 <H-C=O	120.0(fixed)	
a_6 T(Si-O)	212.6(46)	
a_7 T(Si-O')	-27.4(49)	
a_8 T(C-O)	169.0(67)	
a_9 T(C'-O')	207.0(62)	

All distances and amplitudes of vibration are given in pm and all angles are in degrees. Angles 6-9 are torsion angles along the given bond. (fixed)* = fixed after being refined.

TABLE 7.2

MOLECULAR PARAMETERS FOR $SiH_2(OCOH)_2$ (continued)

b) Dependent Distances

	Distance	Amplitude
$d_6(O_2...O_6)$	252.3(2)	6.3(2)
$d_7(Si...C)$	263.9(3)	8.2(3)
$d_8(O_2...O_3)$	272.0(28)	42.0(fixed)*
$d_9(Si...O_6)$	288.2(11)	15.0(9)
$d_{10}(Si...O_7)$	292.8(24)	46.3(fixed)*
$d_{11}(O_3...C_4)$	303.6(24)	15.6(fixed)*
$d_{12}(O_2...C_5)$	395.5(25)	45.6(fixed)*
$d_{13}(O_3...O_6)$	260.7(18)	20.8(fixed)*
$d_{14}(O_2...O_7)$	449.9(23)	18.7(fixed)*
$d_{15}(C_4...C_5)$	438.5(15)	12.2(fixed)*
$d_{16}(O_6...O_7)$	484.5(36)	27.8(fixed)*
$d_{17}(C_5...O_6)$	390.8(17)	15.9(fixed)*
$d_{18}(C_4...O_7)$	517.3(16)	16.8(fixed)*

Numbering :

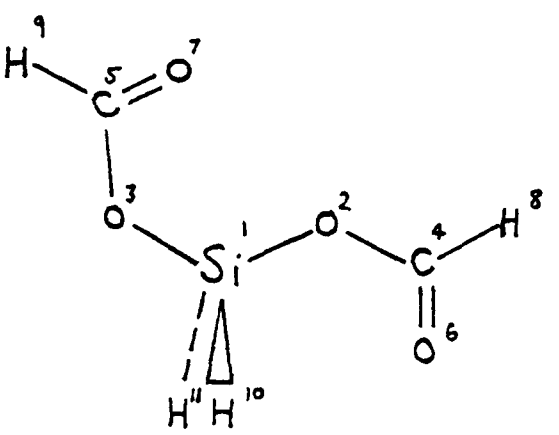

TABLE 7.2

MOLECULAR PARAMETERS FOR $SiH_2(OCOH)_2$ (continued)

Examples of other amplitudes which were fixed

	Amplitude
$(H_{10}\ldots O_2)$	11.0
$(H_{10}\ldots O_6)$	20.0
$(H_8\ldots O_6)$	10.0
$(H_8\ldots O_2)$	10.0
$(H_8\ldots O_3)$	20.0
$(H_{10}\ldots C_4)$	15.0
$(H_8\ldots C_5)$	20.0
$(H_8\ldots Si)$	15.0
$(H_{10}\ldots H_{11})$	10.0
$(H_{10}\ldots H_8)$	20.0
$(H_8\ldots H_9)$	25.0

TABLE 7.3

LEAST SQUARES CORRELATION MATRIX (X100) FOR $SiH_2(OCOH)_2$*

	r3	a3	a4	a6	a8	a9	u3	u4	u9	k2
r1		-44					-65	-42		
r2	43	-42	-41							
r3		-47	-61							
r4			-50							
a2		41		-84		-46				
a3			49	-57						
a4				-45	45					
a6					-67	45				
a7					51					
u2										60
u3								68		
u7									57	

*Only off-diagonal elements with magnitude ≥40 are shown.

present, however, and one of these was found to be close to cis with respect to the Si-O bond, whilst the other was trans. This was rather surprising, since on steric grounds, it would be expected that a trans, trans arrangement would be favoured. The observed cis, trans conformation gives rise to a very short contact of 261pm between the carbonyl oxygen of the cis formate group to the single-bonded oxygen of the trans group. The sum of the Van der Waals radii for two oxygen atoms is 280pm, so although this contact cannot be electrostatic in nature, it obviously does not induce any serious steric strain on the molecule in the gas-phase.

The molecular parameters for the formate groups are quite consistent with those observed for other silyl esters. In silyl formate in the gas-phase, the C=O bond length is 121pm and the OCO angle is 123°, compared with 121pm and 121° respectively for $SiH_2(OCHO)_2$. The H-C=O angle was fixed at 120°, hence the H-C-O angle is ≃119°. This is not unreasonable, since it would be expected that the heavy atom OCO angle would be the widest within the formate group.

TABLE 7.4

COMPARISON OF SPECIFIC BOND LENGTHS, ANGLES AND NON-BONDED DISTANCES IN VARIOUS SILYL ESTERS

Compound (gas-phase)	Si-O	C-O	<SiOC	Si...O	Si...C	Ref.
SiH_3OCHO	169.5(3)	135.1(6)	116.8(5)	286.5(10)	260.1(8)	2
SiH_3OCOCH_3	168.5(3)	135.8(4)	116.5(7)	279.5(13)	259.3(9)	2
$SiH_2(OCHO)_2$	166.7(3)	136.9(3)	120.4(4)	288.2(11) 292.8(24)	263.9(3)	This Work

(distances in pm; angles in degrees)

Comparison of the Si-O and C-O bond lengths in $SiH_2(OCHO)_2$ with those for SiH_3OCHO and SiH_3OCOCH_3, reveals a distinct shortening of the Si-O bond coupled with a lengthening of the C-O bond. In accord with the shortened Si-O bond, which compares with the Schomaker-Stevenson predicted value of 177pm, a clear widening of the SiOC angle is observed relative to the other silyl esters. It can be concluded from this then that there is probably greater π(p—d) character in the Si-O bonds in $SiH_2(OCHO)_2$, although π character in Si-O bonds in silyl esters is known to be low. The Si-O bond length compares with a value of 163pm in $(SiH_3)_2O$[107] and 161pm for the 2-coordinate oxygen in silicates[108] where greater π character exists. The SiOC angle is, as would be expected, intermediate in value between 144.1(8)° for $(SiH_3)_2O$ and 111.5(15)° for $(CH_3)_2O$[109] again reflecting π bonding considerations, although the wider angles observed for $SiH_2(OCOH)_2$ and $(SiH_3)_2O$ also reflect the presence of the larger Si atom. The cis conformations of the two formate group with respect to the C-O bonds induces the aforementioned short Si...O=C contacts of 288.2 and 292.8ppm, which are slightly longer than those observed for SiH_3OCHO and SiH_3OCOCH_3, but consistent with the wider SiOC angles found in $SiH_2(OOCH)_2$. This short intramolecular interaction is almost certainly electrostatic in nature, between the relatively electropositive Si and the electronegative O. This explanation is consistent with the findings that for carbon substituted esters, e.g. CH_3OCOCH_3 this shortening, relative to the sum of the van der Waals radii, is less than that observed for the analogous silyl esters, since carbon is less positive than silicon. It seems then that the additional formate group weakens the effect of the Si...O contacts whilst shortening the Si-O bond lengths. It would be interesting, therefore, to observe

whether this trend continued with increasing substitutions of hydride atoms with formate groups, although steric constraints would undoubtedly become more important with substitution in compounds of this type.

TABLE 7.5

NON-BONDED DISTANCES IN ESTERS IN THE GAS PHASE

Compound	2 bond distance M...C(pm) (M=C or Si)	Sum of Hard Sphere Radii	3 bond distance M...O(pm) (M=C or Si)	Sum of van der Waals Radii
CH_3OCHO	235.2	250(-15)*	268.7	300(-31)*
SiH_3OCHO	260.1	282(-22)	286.5	350(-64)
SiH_3OCOCH_3	259.3	282(-23)	279.5	350(-71)
$SiH_2(OCHO)_2$	263.9	282(-18)	288.2 292.8	350 (-62) (-57)

*The numbers in brackets are the differences between the experimental distances and the sum of the hard sphere or van der Waal's radii.

It is apparent from Table 7.5 that not only the Si...O but also the Si...C distance in silyl esters is shorter than expected. In all cases the Si...C distance is smaller than that predicted by Bartell's hard sphere radii,[110] and again this effect is more significant for silyl esters than for their carbon analogues. It would appear then, that this shortened distance is determined by the effect of the non-bonded eletrostatic Si...O interaction. The Si...O interactions are weaker in $SiH_2(OCHO)_2$ relative to the other silyl esters, and the observed Si...C distance is also consistently longer.

Overall, $SiH_2(OCHO)_2$ is found to possess no symmetry, although the Si-O torsions of 212(7)° and -27(7)°, and the C-O torsions of

169(10)° and 297(9)° indicate that the deviation from an idealised C_S structure with Si-O torsions of 180° and 0° and C-O torsions of 180° is not too great. A possible explanation for this is that in this conformation, eclipsing interactions between the two formate groups are eliminated. A more likely explanation however, is that these torsional deviations are simply due to shrinkage effects, brought about coupled torsional vibrations of very low frequency and very high amplitude. This is quite consistent with the requirement that some very high amplitudes of vibration were necessary for some of the non bonded C...O and O...O distances. Further evidence for a facile interchange of conformation of this type was obtained from the room temperature n.m.r. spectra (^{1}H, ^{13}C and ^{29}Si). On the n.m.r. timescale, these all indicate the magnetic equivalence of both the two formate protons, and the formate carbon atoms indicating that some sort of intramolecular conformational rearrangement must occur. This also helps rationalise the very short O...O contact found between the cabonyl oxygen of the cis formate group and the singly bound oxygen in the other group. It can be seen then, that the introduction of two formate groups around silicon still results in short intramolecular Si...O contacts (as observed in other silyl esters), although these appear to be weakened at the expense of Si-O bonds with apparently more π character.

CHAPTER 8

VIBRATIONAL NUCLEAR MAGNETIC RESONANCE AND MASS SPECTRA OF $SiH_2(OCHO)_2$

8.1 INTRODUCTION

Examples of silicon compounds containing only two Si-O linkages are limited to dialk oxysilanes[111,112] and 'prosiloxane'.[113] Diformatosilane is therefore of interest, since it is the first bis-ester derivative of silane to be prepared. Characterisation of this compound was essential to try and establish principally if there was any evidence for an intramolecular conformational interchange of the formate groups, and also to attempt to deduce whether any intermolecular interactions between the silicon and carbonyl oxygen atoms on neighbouring molecules existed. Vibrational spectroscopy has been used[114, 115] to show that shifts of the carbonyl stretching frequency for silyl and germyl esters on condensation can be indicative of associative intermolecular interactions of this type. Similar studies of the vibrational spectra of $SiH_2(OCHO)_2$, have therefore been undertaken here.

8.2 VIBRATIONAL SPECTRA OF DIFORMATOSILANE

The gas-phase structure determination of $SiH_2(OCHO)_2$ has shown that the molecule, although possessing Si-O and C-O torsions which remove the plane of symmetry expected for a molecule with the C_s point group, is never the less, geometrically very close to this idealised structure. The vibrational spectra have therefore been interpreted on the basis of this assumed C_s symmetry, where the two formate groups are found to be non-identical. This results in a predicted 27 vibrational modes, 18A' and 9A", all of which should be infra-red and Raman active. Vibrations of A" symmetry should give

rise to C band shapes, since the dipole change is perpendicular to the plane of symmetry, and A' vibrations should produce bands which are a mixture of A and B band shapes, since the dipole changes will be in the plane of symmetry.

It would be expected then, that all of the vibrational modes of the formate groups would be expected to produce two bands and in some instances this so, although splittings tend to be more apparent in the condensed phases. The infra-red spectra are shown in Figures 8.1-8.3 and the observed frequencies are given in Table 8.1. The C-H stretches give rise to only one absorption in all of the spectra. The extreme values of 2,985cm^{-1} and 2,944cm^{-1} are observed in the Raman and gas-phase infra-red spectra respectively, with intermediate values of $\simeq$2,965cm^{-1} in the solid and matrix infra-red spectra. In the Si-H stretching region, the matrix infra-red spectrum consists of a doublet with splitting 5cm^{-1}, which is likely to be due to the symmetric (A') and asymmetric(A") stretches with the band at highest frequency assigned as the asymmetric stretch.

The gas-phase and solid infra-red, and the Raman spectra all give a single peak at $\simeq$2,260cm^{-1} although the Raman band appears to be polarised and can therefore be assigned as the symmetric stretch, presumably with the asymmetric band underneath. Below this, the carbonyl absorptions appear. In the gas-phase, a single broad band is observed at 1,744cm^{-1} which shifts to 1,720cm^{-1} in the Raman spectrum, and to 1,710cm^{-1} in the solid phase infra-red spectrum. These shifts are quite consistent with those observed for other silyl esters (see discussion section). The matrix spectrum in these region shows a clear doublet due to the two C=O bonds with a splitting of 15cm^{-1}.

The C-H deformations and C-O stretches are found in the region

Figure 8.1 Infra-red Spectrum of $SiH_2(OCHO)_2$ in the gas-phase.

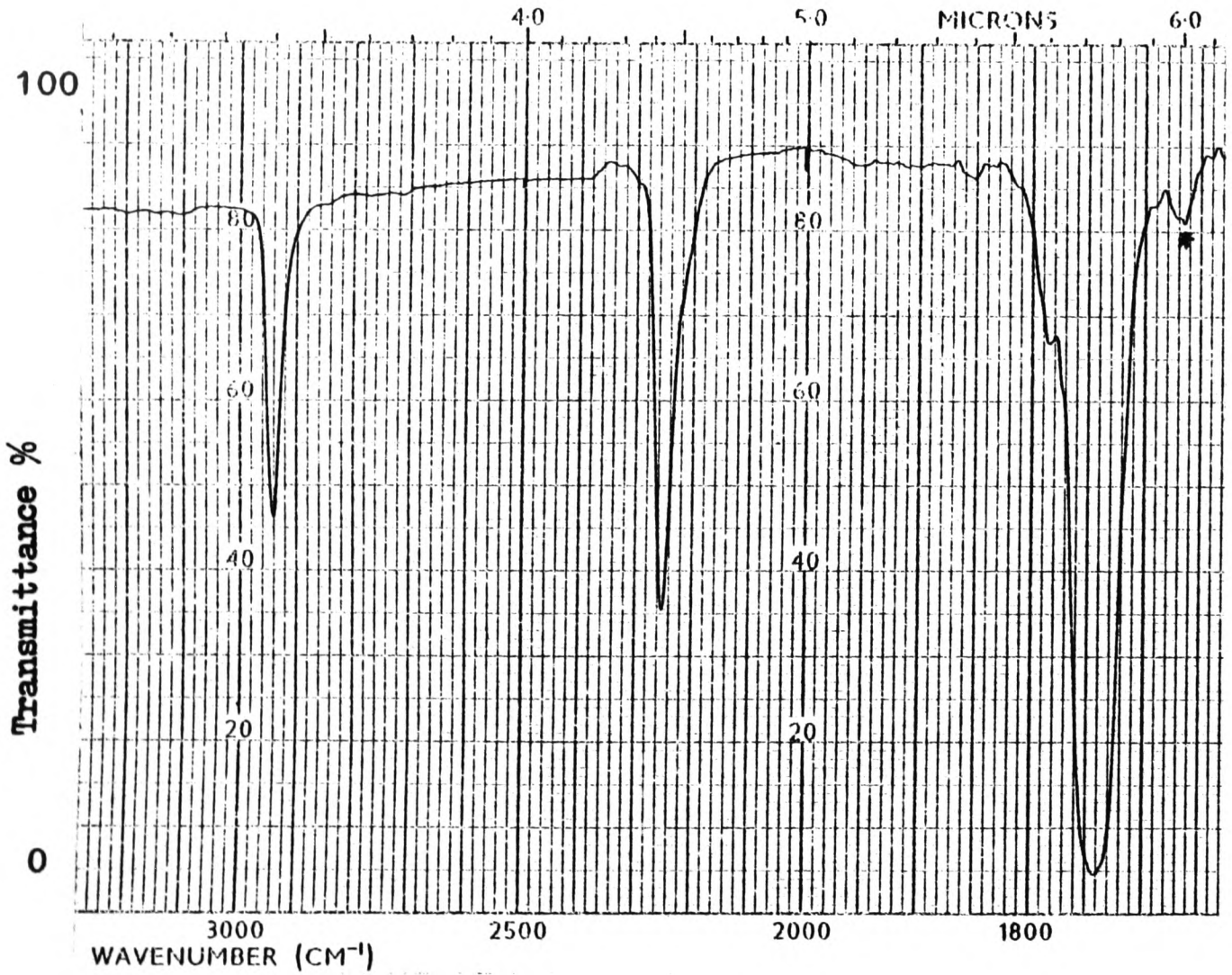

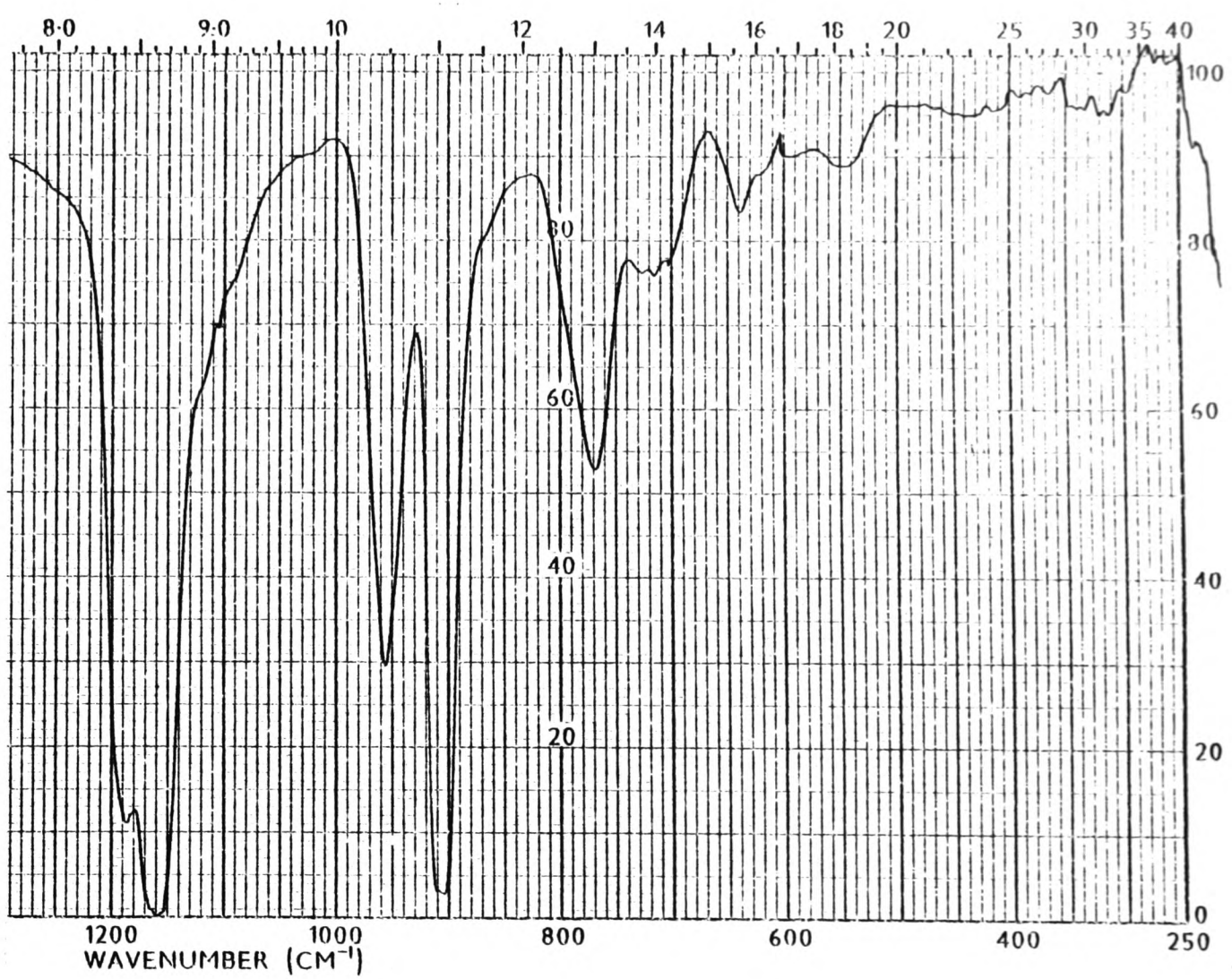

185.

ν

* = Cell blank

Figure 8.2 Infra-red Spectrum of $SiH_2(OCHO)_2$ in an N_2 matrix (1:833).

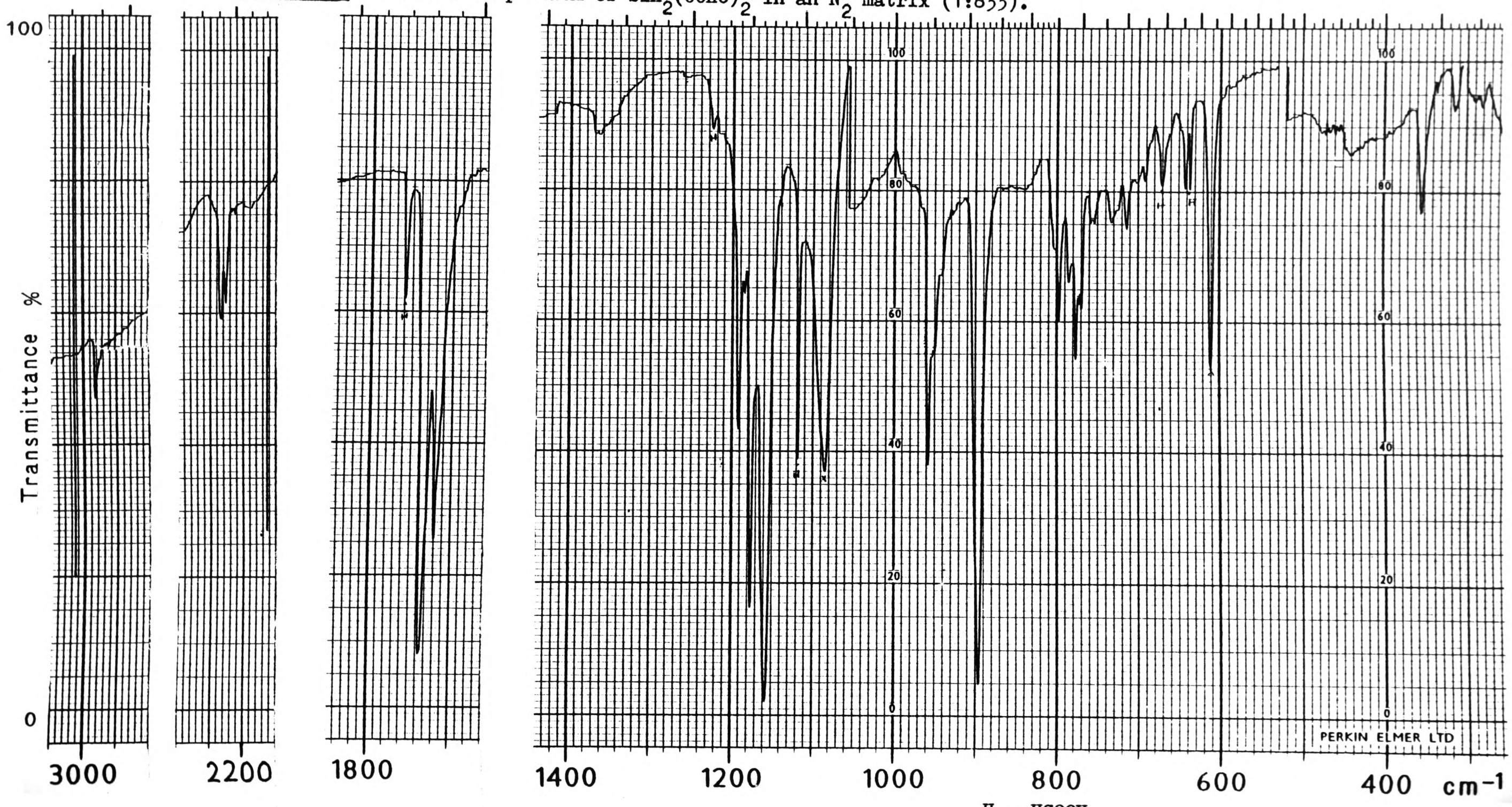

H = HCOOH

x, △ = Cell blank.

Figure 8.3 Infra-red Spectrum of $SiH_2(OCHO)_2$ in the solid phase.

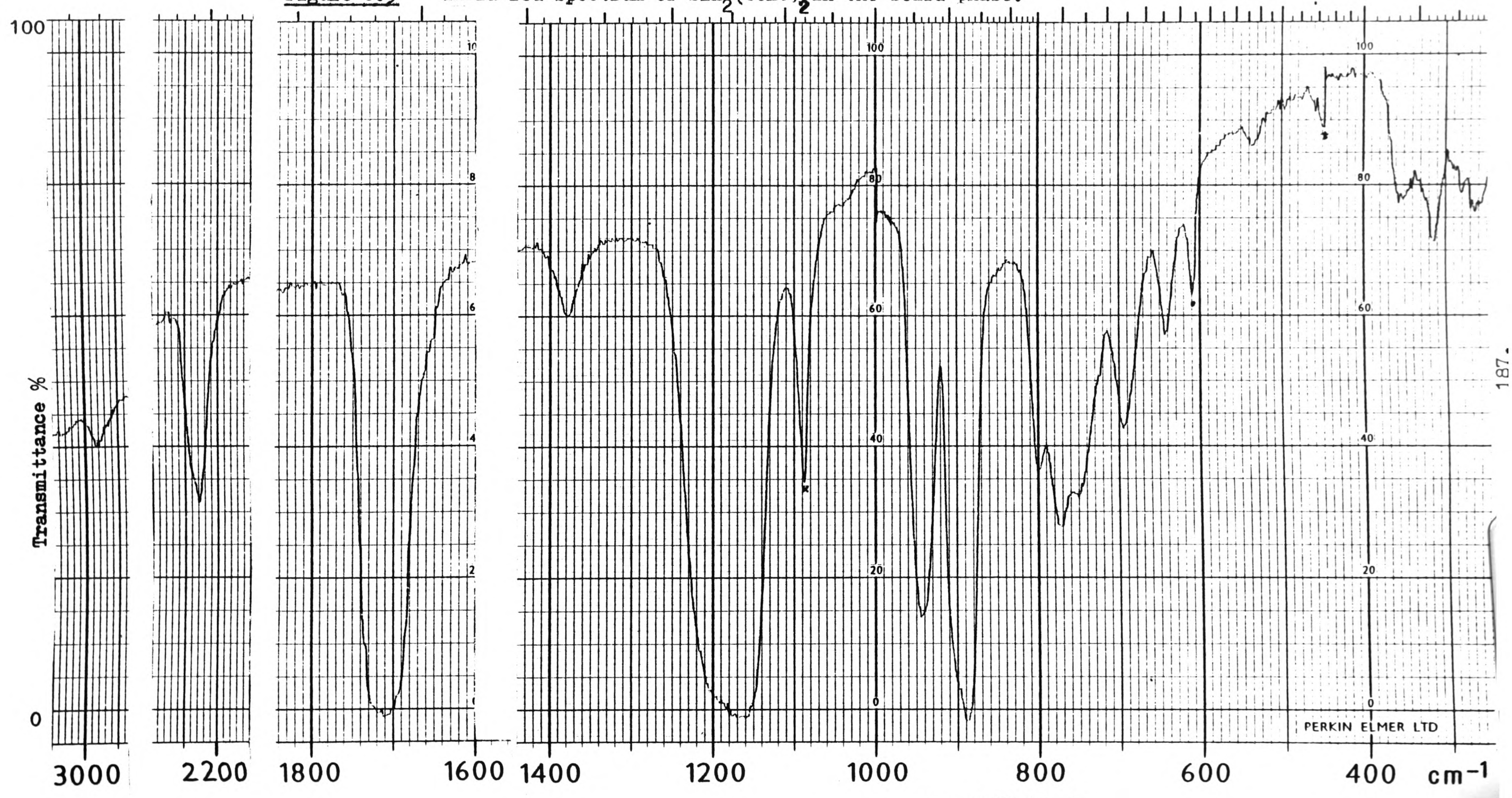

x = Cell blank

. = impurity

phases. The very strong band at 710cm^{-1} in the Raman spectrum appeared to be polarised and was therefore assigned as one of the symmetric Si-O stretches, rather than SiH_2 torsion. This torsion is assigned as the weak band at 715 and 714cm^{-1} in the gas-phase and matrix infra-red spectra respectively. In the gas-phase, this is the only C-type band and must therefore be assigned to an out of plane mode. It is assumed that this band is hidden under the strong ν(Si-O) signal in the Raman spectrum.

The two OCO bending deformations and the SiH_2 rock are observed between 700cm^{-1} and 400cm^{-1}. The OCO deformation consistently appears as a single band at $\simeq$642cm^{-1} in all phases and this assignment contrasts with the suggested assignment of this band at 720cm^{-1} in $SiH_3(OCHO)$.[116] The SiH_2 rock is assigned as the weak band at 550cm^{-1} in the gas-phase and the relatively more intense band at 551cm^{-1} in the Raman spectrum. It is unlikely that the OCO bend and SiH_2 rock have been incorrectly assigned since for compounds containing an $-SiH_2$ group, the rocking deformation generally occurs between 600-450cm^{-1}.[76] Obviously, assignment of these bands would be considerably simplified if significant band shapes were observed.

In the region below 500cm^{-1}, only skeletal deformations involving silicon, and torsional motions about the two C-O and two Si-O bonds are expected to give rise to absorptions. The OSiO deformation is assigned to the bands at 355 and 354cm^{-1} in the matrix and solid infra-red spectra respectively. This is not unreasonable, since the analogous (in terms of mass) $\delta(SiF_2)$ in SiH_2F_2 [117] occurs at 322cm^{-1}. The remaining bands were assigned on the basis of the data for $SiH_3(OCHO)$,[115] with the C-O torsions (2A") assigned to the absorptions at $\simeq$250cm^{-1} in the matrix and solid infra-red spectra, and the δ(SiOC) (A') assigned as the very weak Raman band at 170cm^{-1}.

TABLE 8.1

OBSERVED FREQUENCIES (cm^{-1}) AND ASSIGNMENTS FOR DIFORMATOSILANE

Gas	Infra-Red N_2 Matrix	Solid	Raman Liquid	Assignment
2,944m	2,969w	2,962w	2,985m	ν(CH); 2A'
2,256ms	2,256mw	2,260ms	2,266sp	ν(SiH); A'+A"
	2,251(sh)			
1,744vs br	1,737vs	1,710vs	1,740m,br	ν(C=O); 2A'
	1,722s		1,720ms	
1,370vw	1,372vw	1,378mw	1,387m	δ_i(CH); 2A'
1,188s	1,193ms		)	
			)	
	1,177s		1,200w,br)	ν(C-O); 2A'
			)	
1,162vs	1,165s	1,164vs	)	
	1,159vs			
n.o.	n.o.	1,040vvw	1,045w	δ_o(CH); 2A"
953ms	954ms	943s	957m	δ_s(SiH_2); A'
909(pr),vs	898vs	889vs	908w	δ_w(SiH_2; A'
	805m	800	800m)	
			)	
768m	777m	774ms	760m)	ν(SiO); 2A'
			)	
	771	754	710vs,p)	
	730			
715(PQR)w	714w	696ms	n.o.	δ_t(SiH_2); A"
	693			
640w	642w	644m	640w	δ(OCO); 2A'
550w	477vw?	537w	551mw	ρ(SiH_2); A"

TABLE 8.1

OBSERVED FREQUENCIES (cm^{-1}) AND ASSIGNMENTS FOR DIFORMATOSILANE (continued)

Infra-Red			Raman		Assignment
Gas	N_2 Matrix	Solid	Liquid		
	355w	354m		)	δ(OSiO); A'
				)	
320vvw	314w	318m	325vw	)	
	249w	268m		)	τ(CO); 2A"
				)	
	228w			)	
			170vw		δ(SiOC); 2A'

n.o. = not observed

b.r. = broad

p = polarised

w = weak

m = medium

s = strong

v = very

These compare with $223cm^{-1}$ and $160cm^{-1}$ for the C-O torsion and the SiOC bend respectively in silylformate, where the assignment is made from the Raman polarisation data. No infra-red data for the region below $200cm^{-1}$ is available and so assignment of the two Si-O torsions is not possible.

Spectra were recorded for $SiH_3(OCHO)$ in this region however, and here, as above $200cm^{-1}$, no significant absorptions were detected.

8.1 NUCLEAR MAGNETIC RESONANCE SPECTRA OF DIFORMATOSILANE

^1H, ^{13}C and ^{29}Si n.m.r. spectra were recorded for diformatosilane and the observed chemical shifts (ppm) and coupling constants (Hz) are given below. All chemical shifts are relative to $SiMe_4$.

$\delta(^1\underline{H}C) = 7.12$, $\delta(^1\underline{H}Si) = 4.58$, $\delta(^{13}C) = 158.2$ and $\delta(^{29}Si) = -35.5$

$^1J(CH) = 233.1$, $^1J(SiH) = 281.6$, $^3J(SiH) = 6.8$, $^4J(HH) = 0.5$

($^3J(CH)$ was not observed)

The chemical shifts of the various nuclei are consistent with those of other silylesters[5] and the magnitude of $^1J(SiH)$ and the ^{29}Si spectrum confirm the presence of an $-SiH_2$ group. The ^{13}C and ^{29}Si spectra (see Figure 8.4) are a doublet and triplet of triplets respectively confirming that the two formate groups are equivalent at room temperature on the n.m.r. timescale, in contrast with the electron diffraction and vibrational spectroscopic data.

In an attempt to detect the inequivalence of the formate groups, a subsequent series of ^1H n.m.r. spectra were recorded at low temperature. At 213K, the proton spectrum showed two singlets shifted to lower frequency which appeared as distinct multiplets on line narrowing. The silyl resonance at 4.45ppm was a triplet as expected. The formate signal however, appeared as a pseudo quartet,

due to two overlapping triplets from coupling of the silyl protons to two distinct formate protons. The chemical shifts of these protons were 6.697ppm and 6.690ppm and again $^4J_{HH}$ = 0.5Hz. This process was found to be completely reversible on warming the sample to room temperature, confirming the low temperature inequivalence of the formate groups.

MASS SPECTRUM OF DIFORMATOSILANE

M/e	Relative Abundance	Assigned Species
121	5	$[HSiH_2(OCHO)_2]^+$
120	6	$[SiH_2(OCHO)_2]^+$
119	2	$[SiH(OCOH)_2]$ or $[SiH_2(OCO)(OCOH)]^+$
92	3	$[SiH_2(OH)(OCOH]^+$
91	83	$[SiH_2(O)(OCOH]^+$
75	12	$[SiH_2(OCOH)]^+$
47	97	$[H_2OCOH]^+$
46	100	$[HOCOH]^+$
45	92	$[OCOH]^+$
44	11	$[OCO]^+$
30	2	$[SiH_2]^+$
29	81	$[OCH]^+$ or $[SiH]^+$
28	52	$[CO]^+$ or $[Si]^+$

The mass spectrum of $SiH_2(OCHO)_2$, above, shows a small peak at M/e = 120 due to the parent ion, and also a peak of similar intensity for the $(M+1)^+$ species. The other principal features are the presence of peaks due to the fragment-ions $[HCO]^+$ and $[OCOH]^+$, and the corresponding species $[SiH_2O(OCHO)]^+$ and $[SiH_2(OCHO)]^+$ indicating that fragmentation occurs principally by cleavage of the C-O and Si-O bonds. The base peak at M/e = 46 is due to the formation of $[HOCOH]^+$ by hydrolysis of diformatosilane in the spectrometer.

Figure 8.4 ^{29}Si Nmr Spectrum of $SiH_2(OCHO)_2$.

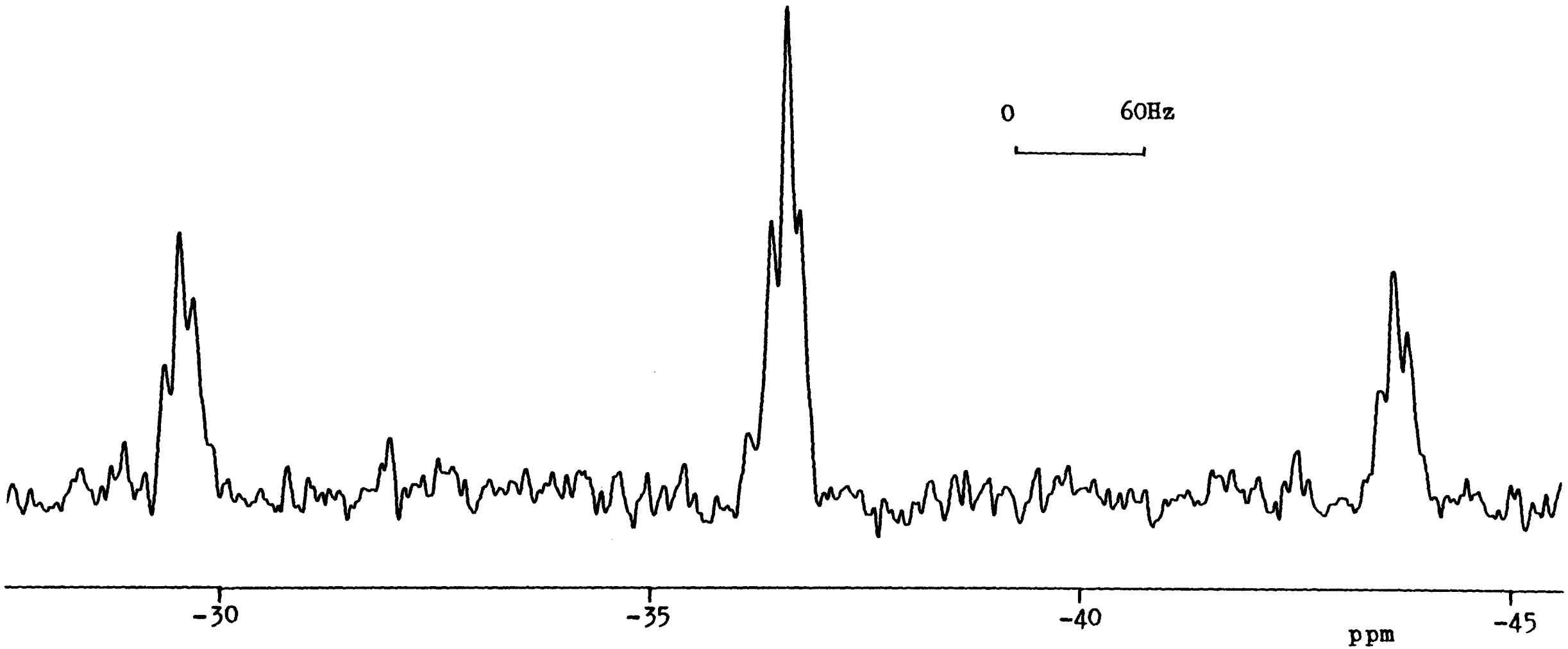

RESULTS AND DISCUSSION

The equivalence of the two formate groups on the n.m.r. timescale, which contrasts with the electron diffraction and vibrational spectroscopic data, indicates that an interchange of the conformations of the two groups must occur. This facile process is probably concerted, and will involve low frequency, high amplitude motions about the Si-O and C-O bonds. This is consistent with the requirement that some large amplitudes of vibration were necessary for some of the non-bonded heavy atom distances between the two formate groups.

Evidence for possible intermolecular association is not as clear. Table 8.2 shows the shifts of the C=O stretching frequency for some silyl esters on condensation.

TABLE 8.2

CARBONYL STRETCHING FREQUENCIES (cm^{-1}) IN VARIOUS PHASES

	$SiH_3(OCHO)$	$SiH_3(OCOCH_3)$	$SiH_2(OCHO)_2$	$SiH_3(OCOCF)_3$
Gas (Infra-Red)	1,734	1,750	1,744	1,790
	31	32	22	19
Liquid (Raman)	1,703 39	1,718 43	1,720 32	1,771 28
	8	11	10	9
Solid (Infra-Red)	1,695	1,707	1,710	1,762

The shifts for the gas to solid phase transition vary between 28-43cm^{-1} and this shift is attributed to weakening of the C=O bond as electron donation from the carbonyl oxygen atom on one molecule to the silicon atom of a neighbouring molecule occurs. Silyl acetate

shows the largest shift and the crystal structure indicates significant intermolecular interactions (Si...O, 2.72Å). This shift alone, however, does not imply association in the solid phase, since shifts for the analogous methyl esters[115] are of a comparable magnitude, but the crystal structure of methyl acetate shows no short intermolecular contacts. Crystal structure determinations for the other silyl esters have not been carried out, and so with only the magnitude of the shifts on condensation known for $SiH_2(OCHO)_2$ it is impossible to evaluate the extent or otherwise of any association in the solid phase. It seems reasonable to assume, however, that since no profound changes occur in the solid phase infra-red spectrum, such as those observed for SiH_2XNMe_2 (see Chapter 5), any intermolecular interactions are likely to be very weak in nature.

APPENDIX I

EXCHANGE REACTIONS OF $SiH_2(OCHO)_2$

Diformatosilane was allowed to react with some silyl and germyl halides in order to study its exchange reactions. In each case, a stoichiometric quantity of the compound was mixed with $SiH_2(OCHO)_2$ and the reaction was followed at room temperature by ^1H n.m.r. spectroscopy using sealed tubes with d_8-toluene as the solvent and reference.[118] Where exchange took place, this clearly occurred at a slow rate relative to the timescale of the n.m.r. experiment, since sharp signals were always observed.

REACTION OF $SiH_2(OCHO)_2$ WITH SiH_3X (X=Cl AND Br)

$SiH_2(OCHO)_2$ and SiH_3X were mixed in the ratio 1:2 respectively and allowed to react. In this stiochiometry, it would be expected that $SiH_3(OCHO)$ and SiH_2X_2 would be the only products if exchange was complete. In both cases, however, as well as these compounds, the mixed species $SiH_2X(OCHO)$ was also formed in significant quantities. The parameters for these species are given below:

$SiH_2Cl(OCHO)$: $\delta H_{Si} = 4.69$ and $\delta H_C = 7.05$

$^1J_{Si-H} = 286.3$, $^1J_{C-H} = 235.6$ and $^4J_{H-H} = 0.5$

$SiH_2Br(OCHO)$: $\delta H_{Si} = 4.75$ and $\delta H_C = 7.02$

$^1J_{Si-H}$, $^1J_{C-H}$ = n.o. and $^4J_{H-H} = 0.5$

δ in ppm, J in H_2 and n.o. = not observed.

REACTION OF $SiH_2(OCHO)_2$ WITH SiH_2X_2 (X=Cl AND Br)

$SiH_2(OCHO)_2$ and SiH_2X_2 were allowed to react in the ratio 1:2, respectively. ^1H n.m.r. clearly showed that an equilibrium had been set up with a mixture of $SiH_2(OCHO)_2$, SiH_2X_2 and $SiH_2X(OCHO)$ present in both cases. Equilibrium constants were evaluated from the relative integrals of the signals and K was found to be 2.23 for X = Cl and 0.84 for X = Br. These show that at room temperature the

equilibrium lies to the left (see below), since K = 4 if the reaction goes halfway.

$$SiH_2(OCHO)_2 + SiH_2X_2 \rightleftharpoons SiH_2X(OCHO)$$

The reaction of $SiH_2(OCHO)_2$ with SiH_2X_2 to give $SiH_2X(OCHO)$ is therefore not synthetically viable if high yields are desired.

REACTION OF $SiH_2(OCHO)_2$ WITH GeH_3X (X=F,Cl AND Br)

When $SiH_2(OCHO)_2$ was mixed with either GeH_3Cl or GeH_3Br, the ^1H n.m.r. spectra contained only signals attributable to the two starting materials and it was therefore concluded that no reaction occurred. With GeH_3F, however, a 1:1 mixture gave a complex array of products. Amongst these products GeH_3OCHO, $SiH_2F(OCHO)$, GeH_4 and SiH_3OCHO were all identified by ^1H n.m.r. Further evidence for the complex nature of this exchange/disproportionation reaction was obtained from the ^{19}F and $^{19}F-[^1H]$ spectra where more species were identified (see Table A).

TABLE A

Species	δ F	$^1J_{H-F}$	$^4J_{H-F}$
SiH_2F_2	-146.9	60.8	-
MHF_3	-135.3	95.8	-
MF_4	-153.4	-	-
$MHF_2(OCHO)$	-137.8	87.6	2.6
$MHF(OCHO)_2$	-141.0	80.6	2.4
$MF(OCHO)_3$	-144.7	-	3.7
$MF_2(OCHO)_2$	-149.3	-	4.2
$MF_3(OCHO)$	-155.4	-	4.9

δ in ppm and J in Hz. M = Si or Ge

$\underline{SiH_2F(OCHO)}$: δH_{Si} = 4.31 δH_C = n.o. δF = -160.3 $^1J_{Si-H}$ = 283.7, $^1J_{Si-F}$ = n.o., $^2J_{H-F}$ = 58.0 $^4J_{H-H}$ = 0.6 and $^4J_{H-F}$ = 1.8

The sample proved too weak to obtain any information from the ^{29}Si spectrum and so it was not possible to deduce whether M was Si or Ge for any of the species. It is worth noting, however, that no GeH_3F was detected after reaction.

APPENDIX II

FUTURE WORK

The use of solid phase vibrational spectroscopic techniques in conjunction with X-ray crystallography has been shown to be a powerful method for investigating intermolecular interactions in crystals.

Of the compounds, SiH_2XNMe_2, only the chloride has been shown crystalographically to be dimeric, thus X-ray crystal structures of the fluoride and iodide are essential to allow comparison with the chloride. Investigations into similar molecules which exhibit association in the solid phase are likely to be limited, since only compounds with one $Si-NMe_2$ unit and relatively small groups on silicon are likely to be suitable candidates.

The compounds, SiX_3NMe_2, where X = F or Cl may form chains in the solid phase, although the relatively large steric bulk of the halogen atoms will possibly preclude this arrangement.

Other series' of molecules which could be prepared and structurally characterised by electron diffraction are $SiHX_2NMe_2$ and $SiHX(NMe_2)_2$ where X is again a halogen atom. For the former series, $SiHCl_2NMe_2$ is discussed here, but the other dihalosilyl-dimethylamines could be examined and compared with the monohalosilyl-dimethylamines reported here. These compounds are likely to be planar with very short silicon-nitrogen bonds.

The compounds $SiHX(NMe_2)_2$ and $SiX(NMe_2)_3$ would allow the effects of increasing steric bulk on the conformation at nitrogen and the Si-N bond length to be established, although some of these compounds, along with the dihalosilyl-dimethylamines, may be relatively involatile.

Far infra-red studies of the monohalosilyl-dimethylamines

discussed here might allow assignment of the low frequency methyl torsions and particularly the deformational modes involving nitrogen. These, in conjunction with normal coordinate analysis studies, would also allow spectroscopic amplitudes of vibration and barriers to internal rotational to be determined.

ANGEWANDTE
CHEMIE
Volume 25 · Number 1
January 1986
Pages 107–108

International Edition in English

Reprint

© VCH Verlagsgesellschaft mbH, Weinheim/Bergstr. 1986

Registered names, trademarks, etc. used in this journal, even without specific indication thereof, are not to be considered unprotected by law. Printed in Germany

The Structure of Chlorosilyl-*N,N*-dimethylamine in the Gaseous and Solid Phases

By *David G. Anderson, Alexander J. Blake, Stephen Cradock,* E. A. V. Ebsworth, David W. H. Rankin,* and *Alan J. Welch*

Silylamines exhibit some striking structural features that are related to the ability of four-covalent silicon to accept additional electrons, using its vacant 3d orbitals. Thus, trisilylamine[1] and disilylamines[2] have planar coordination at nitrogen, while *N,N*-dimethyl(silyl)amine (which appears to have a non-planar nitrogen in the gas phase[3]) forms a cyclic pentamer in the crystal[4] with five-coordinate silicon linked by four-coordinate nitrogen, all the Si–N bonds being equivalent.

[*] Dr. S. Cradock, D. G. Anderson, Dr. A. J. Blake,
Prof. E. A. V. Ebsworth, Dr. D. W. H. Rankin, Dr. A. J. Welch
Department of Chemistry, University of Edinburgh
West Mains Road, Edinburgh EH9 3JJ (Scotland)

As part of systematic a study of silylamines and their structures we have prepared chlorosilyl-*N,N*-dimethylamine **1**. This compound has been briefly reported by *Emsley*.[5] We have synthesized it by reaction of dichlorosilane with two molar equivalents of dimethylamine in the gas phase, and characterized it by its IR and Raman spectra in the gas, liquid, and solid phase, and by its NMR spectra in solution.

$ClH_2Si-N(CH_3)_2$ **1**

The vibrational spectra of **1** are strikingly different in the gas and the annealed solid phases, particularly in the region associated with Si–N stretching modes (600–900 cm^{-1}). A prominent band at 688 cm^{-1} (IR, gas)/694 cm^{-1} (Raman, liquid) is absent in the annealed solid, being apparently replaced by two bands in each spectrum, with frequencies of 796 and 619 cm^{-1} in the IR spectrum, and of 802 and 610 cm^{-1} in the Raman spectrum. These observations suggested that the species present in the annealed solid was not monomeric, as in the gas and the liquid; they would be consistent with a centrosymmetric dimer unit with a Si_2N_2 ring, but do not suffice as proof that such a ring is present. Accordingly, we used electron diffraction in the gas phase and X-ray diffraction in the annealed solid phase in order to determine the molecular structures unequivocally in each case. The results confirmed our initial conjectures from the vibrational spectra, revealing that **1** forms a novel centrosymmetric dimer in the crystal.

According to the electron diffraction pattern gaseous **1** is monomeric, with the expected four-coordinate silicon (Fig. 1a). The Si–N and Si–Cl bond lengths are similar to those found in related compounds, 168.9(4) pm and

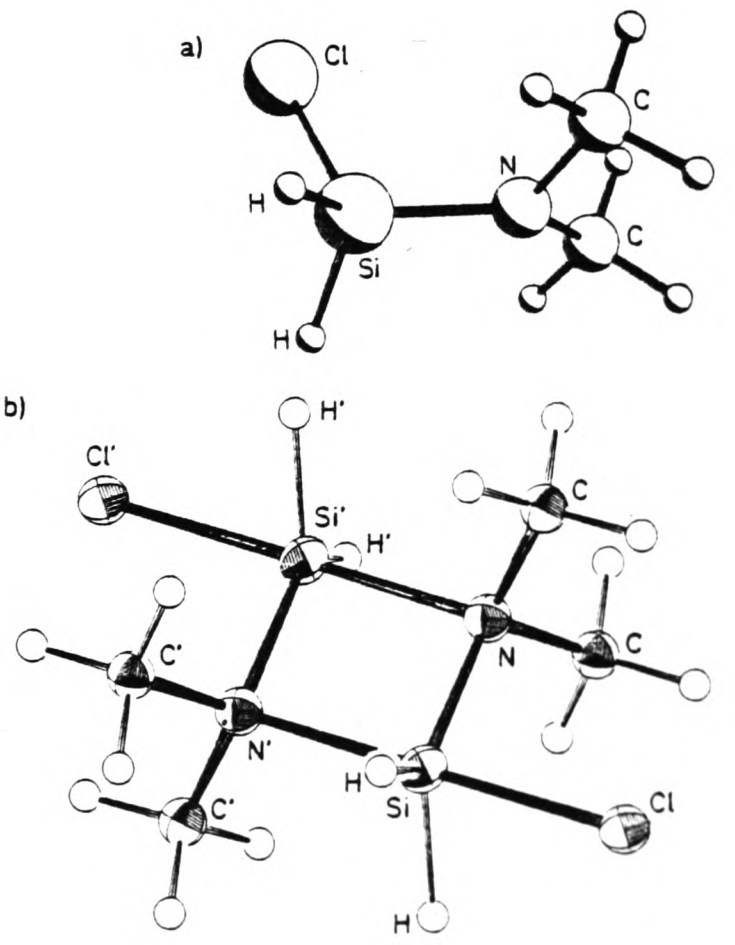

Fig. 1. a) Structure of gaseous monomeric chlorosilyl-*N,N*-dimethylamine **1** at 298 K. Bond lengths [pm] and angles [°]: Si-Cl 207.0(2), Si-N 168.9(4), Si-H 147(2), N-C 146.4(4), C-H 110.2(5); Cl-Si-N 113.0(6), Si-N-C 121(1), C-N-C 115(1). b) Structure of **1** in the crystal at 116 K. The Si_2N_2Cl group is almost planar; the dimer contains a center of inversion. Bond lengths [pm] and angles [°]: Si-Cl 223.1(6), Si-N 181.4(13), Si-H 149(1), N-C 149.8(18), Si-N 205.4(13); Cl-Si-N 96.1(5), Si-N-C 112.8(9), C-N-C 108.8(14), N-Si-N' 83.0(5), Si-N-Si' 97.0(6).

207.0(2) pm respectively. The Si–N bond is slightly shorter than those in other *N,N*-dimethyl(silyl)amines (171–172 pm), which are themselves shorter than those in other silylamines,[6] whereas the Si–Cl bond is somewhat longer than that found in SiH_3Cl (205 pm). The nitrogen appears very slightly non-planar, though this may well be a shrinkage effect, and the ClSiN and CNC planes are almost perpendicular to each other.

The crystal structure[7] consists of well-separated dimers (Fig. 1b), packed in sheets parallel to *ac*, about 500 pm apart, with dimers in one plane above interstices in the plane below. The dimer has crystallographically-required C_{2h} symmetry. The central Si_2N_2 unit is not equilateral; two opposite Si–N distances are 181.4(13) pm, whilst the other two are much longer, 205.4(13) pm. The dimers can therefore be described in terms of two strongly-interacting monomers. The strength of the interaction is shown by the extent to which the normal tetrahedral coordination at Si is distorted in the dimer; the N–Si–Cl angle 96.1(5)° is much smaller than in the gas-phase monomer (113.0(6)°), allowing the additional bond to N′ to develop. The N′···Si–Cl angle is 179.0(4)°, very close to linear, so that Si is adopting trigonal bipyramidal coordination, though the "axis" ClSiN is not strictly perpendicular to the "equatorial plane" containing N′ and the two H atoms attached to Si. The fact that the Cl atom adopts the axial position rather than an equatorial position is in accord with its position in the "apicophilicity series", which has been proposed[12] to account for some observed structures of pentacoordinate phosphorus compounds.

The effect of the additional Si···N′ interaction on the Si–Cl and Si–N bond lengths is striking; these are, respectively, 16 and 12 pm longer in the crystal than in the gas-phase monomer, even though the Si–Cl bond is *trans* to the additional Si···N′ bond and the Si–N bond is almost orthogonal to it. The lengthened Si–Cl bond may be compared with other Si–Cl bonds *trans* to nitrogen at five- or six-coordinated silicon, with lengths such as 227.4 pm and 239.3 pm.[13] The Si–N···Si′ angle (97.0(6)°) probably represents a compromise between 90° (as would be needed for a square Si_2N_2 unit, and as is appropriate to trigonal bipyramidal coordination at Si) and the tetrahedral angle of 109.47°. We may regard the dimer as a "frozen" intermediate in an S_N2 reaction involving attack at Si by N′; the leaving group is Cl, and the putative "product" would be an ionic form of the dimer, with all Si–N bonds equal in length.

Received: September 16, 1985;
supplemented: October 21, 1985 [Z 1464 IE]
German version: *Angew. Chem. 98* (1986) 97

[1] K. Hedberg, *J. Am. Chem. Soc. 77* (1955) 6491.
[2] G. Gundersen, D. W. H. Rankin, H. E. Robertson, *J. Chem. Soc. Dalton Trans. 1985*, 191.
[3] C. Glidewell, D. W. H. Rankin, A. G. Robiette, G. M. Sheldrick, *J. Mol. Struct. 6* (1970) 231.
[4] a) R. Rudmann, W. C. Hamilton, S. Novick, T. D. Goldfarb, *J. Am. Chem. Soc. 89* (1967) 5157; b) A. J. Blake, E. A. V. Ebsworth, A. J. Welch, *Acta Crystallogr. C40* (1984) 895.
[5] J. Emsley, *J. Chem. Soc. A 1968*, 1009.
[6] G. Gundersen, R. Mayo, D. W. H. Rankin, *Acta Chem. Scand. Ser. A 38* (1984) 579.
[7] Monoclinic, space group $C2/m$, $a = 676.59(22)$, $b = 995.0(3)$, $c = 849.40(27)$ pm, $\beta = 114.70(4)°$, $V = 0.5195$ nm^3, $Z = 4$, $\varrho_{calc} = 1.402$ g cm^{-3}, $T = 116$ K, $\mu(Mo_{K\alpha}) = 0.79$ mm^{-1}. A conical crystal (0.27 × 0.20 mm) was grown in a tapered capillary tube in situ on a Weissenberg goniometer and transferred as described previously [8] to an Enraf-Nonius CAD4 diffractometer. From 427 unique data ($1° \leq \Theta \leq 22.5°$), corrected for absorption [9], 282 with $F \geq 4\sigma(F)$ were used to solve (Patterson [10]) and refine (difference Fourier, full-matrix least-squares [11]) the structure. Non-hydrogen atoms were refined anisotropically and, after location, methyl hydrogens were refined as parts of rigid groups; r(Si–H) was constrained to 150 ± 5 pm. Final residuals $R = 0.0970$, $R_w = 0.1097$. The atomic coordinates for this work are available on request from The Director of the Cambridge Crystallographic Data Centre, University Chemical Laboratory, Lensfield Road, Cambridge CB21EW. Any request should be accompanied by the full literature citation for this communication.
[8] A. J. Blake, S. Cradock, E. A. V. Ebsworth, D. W. H. Rankin, A. J. Welch, *J. Chem. Soc. Dalton Trans. 1984*, 2029.
[9] DIFABS. Program to apply empirical absorption corrections. N. Walker, D. Stuart, *Acta Crystallogr. A 39* (1983) 158.
[10] SHELX84. Program for crystal structure solution. G. M. Sheldrick, Universität Göttingen 1983.
[11] SHELX76. Program for crystal structure refinement. G. M. Sheldrick, University of Cambridge, 1976.
[12] R. G. Cavell, D. D. Poulin, K. I. The, A. J. Tomlinson, *J. Chem. Soc. Chem. Commun. 1974*, 19.
[13] G. Sawitzki, H. G. von Schnering, *Chem. Ber. 109* (1976) 3728.

Diformatosilane: Preparation, Characterisation, and Molecular Structure in the Gas Phase by Electron Diffraction †

David G. Anderson and Stephen Cradock *
Department of Chemistry, University of Edinburgh, West Mains Road, Edinburgh EH9 3JJ

The first bis-ester derivative of silane, $SiH_2(OCHO)_2$, has been prepared and characterised by a variety of spectroscopic techniques and by electron diffraction in the gas phase. The electron-diffraction investigation shows it to have an asymmetric conformation, one formate group apparently being close to the *cis* arrangement about its SiO bond, the other close to *trans*. The two formate groups are, however, equivalent on the n.m.r. time-scale.

Some dialkoxysilanes were prepared and characterised many years ago,[1,2] and 'prosiloxane', $(SiH_2O)_n$, has been shown[3] to consist of a mixture of cyclic species with alternating SiH_2 and oxygen moieties. Nevertheless, there are few reports in the literature of compounds containing two oxygen ligands on an SiH_2 group, and this is probably linked with the chemical lability of SiH bonds and the much greater thermodynamic stability of SiO linkages. Thus SiH_4 and methoxysilanes react[2] with liquid CH_3OH or with gaseous CH_3OH in the presence of copper metal liberating H_2, though mono-, di-, and tri-alkoxysilanes seem to be stable when pure. We have shown[4] that simple silyl esters of organic acids $RCOOSiH_3$, where R = H,CH_3, *etc.*, may be prepared under very mild conditions by mixing silyl halides with trialkyltin esters at or below room temperature, and now report that a similar reaction of a dihalogenosilane with tributyltin formate gives a new compound identified as diformatosilane, $SiH_2(OCHO)_2$. We have characterised it by spectroscopic means and have studied its structure in the gas phase by electron diffraction.

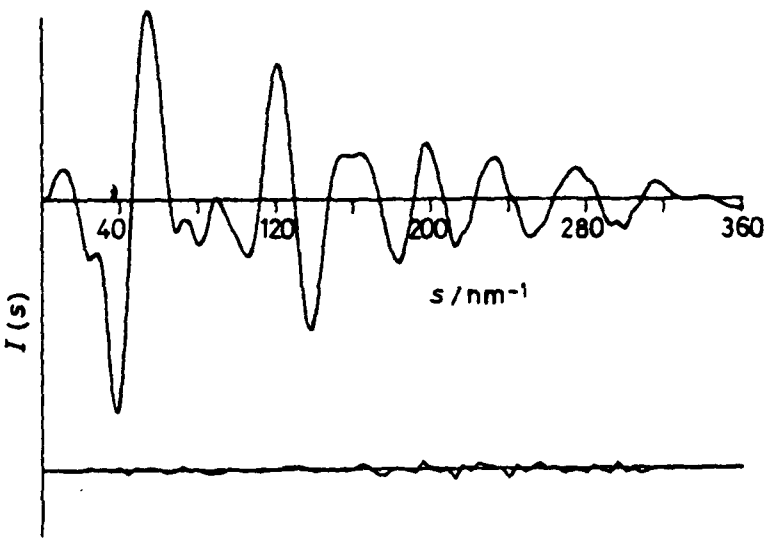

Figure 1. Combined electron-scattering intensities: observed and final difference curves

Experimental

Preparation.—Dibromosilane [prepared from dichlorosilane *via* bis(dimethylamino)silane[5]] (5 mmol) was condensed under vacuum into a glass tap ampoule containing tributyltin formate[6] (12 mmol) at 77 K. The ampoule and its contents were allowed to warm to room temperature with vigorous shaking. After about 1 min, when the viscosity of the contents had noticeably diminished, volatile products were removed by condensation at 77 K in a vacuum system. Trap-to-trap distillation gave *diformatosilane* (3.6 mmol, 72%) which was retained at 227 K but passed a trap at 250 K. The same product could be obtained, in slightly lower yield (61%), by reaction of dichlorosilane with tributyltin formate under similar conditions. Diformatosilane is a colourless liquid, vapour pressure 1.4 mmHg at 271.7 K. It was characterised by mass spectrometry, multinuclear n.m.r., i.r., and Raman spectroscopy, and electron diffraction in the gas phase (see below).

Volatile compounds were prepared and handled using a conventional glass vacuum line, and their identity and purity established by study of the i.r. spectra in the gas phase and of ^1H n.m.r. spectra in solution.

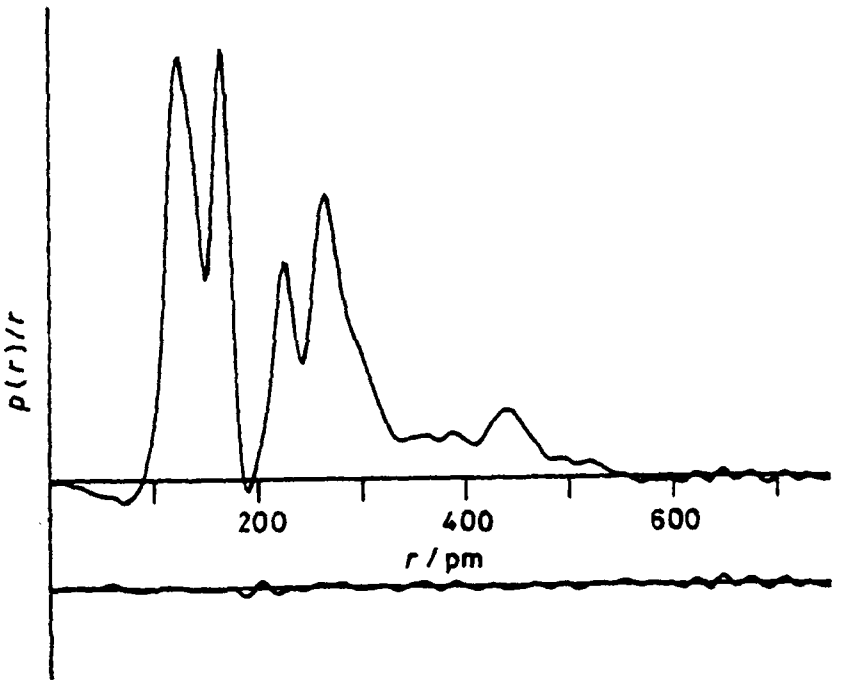

Figure 2. Observed and final difference radial distribution curves. Before Fourier inversion the data were multiplied by $s\cdot\exp[-0.000\,02s^2/(Z_{Si} - f_{Si})(Z_O - f_O)]$

Instrumental.—I.r. spectra of gaseous samples were obtained with a Perkin-Elmer 598 recording spectrophotometer, and of solid and matrix-isolated samples with a Perkin-Elmer 225 spectrometer, samples being held at a controlled temperature between 15 and 100 K on a CsI window cooled by an Air Products DE-202 helium microrefrigerator. Raman spectra of liquid samples were obtained using a Cary 83 spectrometer with an argon-ion laser operating at 488 nm as light source. Proton n.m.r. spectra were obtained using a Bruker WP80 spectrometer operating at 80 MHz, and ^{13}C and ^{29}Si spectra using a Bruker WP200 spectrometer operating at 50.32 and 39.76 MHz

† *Non. S.I. units employed:* mmHg ≈ 134 Pa, eV ≈ 1.60 × 10^{-19} J.

Table 1. Camera distances/mm, s ranges/nm^{-1}, correlation parameters, and scale factors; electron wavelength = 5.693(6) pm

Distance	s	$s_{min.}$	s_{w1}	s_{w2}	$s_{max.}$	Correlation parameter	Scale factor
285.48	2	20	40	124	144	−0.128	0.639(4)
128.36	4	68	80	300	328	−0.075	0.771(13)

Table 2. Infrared and Raman spectra of $SiH_2(OCHO)_2$; n.o. = not observed

I.r.			Raman	
Gas	N_2 matrix	Solid	liquid	Assignment
2 944m	2 969w	2 962w	2 985m	ν(CH); ν_1 and ν_2
2 256ms	2 256mw	2 260ms	2 266s,p	ν(SiH); ν_3, ν_{19}
	2 251(sh)			
1 744vs	1 737vs	1 710vs	1 740m,br	ν(C=O); ν_4, ν_5
	1 722s		1 720ms	
1 370vw	1 372vw	1 378mw	1 387m	δ_i(CH); ν_6, ν_7
1 188s	1 193ms			
	1 177s		1 200w,br	ν(C–O); ν_8, ν_9
1 162vs	1 165s	1 164vs		
	1 159vs			
n.o.	n.o.	1 040vvw	1 045w	δ_o(CH); ν_{20}, ν_{21}
953ms	954ms	943s	957m	$\delta_s(SiH_2)$; ν_{10}
909(*PR*),vs	898vs	889vs	908w	$\delta_w(SiH_2)$; ν_{11}
	805m	800	800m	
768m	777m	774ms	760m	ν(SiO); ν_{12}, ν_{13}
	771	754	710vs,p	
	730			
715(*PQR*)w	714w	696ms	n.o.	$\delta_t(SiH_2)$; ν_{22}
	693			
640w	642w	644m	640w	δ(OCO); ν_{14}, ν_{15}
550w	477vw?	537w	551mw	$\rho(SiH_2)$; ν_{23}
	355w	354m		
320vvw	314w	318m	325vw	δ(OSiO); ν_{16}
	249w	268m		
	228w			τ(CO); ν_{24}, ν_{25}
			170vw	δ(SiOC); ν_{17}, ν_{18}

respectively. The mass spectrum was obtained using an AEI MS902 spectrometer, using 70-eV electron energy.

Electron-diffraction experiments used the Edinburgh apparatus,[7] data being recorded photographically and converted into digital form by the S.E.R.C.-funded microdensitometer service at Daresbury.[8] The data reduction[8] and model refinement[7] were performed with established programs. The sample and nozzles were at 293 K during experiments; three plates were exposed at each of two camera distances, 128 and 285 mm, giving data over a range of 20—328 nm^{-1} in the scattering variable s. The s ranges, weighting points, correlation parameters, scale factors, and electron wavelengths (calculated from diffraction patterns of benzene recorded consecutively with those of the compound) are given in Table 1. The scattering factors of Schäfer *et al.*[9] were used in all calculations. A curve showing the combined intensities and a radial distribution curve are shown in Figures 1 and 2, with the final differences between observed and calculated intensities or $P(r)/r$ shown in each case.

Characterisation.—N.m.r. spectra. Proton, ^{13}C, and ^{29}Si n.m.r. spectra were recorded, giving the following parameters: δ(C*H*) 7.12, δ(Si*H*) 4.58, δ(^{13}C) 158.2, and δ(^{29}Si) −35.5 p.p.m. (all relative to $SiMe_4$); ^1J(CH) 233.1, ^1J(SiH) 281.6, ^3J(SiH) 6.8, and ^4J(HH) 0.5 Hz. No ^{13}C satellites of the Si*H* resonance were observed, so ^3J(CH) is not determined. The two CH protons are effectively equivalent at room temperature. A triplet of triplets in the ^{29}Si spectrum confirms the formulation of the compound as $SiH_2(R_H)_2$, where R_H contains a single proton and is identified as the formate group from its proton and ^{13}C chemical shifts.

Mass spectrum. There was a weak molecular ion peak at m/e = 120, with a strong fragment-ion peak at m/e = 91, corresponding to loss of HCO from the molecular ion. A weaker fragment-ion peak at m/e = 75 is attributable to loss of HCO_2 from the molecular ion, showing that both C–O and Si–O bond cleavage occurs. The $(M + 1)^+$ peak at m/e = 121 was nearly as strong as the molecular ion peak.

Reactions. Some exchange reactions of diformatosilane were investigated using ^1H n.m.r. spectroscopy, small quantities of reactants being mixed in n.m.r. tubes with [$^2H_8$]toluene as solvent and standard. Reactions with SiH_3X (X = Cl or Br) gave $SiH_3(OCHO)$, SiH_2X_2, and a new species in each case, identified on the basis of its ^1H n.m.r. spectrum as $SiH_2X(OCHO)$ [X = Cl, δ(Si*H*) = 4.69 and δ(C*H*) = 7.05 p.p.m., ^1J(SiH) = 286.3, ^1J(CH) = 235.6, and ^4J(HH) = 0.5 Hz; X = Br, δ(Si*H*) = 4.75 and δ(C*H*) = 7.02 p.p.m., ^1J(SiH) = 287.4 and ^4J(HH) = 0.5 Hz]. The same product was also observed in each case when $SiH_2(OCHO)_2$ was mixed with SiH_2X_2. No exchange products were observed when $SiH_2(OCHO)_2$ was mixed with GeH_3X (X = Cl or Br) under the same conditions, but a complex mixture of products was found when it reacted with GeH_3F. The compound $SiH_2F(OCHO)$ was tentatively identified by its ^1H and ^{19}F n.m.r. spectra [δ(Si*H*) = 4.31 and δ(F) = −160.3 p.p.m.; ^1J(SiH) = 283.7, ^2J(HF) = 58.0, ^4J(HH) = 0.6, and ^4J(HF) = 1.8 Hz]. The C*H* signal could not be

identified with any certainty among a group of signals due to various formate-containing species.

Results and Discussion

Vibrational Spectra.—The i.r. and Raman bands recorded for samples of $SiH_2(OCHO)_2$ under various conditions are listed in Table 2, together with a suggested assignment. This assumes a structure based on that found by electron diffraction (see below), idealised so that the two (non-identical) formate groups have a common plane of symmetry. The molecular symmetry is then C_s, and the 27 normal modes are expected to be separable into 18 of a' symmetry and 9 of a'' symmetry. The latter will give rise to a dipole change perpendicular to the plane of symmetry and hence should give type C band contours in the i.r. spectrum of the gas. The only band to show any distinguishable Q branch is the weak band at 715 cm^{-1}, which is therefore assigned to an a'' mode, probably the SiH_2 torsion, which is i.r. active in this molecule solely because of the non-equivalence of the two formate groups. This non-equivalence is also manifested in the clear doubling of the characteristic ν(C–O) bands just below 1 200 cm^{-1} in the gas phase and in the matrix. In the gas phase the other formate modes [ν(CH), ν(C=O), and δ(OCO)] and ν(SiO) give only a single band in each case, but splittings are apparent in some cases in the matrix. The band associated with ν(SiO) splits into several components in the solid and liquid phases as well; the Raman band of the liquid at 710 cm^{-1} is the strongest in the spectrum and is distinctly polarised, so must be assigned to this mode rather than the SiH_2 torsion, whose Raman band is presumably hidden by the stronger ν(SiO) band. This suggests that there may be a change in the conformation, or a mixture of conformations may occur, in the condensed phases, but there is no evidence as to the nature of the conformation(s) in the liquid and solid. The OSiO deformation is assigned to very weak i.r. and Raman bands near 320 cm^{-1}, very close to $\delta(SiF_2)$ for SiH_2F_2 at 322 cm^{-1}.[10]

Other assignments are mainly by analogy with those for silyl formate[4,11] or other SiH_2 compounds.[12] The assignment is almost complete down to 500 cm^{-1}; all fundamentals expected can be assigned in each spectrum, except that the out-of-plane CH deformations of the formate groups are not discernible in the i.r. spectra of the gaseous and matrix samples. A distinct but very weak band in the i.r. spectrum of the solid and a weak band in the Raman spectrum of the liquid are assigned to the expected modes for the two formate groups. Below 500 cm^{-1} we expect three in-plane modes (two SiOC bends and the OSiO bend) and four torsions of a'' symmetry, derived from twisting motions about the C–O and Si–O bonds. As mentioned above, δ(OSiO) can plausibly be assigned near 320 cm^{-1}; the SiOC bonds may be expected below 200 cm^{-1}, and are not observed in our i.r. spectra as a result. An indistinct Raman band on a rapidly rising background near 170 cm^{-1} may be due to one or both of these motions. The CO torsion in silyl formate has been assigned[4] to a weak band at 223 cm^{-1}, and weak bands in the matrix at 249 and 228 cm^{-1} may be due to the corresponding modes here. A moderate band in the i.r. spectrum of the solid at 268 cm^{-1} is probably related, as torsions are often increased in frequency in condensed phases. The SiO torsions give no detectable bands in the i.r. spectrum above 200 cm^{-1} or in the Raman spectrum and remain unassigned. Table 3 shows the very close agreement between the assignments for $SiH_2(OCHO)_2$ and $SiH_3(OCHO)$.[4,11]

Molecular Structure in the Gas Phase.—The results of electron diffraction from a gaseous sample were used to define the molecular structure. The model used assumed planar OCHO groups with identical bond lengths and angles, but allowed independent variation of the torsion angles about the two SiO and the two CO bonds. It proved impossible to fit the data adequately unless the two SiO torsion angles differed by about 180°, so that one C–O–Si–O linkage was close to *cis*, the other close to *trans*, though both Si–O–C=O groups were close to the *cis* conformation (see Figure 3). The resulting Si · · · O=C non-bonded contacts were therefore similar to that found[13] for silyl formate. The two formate groups are not related by symmetry and the molecular structure has no two-fold rotation axis, and apparently not even a mirror plane. This latter feature may simply be due to the shrinkage effects associated with the very low-frequency torsional motions, and we have shown above that the assumption of an idealised molecular structure of C_s symmetry with non-identical formate groups allows us to interpret the vibrational spectra.

Table 3. Corresponding modes of mono- and di-formatosilanes

$SiH_2(OCHO)_2$	$SiH_3(OCHO)$	
2 944	2 945	ν(CH)
1 744	1 750	ν(C=O)
1 370	1 376	δ(CH) in plane
1 188, 1 162	1 195	ν(C–O)
768	808	ν(SiO)
640	720?	δ(OCO)
249, 228	223	τ(CO)
170	160	δ(SiOC)

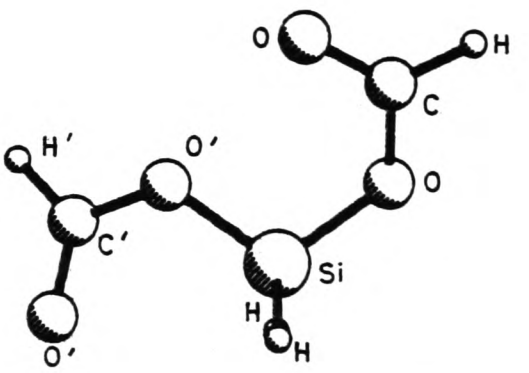

Figure 3. Idealised conformation of $SiH_2(OCHO)_2$

The refined molecular parameters (Table 4) are reasonable, though some of the non-bonded interatomic distances are shorter than those calculated on the basis of normal van der Waals radii. The very short Si · · · O=C and two-bond O · · · O distances (*ca.* 290 and 225 pm respectively) are expected,[13] but there is also a close approach between the carbonyl oxygen of the *cis* formate group and the other single-bonded oxygen of 261 pm, which is much less than the sum of van der Waals radii, 280 pm. It is therefore necessary to suppose that the *cis* conformation is favoured by other factors, despite this close contact. The effective equivalence of the two formate groups on the n.m.r. time-scale shows that the conformations must interchange. The present static but asymmetric model fits the data well, with final R factors of 5.3 (R_G) and 5.9% (R_D).

The final amplitudes [Table 4(*c*)] for non-bonded distances involving non-hydrogen atoms have all been refined at some stage in the analysis, but we cannot claim them to be a unique set all of which are simultaneously determined. It is clear that some very large amplitudes are necessary, and attempts to constrain, for instance, the two non-bonded SiO amplitudes to a common value worsened the fit considerably, though the overall solution still seemed acceptable. The values reported here are those giving the best fit to the data that we have found; if anything the

Table 4. Model parameters (r_a) for diformatosilane

		$SiH_3(OCHO)$
(*a*) Bond lengths/pm		
SiH	151.6(11)	150.0(8)
SiO	166.7(3)	169.5(3)
C–O	136.9(3)	135.1(6)
C=O	121.4(2)	120.9(7)
CH	110.6 (fixed)	112(4)
(*b*) Bond angles/°		
HSiH	110 (fixed)	
OSiO	109.3(25)	
SiOC	120.4(4)	116.8(5)
OCO	121.3(3)	123.5(5)
HCO	120 (fixed)	110 (fixed)
SiO torsion	212(7)	
SiO′ torsion	−27(7)	
OC torsion	169(10) }	201(3)
O′C′ torsion	207(9) }	

(*c*) Interatomic distances and amplitudes/pm

	r_a	u			r_a	u	
SiH	151.6	7.7	f*	H″ ··· H″	248.4	10	f
SiO	166.7	5.1(1)		H″ ··· O	260.0	11	f
C–O	136.9	5.4(2)		H″ ··· C	338.7	15	f
C=O	121.4	4.1(2)		H″ ··· C	382.5	15	f
CH	110.6	7.0	f	H″ ··· C	339.2	15	f
O ··· O	225.3	6.3(2)		H″ ··· C	296.7	15	f
Si ··· C	263.9	8.2(3)		H″ ··· O	355.9	20	f
O ··· O	272.0	42	f*	H″ ··· O	422.3	20	f
Si ··· O	288.2	15.0(9)		H″ ··· O	334.3	20	f
Si ··· O	292.8	46.3	f*	H″ ··· O	286.8	20	f
O ··· C	303.6	15.6	f*	H″ ··· H	428.4	20	f
O ··· C	395.5	45.6	f*	H″ ··· H	471.4	20	f
O ··· O	260.7	20.8	f*	H″ ··· H′	445.4	20	f
O ··· O	449.9	18.7	f*	H″ ··· H′	389.3	20	f
C ··· C	438.5	12.2	f*	H ··· O	201.0	10	f
O ··· O	484.5	27.8	f*	H′ ··· O	213.3	10	f
C ··· O	390.8	16.0	f*	H ··· Si	364.4	15	f
C ··· O	517.3	16.8	f*	H′ ··· Si	360.9	15	f
				H′ ··· O′	413.6	20	f
				H′ ··· O	471.6	20	f
				H ··· C′	547.8	20	f
				H′ ··· C	495.3	20	f
				H ··· O′	626.9	25	f
				H′ ··· O	432.2	25	f
				H ··· H′	600.1	25	f

f = Fixed at this value throughout refinement; f* = fixed after refining to this value.

Table 5. Least-squares correlation matrix (× 100); t = torsion

	Angle OCO	t(SiO)	u(C–O)	u(Si ··· O)	Scale 2
r(SiH)			−65		
r(C–O)	−61				
Angle OSiO		−84			
Angle SiOC		−57			
t(CO)		−67			
u(Si–O)					60
u(C=O)			68		
u(Si ··· C)				57	

Only off-diagonal elements whose magnitude exceeds 50 are shown.

fit is better than expected. The correlation matrix for refining parameters is given in Table 5 in condensed form.

General Discussion and Conclusions.—Diformatosilane, once prepared by an exchange reaction under mild conditions, proves to be reasonably stable, though it is subject to hydrolysis, aerial oxidation, and to other decomposition reactions to give formic acid and other as yet unidentified products. It can be handled *in vacuo*, having a vapour pressure of a few mmHg at room temperature. It undergoes exchange reactions with electronegative groups X on silicon or germanium hydride moieties, yielding mixed compounds $SiH_2X(OCHO)$ (X = F, Cl, or Br) that have as yet been identified only tentatively from ^1H n.m.r. spectra.

The vibrational spectra show clearly the presence of non-identical formate conformations, though on the n.m.r. time-scale the two groups are effectively equivalent. These observations, together with the electron-diffraction evidence for two formate groups with different conformations about their SiO bonds, can be reconciled if a facile interchange of conformation, probably concerted, between the two groups is postulated. (This is equivalent to the existence of a coupled torsional vibration of very low frequency and very high amplitude.) The structure found by analysis of the electron-diffraction data has CO torsion angles slightly different from 180° (defined as *cis*) probably because of shrinkage effects associated with torsional motions. In the same way, the SiO

torsion angles depart from 180° (*cis*) and 0° (*trans*), probably for the same reason. The amplitudes of vibration calculated for the non-bonded distances include some very large values (over 40 pm), which is consonant with high-amplitude torsional motions.

Acknowledgements

It is a pleasure to acknowledge the gift of a cylinder of SiH_2Cl_2, used as the starting material in this investigation, by Union Carbide and the help and encouragement given us in the electron diffraction investigations by Drs. D. W. H. Rankin and H. E. Robertson of this Department.

References

1 W. S. Miller, J. S. Peake, and W. H. Nebergall, *J. Am. Chem. Soc.*, 1957, **79**, 5604.
2 B. Sternbach and A. G. MacDiarmid, *J. Am. Chem. Soc.*, 1959, **81**, 5109.
3 H. J. Campbell-Ferguson, *J. Inorg. Nucl. Chem.*, 1965, **27**, 2121.
4 W. Bett and S. Cradock, *Monatsh. Chem.*, 1980, **111**, 193.
5 D. G. Anderson and S. Cradock, unpublished work.
6 R. A. Cummins and P. Dunn, *Aust. J. Chem.*, 1964, **17**, 185.
7 C. M. Huntley, G. S. Laurenson, and D. W. H. Rankin, *J. Chem. Soc., Dalton Trans.*, 1980, 954.
8 S. Cradock, J. Koprowski, and D. W. H. Rankin, *J. Mol. Struct.*, 1981, **77**, 113.
9 L. Schäfer, A. C. Yates, and R. A. Bonham, *J. Chem. Phys.*, 1971, **55**, 3055.
10 S. Cradock, E. A. V. Ebsworth, and A. G. Robiette, *Trans. Faraday Soc.*, 1964, **60**, 1502.
11 A. G. Robiette and J. C. Thompson, *Spectrochim. Acta*, 1965, **21**, 2023.
12 E. A. V. Ebsworth, M. Onyszchuk, and N. Sheppard, *J. Chem. Soc.*, 1958, 1453.
13 W. Bett, S. Cradock, and D. W. H. Rankin, *J. Mol. Struct.*, 1980, **66**, 159.

Received 31*st May* 1985; *Paper* 5/926

COURSES ATTENDED

"Aspects of Structural Chemistry": Dr. C. Glidewell.

"Modern Inorganic Chemistry": Professor E.A.V. Ebsworth et al.

"NMR Spectroscopy": Dr. I. Sadler.

"Inorganic Postgraduates Lectures": Professor E.A.V. Ebsworth et al.

"The Use of Microcomputers with Instrumentation": Dr. A.G. Rowley and Mr. A. King.

"Topics in Transition Metal Coordination Chemistry": Dr. M. Schrö der.

Attendance at Inorganic Evening Seminars and the USIC Conference for three years.

Attendance at the Second International Platinum Metals Conference.

REFERENCES

1. E. Rutherford, Phil.Mag., 21, (1911), 669.

2. C. Davisson and L.H. Germer, Phys.Rev., 30, (1927), 705.

3. P. Debye, Ann. Physik., 46, (1915), 809.

4. P. Debye, Phys. Z., 31, (1930), 419.

5. G.P. Thomson, Proc.Roy.Soc., A117, (1928), 600.

6. G.P. Thomson, Proc.Roy.Soc., A119, (1928), 651.

7. L. de Broglie, Phil.Mag., 47, (1924), 446.

8. H. Mark and R. Weirl, Naturwiss., 18, (1930), 205.

9. R.A. Bonham, L. Schafer and A.C. Yates, J.Chem.Phys., 55, (1971), 3055.

10. M. Davis, "Electron Diffraction in Gases," Marcel Dekker, (1971).

11. L.S. Bartell, J.Chem.Phys., 23, (1955), 1219.

12. P.M. Morse, Phys.Rev., 34, (1929), 57.

13. R.E. Hilderbrandt, Ph.D. Thesis. Cornell University, 1969.

14. B. Cagnac and J.C. Pebay-Peyroula, "Modern Atomic Physics - Fundamental Principles," MacMillan, London (1975).

15. T.Iijima, M. Kimura and K. Tamagawa, J.Mol.Struct., 30, (1976), 243.

16. S. Cradock, J. Koprowski and D.W.H. Rankin, J.Mol.Struct., 77, (1981), 113.

17. D.M. Bridges, J.M. Freeman, G.C. Holywell and D.W.H. Rankin, J. Organomet.Chem., 32, (1971), 87.

18. B.Beagley, J.M.Freeman, G.C.Holywell and D.W.H. Rankin, J.Chem.Soc., A, (1971), 785.

19. Y. Morino, K. Kuchitsu and Y. Murato, Acta Cryst., 18, (1965), 549.

20. Y. Murato and Y. Morino, Acta Cryst., 20, (1966), 605.

21. Y. Morino, Acta Cryst., 13, (1960), 1107, also O. Bastiansen and M. Traetteberg, Acta Cryst., 13, (1960), 1108.

22. S.J. Cyvin(ed.), "Molecular Structures and Vibrations," Elsevier, (1972), Amsterdam.

23. K. Kuchitsu and S. Konaka, J.Chem.Phys., 45, (1965), 4342. also K. Kuchitsu, J.P. Guillory and L.S. Bartell, J.Chem.Phys., 49, (1968), 2488.

24. W.L. Jolly, J.Am.Chem.Soc., 83, (1961), 335.

25. N.S. Hosmone, Ph.D.Thesis, Edinburgh (1974).

26. L.M. Dennis and P.R. Judy, J.Am.Chem.Soc., 51, (1929) 2321.

27. W. Bett and S. Cradock, Monatsh. Chem., 111, (1980), 193.

28. D.R. Duncan, Inorganic Synth, Vol.1, 151.

29. H.S. Booth and K.S. Willson, Inorganic Synth. Vol.1, 21.

30. M. Linhard, Z. Anorg. Allg.Chem., 236, (1938), 200.

31. Birckenbach and E. Buchner, Ber.Dtsch.Chem.Ges., 73, (1940), 1153.

32. R.A. Cummins and P. Dunn, Aust.J.Chem., 17, (1964), 185.

33. B.J. Aylett and L.K. Peterson, J.Chem.Soc., (1964), 3429.

34. J. Emsley, J.Chem.Soc., A (1968), 1009.

35. S.Sujishi and S.Witz, J.Am.Chem.Soc., 79, (1957), 2447.

36. E.A.V. Ebsworth and M.J. Mays, J.Chem.Soc., (1962), 4844.

37. H.J. Emeleus, A.G. MacDiarmid and A.G. Maddock, J.Inorg.Nuclear Chem., 1, (1955), 194.

38. E.A.V. Ebsworth and M.J. Mays, J.Chem.Soc., (1961), 4879.

39. K. Hedberg, J.Am.Chem.Soc. (1955), 6491.

40. B. Beagley and A.R. Conrad, Trans.Faraday Soc., 66, (1970), 2740.

41. M.J. Barrow and E.A.V. Ebsworth, J.Chem.Soc., Dalton Trans., (1984), 563.

42. E.A.V. Ebsworth, E.K. Murray, D.W.H. Rankin and H.E. Robertson, J.Chem.Soc., Dalton Trans., (1981), 1501.

43. C. Glidewell, D.W.H. Rankin, A.J. Robiette and G.M. Sheldrick, J.Mol.Struct., 4, (1969), 215.

44. G. Gundersen, D.W.H. Rankin and H.E. Robertson, J.Chem.Soc., Dalton Trans., 1, (1985), 191.

45. C. Glidewell, D.W.H. Rankin, A.J. Robiette and G.M. Sheldrick, J.Mol.Struct., 6, (1970), 231.

46. G. Gunderson, R.A. Mayo and D.W.H. Rankin, Acta Chem.Scand.,A, 38 (1984), 579.

47. A.J. Blake, E.A.V. Ebsworth, D.W.H. Rankin, H.E. Robertson, D.E. Smith and A.J. Welch, J.Chem.Soc., Dalton Trans., 1, (1986), 91.

48. J.R. Durig and P.J. Cooper, J.Phys.Chem., 81, (1977), 637.

49. B. Beagley and T.G. Hewitt, Trans. Faraday Soc., 64, (1968), 2561.

50. J.H.M. Terbrake, V. Mom and F.C. Miljlhoff, J.Mol.Struct., 65, (1980), 303.

51. B. Beagley and A.R. Medwid, J.Mol.Struct., 38, (1977), 229.

52. B. Rempfer, H. Oberhammer and N.Auner, J.Am.Chem.Soc., 108, (1986), 3893.

53. L. Pauling, "The Nature of the Chemical Bond", (Cornell U.P., Ithaca, N.Y., 1960) Chp.9.

54. R. Kewley, P.M. McKinney and A.G. Robbiette, J.Mol.Spec., 34, (1970), 390.

55. W. Airey, C. Glidewell, A.G. Robiette, G.M. Sheldrick and J.M. Freeman, J.Mol.Struct., 8, (1971), 423.

56. M. Mitzlaff, R. Holm and R. Hartmann, Z. Naturforsch, 23a, (1968), 65.

57. M. Mitzlaff, R. Holm and R. Hartmann, Z. Naturforsch, 23a, (1968), 1819.

58. L.C. Sams and A.W. Jache, J.Chem.Phys., 47, (1967), 1314.

59. R.G. Cavell, D.D. Poulin, K.I. The and A.J. Tomlinson, J.Chem.Soc., Chem. Comm., (1974), 19.

60. R. Corriu, A. Kpoton, M. Poirier, G. Royo and J. Corey, J. Organomet, Chem., 277, (1984), C25.

61. C. Breliere, F. Carre, R. Corriu, M. Poirier and G. Royo, Organometallics, 5, (1986), 388.

62. R. Rudmann, W.C. Hamilton, S. Novick, T.D. Goldfarb, J.Am.Chem.Soc., 89, (1967), 5157.

63. A.J. Blake, E.A.V. Ebsorth, A.J. Welch, Acta Cryst., C40, (1980), 895.

64. V. Schomaker and D.P. Stevenson, J.Am.Chem.Soc., 63, (1941), 37.

65. C.M. Huntley, Ph.D. Thesis, University of Edinburgh, 1983.

66. R.L. Hilderbrant and S.H.Bauer, J.Mol.Struct., 3 (1969), 325.

67. W.C. Airey, C. Glidewell, A.G. Robiette and G.M. Sheldrick, J.Mol.Struct., 8, (1971), 435.

68. N. Wiberg, K. Schurz, G. Reber and G. Muller, J.Chem.Soc., Chem.Comm., (1986), 591.

69. B. Bak and J. Bruhn, Acta Chem.Scand., 8, (1954), 367.

70. A.V. Belyakov and V.S. Mastryukov, (Unpublished results).

71. S. Cradock, E.A.V. Ebsworth, B.M. Hamill, D.W.H. Rankin, J.M. Wilson and R.A. Whiteford, J.Mol.Struct., 57, (1979), 123.

72. M.J. Buttler and D.C. McKean, Spectrochim. Acta, 21, (1964), 465.

73. G. Gamer and H. Wolff, Spectrochim. Acta, A 29, (1973), 129.

74. M.J. Buttler and D.C. McKeon, Spectrochim. Acta, 21, (1965), 485.

75. T.D. Goldfarb and B.N. Khare, J.Chem.Phys., 46, (1967), 3384.

76. E.A.V. Ebsworth, M. Onyszchuk and N. Sheppard, J.Chem.Soc., (1958), 1453.

77. S.D. Ross, "Inorganic Infra-red and Raman Spectra", (McGraw-Hill Europ.Chem.Ser.), London (1972).

78. I.A. Ellis, Ph.D. thesis, Aberdeen University, (1962).

79. C. Newman, J.K. O'Loane, S.R. Polo and M.K. Wilson, J.Chem.Phys. 25, (1956), 855.

80. D.F. Ball, M.J. Buttler and D.C. McKean, Spectrochim. Acta, 21, (1965), 451.

81. R.N. Dixon and N. Sheppard, Trans.Faraday Soc., 53, (1957), 282.

82. Goubeau and Sommer, Z.Anorg.Chem., 28, (1957), 1.

83. J.R. Durig and C.W. Hawley, J.Chem.Phys., 58, (1973), 237.

84. A.J.F. Clark, J.E. Drake, R.J. Hemming and Quang Shen, Spectrochim. Acta, A 39, (1983), 127.

85. J.A. Cella, J.D. Cargioli and E.A. Williams, J. Organomet. Chem., 186, (1980), 13.

86. R.K. Harris, J. Jones and Soon Ng, J.Mag.Res., 30, (1978), 521.

87. F.A. Cotton and G. Wilinson, "Advanced Inorganic Chemistry", 4th Ed., (Wiley-Interscience), (1980).

88. A.J. Blake, E.A.V. Ebsworth, S.D. Henderson and A.J. Welch, Acta Cryst., (C41),(1985), 1141.

89. A.J. Blake, Personal Communication.

90. M.J. Barrow, E.A.V. Ebsworth and M.M. Harding, (1986), to be published.

91. M.J. Barrow, E.A.V. Ebsworth and M.M. Harding, J.Chem.Soc., Dalton Trans., (1980), 1838.

92. U. Wannagat, Adv.Inorg.Chem. and Radiochem., 6, (1964), 225.

93. H.B. Bürgi, Inorg.Chem., 12, (1973), 2321.

94. H.B. Bürgi, Angew. Chemie.Int.Ed.Engl., 14, (1975), 460.

95. R.J.P. Corriu and G.F. Lanneau, J. Organomet. Chem., 67, (1974), 243.

96. C. Breliere, F. Carre, R.J.P. Corriu, A.De.Saxce, M. Poirier and G. Royo, J. Organomet, Chem., 301, (1986), 131.

97. J. Boyer, R.J.P. Corriu, A. Kpoton, M. Mazhar, M. Poirier and G. Royo, J. Organomet, Chem., 301, (1986), 131.

98. G. Klebe, J. Organomet, Chem., 293, (1985), 147.

99. G. Sawitzki and H.G. Von Schnering, Chem. Ber., 109, (1976), 3728.

100. D. Boal and G.A. Ozin, Can.J. Chem., 51 (1973), 609.

101. H.J. Campbell-Ferguson, E.A.V. Ebsworth, A.J. MacDiarmid and T. Yoshioka, J.Phys.Chem., 71, (1967) 723.

102. L.V. Vilkov and N.A. Tarasenko, J.Chem.Soc., Chem.Comm., (1969), 1176.

103. W. Bett, S. Cradock and D.W.H. Rankin, J.Mol.Struct., 66, (1980), 159.

104. M.J. Barrow, S. Cradock, E.A.V. Ebsworth and D.W.H. Rankin, J.Chem.Soc., Dalton Trans., (1981), 1988.

105. S. Cradock and D.W.H. Rankin, J.Mol.Struct., 69, (1980), 145.

106. M.J. Barrow, E.A.V. Ebsworth, C.M. Huntley and D.W.H. Rankin, J.Chem.Soc., Dalton Trans., (1982), 1131.

107. A. Almenningen, O. Bastiansen, V. Ewing, K. Hedberg and M. Traetteberg, Acta Chem.Scand., 17, (1963), 2455.

108. L.E. Sutton and M.R. Truter (Eds.). "Molecular Structure by Diffraction Methods", (S.P.R.), The Chemical Society, London, (1978), Vol.6.

109. K. Kimura and M. Kubo, J.Chem.Phys., 30, (1959), 151.

110. L.S. Bartell, J.Chem.Phys., 32, (1960), 827.

111. W.S. Miller, J.S. Peake and W.H. Nebergall, J.Am.Chem.Soc., 79, (1957), 5604.

112. B. Sternbach and A.G. McDiarmid, J.Am.Chem.Soc., 81, (1959), 5109.

113. H.J. Campbell-Ferguson, J.Inorg.Chem., 27, (1965), 2121.

114. P.C. Angus and S.R. Stobart, J.Chem.Soc., Dalton Trans., (1975), 2342.

115. W. Bett and S. Cradock, Monatsh.Chem., 111, (1980), 193.

116. A.G. Robiette and J.C. Thompson, Spectrochim. Acta, 21, (1965), 2023.

117. S. Cradock, E.A.V. Ebsworth and A.G. Robiette, Trans. Faraday Soc., 60, (1964), 1502.

118. S. Cradock and E.A.V. Ebsworth, J.Chem.Soc., A, (1967), 1226.